HYDRODYNAMIC IMPROVEMENTS FOR THE DOLPHIN: A SURFACE-PIERCING SEMI-SUBMERSIBLE AUV

MARK-ANDREW BUTT

Hydrodynamic Improvements for the *DOLPHIN*: A Surface-Piercing Semi-Submersible AUV

By
©Mark-Andrew Butt, B. Eng.

A Thesis Submitted to the School of
Graduate Studies in Partial Fulfillment for
the Degree of Master of Engineering

Faculty of Engineering and Applied Science
Memorial University of Newfoundland

May 1999

St. John's Newfoundland Canada

Abstract

In 1996, the Institute for Marine Dynamics (IMD) together with International Submarine Engineering Research Limited (ISER) and Memorial University of Newfoundland (MUN) proposed to design and test a 1/2 scale surface-piercing mast for the *DOLPHIN* semi-submersible vehicle. The proposed mast was required to reduce mast drag, and hence overall vehicle drag, and, to provide improved roll control. To improve vehicle roll control, a new mast was designed with a 25% of chord plain flap over its lower-half and active air ejection over its surface-piercing upper-half. Both methods of roll control were independently tested in the 200m Clear Water Towing Tank at IMD using a 0.516 scale-model of the DOLPHIN. This work was carried out in early 1998.

This thesis presents and discusses the results obtained from the scale-model tests. Specifically, it was found that the existing mast represented 54% of overall vehicle drag at the deepest operating draft, while the proposed mast represented only 26% at this same draft. With air ejection from the proposed mast, the overall drag at the deepest draft increased slightly to 31%.

The basic proposed mast configuration (no air, no flap) provided too much vehicle counter-roll. However, with the inclusion of air ejection on the upper-half of the proposed mast, the vehicle roll moment was considerably reduced. In fact, for some tests the vehicle roll moment was effectively reduced to zero. It was also determined that the 25% of chord flap on the proposed mast was adequate in providing vehicle roll control.

Acknowledgements

I would like to extend my sincere gratitude upon Dr. Neil Bose (MUN) and Dr. Chris D. Williams (IMD) for their support and guidance throughout this thesis. Their patience and understanding of "my way of doing things" was greatly appreciated.

Financial support for the scale-model fabrication and testing came from the Institute for Marine Dynamics (IMD) and International Submarine Engineering Research Limited (ISER). I would also like to thank IMD, ISER and NSERC for financially supporting this thesis through provision of fellowship funding.

Thanks are also extended to the entire staff of IMD and the staff of MUN Technical Services (Engineering) for their assistance throughout this thesis. I would also like to personally thank the following people: Mae Seto (ISE), Spence Butt (IMD), Kent Brett (IMD), Bud Mesh (IMD), Pete Hackett (IMD), John Bell (IMD), Mike Walsh (IMD), Indranath Datta (IMD), Charlie Carter (MUN Tech. Serv.), Mac Mercer (MUN Tech. Serv.), Frank Pippy (MUN Tech. Serv.), Humphrey Dye (MUN Tech. Serv.), Jim Andrews (MUN Tech. Serv.) and Peter Neville (PCN Industrial).

Finally, I would like to thank my family and friends, especially my parents, for their moral support and encouragement during this thesis. I would also like to thank Len and Nancy Barry as well as the entire Earle family (especially their eldest daughter) for their generous hospitality and their hot food over the past two years.

Table of Contents

List of Figures

List of Tables

1.0 Introduction

1.1 DOLPHIN Background

The *DOLPHIN* (Deep Ocean Logging Platform with Hydrographic Instrumentation for Navigation) is a semi-submersible AUV (Autonomous Underwater Vehicle) designed and built by International Submarine Engineering Research Limited (ISER). It was developed as a replacement vessel for the surface launches used by the Canadian Hydrographic Service for echo sounding data collection. Since its initial deployment in the early nineteen eighties the *DOLPHIN* has generated interest in both civilian and military circles and has been adapted to perform many different tasks (Figure 1.01).

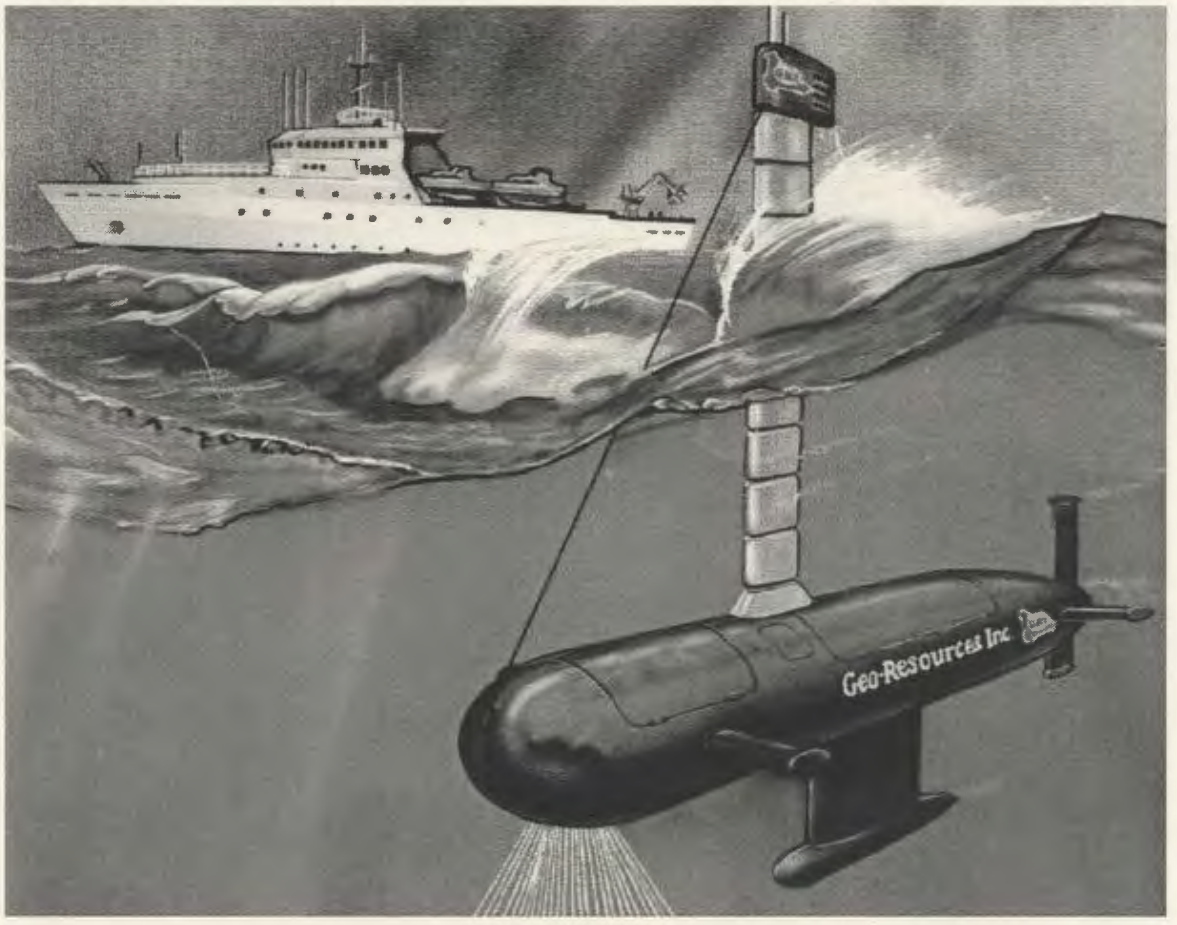

Figure 1.01 – *DOLPHIN Mapping Ocean Floor*

1.2 Description of Existing Mast

A surface-piercing mast is an integral part of the *DOLPHIN* near-surface vehicle. It is used as a conduit for air for the diesel engine and a mount for telemetry equipment which must be above the surface of the water. It consists of a 5" diameter aluminum pipe mounted vertically from the submersible's hull, faired by nine 20" or 25" [508mm or 635mm] free-swiveling fairing segments for a total height (vertical span) of 15' [4.6m] [Watt 1997]. Additionally, since only the aluminum pipe provides the structural support for the mast, a guy wire is required to help support the mast as drag forces act on it. Figure 1.02 shows the *DOLPHIN* in its operating condition as well as the cross-section of the mast fairing segment. The mast has always been suspected of contributing a large portion of the total vehicle drag (approximately 40%).

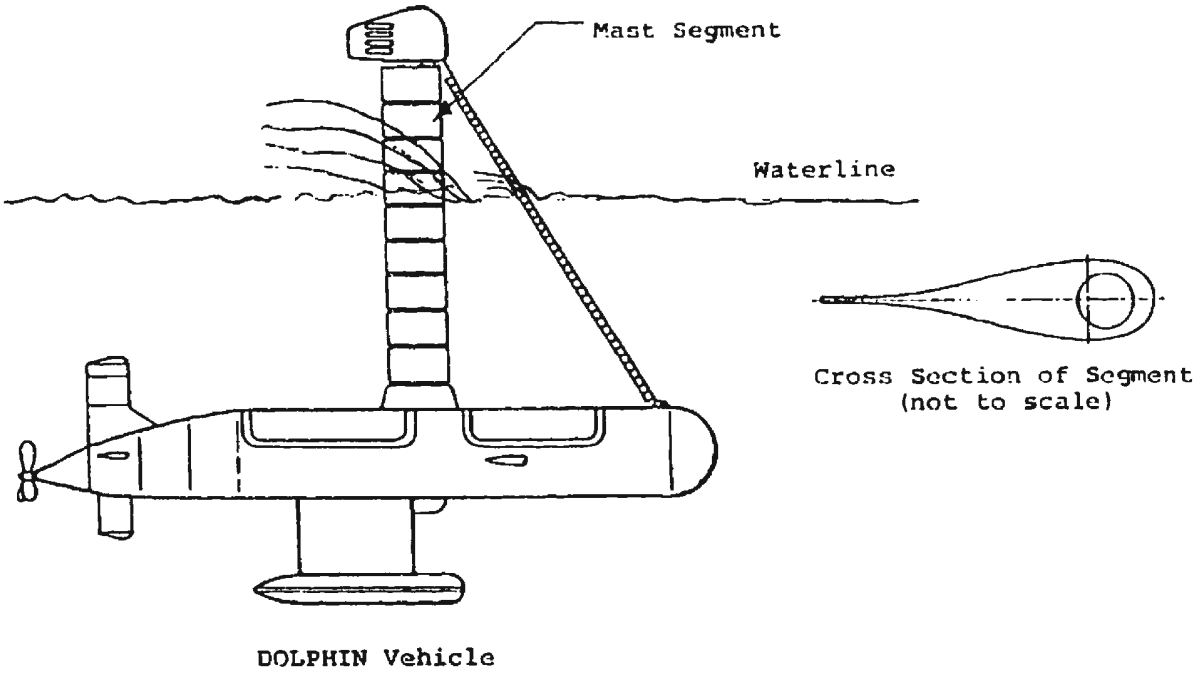

Figure 1.02 – *DOLPHIN Profile and Fairing Segment*

1.3 Current Vehicle Performance

When an underwater vehicle turns, the location where the local cross-flow angle is zero is known as the pivot point. In Figure 1.03 the pivot point is located at the origin of the 'XYZ' coordinate frame (Z* is the turning radius centre). The cross-flow angle is indicated by 'β' in Figure 1.03 ('γ' is the roll angle). Forward of the pivot point the apparent flow comes from the inside of the turn, and aft of the pivot point it comes from outside ('s' in Figure 1.03 indicates the distance from the pivot point to the mid-chord of the appendage). In its present configuration the mast is, in an ideal sense, a passive surface due to the free-swiveling fairing segments. This approach was chosen by ISER because it was noticed that if the mast was rigid and fixed, then when the *DOLPHIN* went into a turn the cross-flow angle onto the 15' mast would cause considerable side force, and hence roll moment.

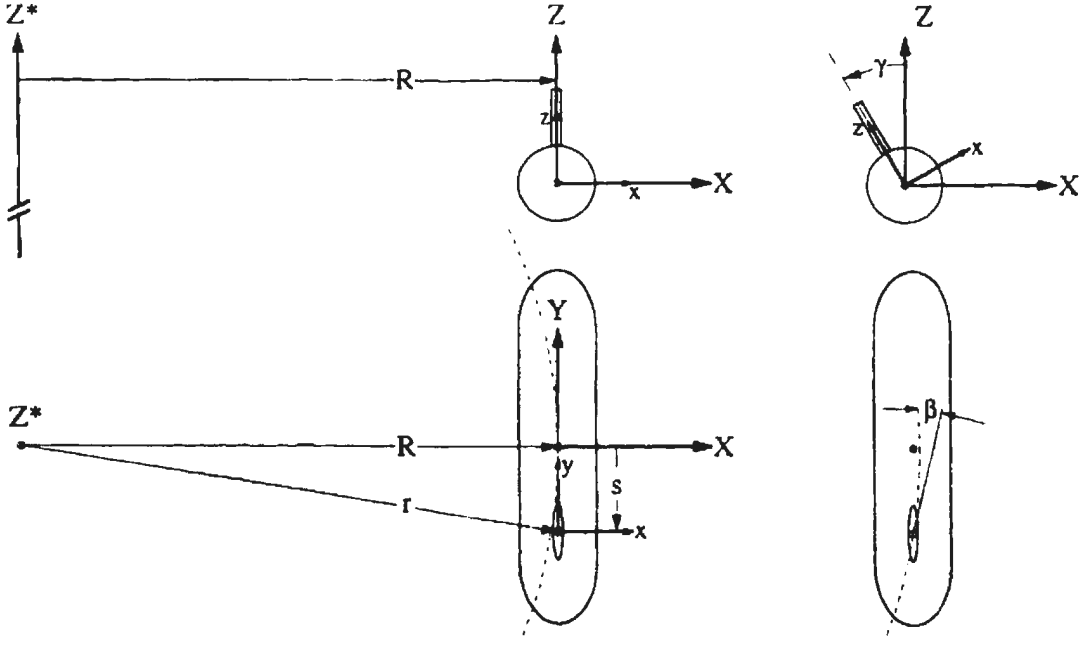

Figure 1.03 – *Pivot Point and Cross-Flow for Underwater Vehicles*

While the mast contributes negligible lift and roll in a turn, the *DOLPHIN*'s keel contributes significant lift and roll. The *DOLPHIN* essentially acts as an airplane with one wing, which in turn produces a large rolling moment on the vehicle such that the keel moves toward the inside of the turn. ISER has partially addressed this problem by reallocating roll control authority to the vehicle's aft planes. However, the resulting lift/roll is still significant enough to require that the *DOLPHIN* make 200' radius turns in order to prevent too much vehicle roll. In fact, roll angles in excess of 30 degrees have been logged during open sea trials. In Figure 1.03, 'R' is the turning radius of the pivot point, while 'r' is the turning radius of the mid-chord of the appendage. The local cross-flow angle at the mid-chord of the keel for a turn of 200' radius is less than 2°.

1.4 ISER's Request for New Mast Design

What is unique to the *DOLPHIN* is that in its present configuration, the pivot point (axis) is located between the mast and the keel [Watt 1997]. This compounds the roll-over problem that was identified in Section 1.3. It should be noted that the *DOLPHIN* is physically capable of initiating 25' radius turns at top speed with its present control surfaces if the rolling problem could be overcome. Through ISER's continuing research and design the *DOLPHIN* has been constantly evolving since its first inception. Therefore, in December 1996, ISER requested that a new surface-piercing mast design be considered. As such, a collaborative research, design and testing plan was set up between ISER, IMD (Institute for Marine Dynamics) and MUN (Memorial University of Newfoundland) to design and test a new surface-piercing mast for the *DOLPHIN*.

1.4.1 Design Constraints for Proposed Mast

ISER requested that the mast be redesigned in order to facilitate the following:

(i) Reduce the overall drag produced by the mast;

(ii) Use the new mast to "counteract" the roll produced by the keel, and;

(iii) Relocate the mast in a more "appropriate" location.

With regards to item (i), the following items were considered:

(a) The new mast had to resist the drag forces without the use of a guy wire. Since the new mast would have lower overall drag forces, this criterion was easy to meet. However, it was required that the new mast provide sufficient strength against the side forces (lift) that would be imposed upon it. For the purposes of this project, an in depth analysis of structural integrity for the prototype (full-scale) mast was not considered. The purpose of this project was to determine the hydrodynamic feasibility of the new mast design.

(b) The cross-sectional hydrodynamic flow section of the mast needed to be modified from its existing section. The current section is an IfS 61 TR 25 rudder type section. ISER had suggested a new mast with a NACA 0015 cross-section. However, while this suggested section may (or may not) have been ideal for fully submerged flow, it may not have been the best (or acceptable) section for surface-piercing flow. Therefore, a suitable mast cross-section was needed to minimize the overall drag forces on the mast.

From item (ii), the new mast was required to be a control surface, and would be integrated into the control architecture of the other control surfaces. The actual control design was not considered as part of this project, it was just kept in mind that the new mast would essentially be a control surface and/or require a control surface. With regards to items (ii) and (iii), the new mast needed to be relocated in a more optimal longitudinal location along the *DOLPHIN*'s hull in order correct the "roll-over" problem.

2.0 Proposed Mast Design Issues

2.1 Proposed Mast Stress Design Issues

With the lack of a guy wire, the new mast required sufficient strength to support drag loads. A constant chord length and thickness for the mast was first assumed. In addition to this, it was assumed that the drag and lift forces were constant with depth (*i.e.* there was a uniform load distribution).

2.1.1 Bending Stress

An ellipse was used to approximate the moment of inertia of the mast about the longitudinal (drag) and lateral (lift) axes. It was determined that for a solid elliptical section that the inertia-ratio of lift to drag is simply the thickness ratio squared (*i.e.* $(t/c)^2$). For example, for an 20" [508mm] chord and 3" [76mm] thickness (t/c=15%) the inertia ratio is 0.0225. In other words, the resisting bending inertia of the mast for lift is only 2.25% of that for the drag. For a hollow section of the above ellipse, this ratio increases to about 5% as the wall thickness goes to zero. To compound this problem, if it is assumed that for some angle of attack that the ratio of the lift coefficient to drag coefficient is, conservatively, 20 to 50, then it is clear that the "path of least resistance" for bending stress is in the lifting direction.

For a uniform load, the bending moment, and hence bending stress, increases parabolically to a maximum at the end affixed to the hull [Hibbeler 1991]. The surface-piercing effects were approximated as a point load acting on the mast at the surface. For a point load, the bending stress increases linearly to a maximum at the end affixed to the hull [Hibbeler 1991]. The most critical area of stress concentration on the mast occurs at the end affixed to the hull, and occurs in the lifting (lateral) direction. It was therefore suggested that the mast chord (and thickness) be tapered from a minimum at the water surface to a maximum at the hull connection to help minimize the stress concentration at the affixed end.

2.1.2 Shear Stress

Shear stress is a function of shear force and the sheared area [Hibbeler 1991]. Since the shear area does not differ between the lateral (drag) and longitudinal (lift) directions, the average shear stress is just a function of shear force (load). For the uniform load, the shear stress will increase linearly from zero at the water surface to a maximum at the hull connection. The surface-piercing point load contributes a constant shear stress along the length of the mast. If a tapered mast is used, then the effective shear area can be increased and the stress concentrations near the hull connection can be reduced.

Ideally then, the size of the mast section at the hull connection would have to be governed by the allowable stress. On the other hand, the size of the surface-piercing section would have to be governed by the necessary air-intake area and the required area for the telemetry. In fact, it may turn out that the section size at the hull connection may be smaller than the requirement for the surface-piercing section. In this case a constant sectional-size mast is all that is required.

Some special considerations were given to the above criteria. With regards to the tapered mast, it should be noted that the tapered mast no longer produces the uniform load distribution assumed previously. The effect is such that for a tapered mast with the same lift (drag) as the constant sectional-size mast, the net force on the mast is located closer to the hull. This causes a reduction in the rolling (pitch) moment. Additionally, if the mast chord is too small (large) then the available lift required to counteract the keel lift is too small (large). Therefore, the proposed mast needed to be designed such that it met the stress requirements, the air-intake and telemetry requirements, is optimized to "complement" the keel and is minimized to reduce drag.

2.2 Proposed Mast Drag Design Issues

2.2.1 Surface-Piercing Drag

At the surface, the resistance of the mast is offered by spray drag and wave making drag. Wave drag is a function of Froude number, Fr, defined as

$$Fr = \frac{V}{\sqrt{g \cdot l}} \qquad \textit{Eq. 2.01}$$

where V is the vehicle speed, g is the acceleration due to gravity, and l is a representative length. For surface-piercing struts (masts), spray drag occurs only for Froude numbers above 0.5 (l is based on chord length). Additionally, wave drag reaches a maximum when the Froude number is 0.5 [Chapman 1971]. Wave formation and wave drag drop off rapidly at higher Froude numbers, and are instead replaced by a thin film of water which flows over the strut above the waterline.

For Froude numbers greater than about three (3), wave drag is negligible and spray drag is independent of Froude number for surface-piercing struts [Chapman 1971]. For a 20" [508mm] chord the speed required for a Froude number of three (3) is about 13 knots [6.7m/s]. This is very close to the operational conditions of the *DOLPHIN*. Therefore, wave making resistance was neglected and spray drag was the only surface-piercing resistance considered for the mast design.

Formation and magnitude of spray drag is influenced by the nose shape. Struts with blunt leading edges, such as airfoils, cause the spray to climb the strut at steep angles and hence greatly increase drag. The NACA 00xx series of airfoils is one of the worst profiles in this regard due to its relatively large leading edge radius. NACA 16-series and 66-series are better choices of airfoil sections suited for surface-piercing applications [Chapman 1971 and Rothblum 1976]. The symmetric double-arc section, with its sharp leading edge is well suited to reduce the spray climb effect [Chapman 1971].

Spray drag is also affected by the location of maximum thickness along the chord (forebody ratio). It was determined that reductions in spray drag could be achieved by moving the location of maximum strut thickness aftward. With regards to the forebody ratio, x/c, the NACA 00xx-series has its location of maximum thickness located at 30% of chord [Abbott 1959]. The 16-series has x/c at about 50% of chord and the 66-series has x/c at about 45% of chord [Abbott 1959], while the symmetric double-arc has, by definition, x/c at exactly 50% of chord. An "asymmetric" double-arc was also considered whose x/c is 65% or 35% of chord depending on the direction of flow (note that this double-arc is still symmetric about its longitudinal axis). When comparing spray drag coefficients obtained by Chapman [Chapman 1971] for 66-series and double-arc sections, the following was determined:

(a) The symmetric double-arc (x/c = 50%) offers a *reduction* in drag of about 25% over the 66-series ($x/c \approx 45\%$).

(b) The asymmetric double-arc (x/c = 35%) *increases* drag by about 40% over the symmetric double-arc.

(c) The asymmetric double-arc (x/c = 65%) *decreases* drag by about:

  (i) 70% over the 66-series;

  (ii) 60% over the symmetric double-arc (x/c = 50%), and;

  (ii) 70% over the asymmetric double-arc (x/c = 35%).

(d) The 66-series airfoil, when operated in "reverse" (x/c is now about 55%), *decreases* spray drag by about 60% compared to its "forward" orientation. This reduction in drag is largely due to the leading edge now being much "finer" (as opposed to the relatively small change in the location of x/c).

(e) The 66-series (forward operating) and the asymmetric double-arc (x/c = 35%) have nearly identical coefficients of spray drag.

From the above, the asymmetric double-arc with x/c = 65% has excellent surface-piercing characteristics, while the symmetric double-arc (x/c = 50%) has the next best performance.

2.2.2 Section Drag

For a chord of 20" [508mm] and a vessel speed of 10 to 20 knots [5.1 to 10.3m/s], the Reynolds number will be about 2.5 to 5.0 × 10^6 respectively. In this regime, from airfoil data [Abbott 1959] for thickness ratios of 15% or less the following was determined for smooth surfaces:

(a) The 66-series and 16-series offer comparable drag coefficients.

(b) The 66-series (and 16-series) offer a *reduction* in drag of about 30% over the NACA 00xx series.

From the above, either the 66-series or 16-series is equally preferable to the NACA 00xx series.

Work done by Chapman [Chapman 1971] at Reynolds numbers of about 1.0 × 10^6 was used to compare 66-series to the double-arc sections. Section drag coefficients (based on $Area = Chord \cdot Vertical\ Span$) suggested the following:

(a) The symmetric double-arc (x/c = 50%), the asymmetric double-arc (x/c = 35%), and the 66-series foil have the same drag coefficients (to within 5%).

(b) The asymmetric double-arc (x/c = 65%) *increases* drag by about 40%.

From the above, the asymmetric double-arc (x/c = 65%) needed to be avoided for submerged application, while the symmetric double-arc (x/c = 50%), the asymmetric double-arc (x/c = 35%), and the 66-series sections were preferred for submerged application.

2.2.3 Mast Raking

Raking or sweeping of the surfacing piercing mast was also considered. Coffee [1953] showed that raking the surface-piecing strut either forward or backward resulted in a reduction of the section drag coefficient. This was expected since raking a given strut reduces the effective thickness ratio to the oncoming flow. However, raking a given strut increases the wetted surface area. Therefore, raking the strut did not reduce the net section drag on the strut. Therefore, from a section drag perspective, there is no advantage in raking the strut. Spray sheet size was somewhat reduced by raking the strut forward, and increased by raking the strut backward. To reduce the complexity of this project, only an un-raked mast was considered for the new design.

2.2.4 Sectional Optimization for Spray Drag and Section Drag

Recall from section 2.2.1 that the optimal section for spray drag was the asymmetric 65% double-arc section (denoted here as DA-65), with the 50% double-arc (DA-50) and 66-series section as secondary choices. Therefore, the "ideal" mast would have a surface-piercing section of the DA-65 type and a submerged section of the DA-35, DA-50 or 66-series section. However, the real world is rarely ideal. Due to oncoming waves the effective mast draft (and hence surface-piercing location) will vary directly with wave height. Therefore, if a DA-65 section is selected for the surface-piercing, then it will spend half a wave cycle in the submerged regime. This will result in an increase in sectional drag for that part of the wave cycle (versus a DA-35, DA-50 or 66-series). Therefore, the symmetric double-arc was used as the foundation for the proposed mast design.

2.3 Side Force and Roll Moment Control

The basic concept for the new mast is for it to just counter-balance the roll produced by the keel when the *DOLPHIN* performs a turn (or for that matter when there is a linear cross-flow). If the mast is rigidly connected to the hull, such that it is located at the same distance back from the pivot point as the keel, then for a mast chord of 20" to 25" [508mm to 635mm] it was determined that 4' to 5' [120cm to 150cm] of mast respectively was required to provided the roll balance. Any more than this and of course the mast would provide too much counter roll. So for a typical mast draft of 9' [2.7m], it was clear then that there would be "too much mast".

In addition to this, when the *DOLPHIN* is in a turn in choppy seas, the effective vessel draft will vary. As a result, the submerged length of the mast will also change, and this in turn causes the net lift and roll on the mast to vary. Moreover, the net lift will vary at the uppermost portion of the mast (*i.e.* where the mast pierces the surface) where the rolling arm is the greatest. The net effect on the *DOLPHIN*'s stability will depend upon: the magnitude of the oncoming waves; the relative frequency (wavelength) of the oncoming waves; the rolling frequency of the *DOLPHIN*; and the effective rolling damping ratio of the *DOLPHIN*. Relatively short (wavelength) waves would be sufficiently far enough away from the natural rolling frequency of the *DOLPHIN* that their effect would be minimal. At the other extreme, it would be expected that in long waves the *DOLPHIN* would simply "follow the surface". The waves of "critical" length, especially those near the natural rolling frequency of the full-scale *DOLPHIN*, would require special attention. Therefore, an additional means of roll moment control was required to maintain vehicle stability in the "critical" sea state.

2.3.1 Flap Design and Configuration

From the above it was obvious then that a means of controlling the side force, and hence the contributed roll moment, on the mast was necessary. It was determined that it may be necessary to dynamically adjust the offset angle (angle of attack) of the mast to compensate for the variable submerged mast length. It was determined however, that if only a few degrees of offset are required, then it may be difficult for the control system to accurately adjust (position) the entire mast. A more appropriate solution was the inclusion of a flap on the mast. The flap had the advantage that it required a larger deflection to achieve the same net lift. This effectively increased the mechanical control resolution of the mast. In addition to this, a flap has a smaller inertial mass and pitching moment and as such requires less control torque to operate [Hoerner 1985]. Depending upon lift requirements the flap concept could be arranged in the following configurations:

(a) The flap runs the entire length of the mast.

- This configuration would require the flap deflection to be dynamically adjusted to compensate for the variable mast draft.

(b) The flap runs only part way up the mast. The flap is on the bottom portion of the mast, and is sized so that it is continuously submerged no matter what the vessel draft.

- This configuration would also require that the flap be dynamically adjusted to compensate for the variable mast draft during sea states.

Depending upon the desired turning radius, the vessel speed, and the average vessel draft, it was determined that the *DOLPHIN* may be required to run in both cases stated above. For this reason, the following mast configuration was considered:

(c). The flap runs part way up the mast as in (b) with a vertical span of 4' to 5' [120cm to 150cm]. However in addition to this, an additional independently controlled flap is added to the upper portion of the mast (*i.e.* the portion that will pierce the surface).

- This configuration would require that the upper flap be adjusted so that it provides *no* lift (and hence *no* roll) in the turn. The advantage of this configuration is that as the vessel draft varies, and hence the submerged mast length varies, the lift/roll contributed by the entire mast section will *not* vary. Moreover, the vertical span of the lower mast section would be selected to just counter-balance the keel (recall Section 2.3). The lower flap would simply perform "supplementary" roll control.

2.3.2 Side Force Control using Air Ejection

Rothblum, Jeffers, and Smith did some work at the David M. Taylor Research and Development Center on methods of controlling side force on surface-piercing struts [Rothblum 1976]. One of the methods used was air entrainment (air ejection) of the strut. The most intriguing result was that if both sides of the strut were entrained with air, then the side force decreased to near zero. A thin, even sheet of air was required on both sides of the strut. Additionally the air sheet needed to be the same size on either side of strut. If these criteria were met, then virtually zero lift over the strut could be achieved for angles of incidence of as high as 15°. This phenomenon was independent of velocity, however the maximum angle of zero lift was related to the airflow ejection rate. Using the results from Rothblum *et al.* [Rothblum 1976], it was determined that for 10 cubic feet of air per minute (CFM) [4.7 *l*/s], 20 CFM [9.4 *l*/s] and 35 CFM [16.5 *l*/s], zero lift was effective up to approximately 6°, 12°, and 15° respectively.

If the air ejection method was used in place of the upper flap in configuration (c) in Section 2.3.1 above, then zero lift and hence zero contributed roll could be achieved with the upper mast section. The lower mast section would be selected so as to just counter-balance the roll contributed by the keel (recall Section 2.3).

It was determined that the "air" required for the air entrainment could in fact be the exhaust from the diesel engine aboard the *DOLPHIN*. To approximate the minimum required volumetric flow rates for the *DOLPHIN* mast, the flow rates used by Rothblum [Rothblum 1976] were extrapolated to the full-scale *DOLPHIN* using a factor based on the cube of the scale (*i.e.* factor = scale^3). To obtain zero lift on the full-scale *DOLPHIN* mast, it was then estimated that between 90 CFM [40 *l*/s] and 350 CFM [165 *l*/s] of exhaust would be required for air entrainment. Using the 363 in^3 [5.9 *l*] engine in the Geo Resources *DOLPHIN* as a baseline at 2800 rpm (revolutions per minute), the intake flow rate of air to the engine was found to be about 300 CFM [140 *l*/s]. This was within the required air flow range, although it should be noted that the exhaust volumetric flow rate would be higher, as the engines in newer *DOLPHIN*s are larger. In addition to this, the *DOLPHIN* uses a turbo charged engine, so in fact the air inflow and hence exhaust outflow would be considerably higher than 300 CFM [140 *l*/s].

2.4 Final Mast Design

The final mast concept had two hydro-dynamically distinct sections. The upper section was optimized for reduced spray drag and section drag (in that order) and had active air ejection to make it effectively a zero lift device. The lower mast section was optimized for strength and reduced section drag (in that order) with an appropriate section chosen for lifting. In addition to this, the vertical span of lower mast section was selected such that it alone provided enough roll moment to counter the roll moment of the keel.

The final design of the new mast was determined during the design and fabrication process of the *DOLPHIN* model (Section 3.6). The final design was inherently a compromise between what was considered "ideal" and what was within the means of fabrication. The full-scale upper section chosen for the proposed mast was a double-arc section with a 22" [560mm] chord and 16% thickness. The lower section selected was a modified double-arc with a 25" [640mm] chord and an 17% thickness. The vertical span of the lower mast section was 5'-3" [160cm]. The modifications required to the lower section were: a leading edge radius of about 2%; a trailing edge with a wedge angle of 22°, and; a 25% of chord plain flap at the trailing edge. In addition to this, a ventilation/end plate was incorporated into the new mast to help minimize interactions between the upper and lower mast sections. The proposed mast design is presented in Figure 2.01.

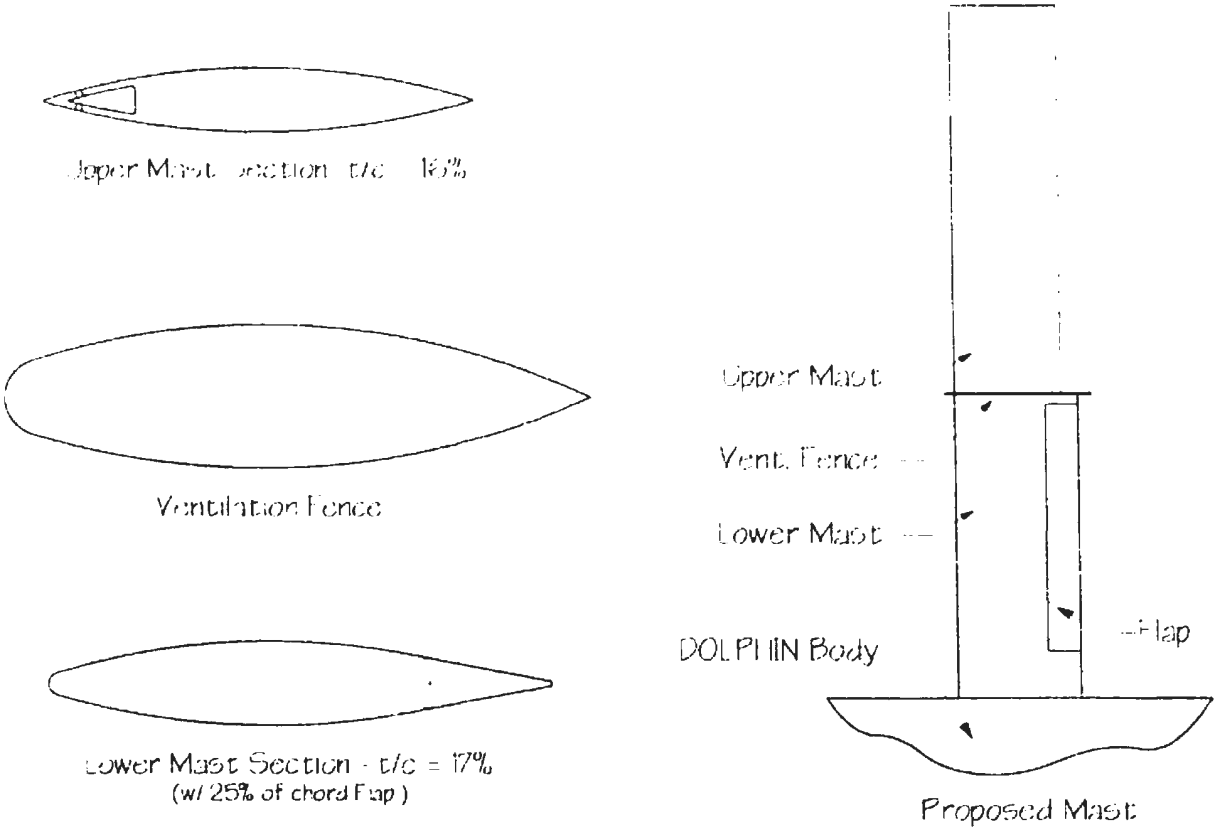

Figure 2.01 – *Proposed Mast Design for DOLPHIN*

3.0 Scale-Model Design and Fabrication

3.1 Scale-Model Constraints and Considerations

The goal of the test program was to compare the relative performance of the proposed (new) mast to that of the existing (old) mast. As such, it was decided that a scale-model of the *DOLPHIN* AUV would be required. The scale-model needed to accurately represent the outer shape of the full-scale vehicle and all relevant appendages. The only appendages included in the scale-model were the keel and the mast. A developmental version of the *DOLPHIN* known as *DOLPHIN* RMS was chosen as the basis for the scale model. The conceptual scale-model of the *DOLPHIN* is shown in Figure 3.01

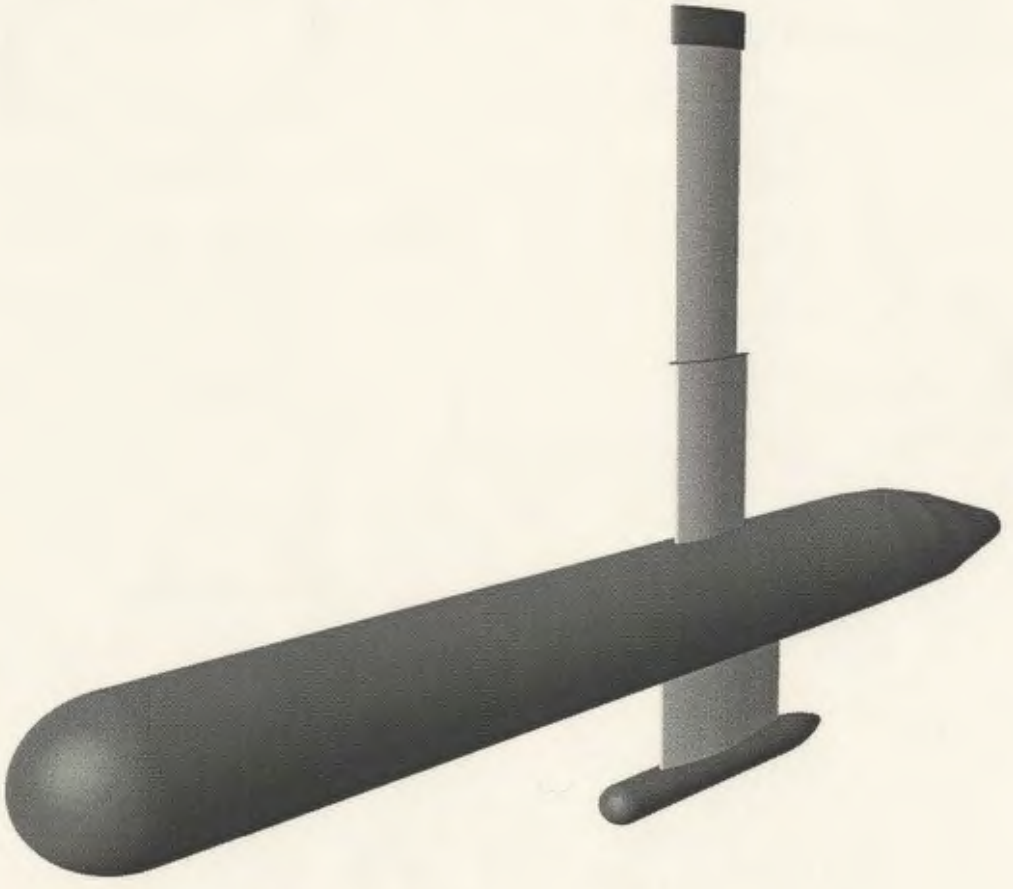

Figure 3.01 – *Conceptual DOLPHIN Scale-Model*

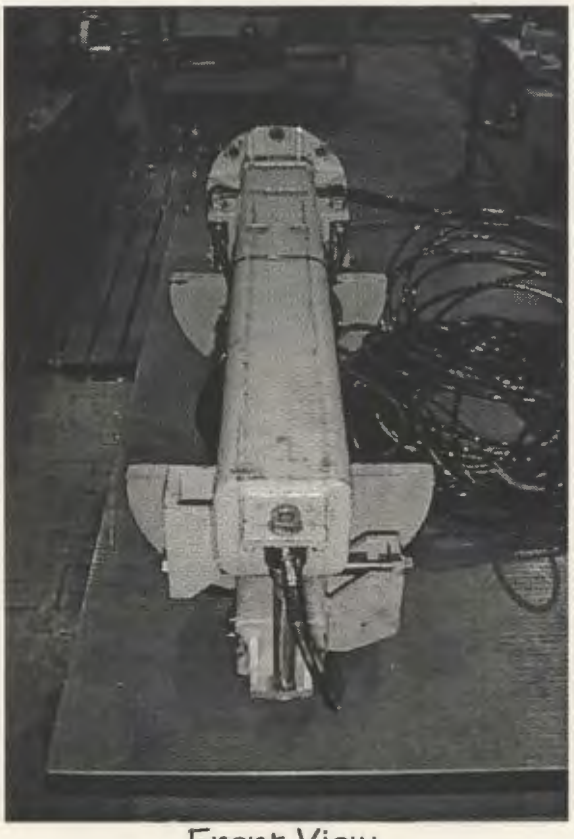

Front View

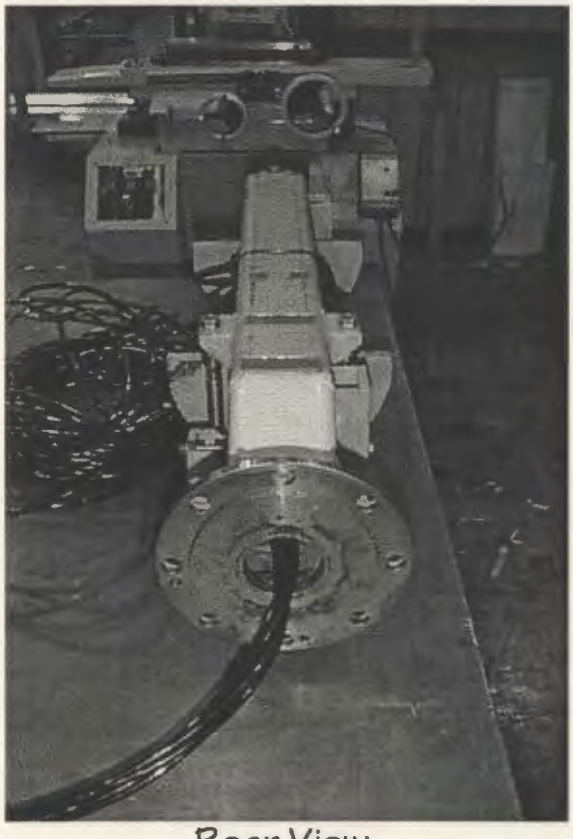

Rear View

Figure 3.02 – *Front and Rear Views of the Tow-Fish Dynamometer*

The scale-model was built around an existing dynamometer and sting. The dynamometer chosen was originally designed for a 12" [300mm] diameter tow-fish model, and hence is referred to as the "tow-fish dynamometer" (Figure 3.02). The tow-fish dynamometer was capable of measuring forces and moments in all 6 degrees of freedom, as well as the associated accelerations. The sting was essentially a 15' [450cm] long heat-treated steel pipe with a 6" [152mm] outside diameter and a 1/2" [13mm] wall thickness. The chosen sting mounted directly to the flange of the tow-fish dynamometer. Figure 3.03 depicts the profile view of the *DOLPHIN* scale-model, as well as the model part names (the masts are not shown to completeness).

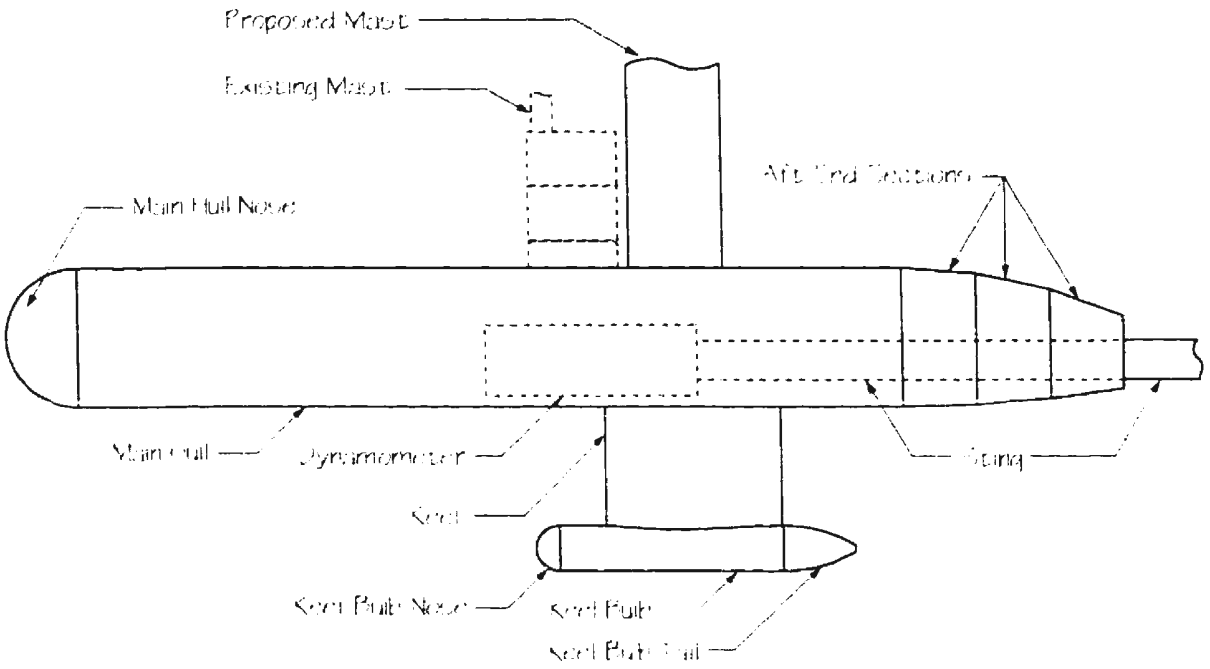

Figure 3.03 – *Profile View of DOLPHIN Scale-Model*

The scale of the *DOLPHIN* model was decided by satisfying the following four constraints:

(a) The scale should be between 1/2 and 2/3;

(b) The sting diameter to model diameter ratio should be between 1/4 and 1/3;

(c) The centre-line of the sting should coincide with the centre-line of the propeller shaft, and;

(d) The dry weight of the scale-model should be less than 1000 pounds.

The diameter of the full scale *DOLPHIN* RMS was 39" [100cm]; it was therefore determined that a scale-model hull diameter between 20" [50cm] and 22" [55cm] would satisfy the above constraints. The final scale was determined during the design process of the model.

3.1.1 Space-Frame Design

The type of design used for the scale-model was determined by ensuring future flexibility of the model. As such, the following items were considered:

(a) The model should be able to accept, at a later date, additional appendages as per the complete *DOLPHIN* RMS;

(b) The model should have an interchangeable aft-end for future *DOLPHIN* designs;

(c) The model should be able to accept additional internal equipment (in addition to the dynamometer) for future tests, and;

(d) The model should provide easy accessibility to its interior.

Based upon these guidelines, a space-frame or web-and-truss design was chosen for the scale-model of the *DOLPHIN*. The space-frame design was used for the main hull, the aft-end, the new mast, and the keel. The space-frame skeleton was wrapped with a "skin" to form the desired outer shape of the vehicle parts. The skin was attached with counter-sunk screws to facilitate removal.

Aluminum alloy was the chosen material used for the space-frame design of vehicle parts. The frame was fastened together with MIG welds. The minimum and maximum thickness of aluminum used were 1/2" [13mm] and 1" [25mm] respectively. This helped minimize warpage and "melt-away" during the welding process. Aluminum alloy was also used for the skin of the model. A 14 gauge (0.064" [1.6mm]) sheet thickness was used for the majority of the skin for the vehicle parts, this was the maximum thickness

that could be easily rolled, yet at the same time was thick enough to accept a counter-sunk machine screw. Alloy 6061-T6 was used for all aluminum in the model. This alloy has high strength combined with excellent corrosion resistance and weldability, as well as good machinability.

3.2 Main-Hull Design

The main-hull was designed to accept the dynamometer, the keel, the masts (old and new), the aft-end, and the hull-nose. Fabrication and assembly of the hull was completed at Technical Services at MUN. The main hull of the *DOLPHIN* has an axi-symmetric circular cross-section, and as such, the webs or ribs could therefore be turned on a lathe. The maximum diameter that could be turned was 20" [508mm]; it was therefore decided that the rib diameter of the main-hull would be 20" [508mm]. Adding the thickness of the outer skin to the hull frame resulted in a model diameter of 20.128" [511.25mm]. Therefore the model scale was determined as 0.516, and the rest of the *DOLPHIN* model was designed based on this scale.

The overall length of the main-hull was 115.5" [293cm] consisting of nine webs; the main-hull was divided into three sub-sections (Figure 3.04). Section 'A' was 48" [122cm] in length with the webs 16" [40cm] on centre. This section was optimized for maximum internal stowage of future equipment and minimized weight. In addition to this, section 'A' was designed to accept the main-hull nose and future appendages. Section 'B' was also 48" [122cm] in length, however, its webs were 12" [30cm] on centre. Since this section was designed to accept the keel, the new mast, the old mast,

and the dynamometer, section 'B' was optimized for maximum strength and maximum flexibility of mast and keel locations. Section 'C' was designed to accept the aft-end as well as provide satisfactory clearance for the sting; its length was 19.5" [50cm].

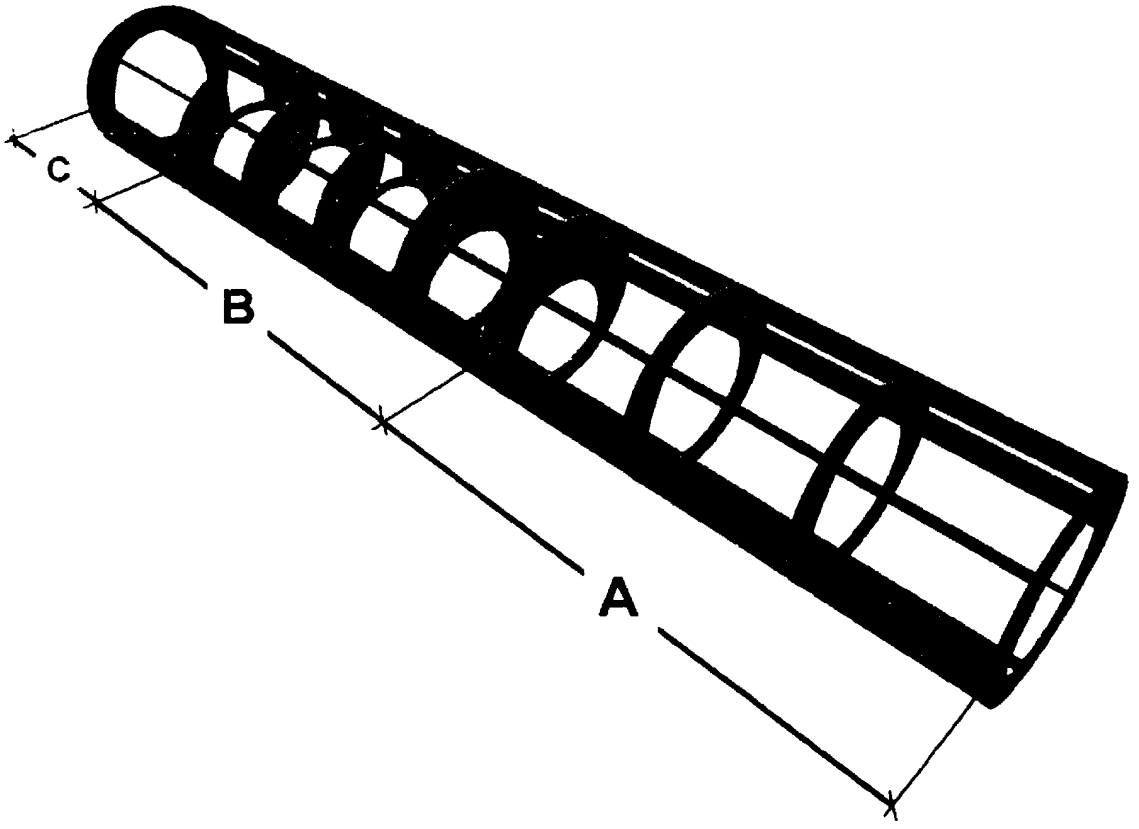

Figure 3.04 – *Main-Hull Space-Frame Design*

Due to limited manufacturing and fabrication techniques at MUN, the *DOLPHIN* model was designed in such a way that its configuration of webs and trusses was also its assembly jig. The result was that three web variations were used in combination with four primary beams (trusses) for the main-hull. The primary beams were orthogonally mounted to the web sections and ran the full length of the main-hull. Figures 3.05 and 3.06 depict the main-hull during fabrication.

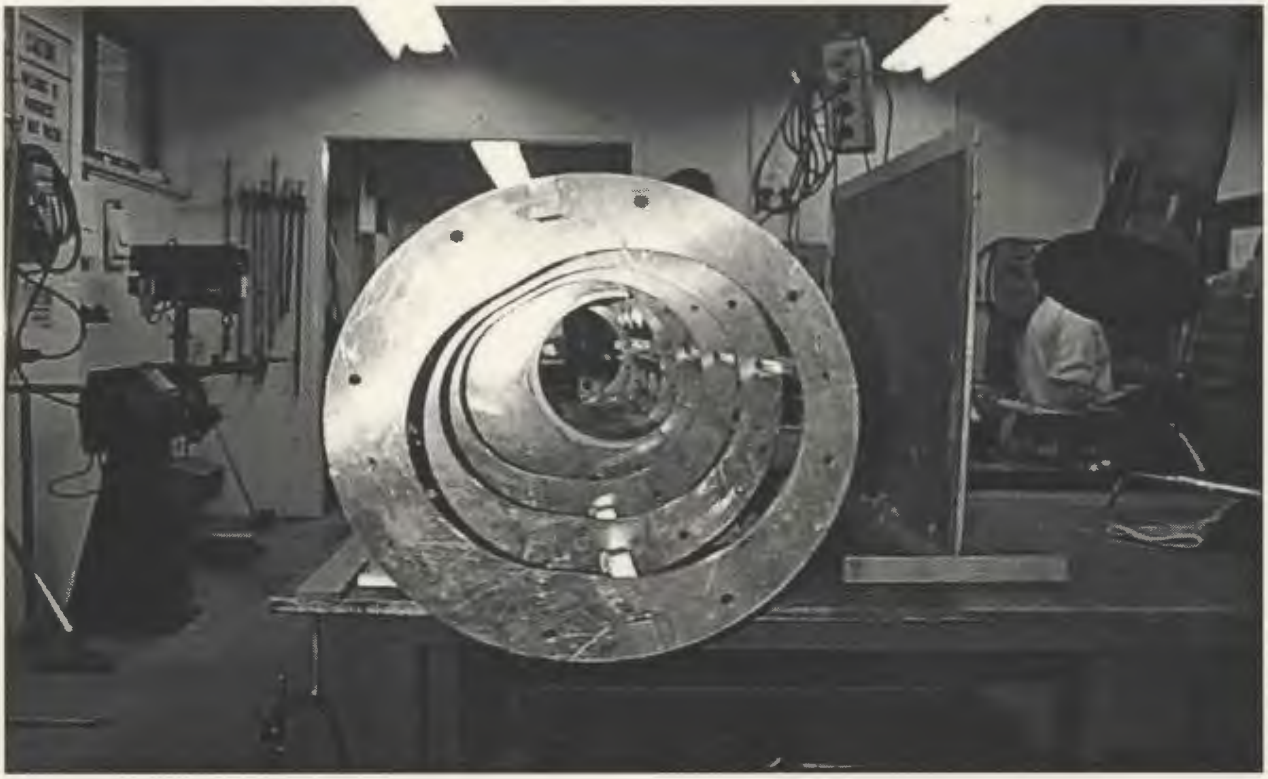

Figure 3.05 – *Front View of Main-Hull Fabrication*

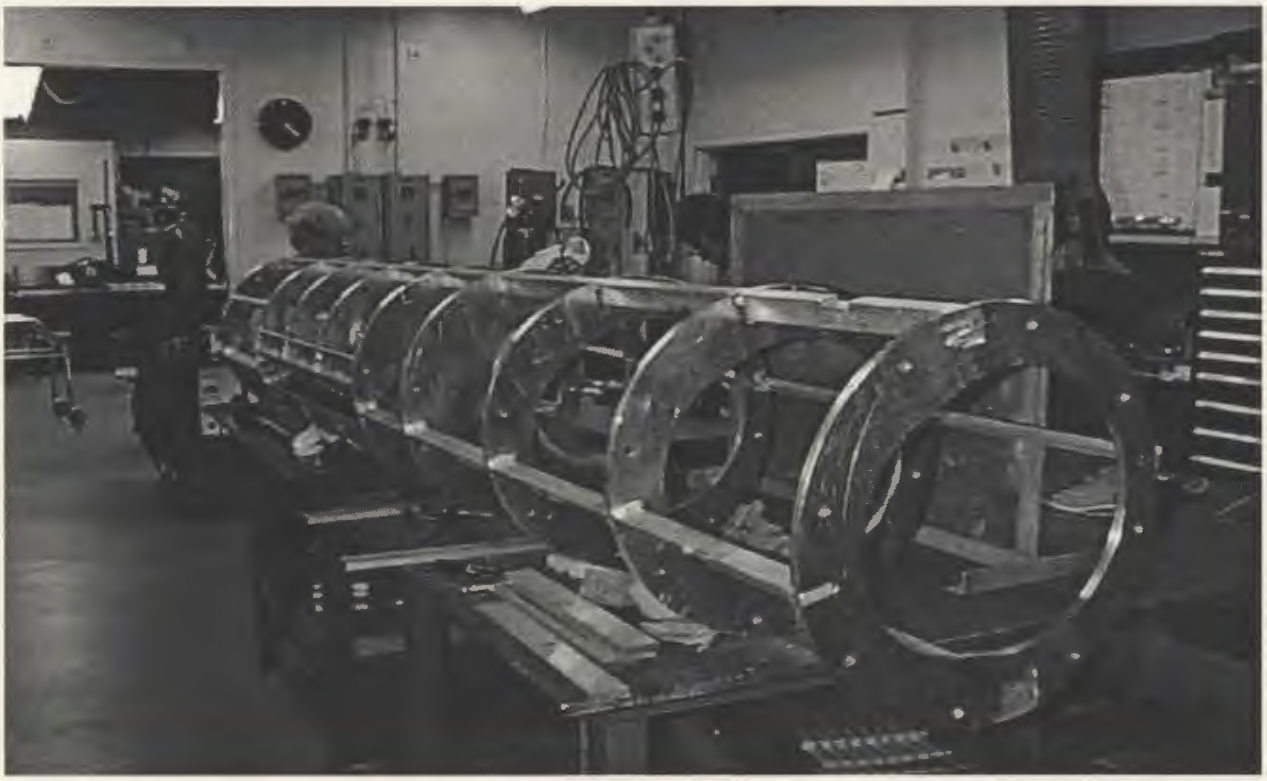

Figure 3.06 – *Left-Front View of Main-Hull Fabrication*

Segments of two of the primary beams of section 'B' would be deleted after the main-hull was fabricated. Also, secondary and tertiary beams were later added to the main-hull. These segments were necessary to stiffen the model, to provide sufficient backing for the skin, and to provide a means of attaching the keel and mast(s) to the main-hull.

3.2.1 Dynamometer Integration

To accept the dynamometer, a dynamometer-tube was integrated into the main-hull. The dynamometer-tube was constructed from the same 12" [300mm] diameter aluminum tubing used for the original "tow-fish". Because it was decided that the centre line of the sting should coincide with the centre line of the propeller shaft, a section of the dynamometer-tube had to be removed. The lower third of the dynamometer-tube was cut away so that it would not protrude through the main-hull. This cut-away was also necessary to provide clearance for the keel attachment, as well as providing easy accessibility to the installed dynamometer. In addition to this, the dynamometer-tube was also designed to accept an existing aluminum canister for additional equipment.

3.3 Aft-End Design

The aft-end of the *DOLPHIN* is vertically asymmetric, and as such, the shaft-line of the *DOLPHIN* is about 1/3 the distance from the bottom of the main-hull. The geometry of the aft-end of the *DOLPHIN* RMS is based on the following equation:

$$D_t = D_h - (D_h - D_{tc}) \cdot \left(\frac{x_t}{x_{tc}} \right)^2 \qquad \textit{Eq. 3.01}$$

where,

D_t = diameter of the aft-end at x_t.

D_h = diameter of the main-hull.

D_{tc} = diameter of the tail-cone.

x_t = position along aft-end.

x_{t_L} = overall length of aft-end.

The above equation is ISE's desired shape for the aft-end of the *DOLPHIN* RMS. The aft-end of the full-scale *DOLPHIN* is in fact comprised of four off-centre conical sub-sections that approximate this theoretical shape. Though the spacing of these sections is not quite equidistant, it was decided to equally space the sub-sections on the scale-model in order to facilitate model fabrication. In addition to this, it was necessary to exclude the fourth (smallest) sub-section to afford a 1" [25mm] mean clearance around the 6" [150mm] diameter sting. To partially compensate for this, the skin of the third sub-section was extended 2" [50mm] over the aft-end frame.

As with the main-hull, it was necessary to design the aft-end configuration such that it too was its own assembly jig. However, because the aft-end is tapered, the primary beams were placed on the inside of the frame. This was the easiest way to mount all four primary beams at right angles to the all four web sections, as well as being able to run the beams the full length of the aft-end section. Secondary beams were also added to stiffen the model and to provide backing for the skin. The space-frame of the aft-end is depicted in Figure 3.07.

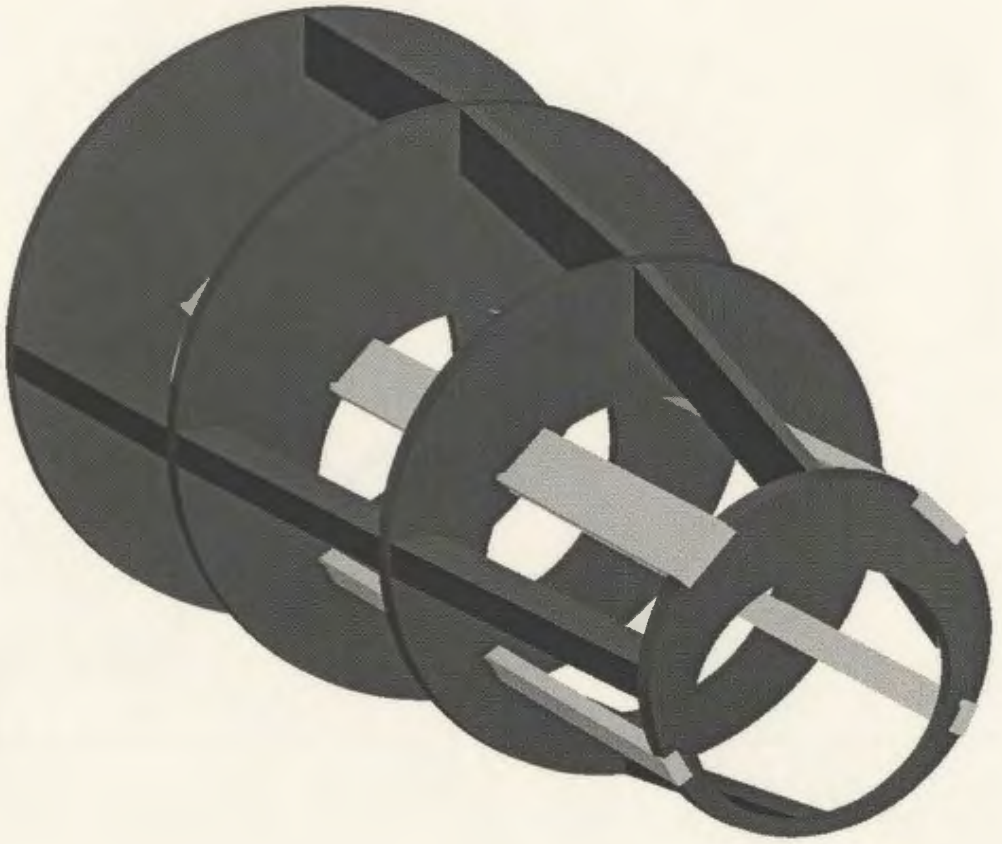

Figure 3.07 – *Aft-End Space-Frame Design*

3.4 Keel Design

The keel for the *DOLPHIN* RMS is a rectangular planform hydrofoil and has a unique cross-section. The cross-section for the model keel was based upon a modified double-arc that closely approximated the full-scale RMS keel. This was done to facilitate the design and fabrication of the keel. The model keel has a 24-1/2" [62cm] chord with a thickness of 3.6" [91mm] (14.7% of chord), and had a leading edge radius of 1/2" [13mm] (2.0% of chord). The model keel had an effective length (vertical span) of 17-1/4" [44cm]. The cross-section of the model keel is shown in Figure 3.08.

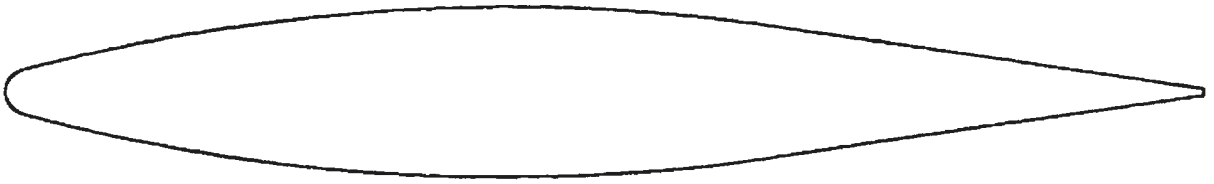

Figure 3.08 – *Cross-Section View of Scale-Model Keel*

The structure of the keel was based on a web-tang design. The tangs in this case were simply trusses that ran through the centre of the webs rather than on their peripheries. For the RMS keel, two tangs of 1" [25mm] by 6" [152mm] sections were inserted through the four web sections. In addition to this, the tangs were designed to provide a means of connecting the keel to the main-hull.

The keel was skinned on each side with 14 gauge aluminum. The skins were fastened to the keel with counter-sunk screws. Where the skins met at the trailing edge of the keel, they were joined with a continuous TIG weld. A 1" [25mm] diameter aluminum alloy rod was used for the leading edge. The skin abutted to this leading edge rod and the gap was filled with body-filler. The completed keel is pictured in Figure 3.09.

The keel for the *DOLPHIN* model was designed to fit into Section 'B' of the main-hull. A requirement of the design was that the keel could be located at various locations along the main-hull. In addition to this, future keel designs needed to be able to be affixed in the same manner as the *DOLPHIN* RMS keel. The result was such that a portion of the keel was inserted into the main-hull and fastened with bolts. The bolt-holes on the keel were 1-1/2" [38mm] on centre, while the holes on the main-hull were 3" [76mm] on

centre. Therefore the keel could be repositioned at 1-1/2" [38mm] intervals. With the RMS keel, it was possible to position the keel 16-1/2" [419mm] forward and 3" [76mm] aft of its design location. It should be noted that once the bolts were tightened, the keel was in fact held in place by the friction load between the main-hull and the keel tangs.

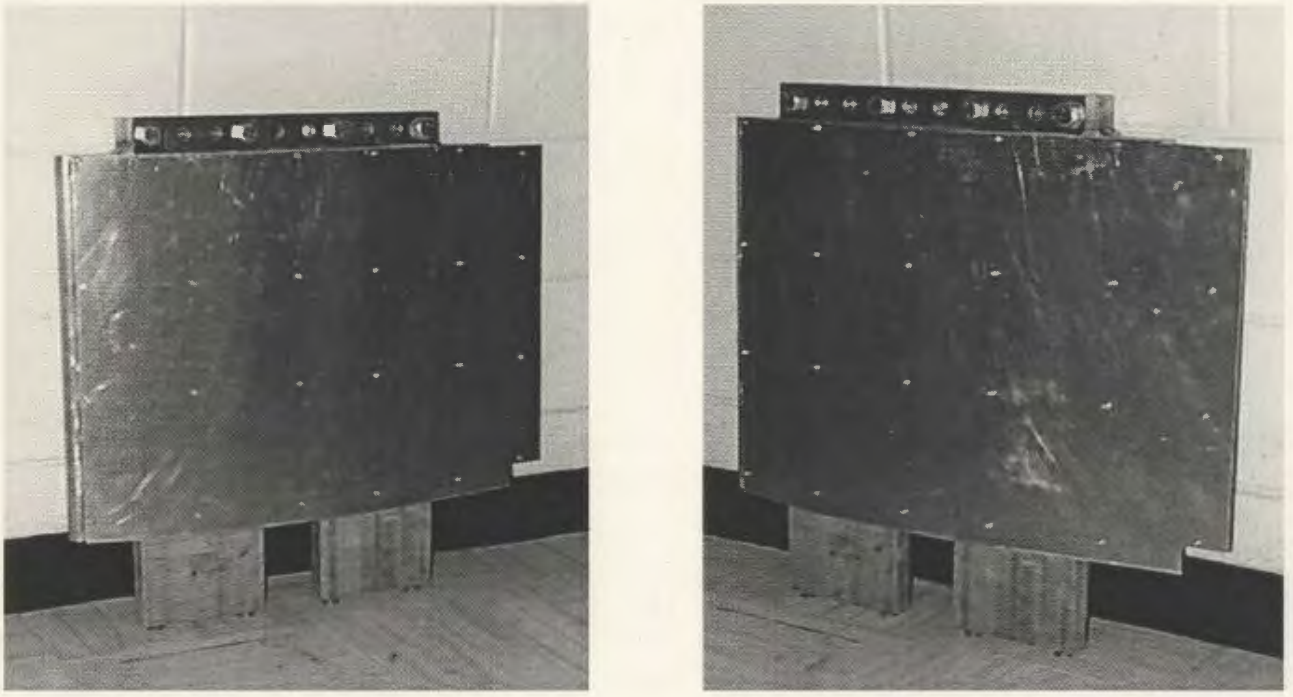

Figure 3.09 – *Completed Scale-Model Keel*

3.4.1 Keel-Bulb Design

Attached to the end of the keel was the keel-bulb (Figure 3.01). The keel-bulb was fabricated from a 6" [152mm] nominal diameter Schedule-40 aluminum pipe. The outside of the bulb was turned down to 6.55" [166.4mm] and the end of the pipe was internally threaded to accept the nose and tail of the keel-bulb. In addition to this, the upper section of the keel-bulb was machined with a cutout that provided a pass-through for the keel so that the tangs could be fastened to the bottom of the keel-bulb.

3.5 *Proposed Mast Design*

The proposed (new) mast for the scale-model *DOLPHIN* had two distinct sections, a lower section and an upper section. Each section was designed to optimize its own specific operational tasks (see Section 2). In addition to this, compromises were made during the design process to facilitate the fabrication of the new mast.

3.5.1 *Lower Mast Design*

The lower section of the new mast, shown in Figure 3.10, was designed to provide lift/roll control and reduced section drag (see Section 2). A modified double-arc with a chord of 13" [330mm] and a thickness of 2-1/4" [57mm] was used for the cross-section of the lower mast section (Figure 3.10). The effective (exposed) length of the lower mast was 32-1/2" [825mm]. The structure of the lower mast was based upon a web-tang design similar to that used for the keel. A 1" [25mm] by 6" [152mm] tang was used for the five web sections. This tang also served as a means of connecting the lower mast to the main-hull. In addition to this, the upper portion of the tang was modified to accept the upper mast section.

It was decided that a 5/8" [16mm] diameter aluminum rod would be used for the leading edge of the lower mast. However, this resulted in a leading edge radius of 2.5% of chord, which was higher than the conceptual design requirement of 2.0% for the lower section of the new mast. It was felt that this larger leading edge radius would not greatly impact the lift or drag performance of the lower mast, and therefore the 5/8" [16mm] diameter aluminum rod was satisfactory.

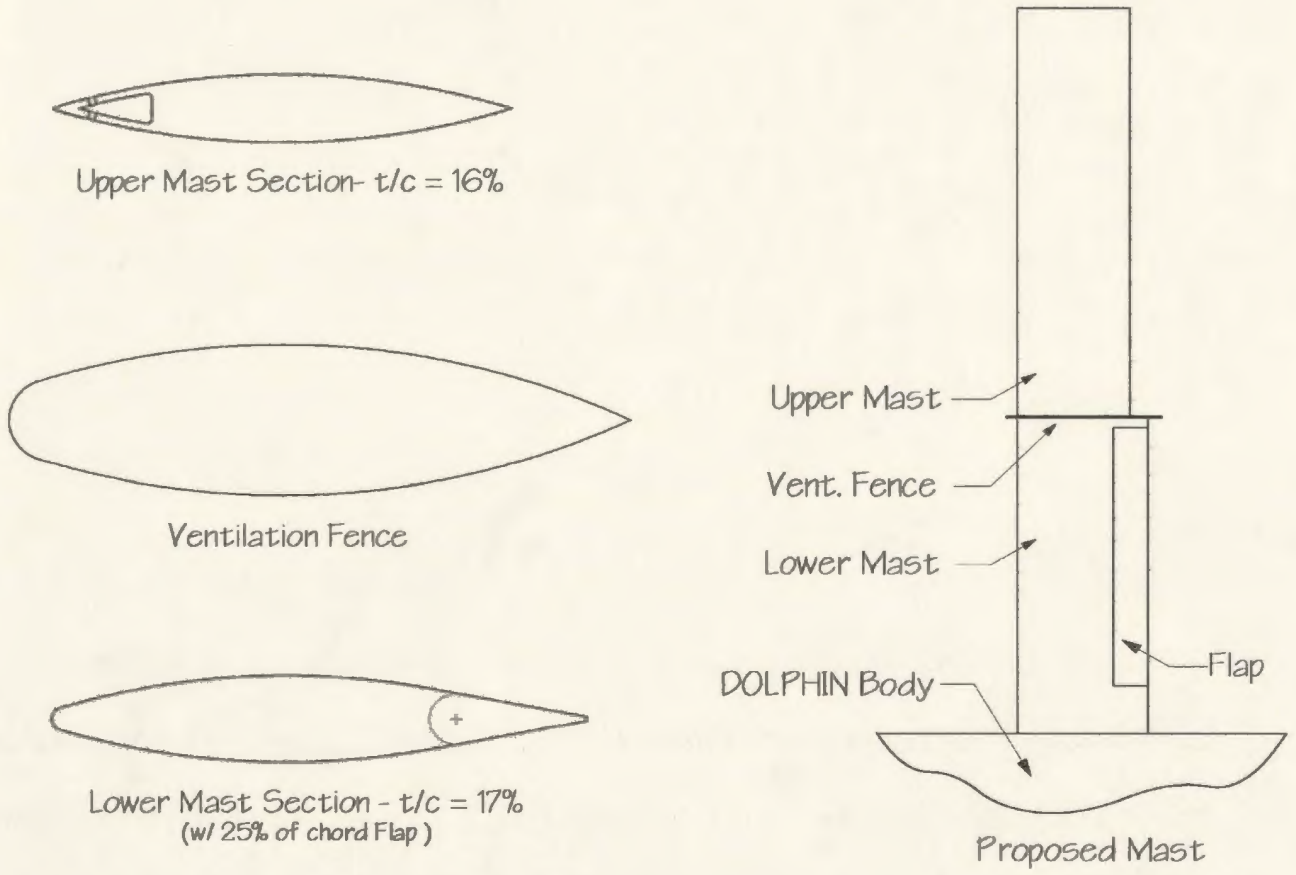

Figure 3.10 - *Proposed Mast Design for Scale-Model*

The lower mast also required an integrated trailing edge plain flap (Figure 3.10). To simplify the fabrication of the flap section it was decided that a trailing wedge shape would be used for the flap. The leading edge of the flap (wedge) would be fabricated from an aluminum pipe (tube) such that the choice of pipe diameter would yield a flap length of 25% chord. A pipe of 1.315" [33.4mm] outside diameter was selected which resulted in a flap length of roughly 24% and a wedge angle of approximately 22°. This trailing wedge design was then re-integrated into the sections of the lower mast that did not have a flap.

To control the attitude of the flap a shaft was required. While an aluminum rod would have provided sufficient strength, it would have been too flexible for practical application. Therefore, a 5/8" [16mm] diameter stainless steel rod was chosen for the shaft. It was necessary to control the flap from above surface so that the *DOLPHIN* model would not have to be raised out of the water each time a flap reconfiguration was required. Therefore, it was decided to pass the flap through the upper section of the new mast and control it from atop the upper mast. In addition to this, brass bushings were fabricated and inserted into the ends of the flap pipe and the web sections where the flap interfaced.

The lower mast section and flap were skinned with 14 gauge aluminum sheet fastened with counter-sunk screws to the web-truss frame. The trailing edge of the flap was fabricated from a single skin which was folded over with a 22° angle. The remainder of the trailing edge of the lower mast was closed up with a TIG weld. Where the skin abutted to the leading edge rod and pipe, body filler was used to fill the gap.

The lower section of the new mast was fastened, like the keel, to Section 'B' of the main-hull. The lower mast had bolt-holes spaced 1-1/2" [38mm] on centre; while the bolt-holes on the main-hull were 3" [76mm] on centre. Therefore the new mast could be repositioned 18" [457mm] forward and 3" [76mm] aft of its design location at 1-1/2" [38mm] intervals. Also, once the bolts were tightened, the friction load between the main-hull and the lower mast tang held the new mast in place.

3.5.2 Upper Mast Design

The upper section of the new mast, shown in Figure 3.10, was designed for reduced spray and sectional drag. A symmetric double-arc with a chord of 11-1/4" [286mm] and thickness of 1-3/4" [44mm] was used for the upper mast (Figure 3.10). The vertical span of the upper mast section was 42" [107cm].

A single 1" [25mm] by 3" [76mm] tang was used for the five webs, with an additional length of roughly 10" [254mm] protruding through the lowest web. This protruding section was inserted into the lower mast section where it was fastened with counter-sunk bolts to the webs of the lower mast.

The upper mast section was skinned with 14 gauge aluminum on each side and fastened to the frame with counter-sunk screws. A series of holes were drilled through the outer surface of the upper foil so that air could be ejected through the holes. The holes were 1mm in diameter and spaced 3.2mm on centre. The holes were all located 0.5" [13mm] aft of the leading edge (4.5% of chord) on both the port and starboard sides. There were roughly 300 holes on each side of the upper mast. The leading and trailing edges of the upper mast were each closed off with a continuous TIG weld.

A means of delivering air to the air-ejection holes on the upper mast was necessary. Rather than deliver the air to the upper holes first, it was decided to deliver the air to the lower holes on the mast first. This would more closely simulate the effect of exhaust leaving the main-hull and entering the bottom portion of the upper mast first.

A 0.675" [17mm] outside diameter aluminum tube was integrated into the forward internal portion of the upper mast. This tube ran the entire length of the upper mast and extended roughly 8" [203mm] beyond the top of the new mast; this tube would deliver air to the upper mast. At the bottom of the tube a slot was cut out so that air could be delivered to the bottom of the upper mast section. Epoxy was used to provide an airtight seal between the air delivery tube and the skin of the upper mast.

The rearward internal portion of the upper mast was designed such that the shaft from the lower mast flap would pass through the upper mast section. A graduated "keel-quadrant" plate was mounted to the top of the upper mast. This keel-quadrant would provide the means of setting and locking the attitude (deflection angle) of the flap.

Figure 3.11 on the following page shows an assembled and "exploded" view of the lower mast and upper mast components. The skin and the ventilation plate are not included in the figure.

3.5.3 Ventilation/End Plate Design

Between the lower and upper mast sections, a ventilation/end plate was required (Figure 3.10). This plate was fabricated from a 3/16" [4.7mm] thick brass plate. The plate was based on a modified double-arc such that its arc was 1.06" [27mm] larger in radius than the arc on the upper mast. This resulted in a minimum overhang of at least 1" [25mm] for the end plate. The leading edge of the plate was modified with a leading edge radius of 1.06" [27mm].

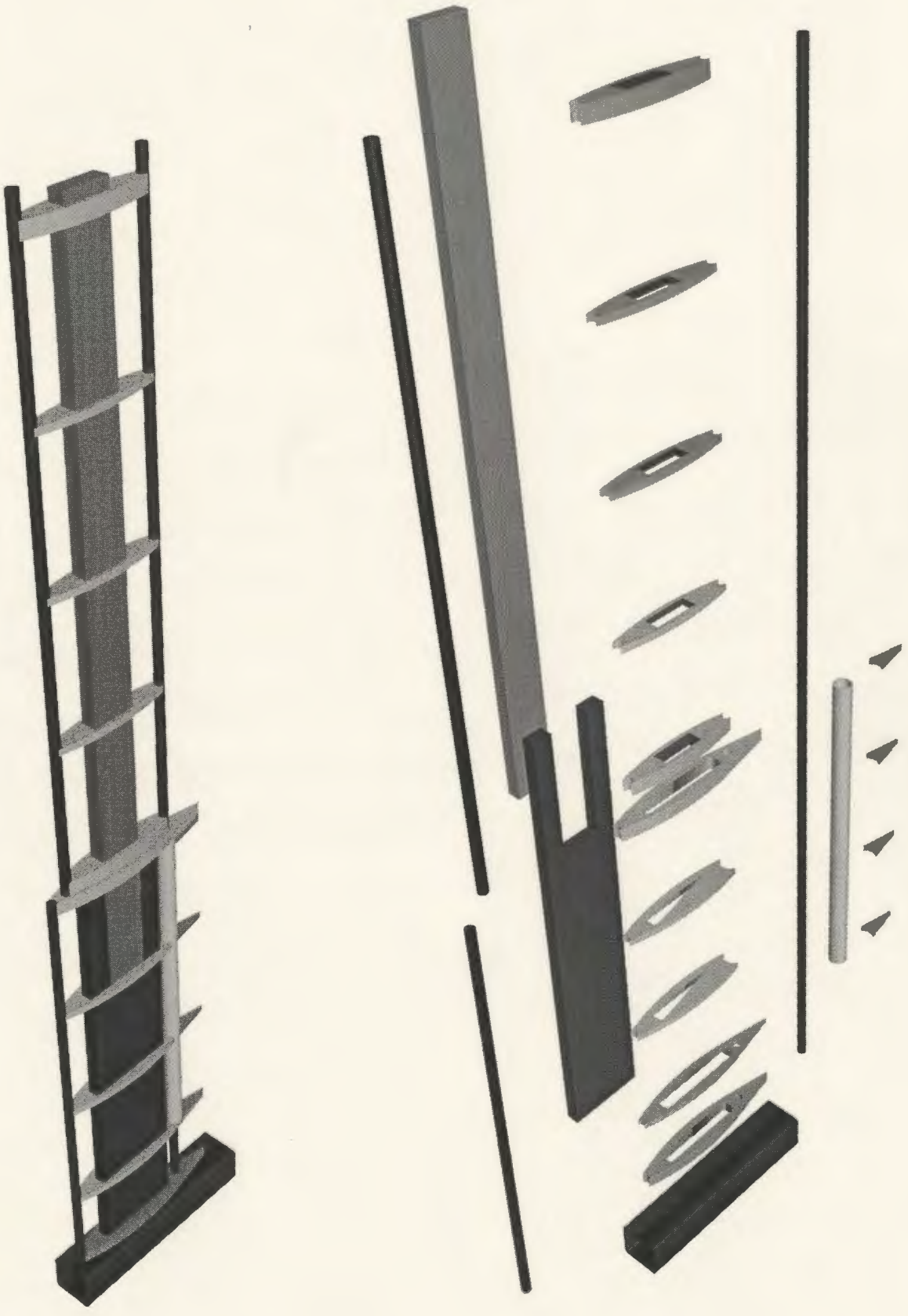

Figure 3.11 – *Assembled and Exploded Views of Proposed Mast Frame*

3.6 *Existing Mast Design*

The existing (old) mast for the *DOLPHIN* RMS is comprised of nine (9) rectangular fairing sections (Figure 3.12). The fairing sections are based upon a IFS-61-TR-25 profile. The scale-model fairing profile was designed using ordinates provided by ISER. PCN Industrial machined the old mast fairings out of Renshape™ using their CNC (Computer Numerically Controlled) facilities. The machined fairings were sealed with Duratec™ and sanded smooth by hand.

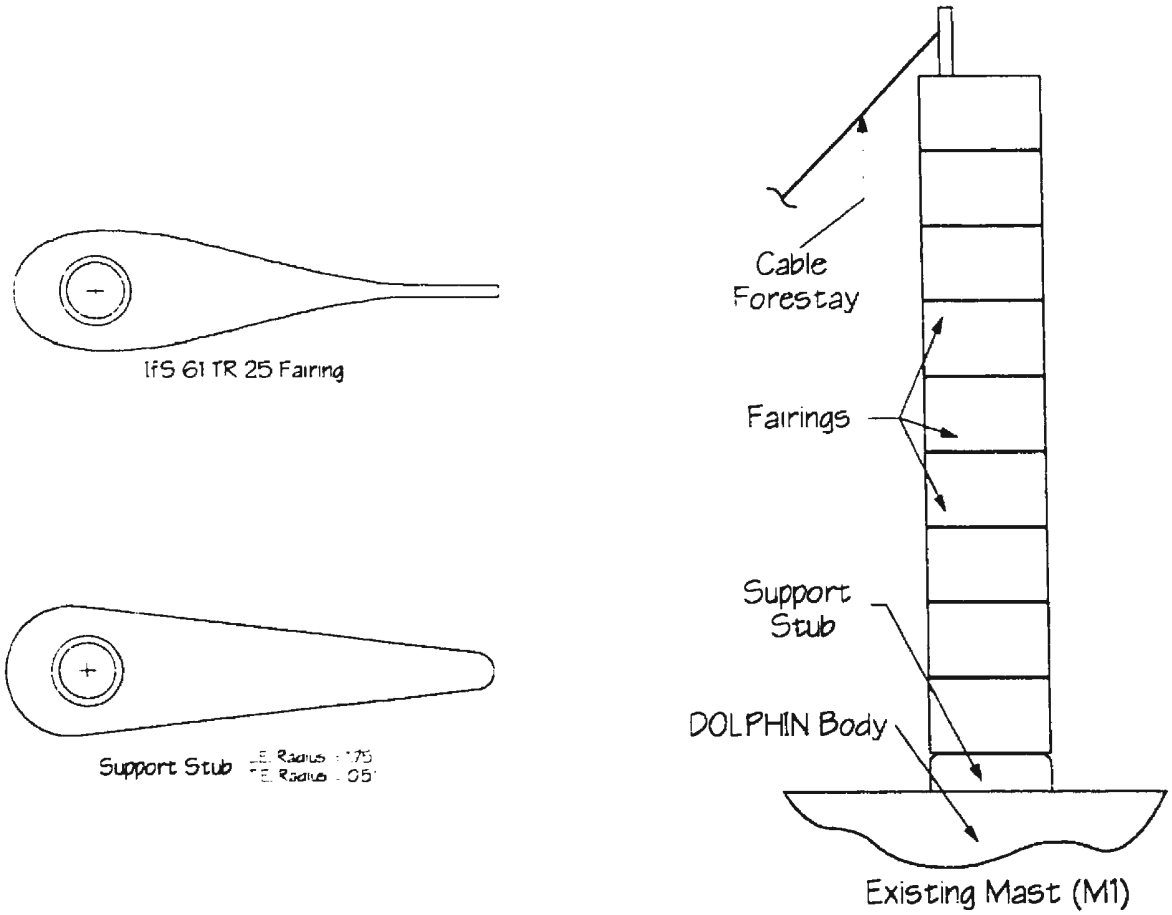

Figure 3.12– *Existing Mast Design for Scale Model*

PVC bushings were used for the fairings so as not to wear down the Renshape™. A 1-1/2" [38mm] diameter aluminum alloy rod was used as the shaft for the old mast fairings. This design of the fairing shaft was integrated into Section 'B' of the main-hull such that it could be fastened in the same manner as the new mast. The result was that the old mast could be repositioned, by 1-1/2" [38mm] increments, from 1-1/2" [38mm] forward to 18" [457mm] aft of its original (existing full-scale) location.

A 3/16" [4.7mm] stainless steel cable was affixed to the top of the fairing shaft with an eyebolt. The other end of this guy wire was attached just behind the nose of the main-hull. The guy wire was tightened via a turnbuckle which was installed on the upper portion of the cable.

3.7 Main-Hull Nose, Keel-Bulb Nose and Keel-Bulb Tail Design

The remaining components of the *DOLPHIN* model were fabricated using Renshape™ milled by the Liné milling machine at IMD. Each component was sealed with Duratec™ and sanded smooth by hand. The main-hull nose was simply a hemisphere section based on a diameter of 20.128"[511.25mm]. The hull nose was attached to Section 'A' of the main-hull with eight 1/2" [13mm] diameter bolts. The keel-bulb nose was also a hemisphere section, but with a diameter of 6.55" [166.4mm]. The end of the nose was threaded so that it could be attached to the keel-bulb. Finally, the keel-bulb tail section was fabricated and similarly affixed to the keel-bulb. Figure 3.13 depicts the keel-bulb tail and nose.

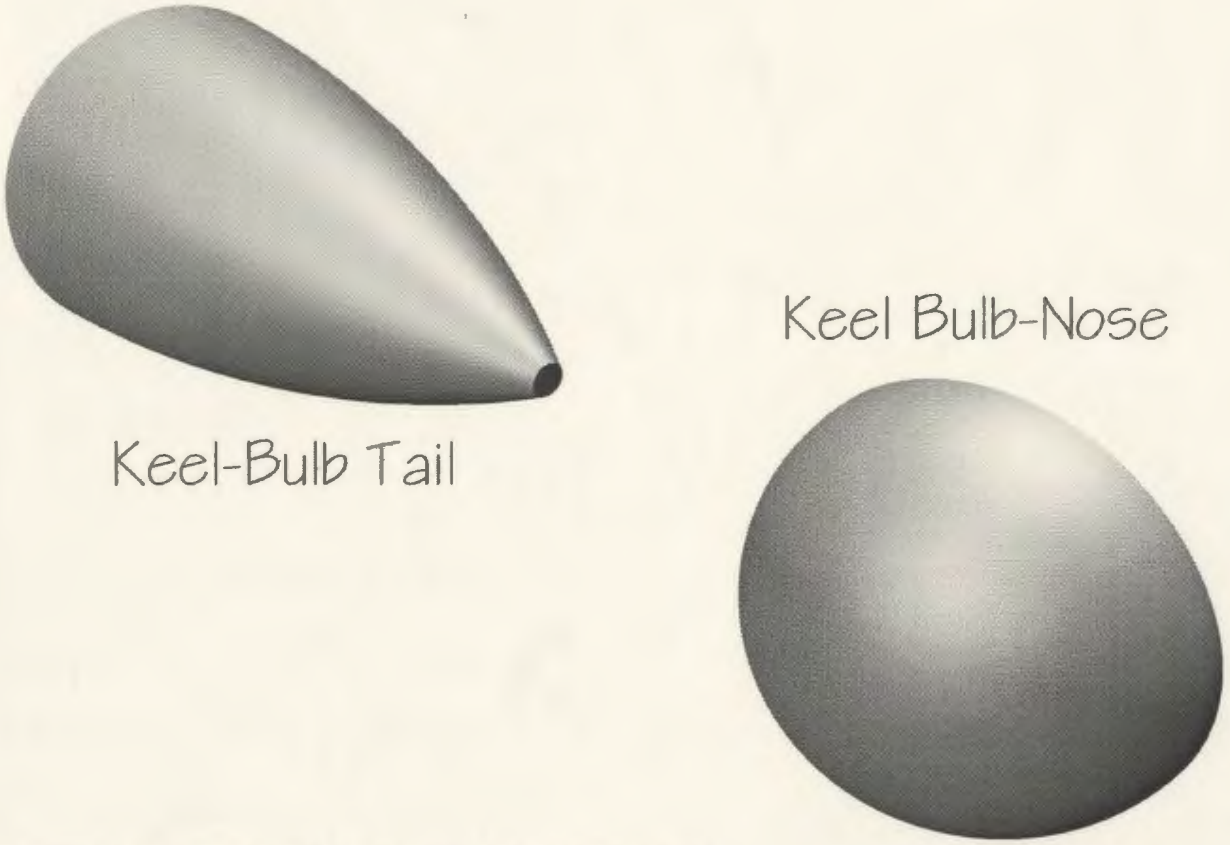

Figure 3.13 – ***Keel-Bulb Tail and Keel-Bulb Nose***

3.8 Scale-Model Painting and Finishing

It was decided to finish all exposed/visible surfaces of the *DOLPHIN* model. This would help minimize oxidation of the aluminum sections, as well as increase model visibility. All exposed aluminum was sprayed with two coats of a zinc-based clear coat to help stabilize the aluminum. It was determined that a flat white colour was optimal for sub-surface visibility. Therefore, two coats of a matte white paint were applied to all components of the model *DOLPHIN* that would be visible. Specifically, this included the entire exterior assembly, with the exception of the upper section of the new mast and the 4 upper fairings of the old mast. These mast sections were given two coats of a matte yellow, as this was a more appropriate colour for observing near-surface effects.

3.9 Complete DOLPHIN Scale-Model

The complete scale-model of the DOLPHIN is shown in Figures 3.14, 3.15 and 3.16.

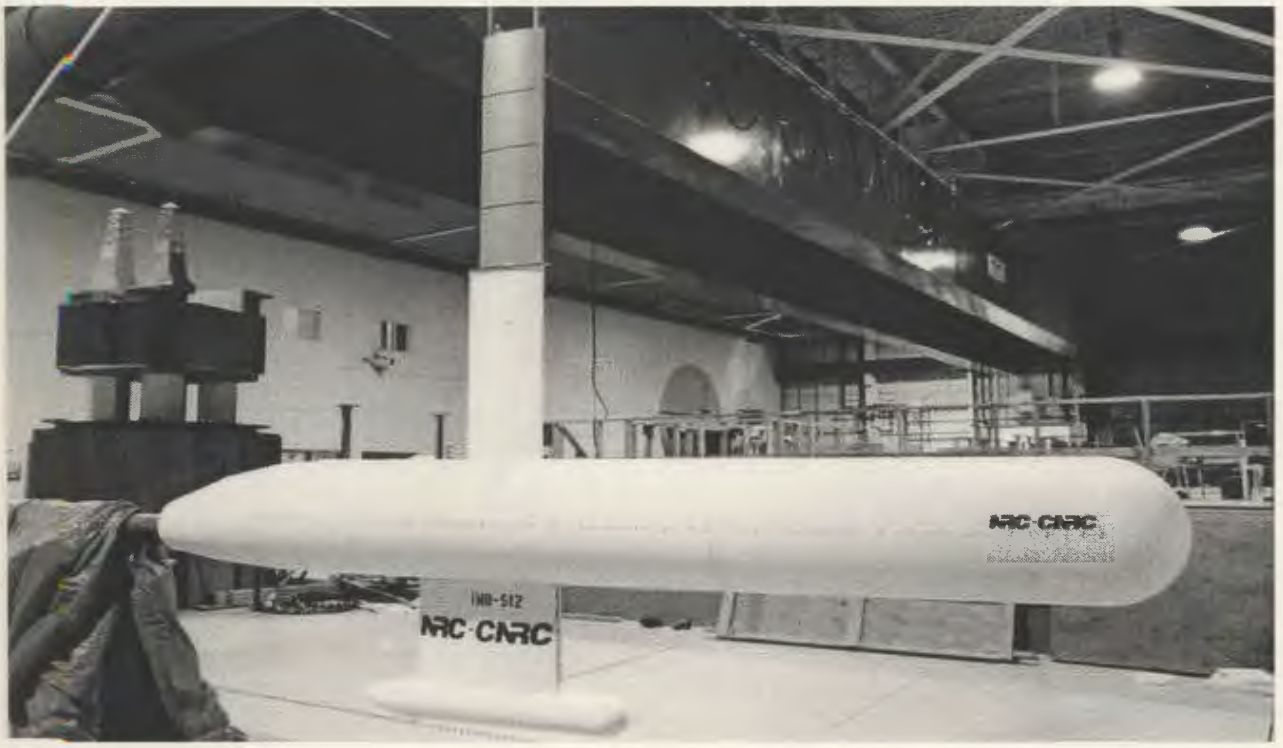

Figure 3.14 – *Right View of DOLPHIN Scale-Model*

Figure 3.15 – *DOLPHIN Front View*

Figure 3.16 – *DOLPHIN Rear View*

4.0 Testing Methodology

4.1 Testing Facilities

A series of captive tests were carried out in the IMD 200m Clear Water Tow Tank (CWTT) using a prototype MDTF (Marine Dynamic Test Facility). To measure the loads and accelerations experienced by the model, the live portion of the 6-DOF (degrees of freedom) tow-fish dynamometer was mounted to the inside of the *DOLPHIN* model. The ground portion of the dynamometer was in turn mounted to a 6" [15cm] diameter sting that extended though the aft end of the *DOLPHIN* model. The sting was in turn connected to the prototype MDTF. Figure 4.01 depicts the actual MDTF with a prototype submarine model attached to it via a sting.

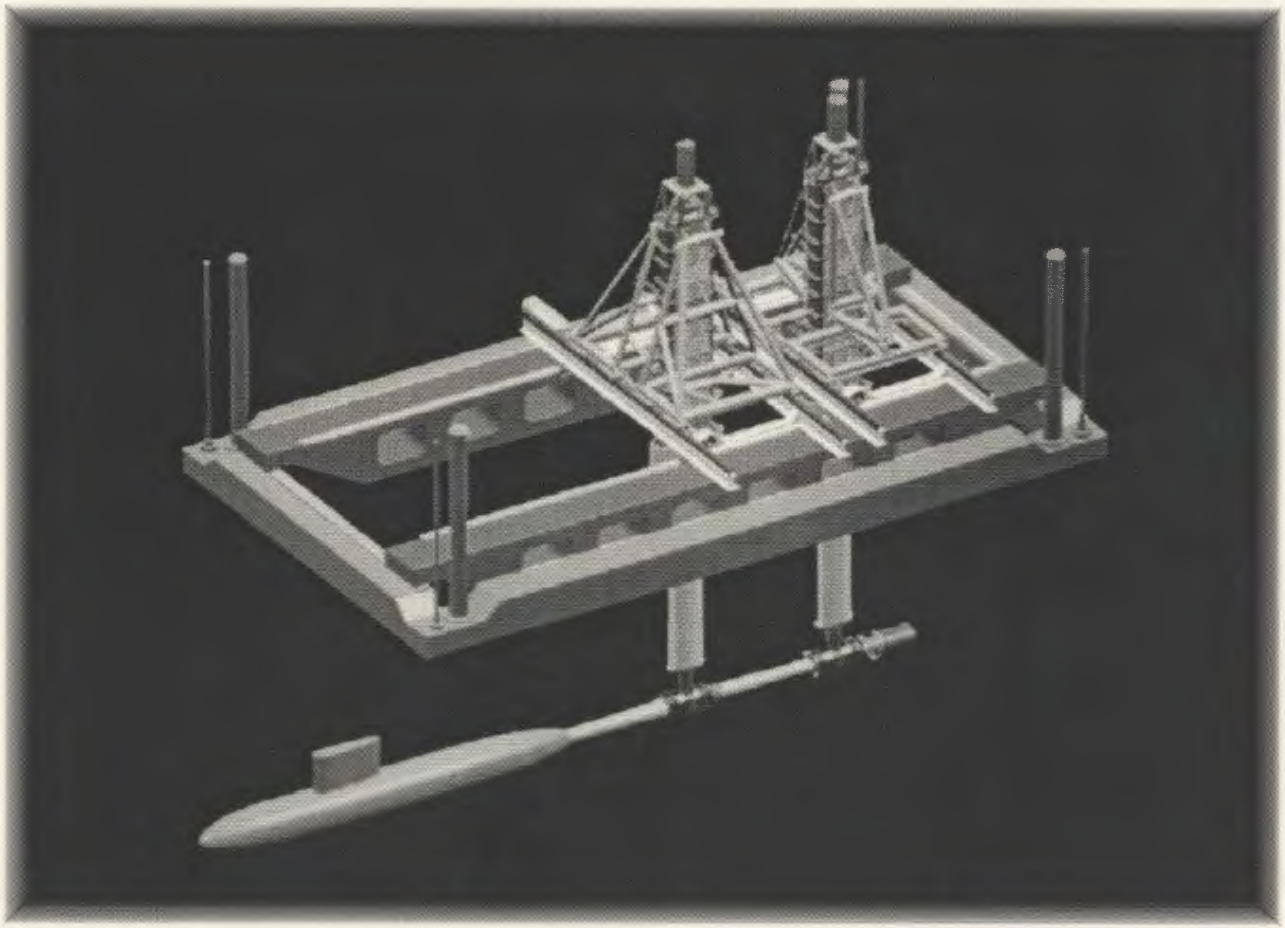

Figure 4.01 – *Marine Dynamic Test Facility with prototype submarine*

Figure 4.02 depicts a schematic of the tow-fish dynamometer (dyno) as well as the six load cell capacities used for this test plan. The data from all six load cells and all six accelerometers were fed to the data collection system onboard the CWTT carriage. Digital photographs were taken of the water surface disturbances for the different mast configurations during testing. In addition to this, motion video was used to observe surface disturbances as well as to monitor the sub-surface effects due to the air ejection.

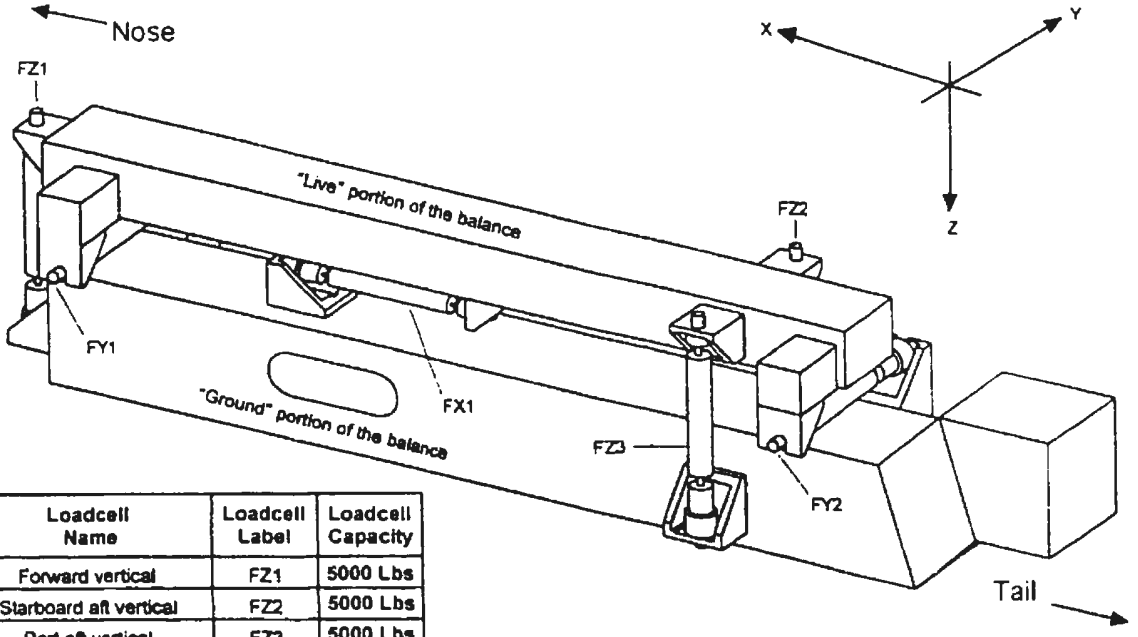

Loadcell Name	Loadcell Label	Loadcell Capacity
Forward vertical	FZ1	5000 Lbs
Starboard aft vertical	FZ2	5000 Lbs
Port aft vertical	FZ3	5000 Lbs
Forward lateral	FY1	3000 Lbs
Aft lateral	FY2	3000 Lbs
Axial	FX1	500 Lbs

Figure 4.02 – *Tow-fish Dynamometer Schematic*

4.2 Test Matrix

For the test program the model yaw angle was varied in increments of 2° from –2° (port) to 10° (starboard); where top-down (plan-view) clockwise rotation is positive. The model pitch and roll angles were fixed for all tests at zero degrees. The six velocities of the model were 2.00m/s, 2.83m/s, 3.46m/s, 4.00m/s, 4.47m/s and 4.90m/s. Three model drafts were used for the test program. Figure 4.03 depicts these drafts as D1, D2 and D3 (the dark horizontal lines on each mast correspond to 1/4" [6mm] wide pin-stripping tape applied to each mast model). These drafts were respectively 43.5" [110cm], 53.5" [136cm] and 63.5" [161cm] as measured from the upper surface of the *DOLPHIN* body.

The model was tested with no mast at draft D1, this configuration was known as M0. The existing mast (configuration M1) and the proposed mast (configuration M2) were tested at all three drafts. In addition to this, the proposed mast was also tested at all drafts with two air ejection rates. Air flows of 20CFM [9.4l/s] (M2B) and 30CFM [14.2l/s] (configuration M2A) were fed to a chamber within the mast during testing by a 5HP [3.7kW] compressor with an 80 gallon [300l] accumulator. The accumulator was fully recharged with air after each test run. Flap angles of –2° to 12° were implemented at model yaw angles of –2°, 0° and 2° at draft D2 only; where top-down (plan-view) clockwise rotation of the flap is positive. The flap configuration was referred to as M2F. The detailed test matrix is contained in "*Appendix A – DOLPHIN Test Matrix*".

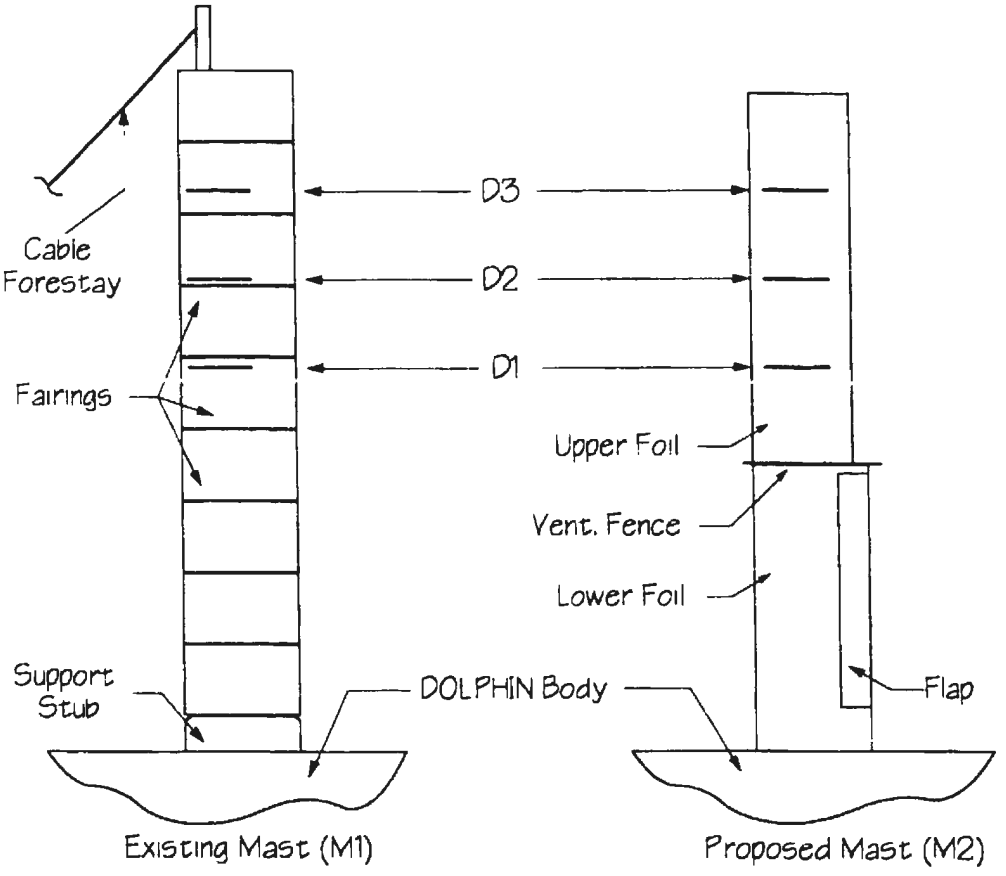

Figure 4.03 – *DOLPHIN model draft locations*

4.3 File Name Convention

The file name convention used for the data collected from the tests is presented below.

The basic file name type is

MastConfiguration_ModelDraft_ModelYaw_ModelVelocity,

where, *MastConfiguration* is replaced by

XM – for no mast (M0)

OM – for old (existing) mast (M1)

NM – for new (proposed) mast (M2).

Replace *ModelDraft* with

D1 – for draft D1

D2 – for draft D2

D3 – for draft D3.

Also, replace *ModelYaw* with

Y## – for positive yaw angles (*i.e.* Y04 for 4° yaw)

YM## – for negative yaw angles (*i.e.* YM02 for –2° yaw).

Finally, replace *ModelVelocity* with

V### – for the velocity in m/s (*i.e.* V283 for 2.83m/s).

Supplementary name extensions include

Q0 – for zero air ejection

Q1 – for 20CFM (M2B) air ejection

Q2 – for 30CFM (M2A) air ejection,

also,

F(M)## – flap angle for M2F tests (*i.e.* F04 and FM02 are 4° and –2° respectively).

For example, file name "XM_D1_Y06_V490" indicates that the model was tested without a mast, at draft D1, at a yaw angle of 6°, and a carriage speed of 4.90m/s.

5.0 Calibrations and Data Correction

5.1 Dynamometer Calibration

After the test plan was completed, a calibration of the dynamometer was carried out. A calibration of the dynamometer was necessary in order to determine both the losses and the crosstalk in the dynamometer. Losses in a dynamometer result when flex links off-axis (non-parallel) to the applied load "absorb" part of the applied load. The effect is such that the load cell(s) parallel to the applied load "sees" less than the full-applied load. Crosstalk occurs when all six load cells (and flex links) are not perfectly mutually orthogonal. The result is that an off-axis flex link will register a false load as it bends. It should be noted that a well designed flex link should not register bending loads, since one design criterion is that the ratio of axial stiffness to bending stiffness is 5000:1. Additionally, in a well-designed dynamometer, the losses vary linearly with the applied load.

To perform the calibration, the sting was mounted to a steel frame such that the *DOLPHIN*/dynamometer assembly could hang freely in air. Known weights were then hung from the *DOLPHIN* at several locations and vehicle orientations and the resulting signals from all six load cells were recorded. These measurements were then used to determine the losses and crosstalk in the dynamometer.

The analysis of the calibration loadings of the x-axis, Fx, is presented here as an example. This calibration procedure and analysis were performed in a similar manner for the other five degrees of freedom.

During the calibration process, it was noticed that hysteresis in some of the load cells was occurring. Specifically, it was noticed that tare measurements taken of each load cell before the weights were hung from the model, did not always coincide with tare measurements taken after the weights were removed. To help reduce the possible occurrences of this hysteresis, three procedures were used. The first was to simply tare both before and after the weights were added, and use the average of these tares as the base tare. In fact, two tares before (Tare 1 & 2) and two tares after (Tare 3 & 4) the loading process were used. Secondly, it was noticed that if the model was shaken just prior to data collection, that the occurrences and magnitude of hysteresis were greatly reduced. Therefore, just prior to each data collection, including all tares and added weights, the model was given an initial oscillation. Thirdly, in addition to incrementally adding weight to the model, the weight was also incrementally removed in the reverse manner. This resulted in two recorded values for each applied load, with the exception of the maximum load.

Table 5.01 on the following page contains the measured (pre-tared) loads recorded by all six load cells; while Table 5.02 contains the tared values for the measured loads. To determine the losses in the axial load (via flex-link X1 and load cell X1), and the crosstalk in the off-axis load cells, Y1, Y2, Z1, Z2 and Z3, the measured (recorded) loads were plotted against the applied axial loads of Fx (Figures 5.01, 5.02 & 5.03). A linear fit was performed on the data sets, and a non-zero intercept was used as it was felt that the tare measurements still exhibited a bias error.

Weight (kg (lbs))	Recorded force in Load Cell (lbs)					
	X1	Y1	Y2	Z1	Z2	Z3
Tare 1	-0.155	-0.244	-0.032	-0.618	1.161	-0.740
Tare 2	-0.144	-0.357	-0.087	-0.739	1.250	-0.839
4 (8.82)	8.337	-0.730	0.268	-0.542	1.142	-0.666
8 (17.6)	16.864	-0.218	-0.020	-0.314	1.122	-0.892
12 (26.5)	25.342	-0.175	-0.006	-0.190	1.049	-1.079
16 (35.3)	33.841	-0.105	-0.031	-0.105	0.975	-1.146
20 (44.1)	42.356	-0.041	-0.043	-0.387	0.821	-1.688
40 (88.2)	85.056	0.218	-0.005	0.187	0.371	-2.285
60 (132)	127.480	0.584	-0.111	0.476	-0.050	-3.048
80 (176)	170.101	0.860	-0.119	0.653	-0.476	-3.778
100 (220)	212.556	1.187	-0.204	1.013	-0.941	-4.406
80 (176)	170.129	0.921	-0.123	0.723	-0.605	-3.562
60 (132)	127.421	0.629	-0.109	0.695	-0.201	-2.921
40 (88.2)	85.067	0.321	-0.052	0.478	0.222	-2.152
20 (44.1)	42.326	0.052	-0.039	0.123	0.661	-1.492
16 (35.3)	33.869	-0.023	-0.026	0.261	0.911	-1.002
12 (26.5)	25.316	-0.102	-0.031	0.105	1.105	-0.902
8 (17.6)	16.871	-0.225	-0.022	0.051	1.262	-0.723
4 (8.82)	8.329	-0.312	-0.051	-0.003	1.313	-0.501
Tare 3	-0.155	0.002	-0.044	-0.043	1.431	-0.478
Tare 4	-0.173	-0.030	-0.018	-0.129	1.422	-0.612

Table 5.01 – *Pre-Tared Calibration Loads for Fx*

Weight (lbs)	Recorded force in Load Cell (lbs)					
	X1	Y1	Y2	Z1	Z2	Z3
8.82	8.494	-0.573	0.314	-0.160	-0.174	0.001
17.6	17.021	-0.060	0.025	0.068	-0.194	-0.225
26.5	25.499	-0.018	0.039	0.192	-0.267	-0.411
35.3	33.998	0.052	0.015	0.278	-0.341	-0.479
44.1	42.513	0.117	0.003	-0.004	-0.495	-1.020
88.2	85.213	0.375	0.040	0.569	-0.945	-1.618
132	127.637	0.741	-0.066	0.858	-1.366	-2.380
176	170.258	1.017	-0.074	1.035	-1.792	-3.111
220	212.713	1.344	-0.159	1.395	-2.257	-3.738
176	170.286	1.078	-0.078	1.105	-1.921	-2.895
132	127.578	0.786	-0.064	1.077	-1.517	-2.254
88.2	85.224	0.478	-0.007	0.860	-1.094	-1.485
44.1	42.483	0.209	0.006	0.505	-0.655	-0.825
35.3	34.026	0.134	0.019	0.643	-0.405	-0.335
26.5	24.473	0.055	0.014	0.487	-0.211	-0.235
17.6	17.178	-0.068	0.023	0.433	-0.054	-0.056
8.82	8.486	-0.155	-0.006	0.379	-0.003	0.166

Table 5.01 – *Tared Calibration Loads for Fx*

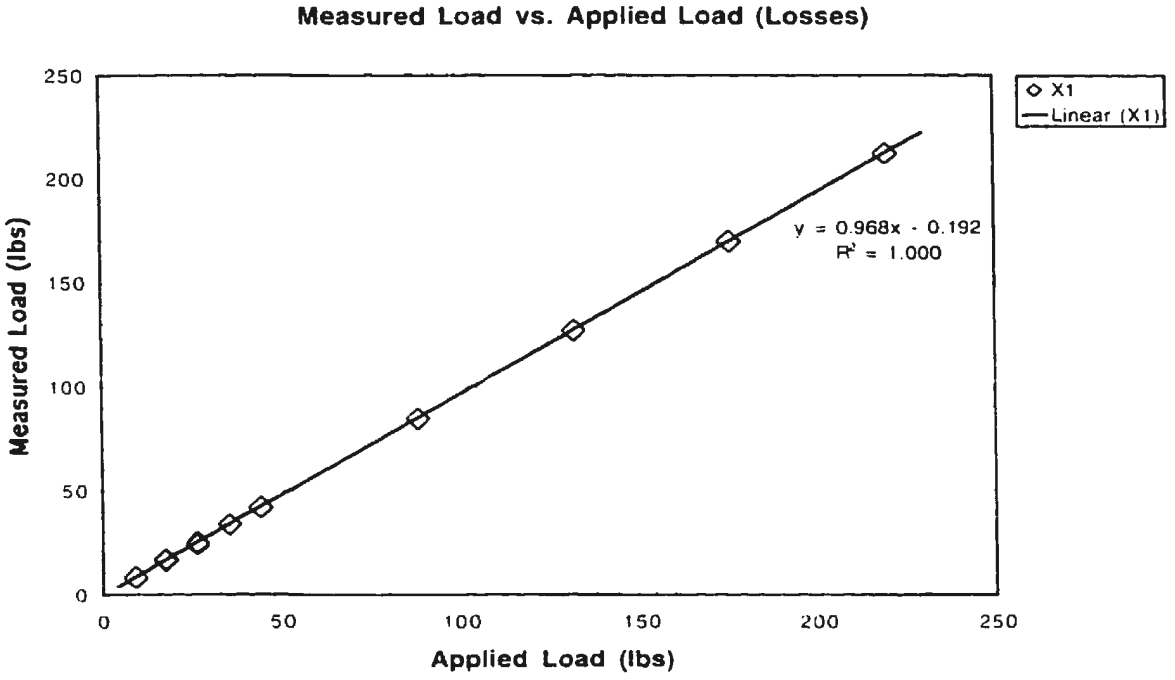

Figure 5.01 – *X1 Load Cell – Measured Load vs. Applied Load (Fx)*

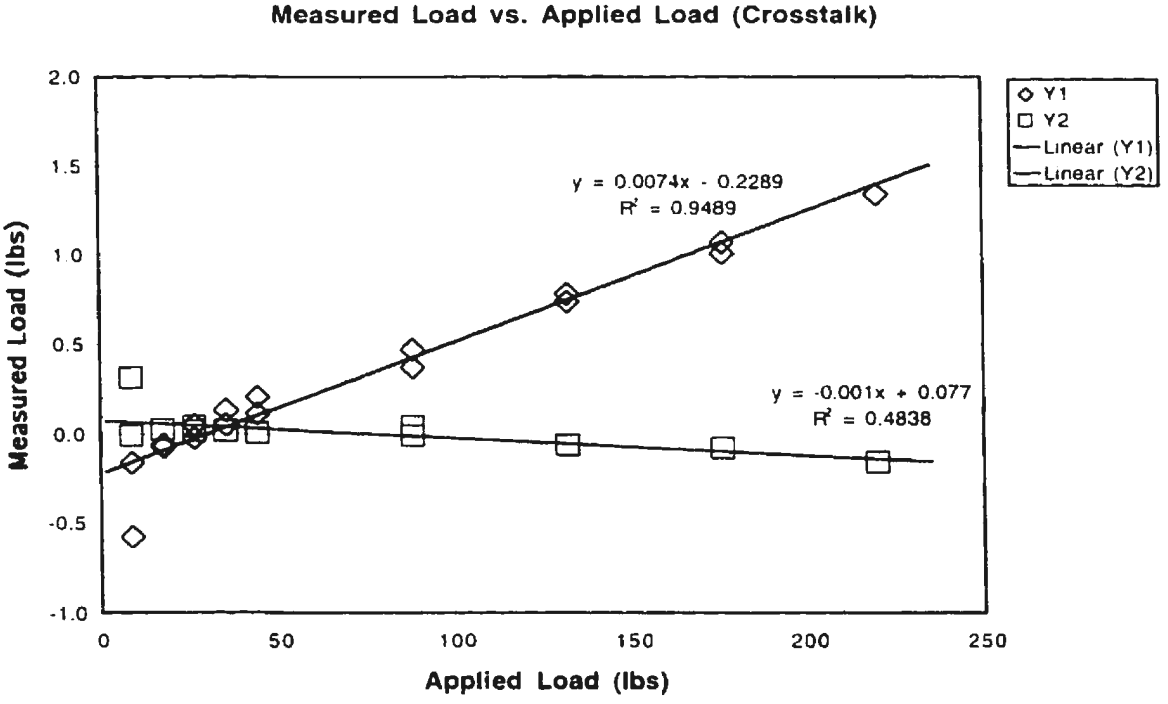

Figure 5.02 – *Y1 and Y2 Load Cells – Measured Load vs. Applied Load (Fx)*

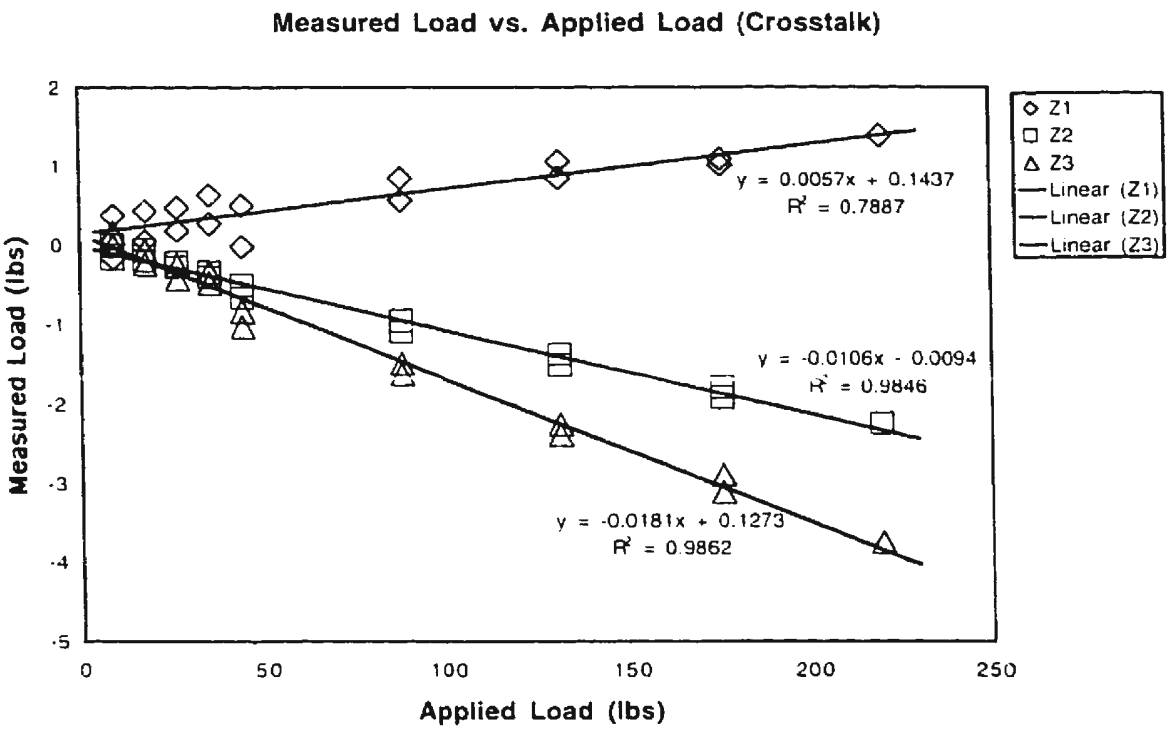

Figure 5.03 – *Z1, Z1 and Z3 Load Cells – Measured Load vs. Applied Load (Fx)*

The linear equation "y = mx + b" calculated for all six load cells was then used to find the associated losses/crosstalk for the x-axis loading case. The slope of the line, "m", was then the loss factor, L_f, in the case of X1; and the slope of the line was the crosstalk factor, C_f, for Y1, Y2, Z1, Z2 and Z3. It should be noted that the crosstalk factors must be used with the applied (true) load of the x-axis (Fx). Therefore, the following equations were written:

"Measured Load (x-axis)" = "L_f" x "Applied Load (x-axis)"; *Eq 5.01*

"Crosstalk Gain (off-axis)" = "C_f" x "Applied Load (x-axis)". *Eq 5.02*

In addition to this, the load gain calculated from the crosstalk factors must be deducted from the measured values of each of the off-axis load cells.

It should be noted that a maximum off-axis loading error of ±0.5° was estimated for the calibration of any axis. In other words, there will be an inherent loss in the loading axis load cell, and a residual gain in the off-axis (orthogonal) load cells. The loss for the loading axis load cell, in this case X1, was simply the cosine of the off-axis loading error. Therefore, for an error of ±0.5°, the off-axis loading loss factor for X1 was 0.99996. This factor is near unity, and therefore the factor was not used to correct the data set of X1. The crosstalk factor for the off-axis load cells was derived from the sine of the loading error. Therefore, for an error of ±0.5°, the off-axis loading gain factor for the off-axis loads cells was ±0.0087. While the absolute magnitude of this number may seem small, its relative magnitude is on order of the crosstalk factors calculated for the off-axis load cells. Table 5.03 is a summary of the losses/crosstalk factors for the x-axis loading case.

Load Cell	L_f	C_f	R^2	Off-axis Corrections		
				Error Magnitude	Min. Mag. C_f	Max. Mag. C_f
X1	**0.968**	N/A	1.000	N/A	N/A	N/A
Y1	N/A	**0.0074**	0.949	0.0087	**-0.0013**	**0.0161**
Y2	N/A	**-0.0010**	0.484	0.0087	**0.0077**	**-0.0097**
Z1	N/A	**0.0057**	0.789	0.0087	**-0.0030**	**0.0144**
Z2	N/A	**-0.0106**	0.985	0.0087	**-0.0019**	**-0.0193**
Z3	N/A	**-0.0181**	0.986	0.0087	**-0.0094**	**-0.0268**

Table 5.03 – *Losses and Crosstalk Factors for Fx*

Consider a sample test run in the tow tank, specifically sample file name: "XM_D1_Y06_V490". The mean loads from this test are reproduced here in Table 5.04. In addition to this, the loads were corrected using the loss factor, L_f, and the maximum magnitude of C_f from Table 5.03. At this point it was assumed that there were no losses or crosstalk in the dynamometer other than those calculated here for the x-axis alone.

Load Cell	Measured Load (N)	Correction Factors		Crosstalk Gain (N)	"True" Load (N)	% Change
		G_f	C_f			
X1	102.3	1.033	N/A	N/A	**105.7**	**+3.30**
Y1	-3031.3	N/A	0.0161	1.70	**-3033.0**	**+0.06**
Y2	800.0	N/A	-0.0097	-1.03	**801.0**	**+0.13**
Z1	-292.7	N/A	0.0144	1.52	**-294.2**	**+0.51**
Z2	4072.3	N/A	-0.0193	-2.04	**4074.3**	**+0.05**
Z3	-3411.5	N/A	-0.0268	-2.83	**-3408.7**	**+0.08**

Table 5.04 – *Sample of Corrected Data for "XM_D1_Y06_V490" (Fx)*

The off-axis loading error of ±0.0087 was written as the percent, ±0.87%, and then directly compared to the percent change of the off-axis load cells from Table 5.04. From this comparison, it was clear that the corrections made to all of the off-axis load cells were smaller than the maximum error due to the off-axis error calibrations. In some load cells, specifically Y1, Z2 and Z3, this difference was an order of magnitude smaller. For this reason, the crosstalk values were not included in any further analysis of the data; to do so would require an exhaustive calibration procedure which was beyond the scope of this project. Only the losses of the loading-axis load cells in the dynamometer were used to correct the test data.

Using the procedure presented above, the loss factor L_f, was determined for the remainder of the load cells. Due to the coupled nature of Z2 and Z3, it was assumed that the losses in these load cells were twinned/coupled; that is to say that their losses were the same. During the analysis of the z-axis, it was determined that there was no discernable difference between the losses of Z1 and the losses Z2/Z3. It was assumed that Y1 and Y2 would have dissimilar losses, with Y2 having a larger loss due its proximity to both Z2 and Z3 (Y1 was located near Z1 only; see Figure 4.02).

Load Cells	Loss Factor "L_f"	95% Confidence Interval	Samples (n)
X1	0.9681	±0.0023	17
Y1	0.9063	±0.0048	78
Y2	0.8652	±0.0040	78
Z1	0.9256	±0.0021	16
Z2	0.9256	±0.0021	16
Z3	0.9256	±0.0021	16

Table 5.05 – *Load Cell Loss Factors for all Six Load Cells*

The loss factors calculated for all six load cells are presented here in Table 5.05. At this point, the loss factors and geometry of the dynamometer were used to calculate the forces and moment equations for the six degrees of freedom. The sign convention for the load cells is such that when they are loaded in tension they will produce a positive load (output voltage); similarly, when they are in compression they will produce a negative load (output voltage). Rewriting Equation 5.01 for any load cell as

$$\text{"Applied Load } (F_A)\text{"} = \text{"}\frac{1}{L_f}\text{"} \times \text{"Measured Load } (F_M)\text{"}; \qquad \textit{Eq. 5.03}$$

and defining the gain factor, G_f, as

$$G_f = \frac{1}{L_f}; \qquad \textit{Eq. 5.04}$$

then the following equation was determined

$$F_A = G_f \cdot F_M. \qquad \textit{Eq. 5.05}$$

Therefore the axial force, AF, derived from the x-axis load cell was defined as

$$AF = -G_{F(X1)} \cdot F_{M(X1)}; \qquad \textit{Eq. 5.06}$$

which was then calculated as

$$AF = -1.0330 \cdot F_{M(X1)} \text{ [N]}; \qquad \textit{Eq. 5.07}$$

where negative values indicate vehicle drag force.

The side force, SF, derived from the y-axis was defined as

$$SF = -G_{F(Y1)} \cdot F_{M(Y1)} - G_{F(Y2)} \cdot F_{M(Y2)}; \qquad \textit{Eq. 5.08}$$

which was simplified to

$$SF = -1.1034 \cdot F_{M(Y1)} - 1.1558 \cdot F_{M(Y2)} \text{ [N]}; \qquad \textit{Eq. 5.09}$$

where positive values represent vehicle lift force to starboard.

The normal force, NF, derived from the z-axis was defined as

$$NF = -G_{F(Z1)} \cdot F_{M(Z1)} - G_{F(Z2)} \cdot F_{M(Z2)} - G_{F(Z3)} \cdot F_{M(Z3)}; \qquad \textit{Eq. 5.10}$$

which was reduced to

$$NF = -1.0804 \cdot \left(F_{M(Z1)} + F_{M(Z2)} + F_{M(Z3)}\right) \text{ [N]}; \qquad \textit{Eq. 5.11}$$

where positive values indicate vehicle heave force downward.

The yawing moment, pitching moment and rolling moment are referenced to the BRC, the balance resolution centre. The BRC for this model was chosen as a point on the centreline of the hull at the leading edge of the keel (Figure 5.04). The coordinates of each load cell relative to the BRC is presented in Table 5.06.

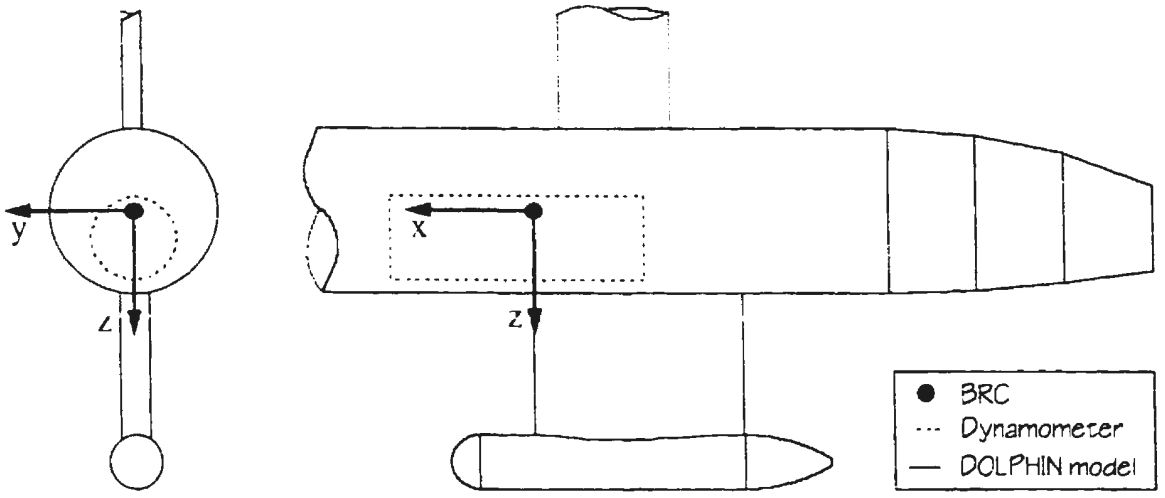

Figure 5.04 – *Front and Profile View of DOLPHIN Model with Location of BRC*

Load Cell	Coordinates of Load Cell axis relative to BRC (mm)		
	X_C	Y_C	Z_C
X1	N/A	0.00	61.52
Y1	336.30	N/A	61.52
Y2	-298.70	N/A	61.52
Z1	412.50	0.00	N/A
Z2	-214.88	76.20	N/A
Z3	-214.88	-76.20	N/A

Table 5.06 – *Load Cell Coordinates Relative to BRC*

The yawing moment, YM, is derived from load cells Y1 and Y2. Using the right hand rule with respect to the z-axis, a positive yawing moment indicates that the nose of the *DOLPHIN* moves to starboard. Therefore, YM was defined as

$$YM = -X_{C(Y1)} \cdot G_{(Y1)} \cdot F_{M(Y1)} - X_{C(Y2)} \cdot G_{(Y2)} \cdot F_{M(Y2)} - Y_{C(X1)} \cdot G_{(X1)} \cdot F_{M(X1)}; \quad Eq.\ 5.12$$

which was simplified to

$$YM = -0.3711 \cdot F_{M(Y1)} + 0.3452 \cdot F_{M(Y2)}\ [\mathrm{N \cdot m}]. \quad Eq.\ 5.13$$

The pitching moment, PM, is defined as positive when the vehicle's nose moves upward. The pitching moment was derived from load cells X1, Z1, Z2 and Z3 as

$$PM = -Z_{C(X1)} \cdot G_{r(X1)} \cdot F_{M(X1)} + X_{C(Z1)} \cdot G_{r(Z1)} \cdot F_{M(Z1)} \\ X_{C(Z2)} \cdot G_{r(Z2)} \cdot F_{M(Z2)} + X_{C(Z3)} \cdot G_{r(Z3)} \cdot F_{M(Z3)}; \qquad \textit{Eq. 5.14}$$

which was simplified to

$$PM = -0.0635 \cdot F_{M(X1)} + 0.4457 \cdot F_{M(Z1)} - 0.2322 \cdot \left(F_{M(Z2)} + F_{M(Z3)}\right) \ [\mathrm{N \cdot m}]. \qquad \textit{Eq. 5.15}$$

The rolling moment, RM, is derived from load cells Y1, Y2, Z2 and Z3. For the *DOLPHIN*, a positive rolling moment would be with the keel moving to port. Therefore, RM was defined as

$$RM = Z_{C(Y1)} \cdot G_{r(Y1)} \cdot F_{M(Y1)} + Z_{C(Y2)} \cdot G_{r(Y2)} \cdot F_{M(Y2)} \\ - Y_{C(Z2)} \cdot G_{r(Z2)} \cdot F_{M(Z2)} - Y_{C(Z3)} \cdot G_{r(Z3)} \cdot F_{M(Z3)}; \qquad \textit{Eq. 5.16}$$

which was simplified to

$$RM = 0.0679 \cdot F_{M(Y1)} + 0.0711 \cdot F_{M(Y2)} \\ -0.0823 \cdot \left(F_{M(Z2)} - F_{M(Z3)}\right) \ [\mathrm{N \cdot m}] \qquad \textit{Eq. 5.17}$$

Table 5.07 below is a summary of the coefficients obtained in Equations 5.07, 5.09, 5.11, 5.13, 5.15 and 5.17. This table was used to convert the measured data into the six forces and moments experienced by the model for each test run.

Forces & Moments	Load Cell					
	X1	**Y1**	**Y2**	**Z1**	**Z2**	**Z3**
AF	-1.0330	N/A	N/A	N/A	N/A	N/A
SF	N/A	-1.1034	-1.1558	N/A	N/A	N/A
NF	N/A	N/A	N/A	-1.0804	-1.0804	-1.0804
YM	N/A	-0.3711	0.3452	N/A	N/A	N/A
PM	-0.0635	N/A	N/A	0.4457	-0.2322	-0.2322
RM	N/A	0.0679	0.0711	N/A	-0.0823	0.0823

Table 5.07 – *Dynamometer Correction Table for All Six Degrees of Freedom*

As an example, the data measured in test run "XM_D1_Y06_V490" were corrected using the factors in Table 5.07; the results are presented here in Table 5.08.

Forces & Moments	Contributing Force(N) or Moment(N·m) from Load Cell						Corrected Forces & Moments
	X1	Y1	Y2	Z1	Z2	Z3	
AF	-105.7	0.0	0.0	0.0	0.0	0.0	-105.7 (N)
SF	0.0	3344.7	-924.6	0.0	0.0	0.0	2420.1 (N)
NF	0.0	0.0	0.0	316.2	-4399.7	3685.8	-397.7 (N)
YM	0.0	1124.9	276.2	0.0	0.0	0.0	1401.1 (N·m)
PM	-6.5	0.0	0.0	-130.5	-945.6	792.2	-290.4 (N·m)
RM	0.0	-205.8	56.9	0.0	-335.2	-280.8	-764.9 (N·m)

Table 5.08 – *Corrected Forces and Moments for Test Run "XM_D1_Y06_V490"*

5.2 *Yaw Angle Corrections*

During the test plan it was noticed that the model was deviating from its "preset" yaw angle, θ_p, by a considerable amount. That is to say that once the model was up to speed, its final yaw angle, θ_R, was larger that the preset angle. It was determined that this was the result of the flexing of the supports of the prototype MDTF system. The amount of flexure in the system was considerable, as at times it was visually estimated that θ_R was 50% greater than θ_p. Therefore, a means of correcting the data was necessary in order to be able to analyze the hydrodynamic loads. In addition to this, it should be noted that there was considerable vibration of the MDTF system during testing.

The lift force that is exerted on a body can be written as [White 1986]

$$Lift = \frac{1}{2} \cdot c_L \cdot \rho \cdot S \cdot V^2; \qquad Eq.\ 5.18$$

if c_L is a function of θ_R, then for low angles of attack ($\theta_R \leq 6^\circ$)

$$c_L = \frac{\delta c_L}{\delta \theta_R} \cdot \theta_R. \qquad Eq.\ 5.19$$

Combining Equations 5.18 and 5.19 yields

$$Lift = \frac{1}{2} \cdot \frac{\delta c_L}{\delta \theta_R} \cdot \rho \cdot S \cdot \theta_R \cdot V^2. \qquad Eq.\ 5.20$$

Next, define the constant 'C_0' as

$$C_0 = \frac{1}{2} \cdot \frac{\delta c_L}{\delta \theta_R} \cdot \rho \cdot S; \qquad Eq.\ 5.21$$

then rewriting Equation 4.20 as

$$Lift = C_0 \cdot \theta_R \cdot V^2. \qquad Eq.\ 5.22$$

The vehicle lift was calculated from the data as

$$Lift = SF \cdot \cos(\theta_R) + AF \cdot \sin(\theta_R). \qquad Eq.\ 5.23$$

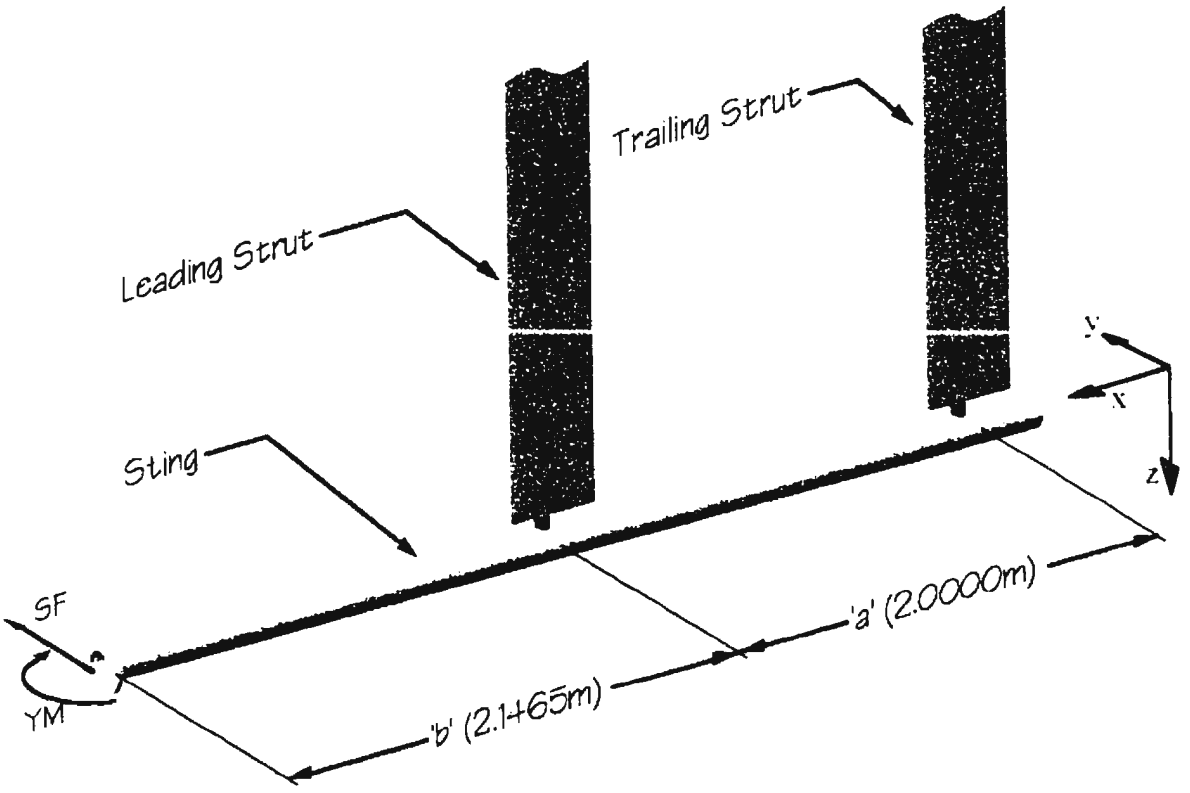

Figure 5.05 – *Prototype MDTF and Sting Configuration*

The method used to find the "true" angle of attack, θ_R, was derived from the mechanics of materials, specifically, the bending of beams. Figure 5.05 depicts the schematic (geometry) of the prototype MDTF showing the sting and the vertical support struts. The deflection, and resultant angle, of the PMDTF system was divided into two sub-systems: the bending of the sting, θ_B, and the flexure of the support struts, θ_F. A means of relating θ_R, θ_B and θ_F with/to the collected data was required.

Using linear superposition, θ_R was defined as

$$\theta_R = \theta_0 + \theta_P + \theta_B + \theta_F; \qquad Eq.\ 5.24$$

where θ_0 is the offset angle from the "true" angle of zero incidence due to initial alignment errors and vehicle asymmetry, and θ_P is the "preset" yaw angle. The expected maximum value for θ_0 was about $\pm 0.25^\circ$.

5.2.1 *Bending of Sting*

In the horizontal plane (xy-plane), the sting behaves like a pinned overhanging beam. It is acted upon by the side force, SF, and the yaw moment, YM, experienced by the dynamometer (Figure 5.05). Using linear superposition, θ_B was further defined as

$$\theta_B = \theta_{B(SF)} + \theta_{B(YM)} \qquad Eq.\ 5.25$$

Using the elastic curve theory for the deflection of beams [Hibbeler 1991], the resultant angle at the end of the beam for an applied point load at the end of the beam was determined as

$$\theta_P = \frac{(2 \cdot a + 3 \cdot b) \cdot b}{6 \cdot E_B \cdot I_B} \cdot P; \qquad Eq.\ 5.26$$

where, the lengths 'a' and 'b' are indicated in Figure 5.05, and E_B and I_B are respectively Young's modulus and the moment of inertia of the sting. The resultant angle at the end of the beam for an applied moment at the end of the beam was determined as

$$\theta_M = \frac{(2 \cdot a + 6 \cdot b)}{6 \cdot E_B \cdot I_B} \cdot M. \qquad Eq.\ 5.27$$

Therefore, using Equations 5.26 and 5.27, Equation 5.25 was rewritten as

$$\theta_B = \frac{(2 \cdot a + 3 \cdot b) \cdot b}{6 \cdot E_B \cdot I_B} \cdot SF + \frac{(2 \cdot a + 6 \cdot b)}{6 \cdot E_B \cdot I_B} \cdot YM. \qquad Eq.\ 5.28$$

It should be noted that a, b, E_B and I_B were constant throughout the test plan. Substituting the known values into Equation 5.28 yielded

$$\theta_B = \frac{1}{6 \cdot E_B \cdot I_B} \cdot [22.4084 \cdot SF + 16.8790 \cdot YM]; \qquad Eq.\ 5.29$$

and, defining the property factor of the sting, P_B, as

$$P_B = \frac{16.8790}{6 \cdot E_B \cdot I_B}; \qquad Eq.\ 5.30$$

then, Equation 5.29 was simplified to

$$\theta_B = P_B \cdot [1.3276 \cdot SF + YM]. \qquad Eq.\ 5.31$$

5.2.2 *Flexing of Support Struts*

The vertical support struts behave like cantilever beams, and their deflection out of the vertical plane (yz-plane) resulted in an offset angle of the sting which was defined as

$$\theta_F = \sin^{-1}\left(\frac{\Delta y_1 + \Delta y_2}{a}\right); \qquad Eq.\ 5.32$$

where

Δy_1 = *Maximum deflection of leading strut*,

and

Δy_2 = *Maximum deflection of trailing strut*.

Using simple beam theory [Hibbeler 1991], the deflection of each strut was defined as

$$\Delta y_1 = \frac{R_1 \cdot L_F^3}{3 \cdot E_F \cdot I_F}; \qquad Eq.\ 5.33$$

and

$$\Delta y_2 = \frac{R_2 \cdot L_F^3}{3 \cdot E_F \cdot I_F}, \qquad Eq.\ 5.34$$

where L_F were the extended length of the support struts, E_F and I_F were respectively Young's modulus and the moment of inertia of each support strut, and R_1 and R_2 were the reactions by the struts as a result of the side force, SF, and the yaw moment, YM. These reactions were determined as

$$R_1 = \frac{(a + b)\cdot SF + YM}{a}; \qquad Eq.\ 5.35$$

and

$$R_2 = \frac{b\cdot SF + YM}{a}. \qquad Eq.\ 5.36$$

Due to the nature of the test facility, the moment of inertia of the support struts (normal to the sting) was a function of the preset angle, θ_p. Therefore, I_F was defined as

$$I_F = I_{x(F)}\left(1 + \left(\frac{I_{z(F)}}{I_{x(F)}} - 1\right)\cdot \sin^2(\theta_p)\right); \qquad Eq.\ 5.37$$

where the inertial ratio was calculated as

$$\frac{I_{z(F)}}{I_{x(F)}} = 2.04. \qquad Eq.\ 5.37$$

Combining and simplifying Equations 5.32 through 5.37 yielded

$$\theta_F = \sin^{-1}\left(\frac{L_F^3}{3\cdot E_F\cdot I_{x(F)}}\cdot\frac{(a + 2\cdot b)\cdot SF + 2\cdot YM}{a^2\cdot\left(1 + \left(\frac{I_{z,F}}{I_{x,F}} - 1\right)\cdot\sin^2(\theta_p)\right)}\right); \qquad Eq.\ 5.39$$

then substituting the known values into Equation 5.39 and simplifying yielded

$$\theta_F = \sin^{-1}\left(\frac{L_F^3}{3\cdot E_F\cdot I_{x(F)}}\cdot\frac{1}{2}\cdot\frac{3.1465\cdot SF + YM}{\left(1 + 1.04\cdot\sin^2(\theta_p)\right)}\right); \qquad Eq.\ 5.40$$

Defining the property factor of the struts, P_F, as

$$P_F = \frac{L_F^3}{6 \cdot E_F \cdot I_{x(F)}}; \qquad \textit{Eq. 5.41}$$

then Equation 5.40 was simplified to

$$\theta_F = \sin^{-1}\left(P_F \cdot \frac{3.1465 \cdot SF + YM}{\left(1 + 1.04 \cdot \sin^2(\theta_p)\right)} \right). \qquad \textit{Eq. 5.42}$$

5.2.3 *Correction Equations*

Using Equations 5.31 and 5.42, Equation 5.24 was expanded to

$$\theta_R = \theta_0 + \theta_p + P_B \cdot [1.3276 \cdot SF + YM] + \sin^{-1}\left(P_F \cdot \frac{3.1465 \cdot SF + YM}{\left(1 + 1.04 \cdot \sin^2(\theta_p)\right)} \right).$$

Eq. 5.43

Then, using Equation 5.43, Equations 5.22 and 5.23 were respectively expanded to

$$Lift = C_0 \cdot \left(\theta_0 + \theta_p + P_B \cdot [1.3276 \cdot SF + YM] + \sin^{-1}\left(P_F \cdot \frac{3.1465 \cdot SF + YM}{\left(1 + 1.04 \cdot \sin^2(\theta_p)\right)} \right) \right) \cdot V^2$$

Eq. 5.44

and

$$Lift = SF \cdot \cos\left(\theta_0 + \theta_p + P_B \cdot [1.3276 \cdot SF + YM] + \sin^{-1}\left(P_F \cdot \frac{3.1465 \cdot SF + YM}{\left(1 + 1.04 \cdot \sin^2(\theta_p)\right)} \right) \right)$$
$$+ AF \cdot \sin\left(\theta_0 + \theta_p + P_B \cdot [1.3276 \cdot SF + YM] + \sin^{-1}\left(P_F \cdot \frac{3.1465 \cdot SF + YM}{\left(1 + 1.04 \cdot \sin^2(\theta_p)\right)} \right) \right)$$

Eq. 5.45

5.2.4 *Correction Procedure and Discussion*

Equations 5.44 and 5.45 were then used in a non-linear regression analysis to find the constants: C_0, θ_O, P_B and P_F. Hand calculations and visual observations suggested that θ_F was larger than θ_B, but of the same order of magnitude. Therefore, P_F and P_B would have the same order of magnitude. In addition to this, C_0, P_B and P_F were constrained to have positive values. As an example, using the data collected for the tests with no mast (file names of the type "XM_D1_Yxx_Vxxx") for cases where θ_P was less than 6°, the following values were calculated

$$C_0 = 13.700 \quad (based\ on\ degrees)$$

$$\theta_O = 0.08852°$$

$$P_B = 0.8637E-6$$

$$P_F = 1.1060E-6$$

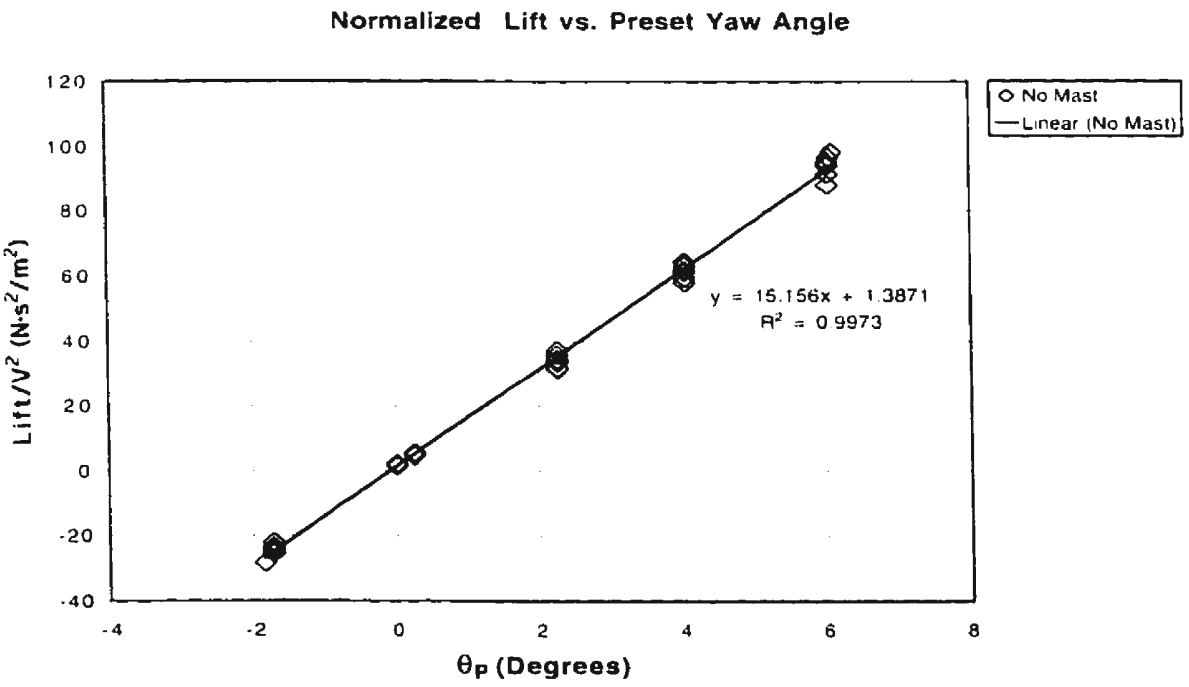

Figure 5.06 – *Normalized Lift vs. Preset Yaw Angle for No Mast Configuration*

Using these results, the "true" angles of attack, θ_R, were calculated using Equation 5.43. Figure 5.06 is a plot of the normalized vehicle lift (Lift / V^2) versus the preset yaw angle, θ_p. Note the increasing vertical spread of the data as θ_p increases. Compare this to Figure 5.07 of the normalized vehicle lift versus the "true" yaw angle, θ_R.

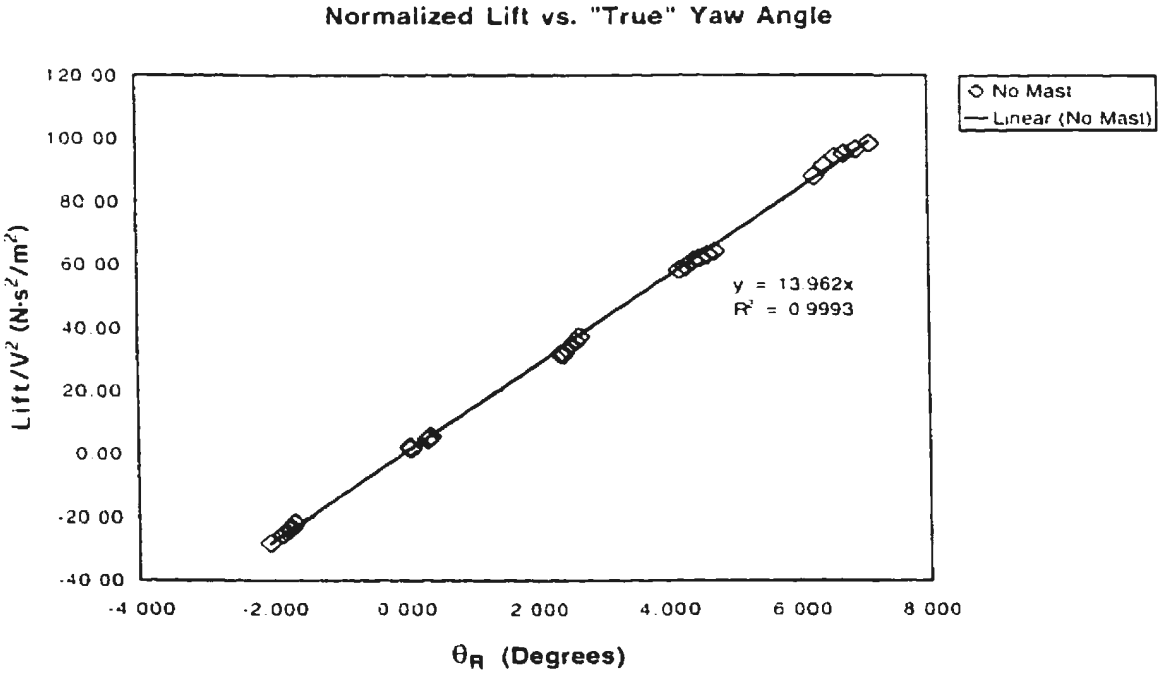

Figure 5.07 – *Normalized Lift vs. "True" Yaw Angle for No Mast Configuration*

The data in Figure 5.07 fit together more appropriately than the data in Figure 5.06. Therefore the calculated values of θ_R provide acceptable estimates for the true yaw angle.

The above procedure was performed for each mast configuration: No Mast (XM), Old Mast (OM), and New Mast (NM). Only values of θ_R less than or equal to 6° were used in the analysis. Therefore, if a value of θ_R was calculated to be larger than 6°, it was

removed from the correction data, and the analysis was performed again. It should be noted that only the constants θ_0, P_B and P_F were required to determine θ_R. In addition to this, P_B remained constant throughout the test plan, while P_F varied slightly because of the change in the amount of exposed strut (due to the raising and lowering of the model during reconfiguration). Also, θ_0 was unique for each of the mast configurations. Table 5.09 summarizes the constants determined for each mast configuration.

Configuration	θ_0 (degrees)	P_B (10^{-6})	P_F (10^{-6})
No Mast (XM)	0.0885	0.8637	1.1060
Old Mast (OM)	0.2368	0.8637	2.4926
New Mast (NM)	0.2401	0.8637	0.9609

Table 5.09 – *Yaw Angle Correction Constants*

6.0 Drag Force Analysis and Observations

The drag force for the *DOLPHIN* model is analyzed in this chapter. Both qualitative and quantitative observations are presented and discussed for the no mast (M0), existing mast (M1) and proposed mast (M2, M2A and M2B) configurations.

6.1 Drag of Existing Mast

The drag on the existing (old) mast configuration, M1, can be broken down into six components: profile drag; ventilation drag; wave drag; spray drag; induced drag; and, the drag from the cable forestay. DREA (Defense Research Establishment Atlantic) and ISER (International Submarine Engineering Research) estimate that the profile drag coefficient (based upon frontal area) is 0.06 [Watt 1997]. Ventilation drag occurs when a pocket of air (vent) opens up aft of the mast extending down into the water from the free surface. Ventilation of the mast configuration M1 was not observed during testing.

Wave drag is a function of Froude number, Fr, defined as

$$Fr = \frac{V}{\sqrt{g \cdot l}} \qquad \textit{Eq. 6.01}$$

where V is the vehicle speed, g is the acceleration due to gravity, and l is a representative length. However, wave drag of surface piercing foils reaches a maximum when the Froude number based on the chord length is about 0.5; additionally, wave drag is negligible at Froude numbers greater than about three [Chapman 1971]. Within this Froude number range, the wave drag on the surface piercing mast undergoes a transformation into spray drag.

For this mast, the steady-state Froude number based on chord length ranged from 1.1 to 2.7 for vehicle velocities of 2.00m/s to 4.90m/s respectively. Figures 6.01 and 6.02 depict the transformation of the wave drag on M1 as the vehicle's velocity ranges from zero to 4.47m/s (Fr=2.5). In Figure 6.01, frame 'A' is the still water condition. In frame 'B' a depression can be seen approximately halfway along the chord.

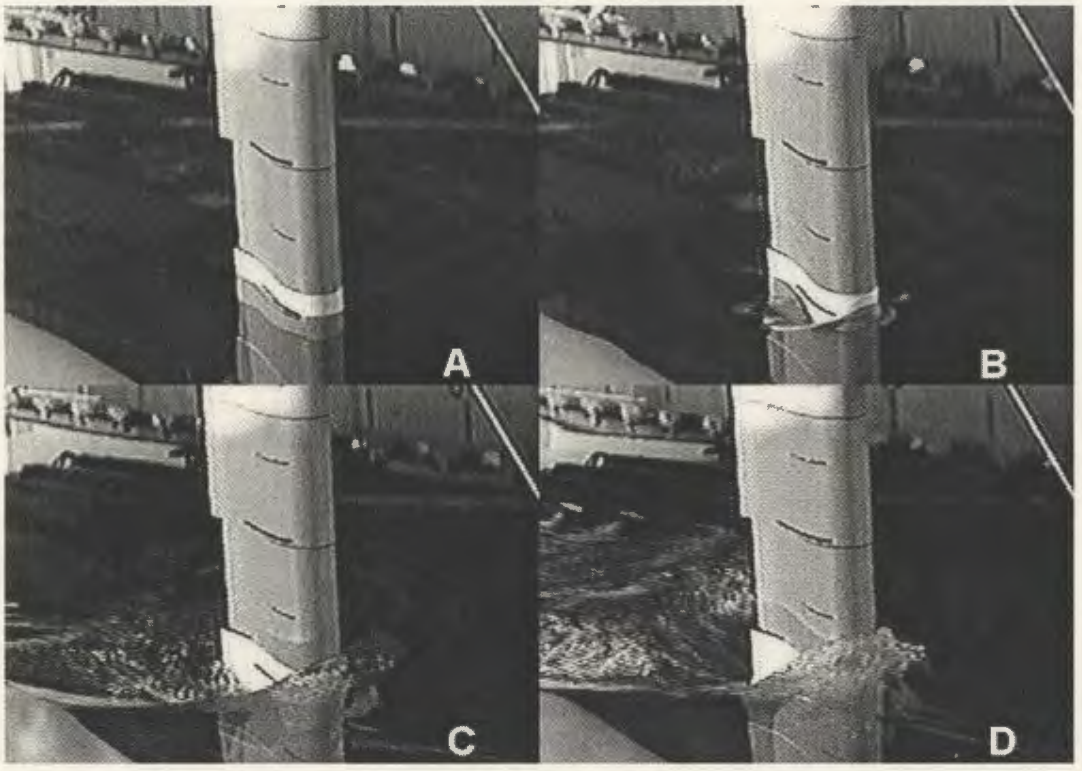

Figure 6.01 - *Existing Mast (M1), @ Draft D1, Yaw = 0°, Frames A, B, C & D*

At higher vehicle velocities, this depression moves rearward, while at the same time a bow (pressure) wave increases in height forward of the leading edge of the fairing (frames 'C' & 'D'). As the Froude number increases the depression vanishes while the pressure wave moves rearward and climbs up and behind the leading edge of the fairings (frames 'E' & 'F' in Figure 6.02). Finally, the pressure wave disappears altogether, and a fully developed spray sheet is formed (frames 'G' & 'H').

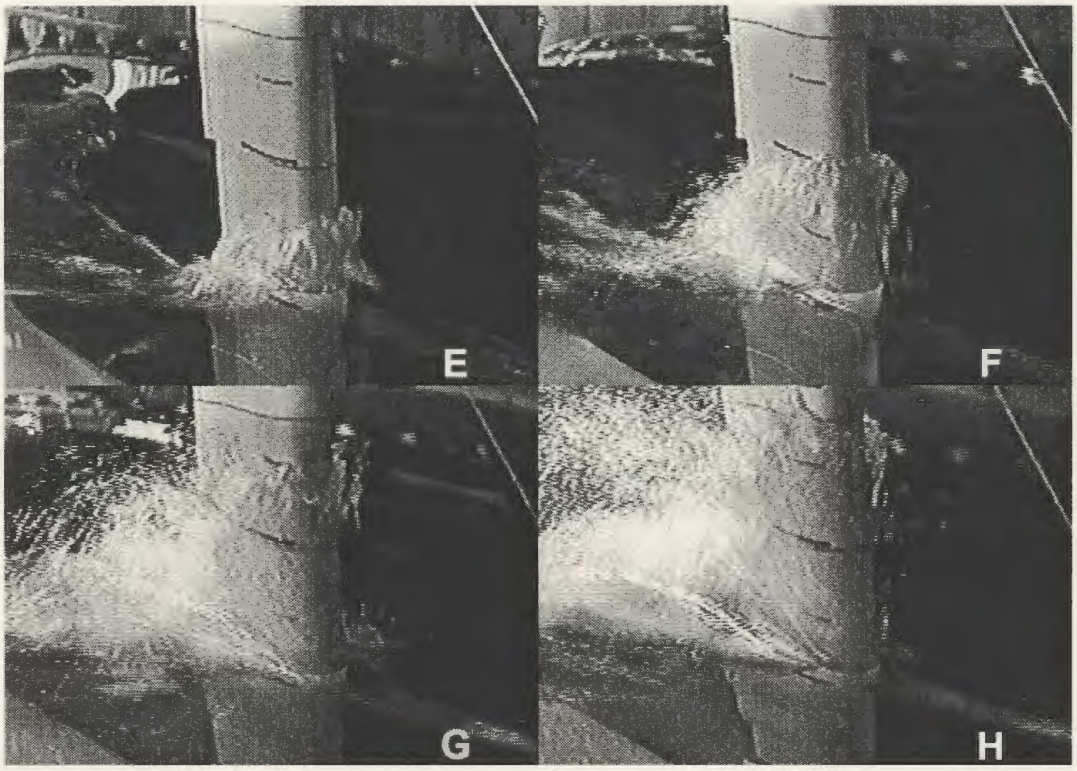

Figure 6.02 - *Existing Mast (M1), @ Draft D1, Yaw = 0°, Frames E, F, G & H*

The spray drag generated on a surface piercing body is independent of Froude number for Froude numbers greater than about three [Chapman 1971]. The spray sheet generated by mast configuration M1 can be seen in Figure 6.03. The spray sheet was extensive at high velocities and it had an estimated height equal to two chord lengths. The spray sheet separated from the mast fairings just aft of the maximum thickness location.

Induced drag for the existing mast configuration occurred when the fairings splayed (yawed) a few degrees relative to each other. The splaying of the mast fairings, both below and above the water surface, can be seen in Figure 6.03. Those fairings below the surface increase the effective profile drag, while those above the surface increase the effective spray drag. ISER confirmed (via verbal communiqué) that when the fairings of

the full-scale DOLPHIN were connected as a single unit, the top speed of the vehicle increased by one knot (increase of roughly 5% to 10%).

Figure 6.03 - *Existing Mast (M1), @ Draft D1, Yaw = 0°, V = 4.47m/s*

In the lower right-hand portion of Figure 6.03 a small amount of spray can been seen coming from the cable forestay. This spray drag, combined with the section and ventilation drag of the submerged cable, constitute the cable forestay drag component of the existing mast.

The size and shape of the spray sheet and the amount of fairing splay did not seem to vary as the yaw angle of the vehicle was varied. This was expected, as the fairings were selected such that they would align with the oncoming flow. However, it was noticed

that for vehicle yaw angles between about ±1°, the ventilation generated by the cable forestay would intersect downstream with the leading edge of the submerged mast fairings. For larger vehicle yaw angles the forestay ventilation "passed on by" the fairings.

The overall vehicle drag at draft D1 for the M1 configuration is presented in Figure 6.04. The symmetric second order polynomial, $Drag = A \cdot \theta^2 + C$ (where A and C are positive constants and θ is yaw angle in degrees) was used to fit the data based on constant velocity. All values of R^2 were at least 0.993. The y-intercept of each plot, C, was used to find the vehicle drag at zero yaw angle for each velocity. These values were then plotted versus the square of vehicle velocity as shown in Figure 6.05.

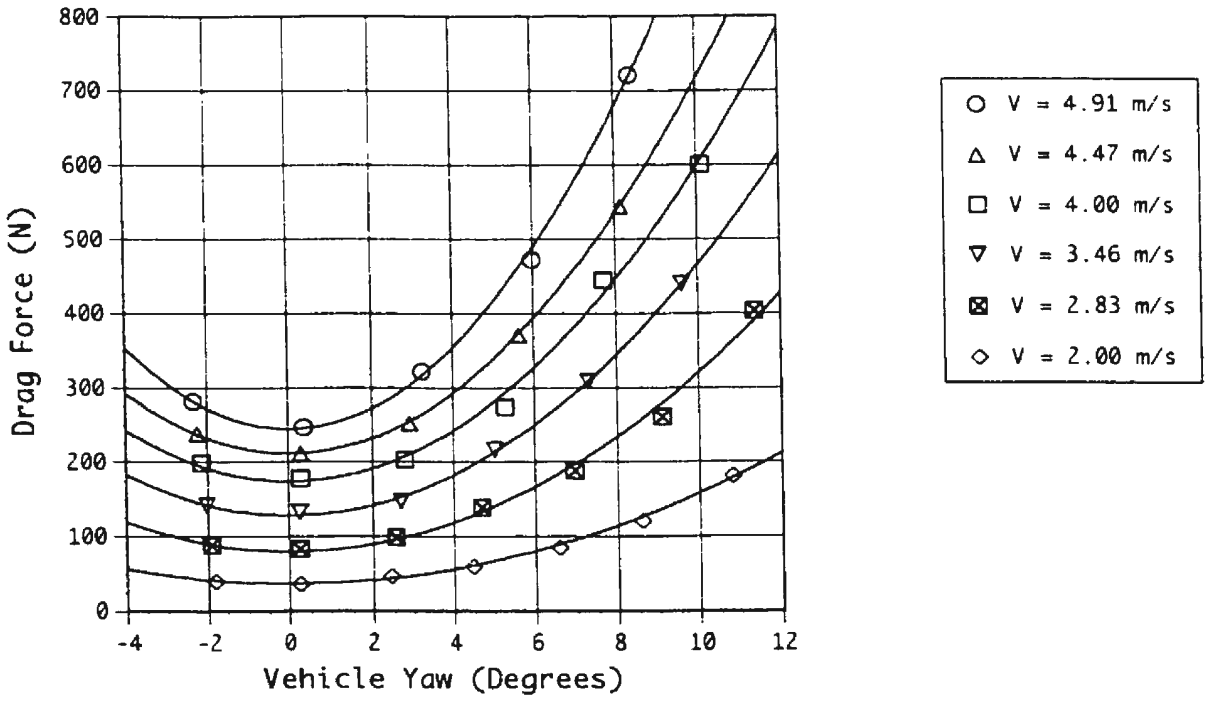

Figure 6.04 - *Drag Force vs. Vehicle Yaw Angle; M1 @ D1*

The vehicle drag at zero yaw angle without any mast, M0, was determined in the same manner as presented above; the results are shown in Figure 6.05. The graph shows that vehicle drag is proportional to the square of the velocity. A linear fit of the data through the origin was performed ($R^2 > 0.995$). The resulting slopes were 10.44 and 6.05 for configurations M1 and M0 respectively. From this, it was determined that for a vehicle draft of D1, the contributed drag from the existing mast represents 42% of the overall vehicle drag.

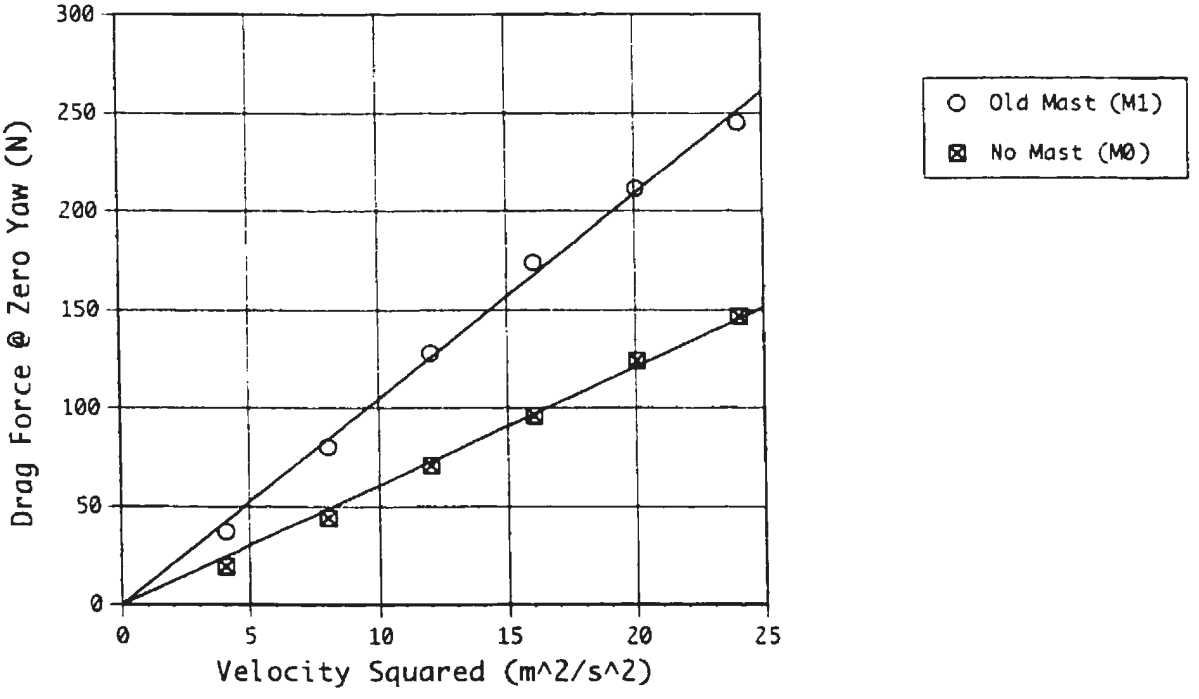

Figure 6.05 - *Drag Force (θ=0°) vs. V^2; Configurations M1 and M0 @ Draft D1*

6.2 *Drag of Proposed Mast*

The drag from the proposed (new) mast configuration, M2, can be broken down into four components: profile drag; ventilation drag; wave drag; and, spray drag. Using work done by Chapman [Chapman 1971], a profile drag coefficient based upon the frontal area of a 16% thick double symmetric-arc was estimated to be 0.024.

For the fixed mast, Froude numbers based on chord length ranged from 1.2 to 2.9 for vehicle velocities of 2.00m/s to 4.90m/s respectively. Figures 6.06 and 6.07 portray the transformation of the wave drag for vehicle velocities ranging from zero to 4.47m/s (Fr=2.6). Frames 'A' through 'H' in Figures 6.06 and 6.07 represent the same velocities as in frames 'A' through 'H' in Figures 6.01 and 6.02 of the existing mast.

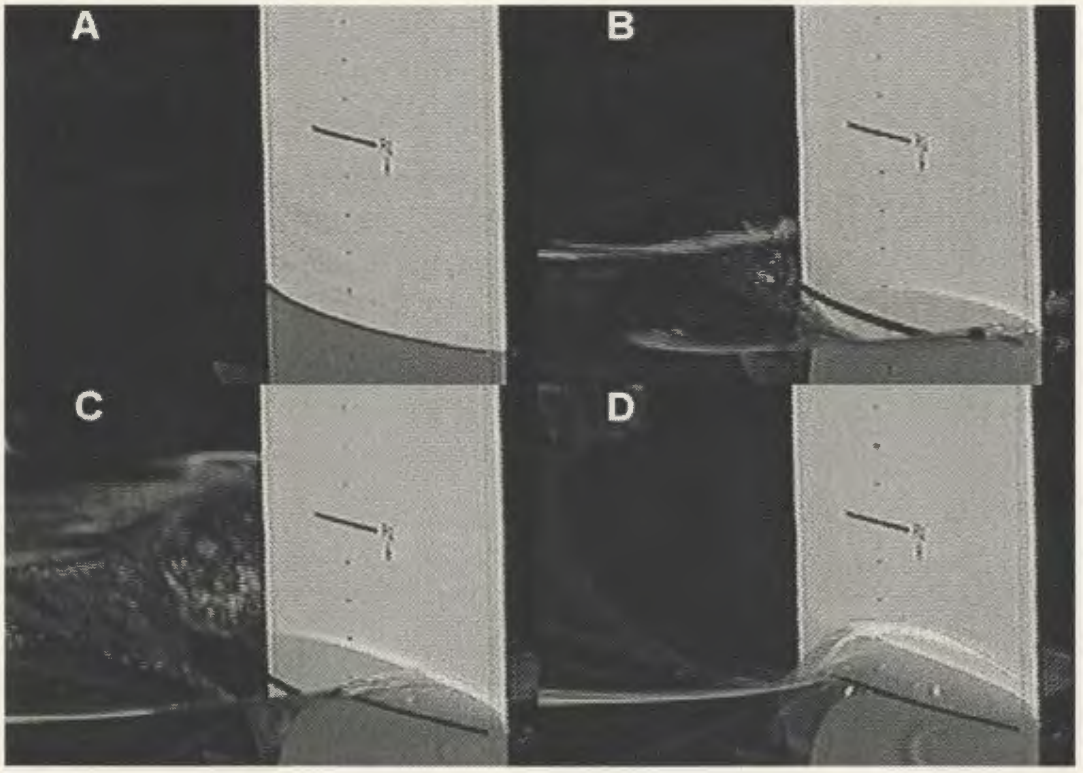

Figure 6.06 - *Proposed Mast (M2), @ Draft D1, Yaw = 0°, Frames A, B, C & D*

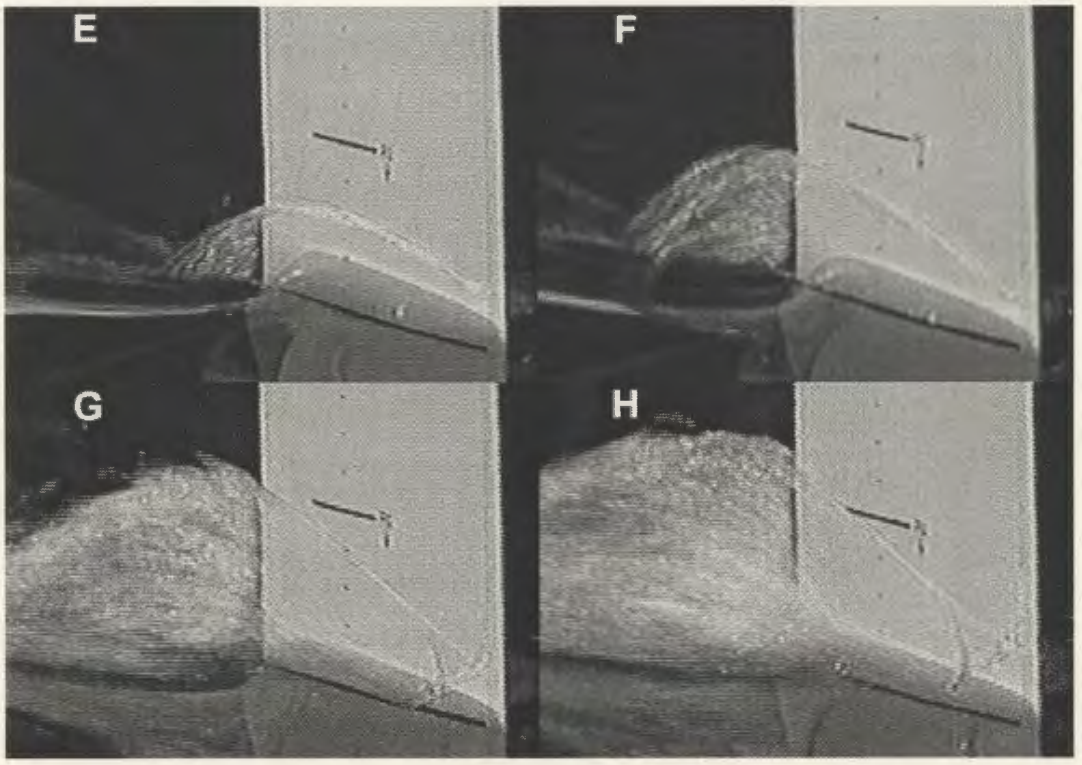

Figure 6.07 - *Proposed Mast (M2), @ Draft D1, Yaw = 0°, Frames E, F, G &H*

Frame 'A' in Figure 6.06 is the still water condition. In frame 'B' a small depression in the water surface is present about two-thirds along the chord. This depression is much smaller than and farther back than the depression on M1 at the same forward speed. In frames 'C' and 'D', the depression moves rearward with diminishing magnitude. In addition to this, a small pressure wave can been seen rising up the sides of the mast.

In frames 'E' and 'F', of Figure 6.07, the pressure wave reaches a maximum, while a spray sheet can be seen rising up and aft of the mast. Frames 'G' and 'H' depict a fully developed spray sheet, with no visible signs of any wave phenomena.

The fully developed spray sheet of M2 at zero vehicle yaw angle, draft D1 and 4.47m/s is shown in Figure 6.08 (the spray on the left side of the figure is from a towing strut). This spray sheet was much smaller than that of M1. The estimated height of the spray sheet was equal to two thirds of the chord length. Unlike M1, the spray sheet did not separate from the mast, rather it "clung" onto either side of the mast, rejoining at the trailing edge.

The size and shape of the spray sheet varied as the vehicle yaw angle varied. In Figure 6.09 the vehicle is yawed 2° to starboard, but its draft and speed are the same as in Figure 6.08. As the yaw angle was increased, the size of the spray sheet correspondingly increased. It was noticed, however, that this increase in spray sheet size occurred only on the high-pressure (port) side of the mast. The spray sheet size and shape remained relatively unchanged on the low-pressure (starboard) side of the mast.

Figure 6.08 - *Proposed Mast (M2), @ Draft D1, Yaw = 0°, V = 4.47m/s*

Figure 6.09 - *Proposed Mast (M2), @ Draft D1, Yaw = 2°, V = 4.47m/s*

Air ejection into the proposed mast configuration, M2B (20CFM [9.4 *l*/s]) and M2A (30CFM [14.2 *l*/s]), did not appreciably change the size or shape of the developed spray sheet. This was expected due to the ejection holes being located just 4.5% of chord aft of the leading edge of the mast. At this forward location, the spray sheet height is minimal and hence interacts with very few if any ejection holes.

Natural ventilation of M2 was not observed for vehicle yaw angle up to and including 4°. Beyond 4°, a small ventilation pocket was observed on the suction side of the mast at the trailing edge. At higher vehicle yaw angle and increased velocities, the ventilation pocket increased its surface opening as well as its penetrating depth.

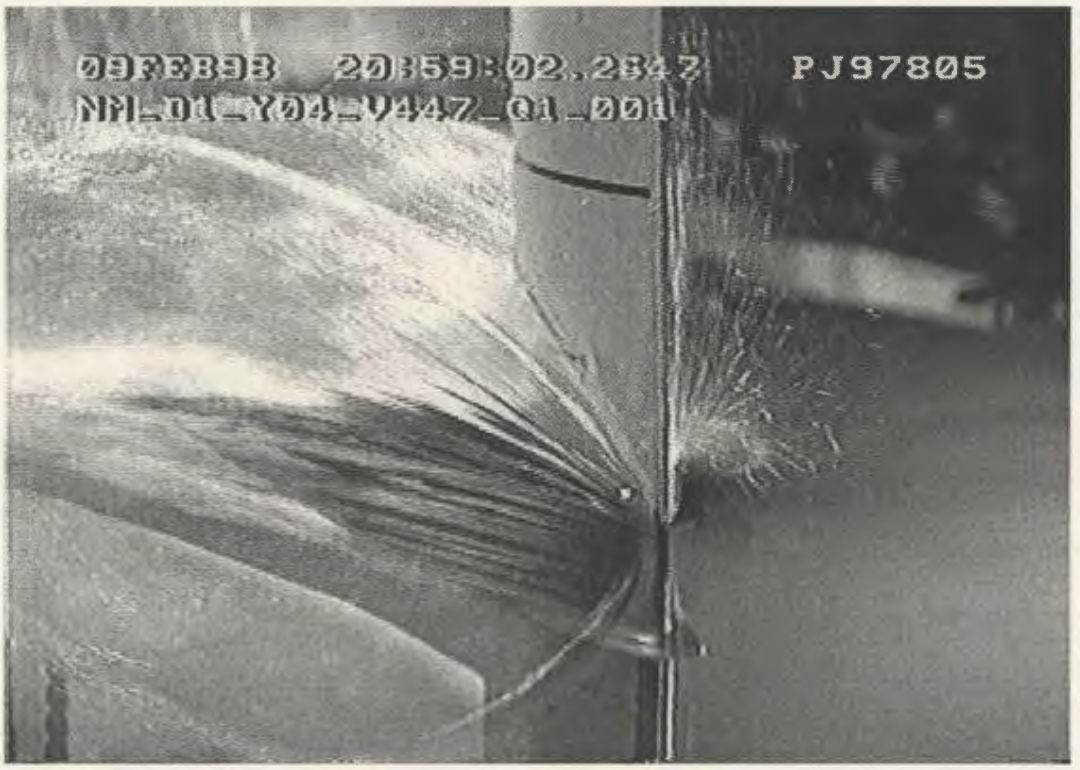

Figure 6.10 - *Proposed Mast w/ 20CFM Air(M2B), @ D1, Yaw = 2°, V = 4.47m/s*

With the air ejection, the formation of the ventilation pocket was initiated at lower vehicle yaw angles. In addition to this, the ventilation pocket was much broader and deeper for M2A/B than for M2 at the same yaw angle and velocity. Under no circumstances was the ventilation pocket observed crossing the ventilation fence. In Figure 6.10 the vehicle is yawed 4° to starboard with 20CFM [9.4 *l*/s] of air ejection (M2B). A ventilation pocket started from the ejection holes and continued beyond the trailing edge of the mast, and extended to the depth of the ventilation plate.

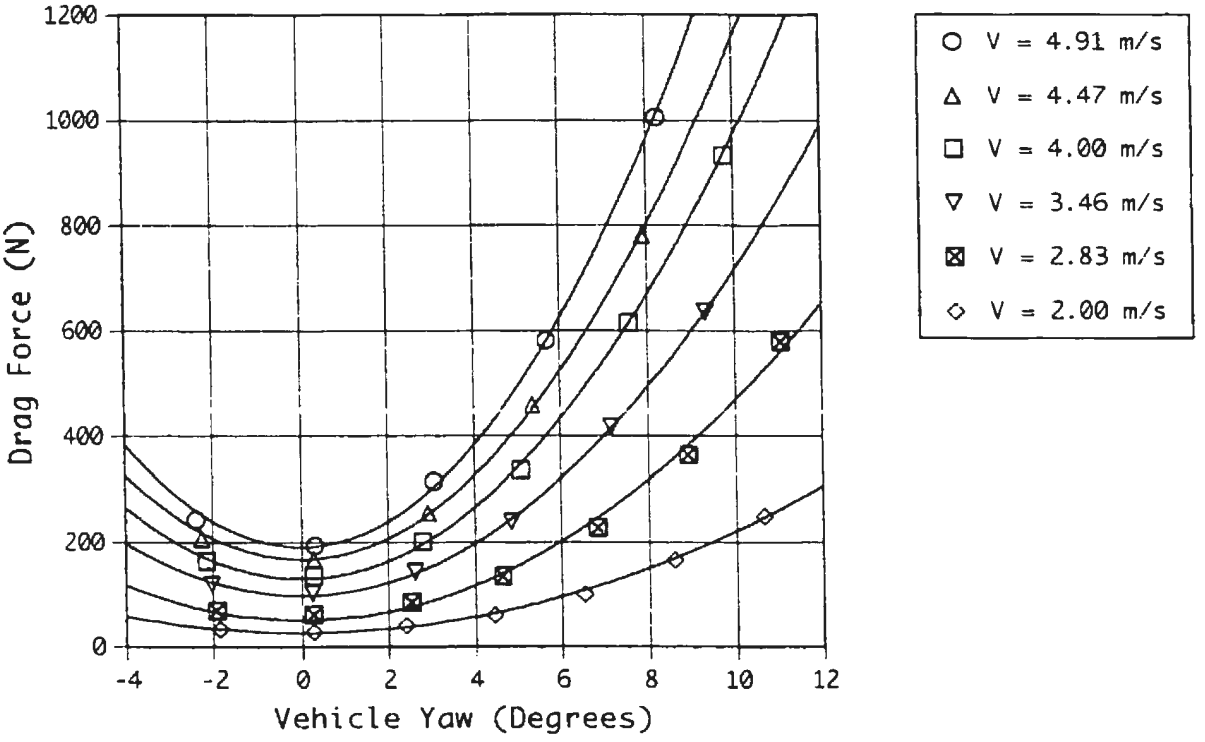

Figure 6.11 - *Drag Force vs. Vehicle Yaw Angle; Configuration M2 @ Draft D1*

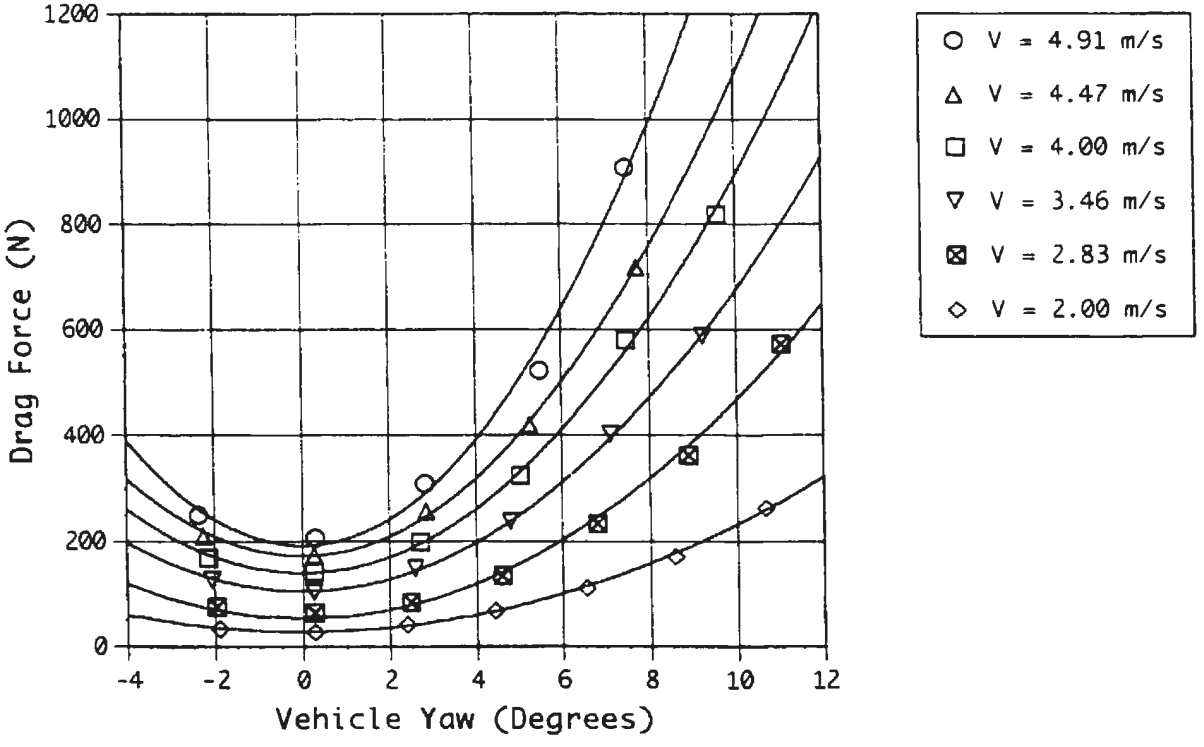

Figure 6.12 - *Drag Force vs. Vehicle Yaw Angle; Configuration M2B @ Draft D1*

The overall vehicle drag at draft D1 with mast configurations M2 and M2B is presented in Figures 6.11 and 6.12 respectively. A symmetric second order polynomial was used to fit the data based on constant velocity. All values of R^2 were at least 0.995. The y-intercept of each plot was used to find the vehicle drag at zero yaw for each velocity and mast. These values were then plotted versus the square of vehicle velocity in Figure 6.13.

Figure 6.13 shows that vehicle drag with mast configurations M2 and M2B is proportional to the square of the velocity. A linear fit of the data for M2 and M2B produced slopes of 8.00 and 8.19 respectively ($R^2 > 0.991$). It was therefore determined that the contributed drag from the proposed mast (M2) represented 24% of the overall vehicle drag, while the drag from the proposed mast with air ejection (M2B) represented 26% of overall vehicle drag.

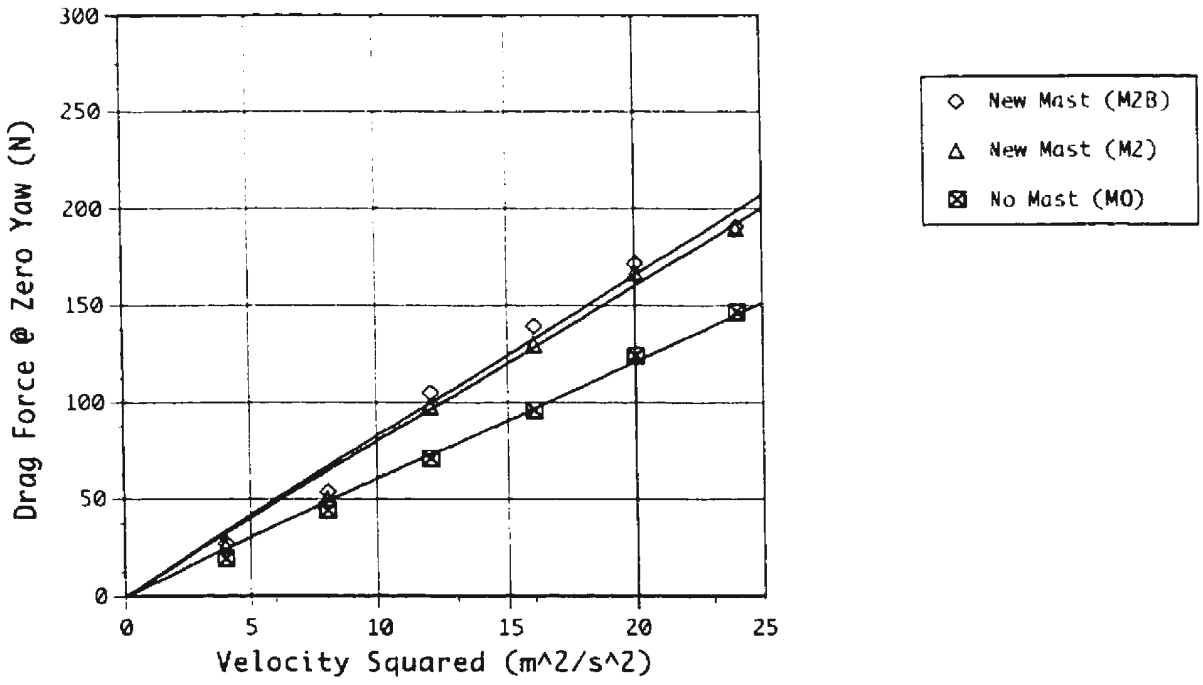

Figure 6.13 - *Drag Force (θ=0°) vs. V^2; Configurations M0, M2 and M2B @ Draft D1*

6.3 *Further Analysis of the Results*

The overall vehicle drag for each mast configuration (at a given draft), as a function of both velocity and yaw angle, can be determined with a multiple non-linear regression analysis of the following equation

$$Drag = A \cdot \theta^2 \cdot V^2 + B \cdot V^2; \qquad Eq.\ 6.02$$

where *Drag*, θ and V are the drag force in Newtons, the yaw angle in degrees and the velocity in metres per second respectively. In Equation 6.02 above, the constant '*A*' represents the rate of increase of drag as the yaw angle increases, while the constant '*B*' represents the magnitude of drag at zero vehicle yaw angle (*i.e.* slope from Figures 6.05 & 6.13). Using Equation 6.02, the overall drag equations for M1, M2, M2A & M0 at draft D1 were determined. Therefore for M1

$$Drag_{M1} = 0.27 \cdot \theta^2 \cdot V^2 + 10.33 \cdot V^2; \qquad Eq.\ 6.03$$

for M2

$$Drag_{M2} = 0.50 \cdot \theta^2 \cdot V^2 + 7.94 \cdot V^2; \qquad Eq.\ 6.04$$

for M2B

$$Drag_{M2A} = 0.47 \cdot \theta^2 \cdot V^2 + 8.11 \cdot V^2; \qquad Eq.\ 6.05$$

and for M0

$$Drag_{M0} = 0.22 \cdot \theta^2 \cdot V^2 + 5.95 \cdot V^2. \qquad Eq.\ 6.06$$

In Equations 6.03 to 6.06, the constants '*B*' are slightly smaller in magnitude than the slopes found in Figures 6.05 & 6.13. This is due in part to the natural weighting of velocity (V^2) in Equation 6.02, compared to the un-weighted analysis (with respect to

velocity) of $Drag = A \cdot \theta^2 + C$ used in Figures 6.04, 6.11 & 6.12. The naturally weighted analysis is preferred here because it was found that larger load-cell forces (*i.e.* higher V) resulted in more precise measurements of external loads. A complete set of plots of the data for all mast configurations is contained in Appendix B.

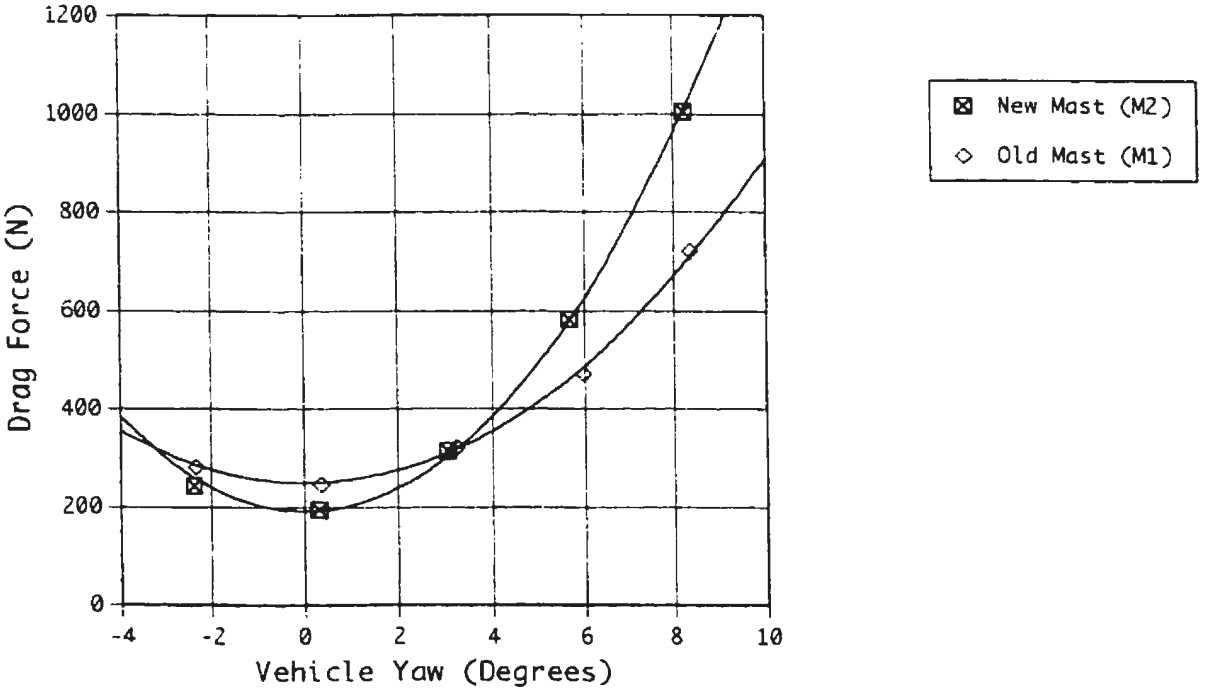

Figure 6.14 - *Drag Force vs. Vehicle Yaw Angle; Config. M1 and M2 @ Draft D1 and 4.91m/s*

From Equations 6.03 and 6.04 it can be seen that the drag of M2 increases at almost twice the rate of M1 as the vehicle yaw angle (θ) increases. This can be seen in Figure 6.14 where data for M1 and M2 at 4.91 m/s are plotted together along with Equations 6.03 and 6.04. Where the curves in Figure 6.14 intersect, the vehicle drag for each mast is equal. The location of this intersection will be referred to as the "equi-drag" angle. The equi-drag angle, θ_{ED}, was calculated by equating Equations 6.03 and 6.04 and solving for θ.

This yielded an angle of 3.2° for θ_{ED}. Therefore, for vehicle yaw angles above 3.2°, the drag of M2 will be greater than the drag of M1.

Mast Configuration	Draft	A	B	R^2
No Mast (M0)	D1	0.224	5.950	0.997
Old Mast (M1)	D1	0.274	10.330	0.997
	D2	0.268	11.792	0.991
	D3	0.252	12.828	0.996
New Mast Q0 (M2)	D1	0.502	7.944	0.998
	D2	0.577	8.066	0.995
	D3	0.657	8.087	0.985
New Mast Q1 (M2B)	D1	0.466	8.110	0.997
	D2	0.554	8.109	0.996
	D3	0.653	8.537	0.985
New Mast Q2 (M2A)	D1	0.480	8.268	0.995
	D2	0.540	8.290	0.996
	D3	0.650	8.682	0.986

Table 6.01 - *Constants 'A' and 'B' Derived from Equation 6.02*

Table 6.01 summarizes the drag calculations for all mast configurations and drafts. The constants '*A*' and '*B*' as well as the corrected R^2 values from Equation 6.02 are tabulated for each mast condition. In Table 6.02, the percent of overall drag at zero yaw angle for each mast configuration is shown, as well as the overall drag percent change (reduction) of the proposed mast configurations compared to M1 (for same draft). In addition to this, the equi-drag angle of the proposed mast configurations compared to M1 (for same draft) is tabulated.

Mast Configuration	Draft	% of overall drag at Zero Yaw	% change compared to M1 at Zero Yaw	θ_{ED} compared to M1
No Mast (M0)	D1	N/A	N/A	N/A
Old Mast (M1)	D1	42%	N/A	N/A
	D2	50%	N/A	N/A
	D3	54%	N/A	N/A
New Mast Q0 (M2)	D1	25%	-23%	3.2
	D2	26%	-32%	3.5
	D3	26%	-37%	3.4
New Mast Q1 (M2B)	D1	27%	-21%	3.4
	D2	27%	-31%	3.6
	D3	30%	-33%	3.3
New Mast Q2 (M2A)	D1	28%	-20%	3.2
	D2	28%	-30%	3.6
	D3	31%	-32%	3.2

Table 6.02 - *Summary of Relative Drag Results*

6.4 Drag Force Conclusions

It was found that the drag from the existing mast represented 42% (Draft D1) to 54% (Draft D3) of overall vehicle drag at zero yaw angle, while the proposed mast drag represented only 25% (Draft D1) to 26% (Draft D3). With air ejection, the overall drag of the proposed mast was slightly higher between 27% (Draft D1) and 31% (Draft D3). This indicates that while there is a small penalty of increased drag by using air ejection, there is still a large reduction in overall vehicle drag.

The overall drag of the vehicle with the proposed mast configurations (M2(A/B)) increased at nearly twice the rate of the existing mast as the yaw angle increased. In fact, above yaw angles of about 3.2° to 3.6° the drag of the proposed mast was higher than the existing mast. It should be recalled from Section 1.3, that under the *DOLPHIN*'s current configuration (*i.e.* the existing mast) cross-flow angles greater than 2° are not possible, therefore this increase in drag of M2(A/B) over M1 is not a performance handicap.

7.0 *Vehicle Lift and Roll Analysis*

The lift force and roll moment for the *DOLPHIN* model are analyzed in this chapter. The chapter concentrates on the lift/roll performance of the basic mast configurations (M0, M1 and M2), the air ejection configuration (M2B) and the flap configuration (M2F).

7.1 *Lift and Roll Performance of Basic Mast Configurations*

As a baseline it is necessary to compare the proposed mast's lift and roll performance to that of the existing mast and no mast configurations. In Figures 7.01, 7.02 and 7.03 the model lift force is plotted versus the model yaw angle (at draft D1) for the case with no mast (M0), existing mast (M1), and the proposed mast (M2) respectively. A linear fit of the data for each velocity set (zero intercept) is included in the figures.

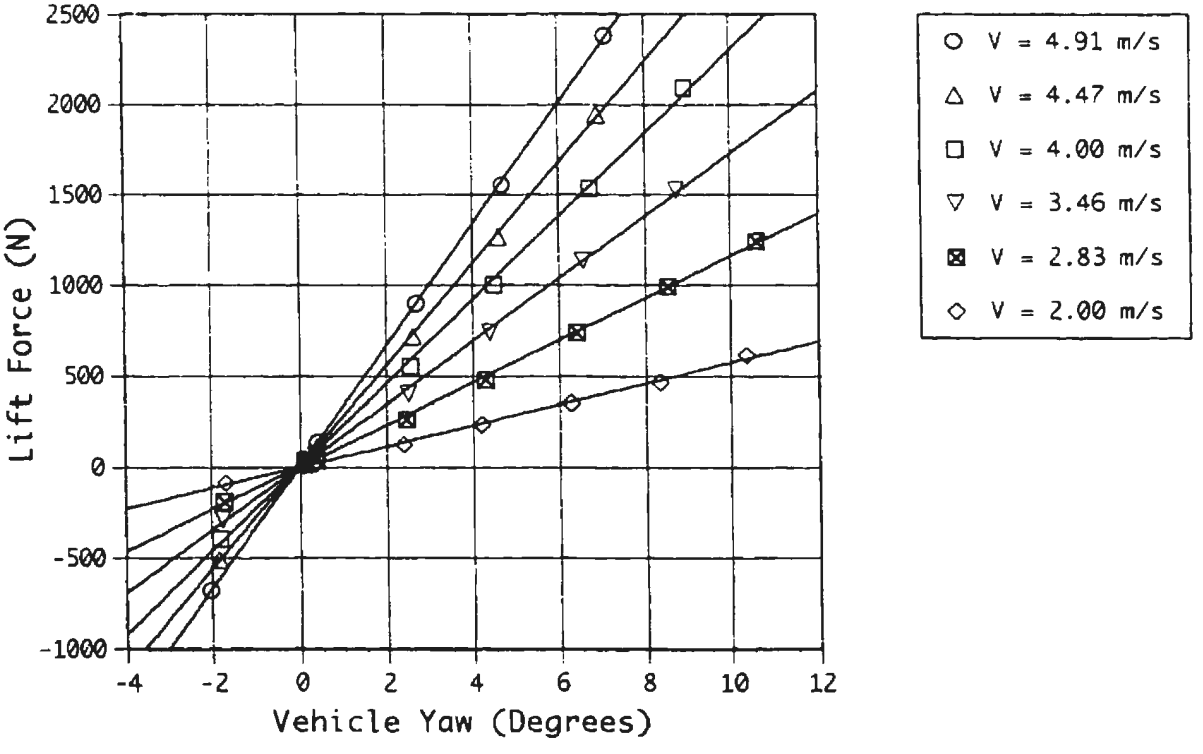

Figure 7.01 – *Lift Force vs. Vehicle Yaw Angle; No Mast (M0) @ Draft D1*

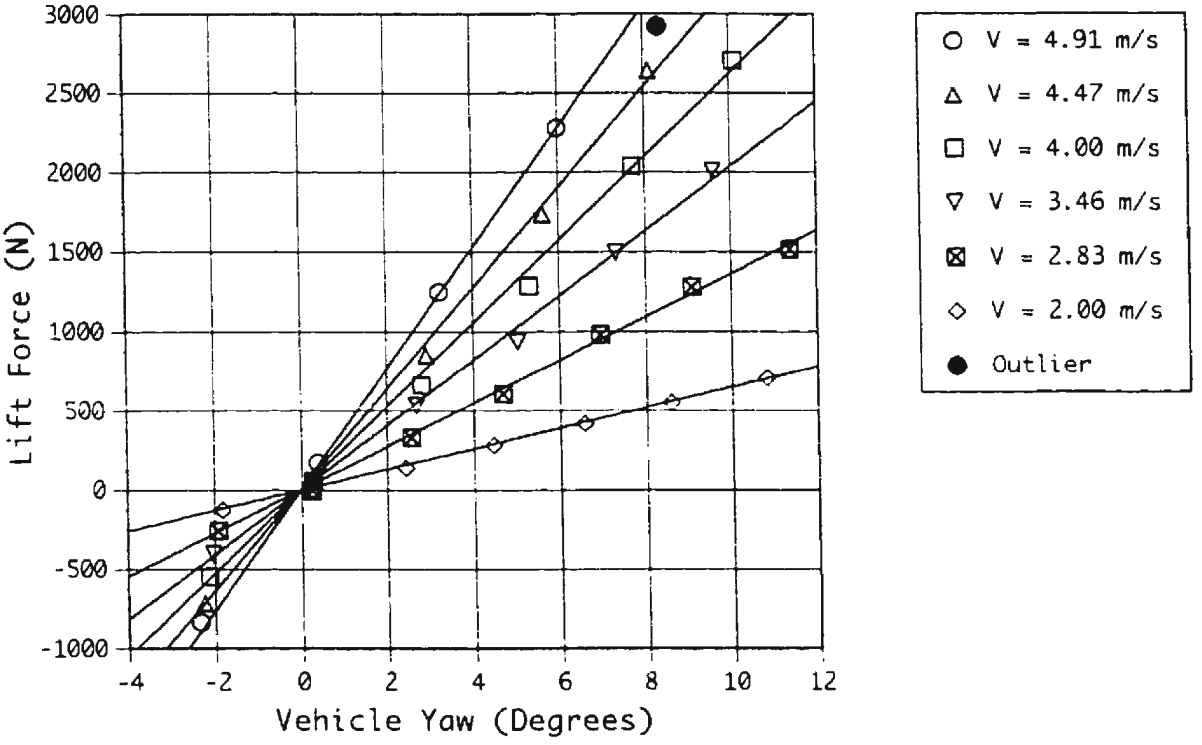

Figure 7.02 – *Lift Force vs. Vehicle Yaw Angle; Existing Mast (M1) @ Draft D1*

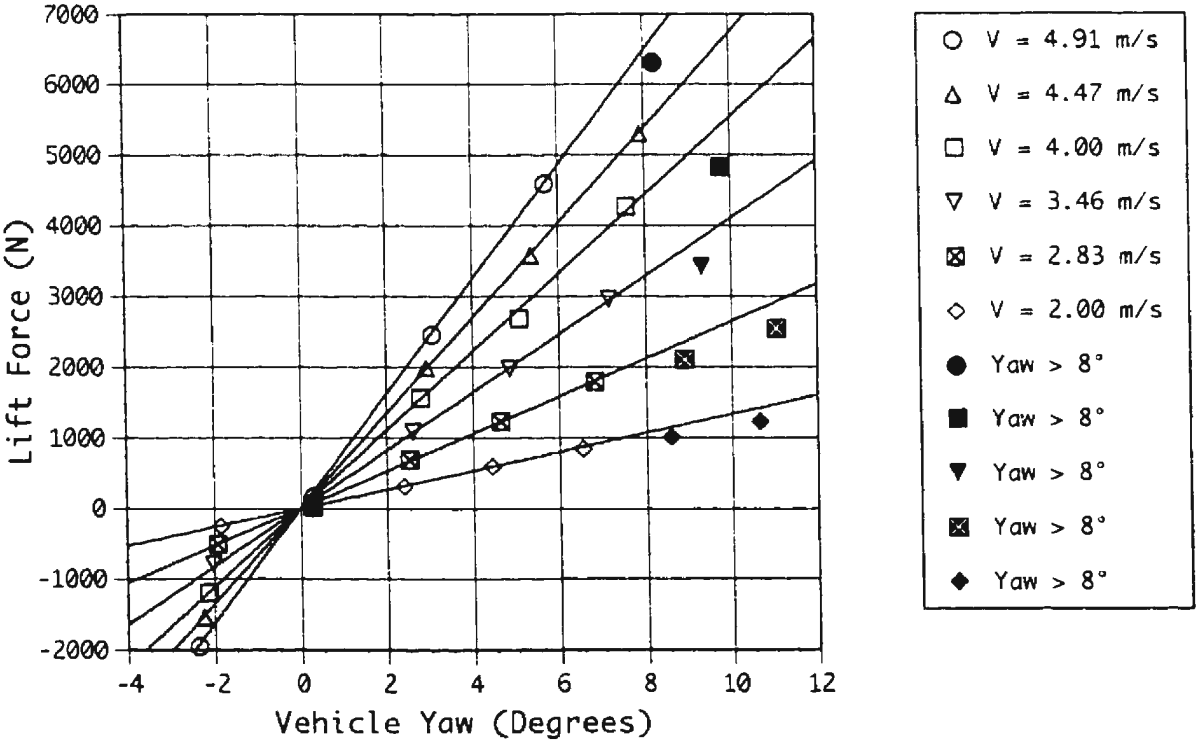

Figure 7.03 – *Lift Force vs. Vehicle Yaw Angle; Proposed Mast (M2) @ Draft D1*

The roll moment versus yaw angle of the model (at draft D1) for the no mast (M0), existing mast (M1), and the proposed mast (M2) cases are presented in Figures 7.04, 7.05 and 7.06 respectively. Again, a linear fit of the data (non-zero intercept) is included in the figures to indicate the linearity of the data for each velocity set. It was determined that for the proposed mast this linearity started to "fall off" for vehicle yaw angles above about 8°. Therefore, it was decided that data above 8° yaw for the proposed mast would not be included as part of any calculations of the lift force or roll moment. In addition to this, any data values that were considered erroneous were deemed "outliers" and were not included in any calculations.

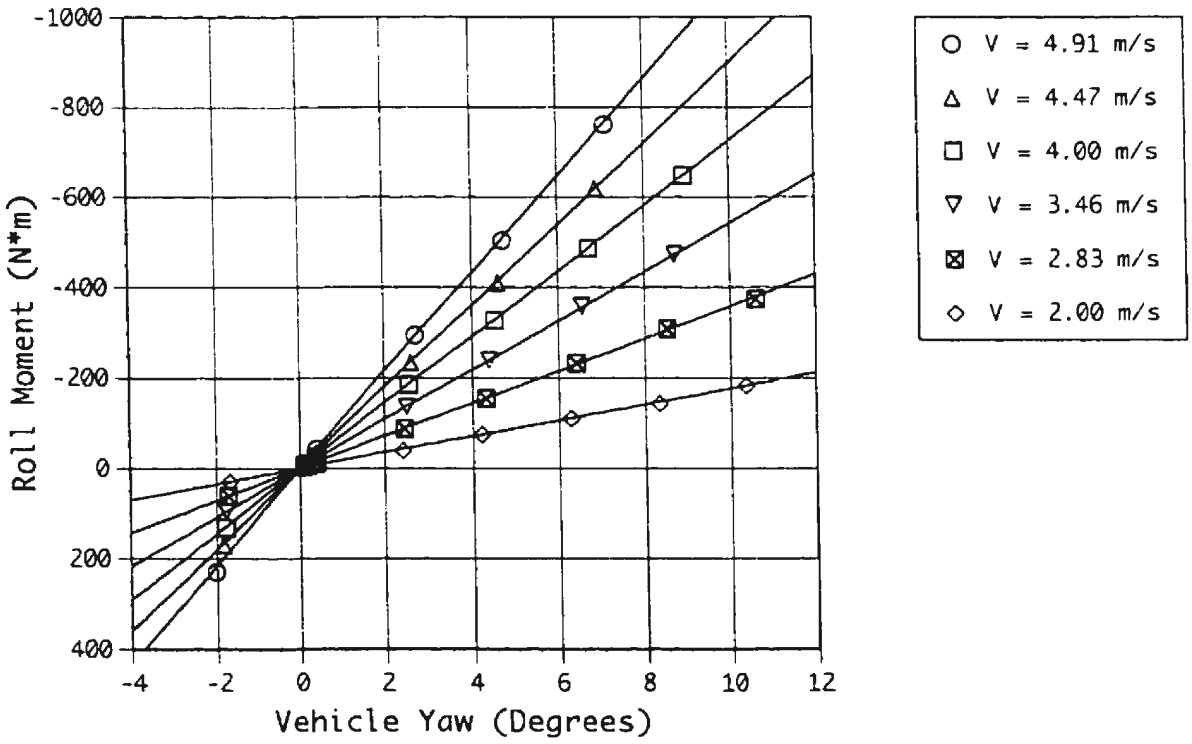

Figure 7.04 – *Roll Moment vs. Vehicle Yaw Angle; No Mast (M0) @ Draft D1*

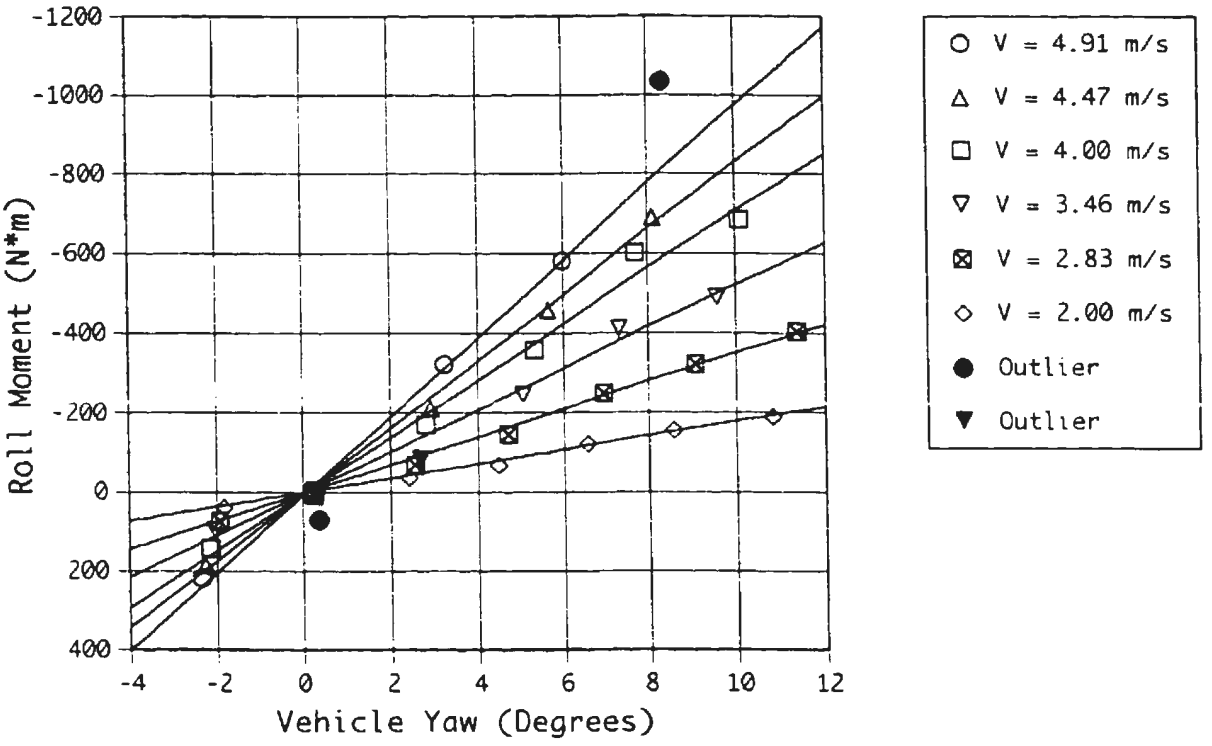

Figure 7.05 – *Roll Moment vs. Vehicle Yaw Angle; Existing Mast (M1) @ Draft D1*

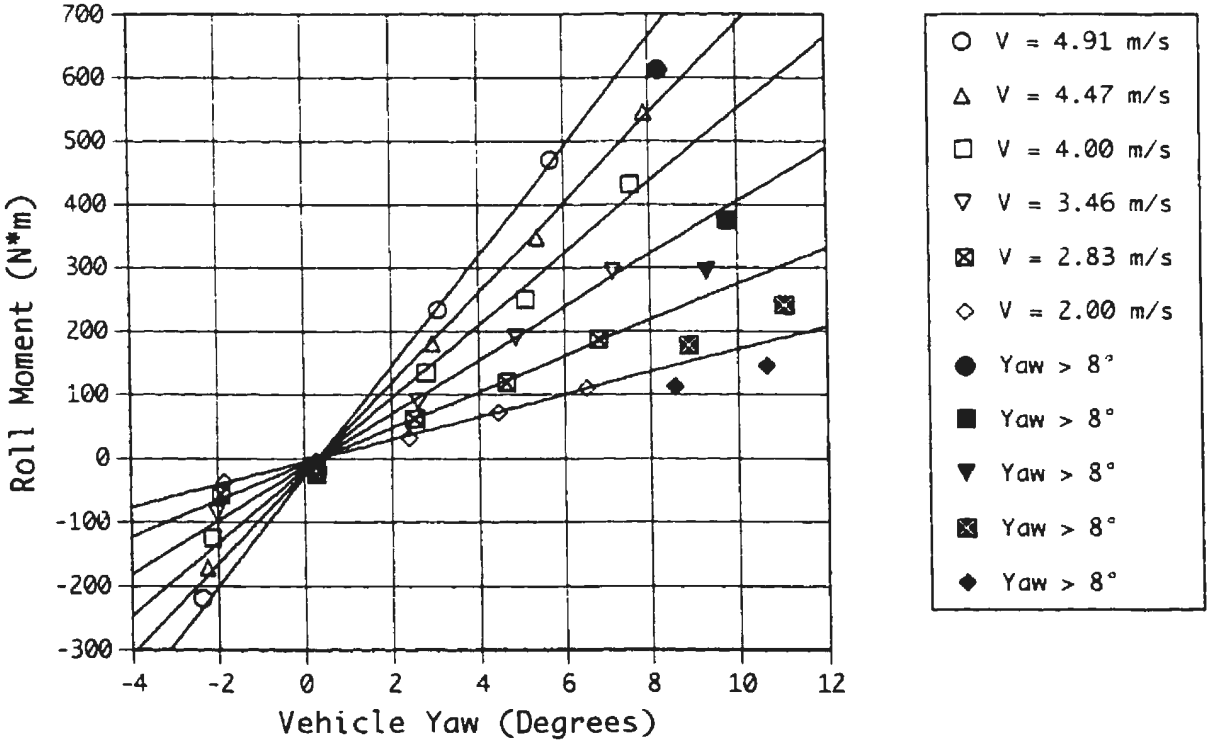

Figure 7.06 – *Roll Moment vs. Vehicle Yaw Angle; Proposed Mast (M2) @ Draft D1*

The overall vehicle lift force and roll moment for each mast configuration (at a given draft), as a function of both velocity and yaw angle, was determined with a multiple non-linear regression analysis. The following regression equations were used for the lift force and roll moment respectively:

$$Lift = C_1 \cdot (\theta_R + \theta_0) \cdot V^2 \ [\mathrm{N}] \qquad Eq.\ 7.01$$

$$Roll = C_1 \cdot (\theta_R + \theta_0) \cdot V^2 \ [\mathrm{N \cdot m}]. \qquad Eq.\ 7.02$$

In the equations above, C_0 and C_1 are the coefficients of interest, θ_R is the corrected "true" yaw angle (in degrees), θ_0 is the offset angle (in degrees) due to initial alignment errors and vehicle asymmetry, and V is the velocity of the vehicle. The coefficients C_0 and C_1 were calculated for the no mast condition (M0), as well as the three drafts for both the existing mast (M1) and the proposed mast (M2). The resulting coefficients as well as the associated R^2 values are listed in Table 7.01.

Mast Configuration	Draft	C_0	C_1	R^2 (C_0)	R^2 (C_1)
No Mast (M0)	D1	14.1	-4.48	0.999	1.000
Old Mast (M1)	D1	16.2	-4.28	0.997	0.993
	D2	15.8	-4.63	0.993	0.992
	D3	15.1	-5.01	0.998	0.987
New Mast Q0 (M2)	D1	33.6	3.53	1.000	0.996
	D2	37.7	7.53	0.999	0.986
	D3	40.4	10.96	0.999	0.991

Table 7.01 – *Coefficients C_0 and C_1 for M0, M1 and M2*

From C_0 in Table 7.01 it can be seen that the lift produced with the proposed mast configuration (M2) is, at a minimum, twice as much as the lift produced by either the no mast (M0) or the existing mast configurations (M1). Also note that the magnitude of the lift produced by the proposed mast (M2) increases with increasing draft, while the magnitude of lift of the existing mast (M1) decreases with increasing draft. The latter result was unexpected and may be related to the splaying of the fairings (Section 6.1).

From C_1 in Table 7.01 it can be seen that the use of the proposed mast (M2) results in a reversal of the direction of the rolling moment when compared to the no mast (M0) and existing mast (M1). In addition to this, it was also noticed that the magnitude of roll of the proposed mast (M2) increases sharply as the draft is increased, while the increase in roll magnitude for the existing mast (M1) was minimal. However, there exists a draft, D0, at which the magnitude of the roll moment is zero for the proposed mast (M2). To calculate this draft, the values of C_1 from Table 7.01 were used in a linear regression with the following equation

$$C_1 = A \cdot Draft + B; \qquad Eq.\ 7.03$$

where A and B were the constants to be calculated, and *Draft* is the draft depth of 43.5", 53.5"and 63.5" for D1, D2 and D3 respectively. The resulting equation ($R^2 = 0.998$) was

$$C_1 = 0.371 \cdot Draft - 12.5. \qquad Eq.\ 7.04$$

For a zero roll moment, C_1 must be identically equal to zero, therefore

$$0 = 0.371 \cdot D0 - 12.5; \qquad Eq.\ 7.05$$

and solving for D0 yielded

$$D0 = 33.7\ [\text{inches}]. \qquad Eq.\ 7.06$$

Therefore, a zero roll condition exists (all else being equal) at a draft of 33.7" [86cm]. This draft is located roughly 3/4" [19mm] above the ventilation fence. Recall from Sections 2.4 and 3.5.1 that the lower mast section was designed (selected) so that it alone would provide enough roll to counter the roll produced by the keel. Therefore, the design of the lower section of the proposed mast configuration is considered to largely meet this criterion.

A synthetic value of C_0 was calculated for draft D0 of the proposed mast. This coefficient was determined by using the values of C_0 from Table 7.01 in the linear regression equation

$$C_0 = A \cdot Draft + B; \qquad Eq.\ 7.07$$

again, where A and B are the constants to be calculated, and *Draft* is the draft depth of 43.5", 53.5"and 63.5" for D1, D2 and D3 respectively. The resulting equation (R^2 = 0.987) is

$$C_0 = 0.340 \cdot Draft + 19.0; \qquad Eq.\ 7.08$$

and substituting a *Draft* of 33.7" yields

$$C_0 = 30.5 \qquad Eq.\ 7.09$$

It should be noted that the procedure used in determining Equations 7.02 through 7.09 is valid only when the upper section of the proposed mast is the surface piercing section.

7.2 Lift and Roll Performance of the Proposed Mast with Air Ejection

Recall from section 2.3.2 that the goal of the air ejection method was to reduce the effective lift force to zero over the upper section of the proposed mast. Ideally, in order for this to occur a thin, evenly distributed air sheet was required on both sides of the upper mast section. However, during tests with air ejection it was noticed that this "ideal" condition was not satisfactorily achieved during the testing.

Firstly, it was observed that the distribution of the ejected air had a variation in sheet thickness along the vertical span of the upper mast section. The thickness of the air sheet was greatest on the lower third (roughly from D0 to D1) of the upper mast section, while it was minimal over the middle third (roughly from D1 to D2). The upper third of the upper mast section (roughly from D2 to D3) had an intermediate air sheet thickness. Secondly, the air sheet on the high-pressure side of the upper mast started to thin as the vehicle was yawed away from zero degrees. Eventually, the air sheet on the high-pressure side was completely depleted, with all the air therefore ejecting out onto the low-pressure side. It was noticed that for yaw angles of *less than* 4°, the low/high-pressure symmetry of the air sheet *was* satisfactory. Thirdly, it was observed that the air sheet was excessively thick for some of the lower velocity tests.

The model lift force is plotted versus the model yaw angle for the proposed mast with the air ejection rate of 20CFM [9.4 *l*/s] (M2B) for vehicle drafts D1, D2 and D3 in Figures 7.07, 7.08 and 7.09 respectively. A linear fit of each velocity set (zero intercept) is derived solely from yaw angles of less than 4° and is included in the figures. Note that as the draft is increased, that the data points above 4° diverge from the linear fit.

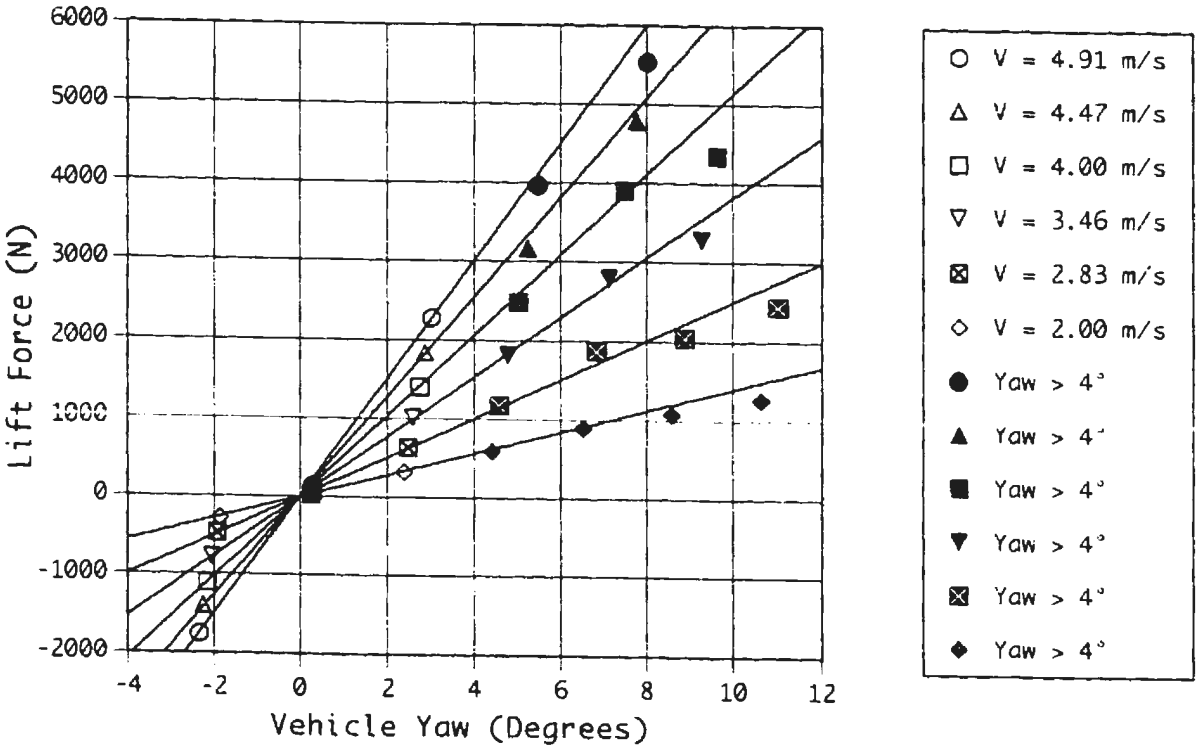

Figure 7.07 – *Lift Force vs. Vehicle Yaw Angle; Proposed Mast w/ Air (M2B) @ Draft D1*

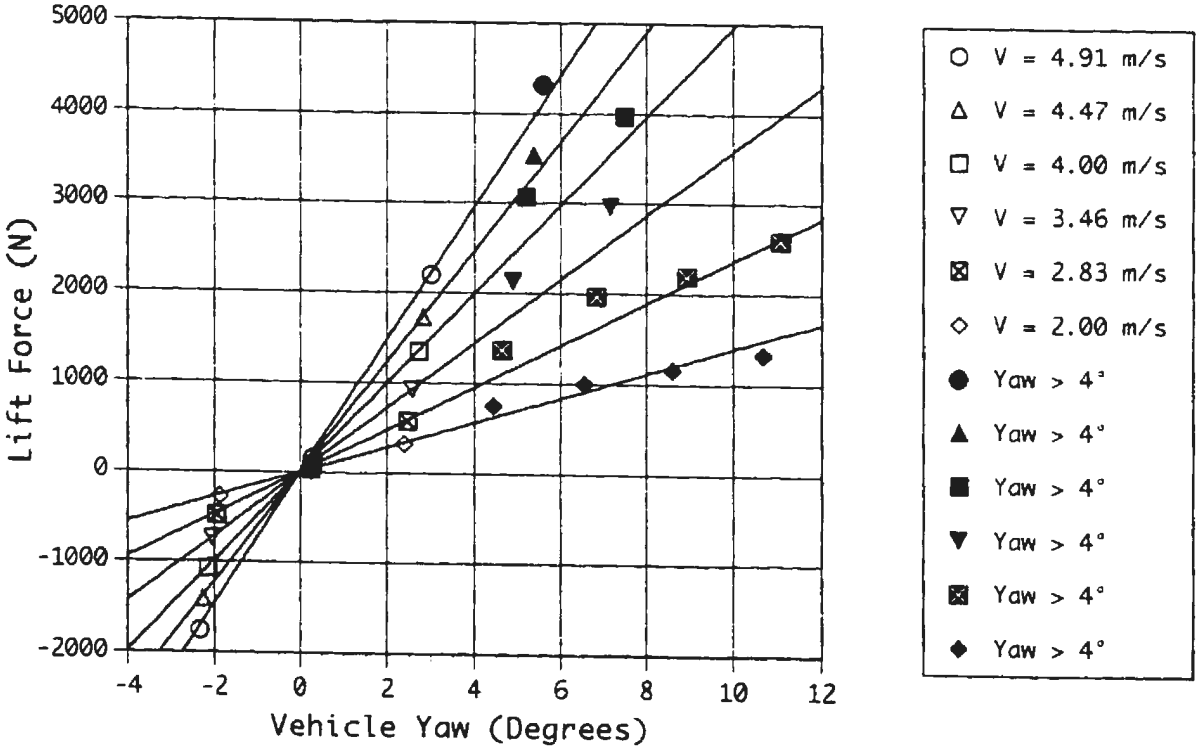

Figure 7.08 – *Lift Force vs. Vehicle Yaw Angle; Proposed Mast w/ Air (M2B) @ Draft D2*

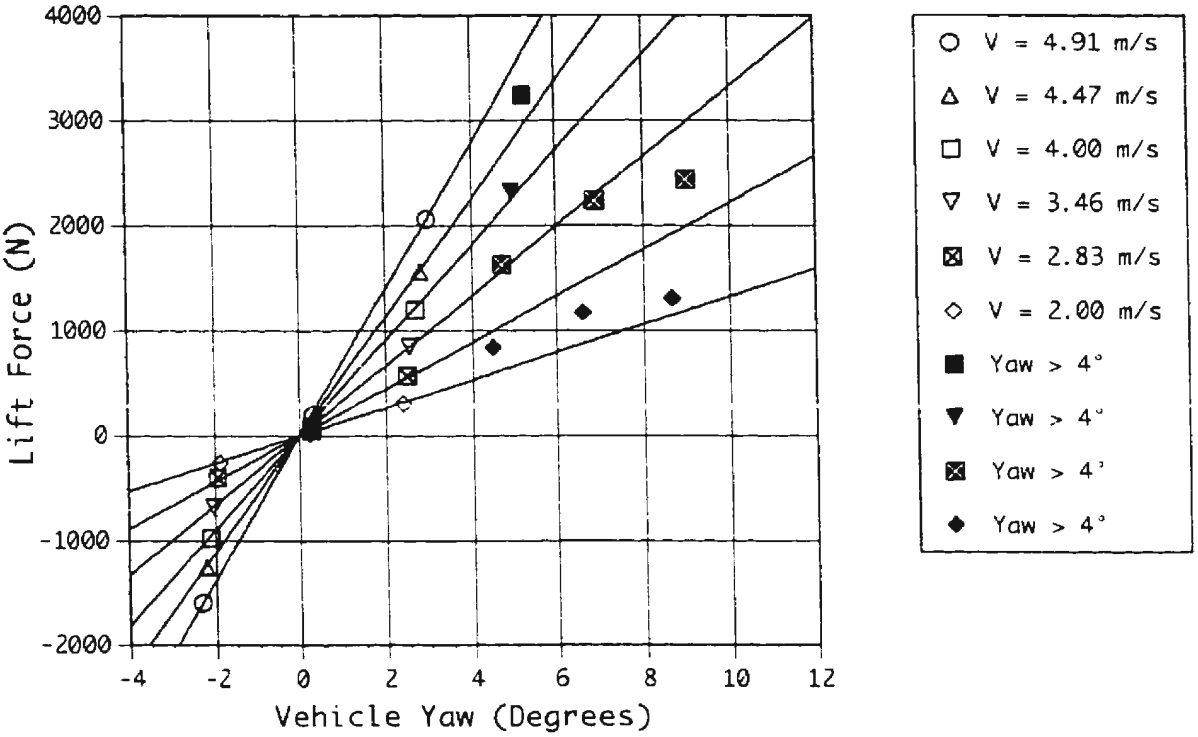

Figure 7.09 – *Lift Force vs. Vehicle Yaw Angle; Proposed Mast w/ Air (M2B) @ Draft D3*

The model roll moment is plotted versus the model yaw angle for the proposed mast with 20CFM [9.4 *l*/s] of air ejection (M2B) for vehicle drafts D1, D2 and D3 in Figures 7.10, 7.11 and 7.12 respectively. As can be seen in the figures, the data collected for the roll moment due to the air ejection is not as "orderly" as the data analyzed up to this point. As a result, a cubic spline was used to indicate the "trend" of each velocity set of data as the yaw angle was increased. As previously mentioned, for vehicle yaw angles above 4° the air sheet pattern is not well behaved and this can be seen in the plots. However, for yaw angles of less than 4° the roll moment of each draft is reasonably regular. For yaw angles of up to 4° in Figures 7.10, 7.11 and 7.12 it was observed that: D1 exhibits a roughly positive slope; D2 exhibits a near zero slope (with the exception of V = 2.00m/s), and; D3 exhibits a roughly negative slope (with the exception of V = 2.00m/s).

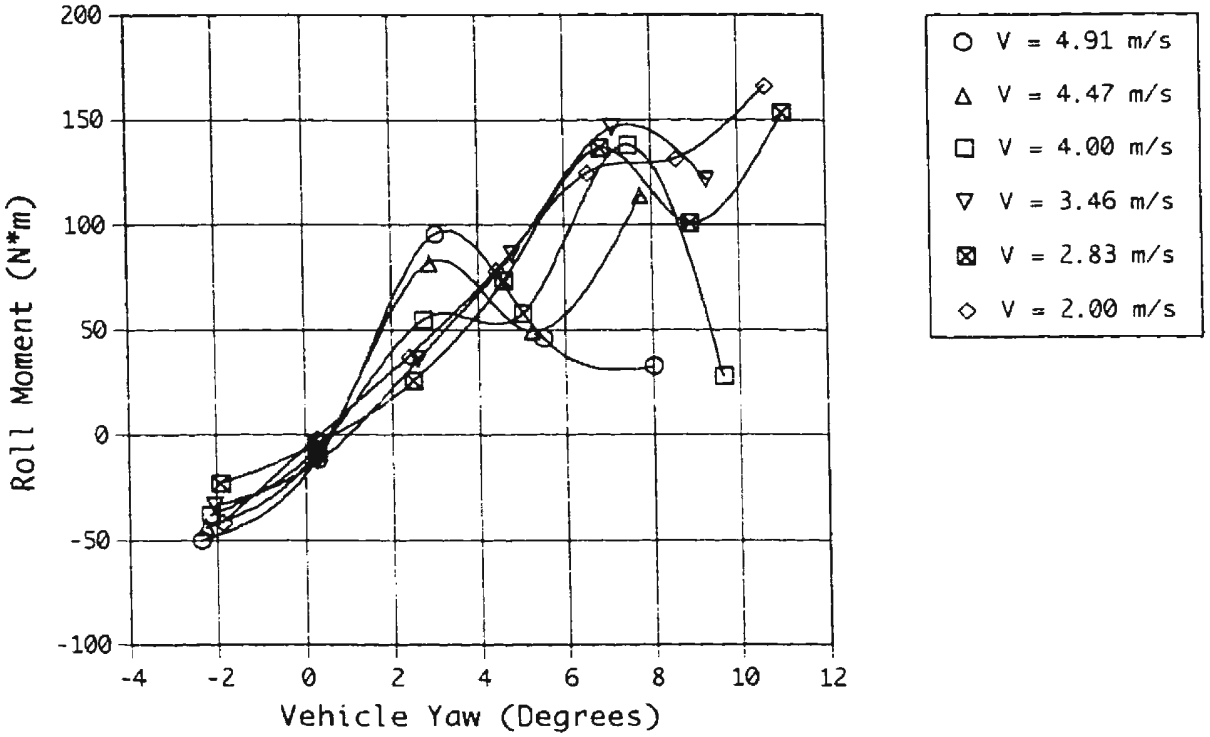

Figure 7.10 – *Roll Moment vs. Vehicle Yaw Angle; Proposed Mast w/ Air (M2B) @ Draft D1*

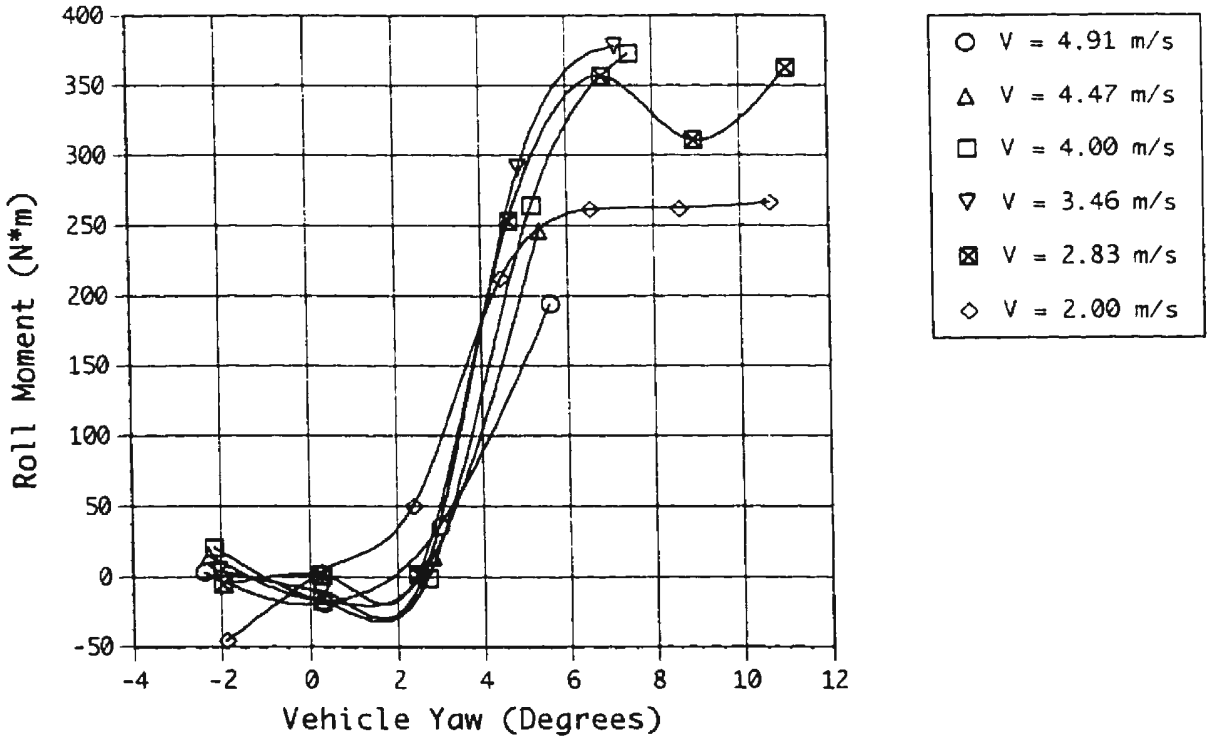

Figure 7.11 – *Roll Moment vs. Vehicle Yaw Angle; Proposed Mast w/ Air (M2B) @ Draft D2*

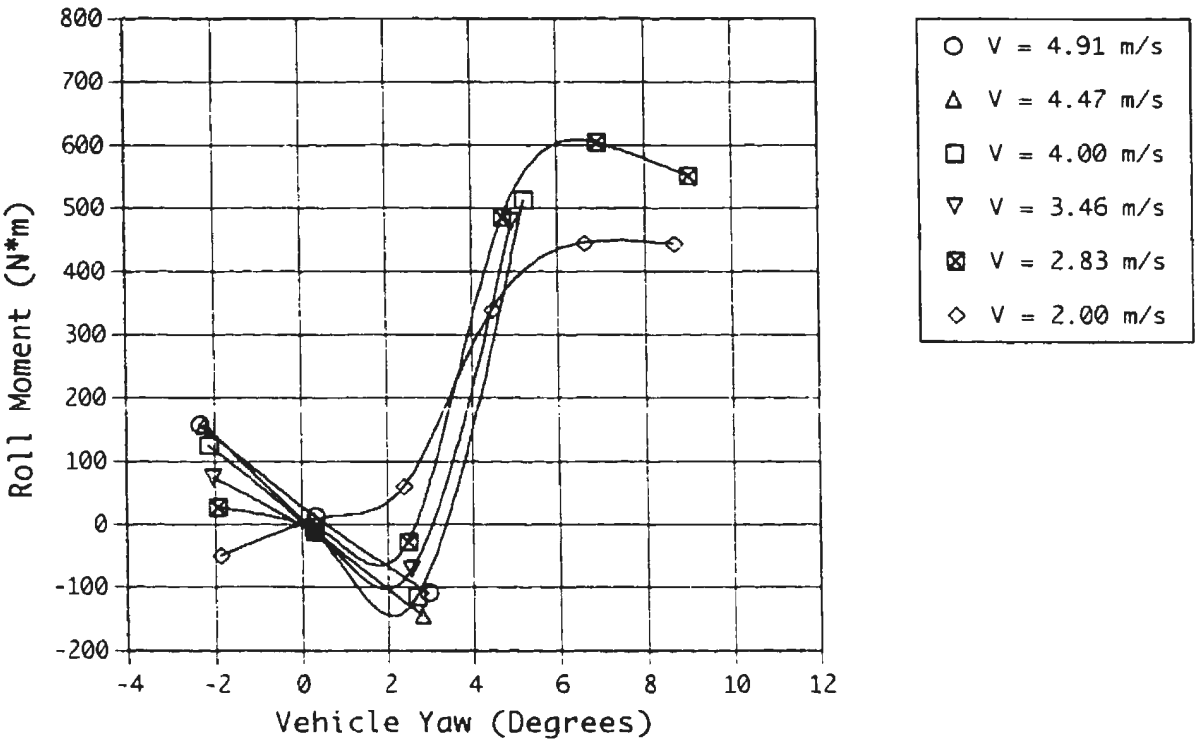

Figure 7.12 - *Roll Moment vs. Vehicle Yaw Angle; Proposed Mast w/ Air (M2B) @ Draft D3*

Using Equations 7.01 and 7.02, the lift force and roll moment for configuration M2B were regressed to obtain the coefficients C_0 and C_1. For the analysis, only yaw angles of less than 4° were considered. In addition to this, the lowest two vehicle velocities, 2.00m/s and 2.83m/s, were also excluded from the analysis. The resulting coefficients, together with the results of Section 7.2, are listed in Table 7.02.

From the results of the proposed mast (M2 and M2B) in Table 7.02, it can be seen that for a given draft the addition of air ejection reduces the overall vehicle lift force (C_0). It is also noted that for the air ejection (M2B), that the overall vehicle lift force (C_0) decreases as the draft is increased. With regards to the roll performance of the air ejected mast (M2B), note that for a given draft that the magnitude of the overall vehicle roll

moment (C_1) of configuration M2B (air) is lower than both M2 (no air) and the existing mast M1. In fact, the magnitude of the roll moment at D3 for M2B (air) is less than the magnitude of roll at D1 for either M2 (no air) or M1 (existing mast).

Mast Configuration	Draft	C_0	C_1	R^2 (C_0)	R^2 (C_1)
No Mast (M0)	D1	14.1	-4.48	0.999	1.000
Old Mast (M1)	D1	16.2	-4.28	0.997	0.993
	D2	15.8	-4.63	0.993	0.992
	D3	15.1	-5.01	0.998	0.987
New Mast Q0 (M2)	D0	30.5	0.00	0.987	0.998
	D1	33.6	3.53	1.000	0.996
	D2	37.7	7.53	0.999	0.986
	D3	40.4	10.96	0.999	0.991
New Mast Q1 (M2B)	D1	31.4	1.18	0.999	0.936
	D2	30.4	0.11	0.999	0.027
	D3	28.3	-2.47	0.999	0.953

Table 7.02 – *Coefficients C_0 and C_1 for M0, M1, M2 and M2B*

Some additional results can be extracted from Table 7.02 with regards to the air ejected mast (M2B). Note that the overall vehicle roll moment (C_1) is nearly zero for draft D2 (the extremely low R^2 value is a result of the data for the roll moment of D2 being very near zero). If the overall vehicle lift force (C_0) and roll moment (C_1) of M2B (air) at D2 is directly compared to the overall vehicle lift force (C_0) and roll moment (C_1) of M2 (no air) at the synthetic draft, it can be seen that lift force and roll moment are essentially the same. In fact the difference in lift force is less than 0.5%. Therefore it can be concluded that at a draft D2 for the air ejected mast (M2B), that the net lift force generated by the air ejected section (*i.e.* D0 to D2) is essentially zero.

Due to the positive roll coefficient (C_l) at draft D1 for M2B (air), and the fact that the overall lift (C_0) of M2B (air) at D1 is greater than that of M2 (no air) at D0, it can be concluded that the there is still some "leftover" lift on the air ejected section (*i.e.* D0 to D1). However, because of the negative roll coefficient (C_l) at draft D3 for M2B (air), and the fact that the overall lift (C_0) of M2B (air) at D3 is less than that of M2 (no air) at D0, it can be concluded that there is a "reverse lift" on the air ejection section (*i.e.* D0 to D3). That is to say that the ejected air causes a counter thrust which acts in the opposite direction than would normally be expected.

7.3 *Lift and Roll Performance of the Proposed Mast Flap Configuration*

The effect of the flap on the lower section of the proposed mast can be thought of as an additional appendage. Therefore, the performance of the vehicle with the flap can be added to the performance of the overall vehicle without the flap. Rewriting Equations 7.01 and 7.02 to include the flap performance yields, for the vehicle lift force and roll moment respectively,

$$Lift = C_0 \cdot (\theta_R + \theta_0) \cdot V^2 + C_2 \cdot \theta_F \cdot V^2 \ [\mathrm{N}]; \qquad \textit{Eq. 7.10}$$

$$Roll = C_1 \cdot (\theta_R + \theta_0) \cdot V^2 + C_3 \cdot \theta_F \cdot V^2 \ [\mathrm{N \cdot m}]. \qquad \textit{Eq. 7.11}$$

In the above equations, C_2 and C_3 represent the magnitude of performance of the flap for vehicle lift force and roll moment respectively, and θ_F is the flap deflection angle in degrees. In order to present the data with both the vehicle yaw angle (θ_R) and mast flap angle (θ_F) it is necessary to "normalize" the data with respect to the velocity. Therefore, dividing Equations 7.10 and 7.11 by V^2 yields

$$\frac{Lift}{V^2} = C_0 \cdot (\theta_R + \theta_0) + C_2 \cdot \theta_F \left[\frac{\mathrm{N}}{\mathrm{m^2/s^2}}\right]; \qquad \textit{Eq. 7.12}$$

$$\frac{Roll}{V^2} = C_1 \cdot (\theta_R + \theta_0) + C_3 \cdot \theta_F \left[\frac{\mathrm{N \cdot m}}{\mathrm{m^2/s^2}}\right]. \qquad \textit{Eq. 7.13}$$

The data for the flap was then normalized by dividing by the velocity squared. The results are plotted for the normalized lift force and roll moment versus vehicle yaw angle in Figures 7.13 and 7.14 respectively ('V^2' is indicated by 'W' in the figures).

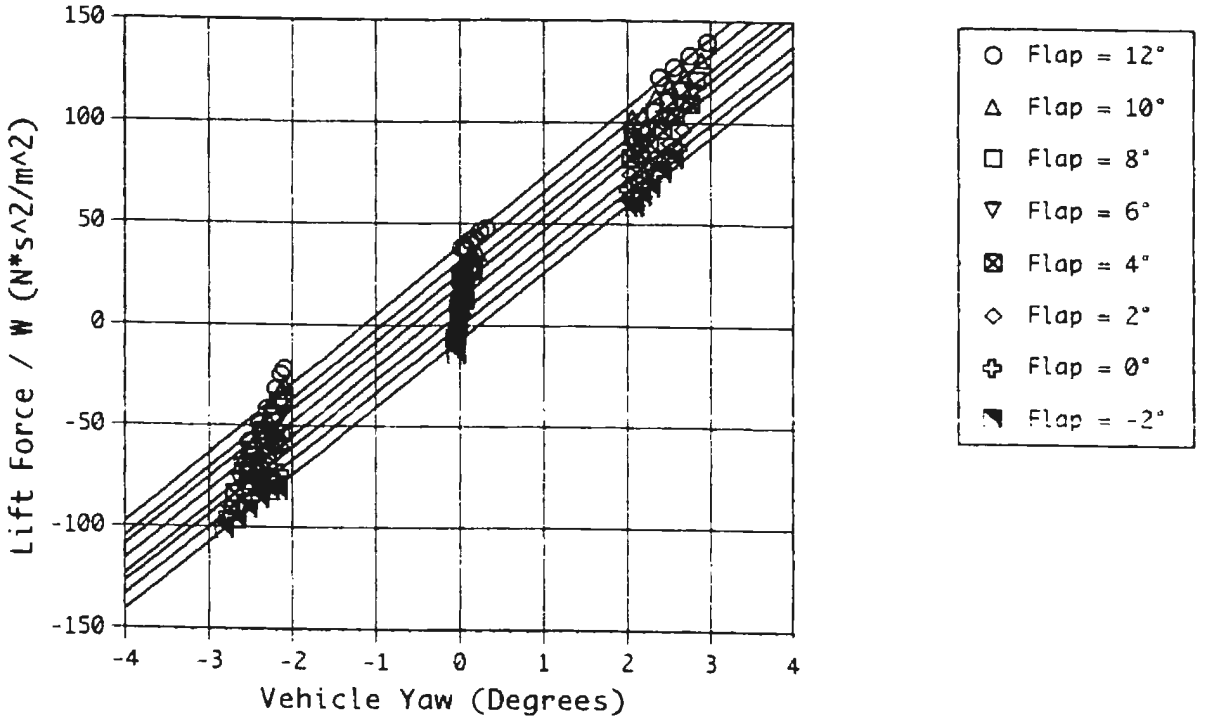

Figure 7.13 – *Normalized Lift Force vs. Vehicle Yaw Angle; Flapped Mast (M2F) @ D2*

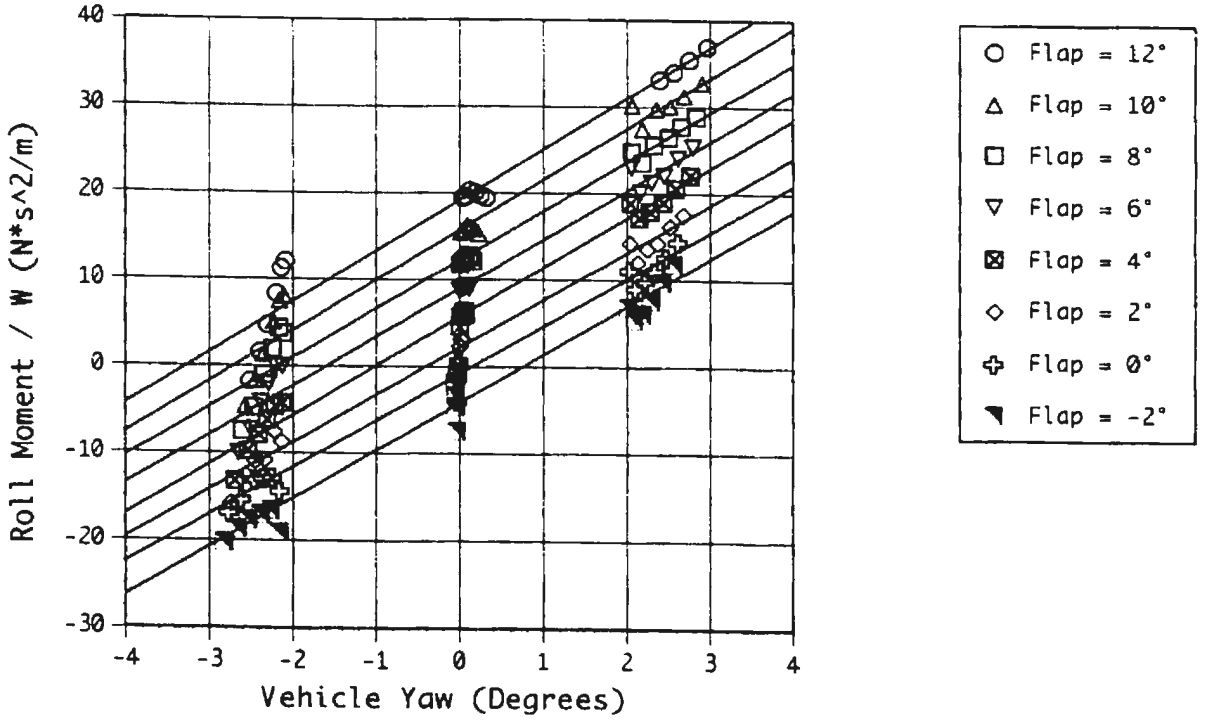

Figure 7.14 – *Normalized Roll Moment vs. Vehicle Yaw Angle; Flapped Mast (M2F) @ D2*

In Figures 7.13 and 7.14, a linear fit of the data is presented based on Equations 7.12 and 7.13 respectively. The slope of the lines in Figures 7.13 and 7.14 represent the coefficients C_0 and C_1 from Equations 7.12 and 7.13. The coefficients C_2 and C_3 can be derived from the intercepts at zero yaw angle in Figures 7.13 and 7.14 respectively.

The data as presented in Figures 7.13 and 7.14 are rather congested. Therefore in Figures 7.15 and 7.16 the data is re-plotted, but only for flap angles of –2°, 4° and 10°. The solid lines in the figures again represent linear normalized fits of the data based on Equations 7.12 and 7.13. The solid gray lines in Figure 7.16 represent linear fits of the data based on Equation 7.11.

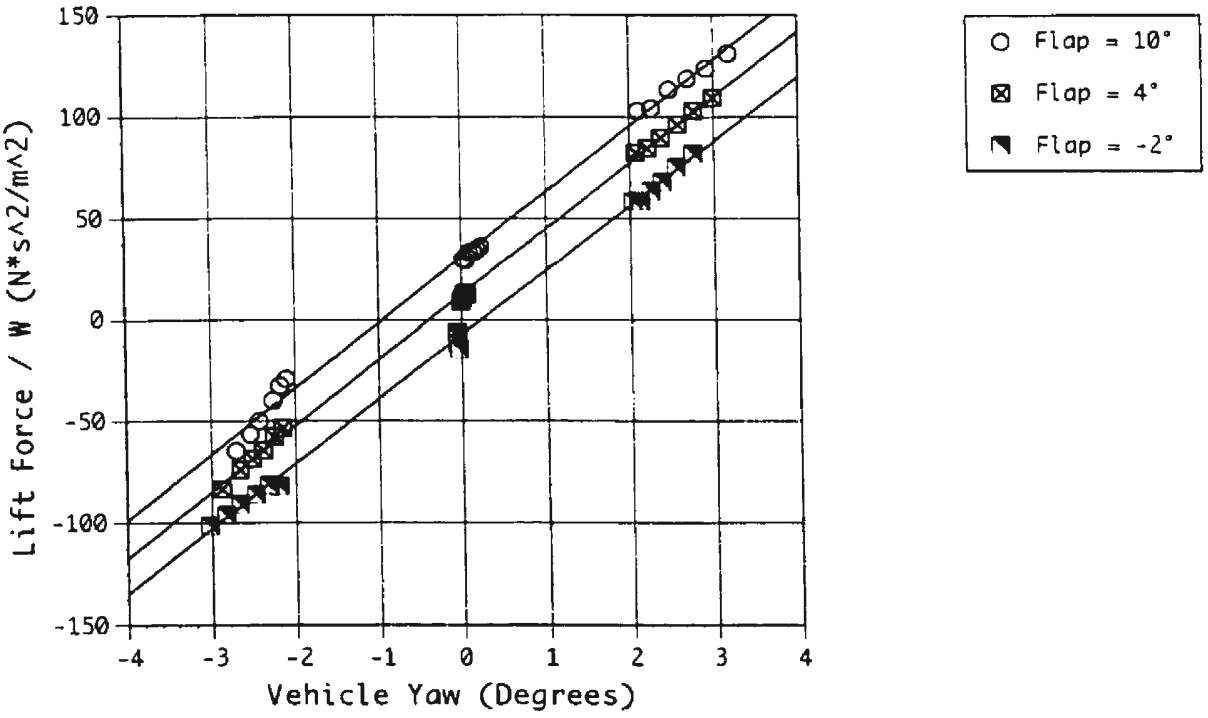

Figure 7.15 – *Normalized Lift Force vs. Vehicle Yaw Angle; Flapped Mast (M2F) @ D2*

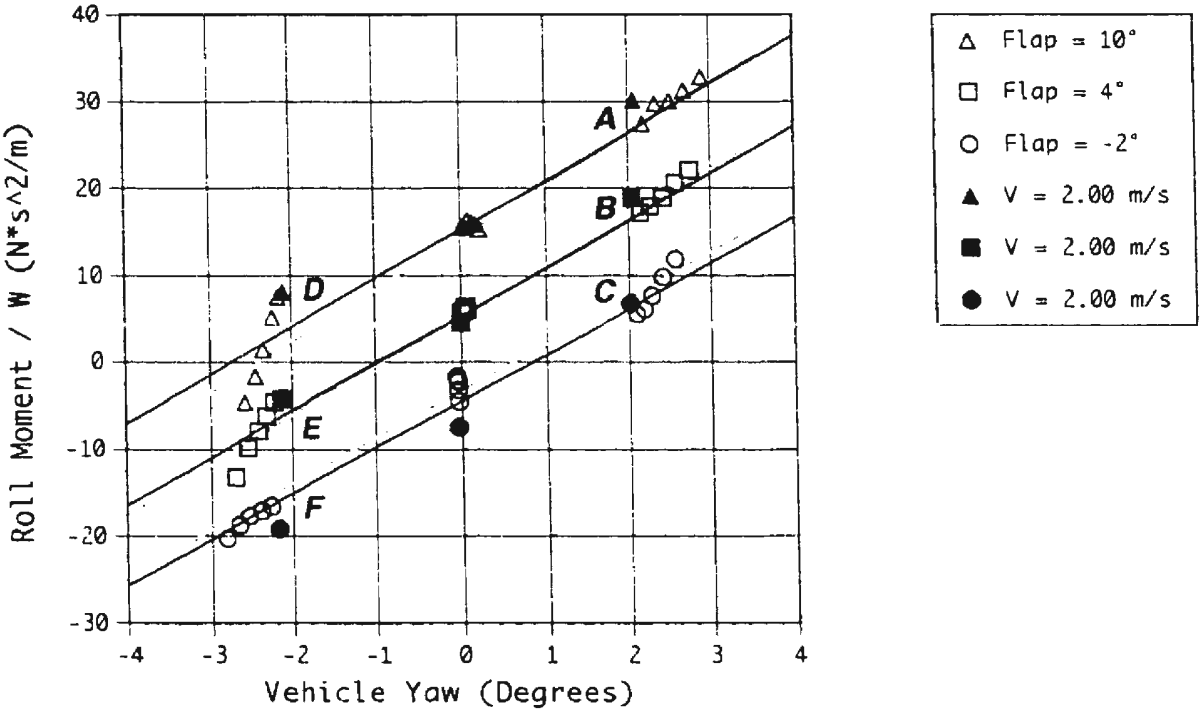

Figure 7.16 – *Normalized Roll Moment vs. Vehicle Yaw Angle; Flapped Mast (M2F) @ D2*

From Figure 7.16 it can be seen that Equations 7.11 and 7.13 yield different results. This is evident by the different slopes and intercepts (at zero yaw angle) for the solid and dashed lines. The main reason for the disagreement between Equations 7.11 and 7.13 is that some of the data for the flap tests does not correlate directly to velocity squared. This can be seen in Figure 7.16 (and to a lesser extent in Figure 7.15) where there is a vertical spread of the normalized data at '*C*', '*D*' and '*E*' with respect to the linear fit. On the other hand, the normalized data at '*A*', '*B*' and '*F*' correlate quite well (neglecting V = 2.00m/s) with respect to the linear fit.

Upon closer examination it was noticed that for data sets '*C*', '*D*' and '*E*' that the flap angle is opposite in sign to the yaw angle, while for '*A*', '*B*' and '*F*' the flap angle and the yaw angle have the same sign. This result is important because as can be seen in Figures 7.14 and 7.16, the zero roll condition (where the linear fits intersect zero roll moment) can only be achieved when the flap is deflected in the opposite sense to the vehicle yaw angle.

Because of the above results, an analytical solution of C_2 and C_1 would not be valid. In other words, because of the opposite sign condition, the assumption in Equations 7.10 through 7.13 that the data is proportional to velocity squared is incorrect. However, the effectiveness of the flap can still be gauged by using Figures 7.14 and 7.16. If the linear fits of the data in these figures is used as a rough guide, then the flap angle required for zero roll moment can be approximated. For example, for a vehicle yaw angle of -1°, a flap deflection of 4° is required to eliminate the roll moment. However, because of the vertical spread of the data this flap angle is only a representative of the intermediate velocities (V = 3.46 m/s and 4.00 m/s). For the higher velocities (V = 4.47 m/s and 4.91 m/s) a larger flap angle would be required, while for the lower velocities (V = 2.00 m/s and 2.83 m/s) a smaller flap angle would be required to achieve zero roll moment.

7.4 Lift Force and Roll Moment Conclusions

One of the goals of this project was to use the proposed mast to control the vehicle roll moment. It was found that the basic proposed mast configuration (*i.e.* no air no flap) provided too much counter-roll for drafts D1, D2 and D3. This was expected, since the mast was designed such that only the lower portion would provide sufficient counter-roll to eliminate the roll moment. The draft D0, at which zero roll moment occurred, was found to be within 3/4" of the design location.

With the inclusion of air ejection, it was found that the magnitude of the overall vehicle roll moment was lower than both the basic proposed mast and the existing mast. In fact, the magnitude of the roll moment at draft D3 for air ejection was less than the magnitude of the roll moment at D1 for both the basic proposed mast and the existing mast. However, because a thin, evenly distributed air sheet was not always observed during testing, the behavior of the ejection was neither what was desired nor considered ideal.

The results of the flap configuration tests indicate that the 25% plain flap included on the lower section of the proposed mast is adequate to provide vehicle roll control. However, the effectiveness of the flap did not correlate well with velocity squared, and as a result, unique flap angles are required for each velocity in order to eliminate the roll moment. Therefore, the roll control via flap deflection would have to be incorporated into the active control system of the *DOLPHIN*.

8.0 Conclusions

Through ISER's (International Submarine Engineering Research) continuing research and design, the *DOLPHIN* has been constantly evolving since its first deployment. Therefore, in December 1996, ISER requested that a new surface-piercing mast design be considered. As such, a collaborative research, design and testing plan was set up between ISER, IMD (Institute for Marine Dynamics) and MUN (Memorial University of Newfoundland) to design and test a new surface-piercing mast for the *DOLPHIN*.

Research and literature were collected and examined on such subjects as surface piercing struts, hydrofoil sections, flap performance, and secondary means of controlling side-force such as spoilers and air-entrainment. A symmetric double-arc shape was selected as the new section for the upper-half of the mast. Active air-entrainment was implemented into the upper mast as a secondary means of regulating vehicle side force. The profile for the lower-half of the mast was based upon a modified double-arc. In addition to this, a 25% of chord plain flap was integrated into the lower mast to control vehicle lift force and roll moment.

A scale model of the DOLPHIN was designed and fabricated to test the performance of the new mast. The DOLPHIN model was tested in the IMD CWTT (Clear Water Tow Tank) using the prototype MDTF (Marine Dynamic Test Facility). The model was tested at various vehicle drafts, speeds, yaw angles, and mast configurations. All six forces and moments on the DOLPHIN model were measured with an internal six degrees-of-freedom dynamometer.

After the test plan was completed it was necessary to perform a calibration of the dynamometer. A calibration of the dynamometer was necessary in order to determine the load interactions within the dynamometer. In addition to this, it was noticed during testing, that the model was deviating from its "preset" yaw angle by a considerable amount. It was determined that this was the result of the flexing of the support struts of the prototype MDTF system. Therefore the data was corrected in order to be able to analyze the hydrodynamic loads.

The primary goal of this project was to reduce the overall vehicle drag of DOLPHIN by reducing the drag of its surface-piercing mast. It was found that the drag from the existing mast represented 42% to 54% of overall vehicle drag at zero vehicle yaw angle, while the proposed mast drag represented only 25% to 26%. With air ejection, the contributed drag of the proposed mast was slightly higher between 27% to 31% of overall vehicle drag. This indicated that while there was a small penalty of increased drag by using air ejection, there was still a large reduction in overall vehicle drag relative to the existing mast.

The overall drag of the vehicle with the proposed mast increased at nearly twice the rate of the existing mast as the yaw angle increased. In fact, above yaw angles of about 3.2° to 3.6° the drag of the proposed mast was higher than the existing mast. It should be noted however, that under DOLPHIN's current configuration cross-flow angles greater than 2° are not maintainable, therefore the increased drag of the proposed mast over existing mast at higher yaw angles is not a performance handicap.

The secondary goal of this project was to use the proposed mast to control vehicle roll. It was found that the basic proposed mast configuration (with no air or flap) provided too much counter-roll for all three drafts tested. This was expected, since the mast was designed such that the lower portion alone was to provide sufficient counter-roll to eliminate the roll moment. The draft at which zero roll moment occurred (D0) was found to be within 3/4" of its design location.

With the inclusion of air ejection on the proposed mast, it was found that the magnitude of the overall vehicle roll moment was lower than both the basic proposed mast and the existing mast. In fact, the magnitude of the roll moment at the deepest draft (D3) for air ejection was less than the magnitude of the roll moment at shallowest draft (D1) for both the basic proposed mast and the existing mast. However, because a thin, evenly distributed air sheet was not always observed during testing, the behavior of the ejection was neither what was desired nor considered ideal.

The results of the flap configuration tests indicate that the 25% of chord plain flap included on the lower section of the proposed mast is adequate to provide vehicle roll control. However, the effectiveness of the flap did not correlate well with velocity squared. In other words, the data for the flap tests was not proportional to velocity squared. As a result, in order to eliminate the roll moment unique flap angles would be required for each vehicle velocity. Therefore, the roll control via flap deflection would have to be incorporated into the active control system of the *DOLPHIN*.

List of Cited References

Abbott, Ira Herbert and Albert E. von Doenhoff (1959). *Theory of Wing Sections*, Dover Publications, New York, NY, 693 p.

Chapman, R.B. (1971). *Spray Drag of Surface-Piercing Struts*, Naval Undersea Research & Development Center, San Diego, 33 p.

Coffee, Claude W. Jr. and Robert E. Mckann (December 1953). Hydrodynamic Drag of 12- and 21-Percent-Thick Surface-Piercing Struts, National Advisory Committee for Aeronautics, Langley Field, VA, 27 p.

Hibbeler, R. C. (1991). *Mechanics of Materials*, MacMillan Publishing Company, Inc., New York, NY, 794 p.

Hoerner, Sighard F. and Henry V. Borst (1985). *Fluid-Dynamic Lift: Practical Information on Aerodynamic and Hydrodynamic Lift* (Second Edition), published by the author, Bricktown, NJ, 507 p.

Rothblum, Richard S., Michael F. Jeffers and Russel P. Smith (1976). *Methods for Controlling the Sideforce on Surface-Piercing Hydrofoil Struts*, David W. Taylor Naval Ship Research and Development Center, Bethesda, MD, 113 p.

Watt, G.D., Mae Seto and Terry Brockett (1997). *Hydrodynamic Considerations for Semi-Submersible Minehunting Vehicles*, 4th Canadian Marine & Structures Conference, Ottawa, ON, 10 p.

White, Frank M. (1986). *Fluid Mechanics (Second Edition)*, McGraw-Hill, Inc, New York, NY, 732 p.

Bibliography

Abbott, Ira Herbert and Albert E. von Doenhoff (1959). *Theory of Wing Sections*, Dover Publications, New York, NY, 693 p.

Beukelman, W. (1993). *Lift and Drag for a Low Aspect-Ratio Surface-Piercing Wing-Model in Deep and Shallow Water*, Delft University of Technology, Ship Hydromechanics Laboratory, Delft, Netherlands, 25 p.

Beukelman, W. (1995). *Manoeuvering Derivatives for a Low Aspect-Ratio Surface-Piercing Wing-Model in Deep and Shallow Water*, Delft University of Technology, Faculty of Mechanical Engineering and Marine Technology, Ship Hydromechanics Laboratory, Delft, Netherlands, 76 p.

Brug, J. B. van den, W. Beukelman and G. J. Prins (1971). *Hydrodynamic Forces on a Surface-Piercing Flat Plate*, Delft University of Technology, Shipbuilding Laboratory, Delft, Netherlands, 93 p.

Butt, Mark-Andrew, Neil Bose, Indra Datta and Christoper D. Williams (1998). Mast/Snorkel Tests for the DOLPHIN Semi-Submersible AUV, 1998 ATTC Conference, Iowa City, IO, 7 p.

Chapman, R. B. (1977). *Experimental Forces and Free-Surface Elevations for a Yawed Surface-Piercing Plate*, David W. Taylor Naval Ship Research and Development Center, Bethesda, MD, 38 p.

Chapman, R.B. (1971). *Spray Drag of Surface-Piercing Struts*, Naval Undersea Research & Development Center, San Diego, 33 p.

Coffee, Claude W. Jr. and Robert E. Mckann (December 1953). Hydrodynamic Drag of 12- and 21-Percent-Thick Surface-Piercing Struts, National Advisory Committee for Aeronautics, Langley Field, VA, 27 p.

Eames, M. C. (April 1983). *A Review of Hydrofoil Development in Canada – Part 2*, High-Speed Surface Craft, pp. 38-42.

Eames, M. C. (February 1983). *A Review of Hydrofoil Development in Canada – Part 1*, High-Speed Surface Craft, pp. 30-34.

Granville, Paul S. (1969). *Geometrical Characteristics of Streamlined Shapes*, Journal of Ship Research, Washington, DC, pp. 299-313.

Henry, Chuck (October 1995). *On Optimum Turning Configurations with Fixed-Fin Stabilization*, IEEE Journal of Oceanic Engineering, pp. 268-275.

Hibbeler, R. C. (1989). *Engineering Mechanics – Statics and Dynamics (Fifth Edition)*, MacMillan Publishing Company, Inc., New York, NY, 552 p.

Hibbeler, R. C. (1991). *Mechanics of Materials*, MacMillan Publishing Company, Inc., New York, NY, 794 p.

Hoerner, Sighard F. (1965). *Fluid-Dynamic Drag: Practical Information on Aerodynamic Drag and Hydrodynamic Resistance*, published by the author, Midland Park, NJ, 1 v.

Hoerner, Sighard F. and Henry V. Borst (1985). *Fluid-Dynamic Lift: Practical Information on Aerodynamic and Hydrodynamic Lift* (Second Edition), published by the author, Bricktown, NJ, 507 p.

Jeffrey, N. E. and M. C. Eames (April 1973). *Canadian Advances in Surface-Piercing Hydrofoils*, Journal of Hydronautics, pp. 85-92.

Johnston, Robert J. (October 1982). *History of U.S. Involvement in Devolping the Hydrofoil – Part 3*, High-Speed Surface Craft, pp. 30-34.

Kaiho, Toshimitsu (1978). *A New Method for Solving Surface-Piercing-Struts Problems*, Department of Naval Architecture and Marine Engineering (Series) 196, 54 p.

Layne, Douglas E. (1975). *Effects of External Stiffeners on the Ventilation, Force and Cavitation Characteristics of a Surface-Piercing Hydrofoil Strut*, David Taylor Naval Ship Research and Development Center, Bethesda, MD, 28 p.

Nahon, Meyer (1996). *A Simplified Dynamics Model for Autonomous Underwater Vehicles*, IEEE Journal of Oceanic Engineering, pp.373-379.

Nelka, John J. (1974). *Effects of Mid-Chord Flaps on the Ventilation and Force Characteristics of a Surface-Piercing Hydrofoil Strut*, David W. Taylor Naval Ship Research and Development Center, Bethesda, MD, 60 p.

Prandtl, L. and O. G. Tietjens (1934). *Applied Hydro- and Aeromechanics*, Dover Publications, Inc., New York, NY, 311 p.

Ransleben G. E. Jr. (March 1969). *Experimental Determination of Steady and Unsteady Loads on a Surface Piercing, Ventilated Hydrofoil*, Journal of Ship Research, pp. 1-11.

Riegels, Freidrich Wilhelm (translated by D.G. Randall) (1961). *Aerofoil Sections: Results from Wind-Tunnel Investigations, Theoretical Foundations*, Butterworths, London, 281 p.

Rothblum, Richard S., Michael F. Jeffers and Russel P. Smith (1976). *Methods for Controlling the Sideforce on Surface-Piercing Hydrofoil Struts*, David W. Taylor Naval Ship Research and Development Center, Bethesda, MD, 113 p.

Swales, P.D., R.C. Mcgregor and A.J. Wright (April 1974). *Correlation of Force Measurements and Separated Flow Regions on Surface-Piercing Struts*, Journal of Hydronautics, pp. 72--73.

Watt, G.D., Mae Seto and Terry Brockett (1997). *Hydrodynamic Considerations for Semi-Submersible Minehunting Vehicles*, 4th Canadian Marine & Structures Conference, Ottawa, ON, 10 p.

White, Frank M. (1986). *Fluid Mechanics (Second Edition)*, McGraw-Hill, Inc, New York, NY, 732 p.

Yim, Bohyun (1975). *Theory of Ventilating or Cavitating Flows about Symmetric Surface-Piercing Struts*, David W. Taylor Naval Ship Research and Development Center, Bethesda, MD, 44 p.

Appendix A

DOLPHIN Test Matrix

Run Number	Model Configuration	Draft Depth	Yaw (Deg)	Carriage Speed (m/s)	Air Flow	Flap (Deg)	Data 'File Name'
1	No Mast	D2	0	2.00 & 2.83			XM_D1_Y00_V200
2	No Mast	D2	0	3.46 & 4.00			XM_D1_Y00_V346
3	No Mast	D2	0	4.47			XM_D1_Y00_V447
4	No Mast	D2	0	4.90			XM_D1_Y00_V490
5	No Mast	D2	-2	2.00 & 2.83			XM_D1_YM02_V200
6	No Mast	D2	-2	3.46 & 4.00			XM_D1_YM02_V346
7	No Mast	D2	-2	4.47			XM_D1_YM02_V447
8	No Mast	D2	-2	4.90			XM_D1_YM02_V490
9	No Mast	D2	2	2.00 & 2.83			XM_D1_Y02_V200
10	No Mast	D2	2	3.46 & 4.00			XM_D1_Y02_V346
11	No Mast	D2	2	4.47			XM_D1_Y02_V447
12	No Mast	D2	2	4.90			XM_D1_Y02_V490
13	No Mast	D2	4	2.00 & 2.83			XM_D1_Y04_V200
14	No Mast	D2	4	3.46 & 4.00			XM_D1_Y04_V346
15	No Mast	D2	4	4.47			XM_D1_Y04_V447
16	No Mast	D2	4	4.90			XM_D1_Y04_V490
17	No Mast	D2	6	2.00 & 2.83			XM_D1_Y06_V200
18	No Mast	D2	6	3.46 & 4.00			XM_D1_Y06_V346
19	No Mast	D2	6	4.47			XM_D1_Y06_V447
20	No Mast	D2	6	4.90			XM_D1_Y06_V490
21	No Mast	D2	8	2.00 & 2.83			XM_D1_Y08_V200
22	No Mast	D2	8	3.46 & 4.00			XM_D1_Y08_V346
23	No Mast	D2	10	2.00 & 2.83			XM_D1_Y10_V200
24	Old Mast	D1	0	2.00 & 2.83			OM_D1_Y00_V200
25	Old Mast	D1	0	3.46 & 4.00			OM_D1_Y00_V346
26	Old Mast	D1	0	4.47			OM_D1_Y00_V447
27	Old Mast	D1	0	4.90			OM_D1_Y00_V490
28	Old Mast	D1	-2	2.00 & 2.83			OM_D1_YM02_V200
29	Old Mast	D1	-2	3.46 & 4.00			OM_D1_YM02_V346
30	Old Mast	D1	-2	4.47			OM_D1_YM02_V447
31	Old Mast	D1	-2	4.90			OM_D1_YM02_V490
32	Old Mast	D1	2	2.00 & 2.83			OM_D1_Y02_V200
33	Old Mast	D1	2	3.46 & 4.00			OM_D1_Y02_V346
34	Old Mast	D1	2	4.47			OM_D1_Y02_V447
35	Old Mast	D1	2	4.90			OM_D1_Y02_V490
36	Old Mast	D1	4	2.00 & 2.83			OM_D1_Y04_V200
37	Old Mast	D1	4	3.46 & 4.00			OM_D1_Y04_V346
38	Old Mast	D1	4	4.47			OM_D1_Y04_V447
100	Old Mast	D1	4	4.90			OM_D1_Y04_V490
101	Old Mast	D1	6	2.00 & 2.83			OM_D1_Y06_V200
102	Old Mast	D1	6	3.46 & 4.00			OM_D1_Y06_V346
103	Old Mast	D1	6	4.47			OM_D1_Y06_V447
104	Old Mast	D1	6	4.90			OM_D1_Y06_V490
105	Old Mast	D1	8	2.00 & 2.83			OM_D1_Y08_V200
106	Old Mast	D1	8	3.46 & 4.00			OM_D1_Y08_V346
107	Old Mast	D1	10	2.00 & 2.83			OM_D1_Y10_V200
108	Old Mast	D2	0	2.00 & 2.83			OM_D2_Y00_V200
109	Old Mast	D2	0	3.46 & 4.00			OM_D2_Y00_V346
110	Old Mast	D2	0	4.47			OM_D2_Y00_V447
111	Old Mast	D2	0	4.90			OM_D2_Y00_V490

Run Number	Model Configuration	Draft Depth	Yaw (Deg)	Carriage Speed (m/s)	Air Flow	Flap (Deg)	Data 'File Name'
112	Old Mast	D2	-2	2.00 & 2.83			OM_D2_YM02_V200
113	Old Mast	D2	-2	3.46 & 4.00			OM_D2_YM02_V346
114	Old Mast	D2	-2	4.47			OM_D2_YM02_V447
115	Old Mast	D2	-2	4.90			OM_D2_YM02_V490
116	Old Mast	D2	2	2.00 & 2.83			OM_D2_Y02_V200
117	Old Mast	D2	2	3.46 & 4.00			OM_D2_Y02_V346
118	Old Mast	D2	2	4.47			OM_D2_Y02_V447
119	Old Mast	D2	2	4.90			OM_D2_Y02_V490
120	Old Mast	D2	4	2.00 & 2.83			OM_D2_Y04_V200
121	Old Mast	D2	4	3.46 & 4.00			OM_D2_Y04_V346
122	Old Mast	D2	4	4.47			OM_D2_Y04_V447
123	Old Mast	D2	4	4.90			OM_D2_Y04_V490
124	Old Mast	D2	6	2.00 & 2.83			OM_D2_Y06_V200
125	Old Mast	D2	6	3.46 & 4.00			OM_D2_Y06_V346
126	Old Mast	D2	8	2.00 & 2.83			OM_D2_Y08_V200
127	Old Mast	D2	10	2.00 & 2.83			OM_D2_Y10_V200
128	Old Mast	D3	0	2.00 & 2.83			OM_D3_Y00_V200
129	Old Mast	D3	0	3.46 & 4.00			OM_D3_Y00_V346
130	Old Mast	D3	0	4.47			OM_D3_Y00_V447
131	Old Mast	D3	0	4.90			OM_D3_Y00_V490
132	Old Mast	D3	-2	2.00 & 2.83			OM_D3_YM02_V200
133	Old Mast	D3	-2	3.46 & 4.00			OM_D3_YM02_V346
134	Old Mast	D3	-2	4.47			OM_D3_YM02_V447
135	Old Mast	D3	-2	4.90			OM_D3_YM02_V490
136	Old Mast	D3	2	2.00 & 2.83			OM_D3_Y02_V200
137	Old Mast	D3	2	3.46 & 4.00			OM_D3_Y02_V346
138	Old Mast	D3	2	4.47			OM_D3_Y02_V447
139	Old Mast	D3	2	4.90			OM_D3_Y02_V490
140	Old Mast	D3	4	2.00 & 2.83			OM_D3_Y04_V200
141	Old Mast	D3	4	3.46 & 4.00			OM_D3_Y04_V346
142	Old Mast	D3	6	2.00 & 2.83			OM_D3_Y06_V200
143	Old Mast	D3	8	2.00 & 2.83			OM_D3_Y08_V200
144	New Mast, No Air	D1	0	2.00 & 2.83	Q0		NM_D1_Y00_V200_Q0
145	New Mast, Low Air	D1	0	2.00 & 2.83	Q1		NM_D1_Y00_V200_Q1
146	New Mast, High Air	D1	0	2.00 & 2.83	Q2		NM_D1_Y00_V200_Q2
147	New Mast, No Air	D1	0	3.46 & 4.00	Q0		NM_D1_Y00_V346_Q0
148	New Mast, Low Air	D1	0	3.46 & 4.00	Q1		NM_D1_Y00_V346_Q1
149	New Mast, High Air	D1	0	3.46 & 4.00	Q2		NM_D1_Y00_V346_Q2
150	New Mast, No Air	D1	0	4.47	Q0		NM_D1_Y00_V447_Q0
151	New Mast, Low Air	D1	0	4.47	Q1		NM_D1_Y00_V447_Q1
152	New Mast, High Air	D1	0	4.47	Q2		NM_D1_Y00_V447_Q2
153	New Mast, No Air	D1	0	4.90	Q0		NM_D1_Y00_V490_Q0
154	New Mast, Low Air	D1	0	4.90	Q1		NM_D1_Y00_V490_Q1
155	New Mast, High Air	D1	0	4.90	Q2		NM_D1_Y00_V490_Q2
156	New Mast, No Air	D1	-2	2.00 & 2.83	Q0		NM_D1_YM02_V200_Q0
157	New Mast, Low Air	D1	-2	2.00 & 2.83	Q1		NM_D1_YM02_V200_Q1
158	New Mast, High Air	D1	-2	2.00 & 2.83	Q2		NM_D1_YM02_V200_Q2
159	New Mast, No Air	D1	-2	3.46 & 4.00	Q0		NM_D1_YM02_V346_Q0
160	New Mast, Low Air	D1	-2	3.46 & 4.00	Q1		NM_D1_YM02_V346_Q1
161	New Mast, High Air	D1	-2	3.46 & 4.00	Q2		NM_D1_YM02_V346_Q2

Run Number	Model Configuration	Draft Depth	Yaw (Deg)	Carriage Speed (m/s)	Air Flow	Flap (Deg)	Data 'File Name'
162	New Mast, No Air	D1	-2	4.47	Q0		NM_D1_YM02_V447_Q0
163	New Mast, Low Air	D1	-2	4.47	Q1		NM_D1_YM02_V447_Q1
164	New Mast, High Air	D1	-2	4.47	Q2		NM_D1_YM02_V447_Q2
165	New Mast, No Air	D1	-2	4.90	Q0		NM_D1_YM02_V490_Q0
166	New Mast, Low Air	D1	-2	4.90	Q1		NM_D1_YM02_V490_Q1
167	New Mast, High Air	D1	-2	4.90	Q2		NM_D1_YM02_V490_Q2
168	New Mast, No Air	D1	2	2.00 & 2.83	Q0		NM_D1_Y02_V200_Q0
169	New Mast, Low Air	D1	2	2.00 & 2.83	Q1		NM_D1_Y02_V200_Q1
170	New Mast, High Air	D1	2	2.00 & 2.83	Q2		NM_D1_Y02_V200_Q2
171	New Mast, No Air	D1	2	3.46 & 4.00	Q0		NM_D1_Y02_V346_Q0
172	New Mast, Low Air	D1	2	3.46 & 4.00	Q1		NM_D1_Y02_V346_Q1
173	New Mast, High Air	D1	2	3.46 & 4.00	Q2		NM_D1_Y02_V346_Q2
174	New Mast, No Air	D1	2	4.47	Q0		NM_D1_Y02_V447_Q0
175	New Mast, Low Air	D1	2	4.47	Q1		NM_D1_Y02_V447_Q1
176	New Mast, High Air	D1	2	4.47	Q2		NM_D1_Y02_V447_Q2
177	New Mast, No Air	D1	2	4.90	Q0		NM_D1_Y02_V490_Q0
178	New Mast, Low Air	D1	2	4.90	Q1		NM_D1_Y02_V490_Q1
179	New Mast, High Air	D1	2	4.90	Q2		NM_D1_Y02_V490_Q2
180	New Mast, No Air	D1	4	2.00 & 2.83	Q0		NM_D1_Y04_V200_Q0
181	New Mast, Low Air	D1	4	2.00 & 2.83	Q1		NM_D1_Y04_V200_Q1
182	New Mast, High Air	D1	4	2.00 & 2.83	Q2		NM_D1_Y04_V200_Q2
183	New Mast, No Air	D1	4	3.46 & 4.00	Q0		NM_D1_Y04_V346_Q0
184	New Mast, Low Air	D1	4	3.46 & 4.00	Q1		NM_D1_Y04_V346_Q1
185	New Mast, High Air	D1	4	3.46 & 4.00	Q2		NM_D1_Y04_V346_Q2
186	New Mast, No Air	D1	4	4.47	Q0		NM_D1_Y04_V447_Q0
187	New Mast, Low Air	D1	4	4.47	Q1		NM_D1_Y04_V447_Q1
188	New Mast, High Air	D1	4	4.47	Q2		NM_D1_Y04_V447_Q2
189	New Mast, No Air	D1	4	4.90	Q0		NM_D1_Y04_V490_Q0
190	New Mast, Low Air	D1	4	4.90	Q1		NM_D1_Y04_V490_Q1
191	New Mast, High Air	D1	4	4.90	Q2		NM_D1_Y04_V490_Q2
192	New Mast, No Air	D1	6	2.00 & 2.83	Q0		NM_D1_Y06_V200_Q0
193	New Mast, Low Air	D1	6	2.00 & 2.83	Q1		NM_D1_Y06_V200_Q1
194	New Mast, High Air	D1	6	2.00 & 2.83	Q2		NM_D1_Y06_V200_Q2
195	New Mast, No Air	D1	6	3.46 & 4.00	Q0		NM_D1_Y06_V346_Q0
196	New Mast, Low Air	D1	6	3.46 & 4.00	Q1		NM_D1_Y06_V346_Q1
197	New Mast, High Air	D1	6	3.46 & 4.00	Q2		NM_D1_Y06_V346_Q2
198	New Mast, No Air	D1	6	4.47	Q0		NM_D1_Y06_V447_Q0
199	New Mast, Low Air	D1	6	4.47	Q1		NM_D1_Y06_V447_Q1
200	New Mast, High Air	D1	6	4.47	Q2		NM_D1_Y06_V447_Q2
201	New Mast, No Air	D1	6	4.90	Q0		NM_D1_Y06_V490_Q0
202	New Mast, Low Air	D1	6	4.90	Q1		NM_D1_Y06_V490_Q1
203	New Mast, High Air	D1	6	4.90	Q2		NM_D1_Y06_V490_Q2
204	New Mast, No Air	D1	8	2.00 & 2.83	Q0		NM_D1_Y08_V200_Q0
205	New Mast, Low Air	D1	8	2.00 & 2.83	Q1		NM_D1_Y08_V200_Q1
206	New Mast, High Air	D1	8	2.00 & 2.83	Q2		NM_D1_Y08_V200_Q2
207	New Mast, No Air	D1	8	3.46 & 4.00	Q0		NM_D1_Y08_V346_Q0
208	New Mast, Low Air	D1	8	3.46 & 4.00	Q1		NM_D1_Y08_V346_Q1
209	New Mast, High Air	D1	8	3.46 & 4.00	Q2		NM_D1_Y08_V346_Q2
210	New Mast, No Air	D1	10	2.00 & 2.83	Q0		NM_D1_Y10_V200_Q0
211	New Mast, Low Air	D1	10	2.00 & 2.83	Q1		NM_D1_Y10_V200_Q1
212	New Mast, High Air	D1	10	2.00 & 2.83	Q2		NM_D1_Y10_V200_Q2

Run Number	Model Configuration	Draft Depth	Yaw (Deg)	Carriage Speed (m/s)	Air Flow	Flap (Deg)	Data 'File Name'
213	New Mast, No Air	D2	0	2.00 & 2.83	Q0		NM_D2_Y00_V200_Q0
214	New Mast, Low Air	D2	0	2.00 & 2.83	Q1		NM_D2_Y00_V200_Q1
215	New Mast, High Air	D2	0	2.00 & 2.83	Q2		NM_D2_Y00_V200_Q2
216	New Mast, No Air	D2	0	3.46 & 4.00	Q0		NM_D2_Y00_V346_Q0
217	New Mast, Low Air	D2	0	3.46 & 4.00	Q1		NM_D2_Y00_V346_Q1
218	New Mast, High Air	D2	0	3.46 & 4.00	Q2		NM_D2_Y00_V346_Q2
219	New Mast, No Air	D2	0	4.47	Q0		NM_D2_Y00_V447_Q0
220	New Mast, Low Air	D2	0	4.47	Q1		NM_D2_Y00_V447_Q1
221	New Mast, High Air	D2	0	4.47	Q2		NM_D2_Y00_V447_Q2
222	New Mast, No Air	D2	0	4.90	Q0		NM_D2_Y00_V490_Q0
223	New Mast, Low Air	D2	0	4.90	Q1		NM_D2_Y00_V490_Q1
224	New Mast, High Air	D2	0	4.90	Q2		NM_D2_Y00_V490_Q2
225	New Mast, No Air	D2	-2	2.00 & 2.83	Q0		NM_D2_YM02_V200_Q0
226	New Mast, Low Air	D2	-2	2.00 & 2.83	Q1		NM_D2_YM02_V200_Q1
227	New Mast, High Air	D2	-2	2.00 & 2.83	Q2		NM_D2_YM02_V200_Q2
228	New Mast, No Air	D2	-2	3.46 & 4.00	Q0		NM_D2_YM02_V346_Q0
229	New Mast, Low Air	D2	-2	3.46 & 4.00	Q1		NM_D2_YM02_V346_Q1
230	New Mast, High Air	D2	-2	3.46 & 4.00	Q2		NM_D2_YM02_V346_Q2
231	New Mast, No Air	D2	-2	4.47	Q0		NM_D2_YM02_V447_Q0
232	New Mast, Low Air	D2	-2	4.47	Q1		NM_D2_YM02_V447_Q1
233	New Mast, High Air	D2	-2	4.47	Q2		NM_D2_YM02_V447_Q2
234	New Mast, No Air	D2	-2	4.90	Q0		NM_D2_YM02_V490_Q0
235	New Mast, Low Air	D2	-2	4.90	Q1		NM_D2_YM02_V490_Q1
236	New Mast, High Air	D2	-2	4.90	Q2		NM_D2_YM02_V490_Q2
237	New Mast, No Air	D2	2	2.00 & 2.83	Q0		NM_D2_Y02_V200_Q0
238	New Mast, Low Air	D2	2	2.00 & 2.83	Q1		NM_D2_Y02_V200_Q1
239	New Mast, High Air	D2	2	2.00 & 2.83	Q2		NM_D2_Y02_V200_Q2
240	New Mast, No Air	D2	2	3.46 & 4.00	Q0		NM_D2_Y02_V346_Q0
241	New Mast, Low Air	D2	2	3.46 & 4.00	Q1		NM_D2_Y02_V346_Q1
242	New Mast, High Air	D2	2	3.46 & 4.00	Q2		NM_D2_Y02_V346_Q2
243	New Mast, No Air	D2	2	4.47	Q0		NM_D2_Y02_V447_Q0
244	New Mast, Low Air	D2	2	4.47	Q1		NM_D2_Y02_V447_Q1
245	New Mast, High Air	D2	2	4.47	Q2		NM_D2_Y02_V447_Q2
246	New Mast, No Air	D2	2	4.90	Q0		NM_D2_Y02_V490_Q0
247	New Mast, Low Air	D2	2	4.90	Q1		NM_D2_Y02_V490_Q1
248	New Mast, High Air	D2	2	4.90	Q2		NM_D2_Y02_V490_Q2
249	New Mast, No Air	D2	4	2.00 & 2.83	Q0		NM_D2_Y04_V200_Q0
250	New Mast, Low Air	D2	4	2.00 & 2.83	Q1		NM_D2_Y04_V200_Q1
251	New Mast, High Air	D2	4	2.00 & 2.83	Q2		NM_D2_Y04_V200_Q2
252	New Mast, No Air	D2	4	3.46 & 4.00	Q0		NM_D2_Y04_V346_Q0
253	New Mast, Low Air	D2	4	3.46 & 4.00	Q1		NM_D2_Y04_V346_Q1
254	New Mast, High Air	D2	4	3.46 & 4.00	Q2		NM_D2_Y04_V346_Q2
255	New Mast, No Air	D2	4	4.47	Q0		NM_D2_Y04_V447_Q0
256	New Mast, Low Air	D2	4	4.47	Q1		NM_D2_Y04_V447_Q1
257	New Mast, High Air	D2	4	4.47	Q2		NM_D2_Y04_V447_Q2
258	New Mast, No Air	D2	4	4.90	Q0		NM_D2_Y04_V490_Q0
259	New Mast, Low Air	D2	4	4.90	Q1		NM_D2_Y04_V490_Q1
260	New Mast, High Air	D2	4	4.90	Q2		NM_D2_Y04_V490_Q2
261	New Mast, No Air	D2	6	2.00 & 2.83	Q0		NM_D2_Y06_V200_Q0
262	New Mast, Low Air	D2	6	2.00 & 2.83	Q1		NM_D2_Y06_V200_Q1
263	New Mast, High Air	D2	6	2.00 & 2.83	Q2		NM_D2_Y06_V200_Q2

Run Number	Model Configuration	Draft Depth	Yaw (Deg)	Carriage Speed (m/s)	Air Flow	Flap (Deg)	Data 'File Name'
264	New Mast, No Air	D2	6	3.46 & 4.00	Q0		NM_D2_Y06_V346_Q0
265	New Mast, Low Air	D2	6	3.46 & 4.00	Q1		NM_D2_Y06_V346_Q1
266	New Mast, High Air	D2	6	3.46 & 4.00	Q2		NM_D2_Y06_V346_Q2
267	New Mast, No Air	D2	8	2.00 & 2.83	Q0		NM_D2_Y08_V200_Q0
268	New Mast, Low Air	D2	8	2.00 & 2.83	Q1		NM_D2_Y08_V200_Q1
269	New Mast, High Air	D2	8	2.00 & 2.83	Q2		NM_D2_Y08_V200_Q2
270	New Mast, No Air	D2	10	2.00 & 2.83	Q0		NM_D2_Y10_V200_Q0
271	New Mast, Low Air	D2	10	2.00 & 2.83	Q1		NM_D2_Y10_V200_Q1
272	New Mast, High Air	D2	10	2.00 & 2.83	Q2		NM_D2_Y10_V200_Q2
273	New Mast, No Air	D3	0	2.00 & 2.83	Q0		NM_D3_Y00_V200_Q0
274	New Mast, Low Air	D3	0	2.00 & 2.83	Q1		NM_D3_Y00_V200_Q1
275	New Mast, High Air	D3	0	2.00 & 2.83	Q2		NM_D3_Y00_V200_Q2
276	New Mast, No Air	D3	0	3.46 & 4.00	Q0		NM_D3_Y00_V346_Q0
277	New Mast, Low Air	D3	0	3.46 & 4.00	Q1		NM_D3_Y00_V346_Q1
278	New Mast, High Air	D3	0	3.46 & 4.00	Q2		NM_D3_Y00_V346_Q2
279	New Mast, No Air	D3	0	4.47	Q0		NM_D3_Y00_V447_Q0
280	New Mast, Low Air	D3	0	4.47	Q1		NM_D3_Y00_V447_Q1
281	New Mast, High Air	D3	0	4.47	Q2		NM_D3_Y00_V447_Q2
282	New Mast, No Air	D3	0	4.90	Q0		NM_D3_Y00_V490_Q0
283	New Mast, Low Air	D3	0	4.90	Q1		NM_D3_Y00_V490_Q1
284	New Mast, High Air	D3	0	4.90	Q2		NM_D3_Y00_V490_Q2
285	New Mast, No Air	D3	-2	2.00 & 2.83	Q0		NM_D3_YM02_V200_Q0
286	New Mast, Low Air	D3	-2	2.00 & 2.83	Q1		NM_D3_YM02_V200_Q1
287	New Mast, High Air	D3	-2	2.00 & 2.83	Q2		NM_D3_YM02_V200_Q2
288	New Mast, No Air	D3	-2	3.46 & 4.00	Q0		NM_D3_YM02_V346_Q0
289	New Mast, Low Air	D3	-2	3.46 & 4.00	Q1		NM_D3_YM02_V346_Q1
290	New Mast, High Air	D3	-2	3.46 & 4.00	Q2		NM_D3_YM02_V346_Q2
291	New Mast, No Air	D3	-2	4.47	Q0		NM_D3_YM02_V447_Q0
292	New Mast, Low Air	D3	-2	4.47	Q1		NM_D3_YM02_V447_Q1
293	New Mast, High Air	D3	-2	4.47	Q2		NM_D3_YM02_V447_Q2
294	New Mast, No Air	D3	-2	4.90	Q0		NM_D3_YM02_V490_Q0
295	New Mast, Low Air	D3	-2	4.90	Q1		NM_D3_YM02_V490_Q1
296	New Mast, High Air	D3	-2	4.90	Q2		NM_D3_YM02_V490_Q2
297	New Mast, No Air	D3	2	2.00 & 2.83	Q0		NM_D3_Y02_V200_Q0
298	New Mast, Low Air	D3	2	2.00 & 2.83	Q1		NM_D3_Y02_V200_Q1
299	New Mast, High Air	D3	2	2.00 & 2.83	Q2		NM_D3_Y02_V200_Q2
300	New Mast, No Air	D3	2	3.46 & 4.00	Q0		NM_D3_Y02_V346_Q0
301	New Mast, Low Air	D3	2	3.46 & 4.00	Q1		NM_D3_Y02_V346_Q1
302	New Mast, High Air	D3	2	3.46 & 4.00	Q2		NM_D3_Y02_V346_Q2
303	New Mast, No Air	D3	2	4.47	Q0		NM_D3_Y02_V447_Q0
304	New Mast, Low Air	D3	2	4.47	Q1		NM_D3_Y02_V447_Q1
305	New Mast, High Air	D3	2	4.47	Q2		NM_D3_Y02_V447_Q2
306	New Mast, No Air	D3	2	4.90	Q0		NM_D3_Y02_V490_Q0
307	New Mast, Low Air	D3	2	4.90	Q1		NM_D3_Y02_V490_Q1
308	New Mast, High Air	D3	2	4.90	Q2		NM_D3_Y02_V490_Q2
309	New Mast, No Air	D3	4	2.00 & 2.83	Q0		NM_D3_Y04_V200_Q0
310	New Mast, Low Air	D3	4	2.00 & 2.83	Q1		NM_D3_Y04_V200_Q1
311	New Mast, High Air	D3	4	2.00 & 2.83	Q2		NM_D3_Y04_V200_Q2
312	New Mast, No Air	D3	4	3.46 & 4.00	Q0		NM_D3_Y04_V346_Q0
313	New Mast, Low Air	D3	4	3.46 & 4.00	Q1		NM_D3_Y04_V346_Q1
314	New Mast, High Air	D3	4	3.46 & 4.00	Q2		NM_D3_Y04_V346_Q2

Run Number	Model Configuration	Draft Depth	Yaw (Deg)	Carriage Speed (m/s)	Air Flow	Flap (Deg)	Data 'File Name'
315	New Mast, No Air	D3	6	2.00 & 2.83	Q0		NM_D3_Y06_V200_Q0
316	New Mast, Low Air	D3	6	2.00 & 2.83	Q1		NM_D3_Y06_V200_Q1
317	New Mast, High Air	D3	6	2.00 & 2.83	Q2		NM_D3_Y06_V200_Q2
318	New Mast, No Air	D3	8	2.00 & 2.83	Q0		NM_D3_Y08_V200_Q0
319	New Mast, Low Air	D3	8	2.00 & 2.83	Q1		NM_D3_Y08_V200_Q1
320	New Mast, High Air	D3	8	2.00 & 2.83	Q2		NM_D3_Y08_V200_Q2
321	New Mast, Flap	D2	0	2.00 & 2.83		-2	NM_D2_Y00_V200_FM02
322	New Mast, Flap	D2	0	3.46 & 4.00		-2	NM_D2_Y00_V346_FM02
323	New Mast, Flap	D2	0	4.47		-2	NM_D2_Y00_V447_FM02
324	New Mast, Flap	D2	0	4.90		-2	NM_D2_Y00_V490_FM02
325	New Mast, Flap	D2	0	2.00 & 2.83		0	NM_D2_Y00_V200_F00
326	New Mast, Flap	D2	0	3.46 & 4.00		0	NM_D2_Y00_V346_F00
327	New Mast, Flap	D2	0	4.47		0	NM_D2_Y00_V447_F00
328	New Mast, Flap	D2	0	4.90		0	NM_D2_Y00_V490_F00
329	New Mast, Flap	D2	0	2.00 & 2.83		2	NM_D2_Y00_V200_F02
330	New Mast, Flap	D2	0	3.46 & 4.00		2	NM_D2_Y00_V346_F02
331	New Mast, Flap	D2	0	4.47		2	NM_D2_Y00_V447_F02
332	New Mast, Flap	D2	0	4.90		2	NM_D2_Y00_V490_F02
333	New Mast, Flap	D2	0	2.00 & 2.83		4	NM_D2_Y00_V200_F04
334	New Mast, Flap	D2	0	3.46 & 4.00		4	NM_D2_Y00_V346_F04
335	New Mast, Flap	D2	0	4.47		4	NM_D2_Y00_V447_F04
336	New Mast, Flap	D2	0	4.90		4	NM_D2_Y00_V490_F04
337	New Mast, Flap	D2	0	2.00 & 2.83		6	NM_D2_Y00_V200_F06
338	New Mast, Flap	D2	0	3.46 & 4.00		6	NM_D2_Y00_V346_F06
339	New Mast, Flap	D2	0	4.47		6	NM_D2_Y00_V447_F06
340	New Mast, Flap	D2	0	2.00 & 2.83		8	NM_D2_Y00_V200_F08
341	New Mast, Flap	D2	0	3.46 & 4.00		8	NM_D2_Y00_V346_F08
342	New Mast, Flap	D2	0	2.00 & 2.83		10	NM_D2_Y00_V200_F10
343	New Mast, Flap	D2	-2	2.00 & 2.83		-2	NM_D2_YM02_V200_FM02
344	New Mast, Flap	D2	-2	3.46 & 4.00		-2	NM_D2_YM02_V346_FM02
345	New Mast, Flap	D2	-2	4.47		-2	NM_D2_YM02_V447_FM02
346	New Mast, Flap	D2	-2	4.90		-2	NM_D2_YM02_V490_FM02
347	New Mast, Flap	D2	-2	2.00 & 2.83		0	NM_D2_YM02_V200_F00
348	New Mast, Flap	D2	-2	3.46 & 4.00		0	NM_D2_YM02_V346_F00
349	New Mast, Flap	D2	-2	4.47		0	NM_D2_YM02_V447_F00
350	New Mast, Flap	D2	-2	4.90		0	NM_D2_YM02_V490_F00
351	New Mast, Flap	D2	-2	2.00 & 2.83		2	NM_D2_YM02_V200_F02
352	New Mast, Flap	D2	-2	3.46 & 4.00		2	NM_D2_YM02_V346_F02
353	New Mast, Flap	D2	-2	4.47		2	NM_D2_YM02_V447_F02
354	New Mast, Flap	D2	-2	4.90		2	NM_D2_YM02_V490_F02
355	New Mast, Flap	D2	-2	2.00 & 2.83		4	NM_D2_YM02_V200_F04
356	New Mast, Flap	D2	-2	3.46 & 4.00		4	NM_D2_YM02_V346_F04
357	New Mast, Flap	D2	-2	4.47		4	NM_D2_YM02_V447_F04
358	New Mast, Flap	D2	-2	4.90		4	NM_D2_YM02_V490_F04
359	New Mast, Flap	D2	-2	2.00 & 2.83		6	NM_D2_YM02_V200_F06
360	New Mast, Flap	D2	-2	3.46 & 4.00		6	NM_D2_YM02_V346_F06
361	New Mast, Flap	D2	-2	4.47		6	NM_D2_YM02_V447_F06
362	New Mast, Flap	D2	-2	2.00 & 2.83		8	NM_D2_YM02_V200_F08
363	New Mast, Flap	D2	-2	3.46 & 4.00		8	NM_D2_YM02_V346_F08
364	New Mast, Flap	D2	-2	2.00 & 2.83		10	NM_D2_YM02_V200_F10

Run Number	Model Configuration	Draft Depth	Yaw (Deg)	Carriage Speed (m/s)	Air Flow	Flap (Deg)	Data 'File Name'
365	New Mast, Flap	D2	2	2.00 & 2.83		-2	NM_D2_Y02_V200_FM02
366	New Mast, Flap	D2	2	3.46 & 4.00		-2	NM_D2_Y02_V346_FM02
367	New Mast, Flap	D2	2	4.47		-2	NM_D2_Y02_V447_FM02
368	New Mast, Flap	D2	2	4.90		-2	NM_D2_Y02_V490_FM02
369	New Mast, Flap	D2	2	2.00 & 2.83		0	NM_D2_Y02_V200_F00
370	New Mast, Flap	D2	2	3.46 & 4.00		0	NM_D2_Y02_V346_F00
371	New Mast, Flap	D2	2	4.47		0	NM_D2_Y02_V447_F00
372	New Mast, Flap	D2	2	4.90		0	NM_D2_Y02_V490_F00
373	New Mast, Flap	D2	2	2.00 & 2.83		2	NM_D2_Y02_V200_F02
374	New Mast, Flap	D2	2	3.46 & 4.00		2	NM_D2_Y02_V346_F02
375	New Mast, Flap	D2	2	4.47		2	NM_D2_Y02_V447_F02
376	New Mast, Flap	D2	2	4.90		2	NM_D2_Y02_V490_F02
377	New Mast, Flap	D2	2	2.00 & 2.83		4	NM_D2_Y02_V200_F04
378	New Mast, Flap	D2	2	3.46 & 4.00		4	NM_D2_Y02_V346_F04
379	New Mast, Flap	D2	2	4.47		4	NM_D2_Y02_V447_F04
380	New Mast, Flap	D2	2	4.90		4	NM_D2_Y02_V490_F04
381	New Mast, Flap	D2	2	2.00 & 2.83		6	NM_D2_Y02_V200_F06
382	New Mast, Flap	D2	2	3.46 & 4.00		6	NM_D2_Y02_V346_F06
383	New Mast, Flap	D2	2	4.47		6	NM_D2_Y02_V447_F06
384	New Mast, Flap	D2	2	2.00 & 2.83		8	NM_D2_Y02_V200_F08
385	New Mast, Flap	D2	2	3.46 & 4.00		8	NM_D2_Y02_V346_F08
386	New Mast, Flap	D2	2	2.00 & 2.83		10	NM_D2_Y02_V200_F10
387	New Mast, Flap	D2	-2	2.00 & 2.83		-2	NM_D2_YM02_V200_FM02
388	New Mast, Flap	D2	-2	3.46 & 4.00		-2	NM_D2_YM02_V346_FM02
389	New Mast, Flap	D2	-2	4.47		-2	NM_D2_YM02_V447_FM02
390	New Mast, Flap	D2	-2	4.90		-2	NM_D2_YM02_V490_FM02
391	New Mast, Flap	D2	-2	2.00 & 2.83		0	NM_D2_YM02_V200_F00
392	New Mast, Flap	D2	-2	3.46 & 4.00		0	NM_D2_YM02_V346_F00
393	New Mast, Flap	D2	-2	4.47		0	NM_D2_YM02_V447_F00
394	New Mast, Flap	D2	-2	4.90		0	NM_D2_YM02_V490_F00
395	New Mast, Flap	D2	-2	2.00 & 2.83		2	NM_D2_YM02_V200_F02
396	New Mast, Flap	D2	-2	3.46 & 4.00		2	NM_D2_YM02_V346_F02
397	New Mast, Flap	D2	-2	4.47		2	NM_D2_YM02_V447_F02
398	New Mast, Flap	D2	-2	4.90		2	NM_D2_YM02_V490_F02
399	New Mast, Flap	D2	-2	2.00 & 2.83		4	NM_D2_YM02_V200_F04
400	New Mast, Flap	D2	-2	3.46 & 4.00		4	NM_D2_YM02_V346_F04
401	New Mast, Flap	D2	-2	4.47		4	NM_D2_YM02_V447_F04
402	New Mast, Flap	D2	-2	4.90		4	NM_D2_YM02_V490_F04
403	New Mast, Flap	D2	-2	2.00 & 2.83		6	NM_D2_YM02_V200_F06
404	New Mast, Flap	D2	-2	3.46 & 4.00		6	NM_D2_YM02_V346_F06
405	New Mast, Flap	D2	-2	4.47		6	NM_D2_YM02_V447_F06
406	New Mast, Flap	D2	-2	4.90		6	NM_D2_YM02_V490_F06
407	New Mast, Flap	D2	-2	2.00 & 2.83		8	NM_D2_YM02_V200_F08
408	New Mast, Flap	D2	-2	3.46 & 4.00		8	NM_D2_YM02_V346_F08
409	New Mast, Flap	D2	-2	4.47		8	NM_D2_YM02_V447_F08
410	New Mast, Flap	D2	-2	4.90		8	NM_D2_YM02_V490_F08
411	New Mast, Flap	D2	-2	2.00 & 2.83		10	NM_D2_YM02_V200_F10
412	New Mast, Flap	D2	-2	3.46 & 4.00		10	NM_D2_YM02_V346_F10
413	New Mast, Flap	D2	-2	4.47		10	NM_D2_YM02_V447_F10
414	New Mast, Flap	D2	-2	4.90		10	NM_D2_YM02_V490_F10

Run Number	Model Configuration	Draft Depth	Yaw (Deg)	Carriage Speed (m/s)	Air Flow	Flap (Deg)	Data 'File Name'
415	New Mast, Flap	D2	-2	2.00 & 2.83		12	NM_D2_YM02_V200_F12
416	New Mast, Flap	D2	-2	3.46 & 4.00		12	NM_D2_YM02_V346_F12
417	New Mast, Flap	D2	-2	4.47		12	NM_D2_YM02_V447_F12
418	New Mast, Flap	D2	-2	4.90		12	NM_D2_YM02_V490_F12
419	New Mast, Flap	D2	2	2.00 & 2.83		-2	NM_D2_Y02_V200_FM02
420	New Mast, Flap	D2	2	3.46 & 4.00		-2	NM_D2_Y02_V346_FM02
421	New Mast, Flap	D2	2	4.47		-2	NM_D2_Y02_V447_FM02
422	New Mast, Flap	D2	2	4.90		-2	NM_D2_Y02_V490_FM02
423	New Mast, Flap	D2	2	2.00 & 2.83		0	NM_D2_Y02_V200_F00
424	New Mast, Flap	D2	2	3.46 & 4.00		0	NM_D2_Y02_V346_F00
425	New Mast, Flap	D2	2	4.47		0	NM_D2_Y02_V447_F00
426	New Mast, Flap	D2	2	4.90		0	NM_D2_Y02_V490_F00
427	New Mast, Flap	D2	2	2.00 & 2.83		2	NM_D2_Y02_V200_F02
428	New Mast, Flap	D2	2	3.46 & 4.00		2	NM_D2_Y02_V346_F02
429	New Mast, Flap	D2	2	4.47		2	NM_D2_Y02_V447_F02
430	New Mast, Flap	D2	2	4.90		2	NM_D2_Y02_V490_F02
431	New Mast, Flap	D2	2	2.00 & 2.83		4	NM_D2_Y02_V200_F04
432	New Mast, Flap	D2	2	3.46 & 4.00		4	NM_D2_Y02_V346_F04
433	New Mast, Flap	D2	2	4.47		4	NM_D2_Y02_V447_F04
434	New Mast, Flap	D2	2	4.90		4	NM_D2_Y02_V490_F04
435	New Mast, Flap	D2	2	2.00 & 2.83		6	NM_D2_Y02_V200_F06
436	New Mast, Flap	D2	2	3.46 & 4.00		6	NM_D2_Y02_V346_F06
437	New Mast, Flap	D2	2	4.47		6	NM_D2_Y02_V447_F06
438	New Mast, Flap	D2	2	4.90		6	NM_D2_Y02_V490_F06
439	New Mast, Flap	D2	2	2.00 & 2.83		8	NM_D2_Y02_V200_F08
440	New Mast, Flap	D2	2	3.46 & 4.00		8	NM_D2_Y02_V346_F08
441	New Mast, Flap	D2	2	4.47		8	NM_D2_Y02_V447_F08
442	New Mast, Flap	D2	2	4.90		8	NM_D2_Y02_V490_F08
443	New Mast, Flap	D2	2	2.00 & 2.83		10	NM_D2_Y02_V200_F10
444	New Mast, Flap	D2	2	3.46 & 4.00		10	NM_D2_Y02_V346_F10
445	New Mast, Flap	D2	2	4.47		10	NM_D2_Y02_V447_F10
446	New Mast, Flap	D2	2	4.90		10	NM_D2_Y02_V490_F10
447	New Mast, Flap	D2	2	2.00 & 2.83		12	NM_D2_Y02_V200_F12
448	New Mast, Flap	D2	2	3.46 & 4.00		12	NM_D2_Y02_V346_F12
449	New Mast, Flap	D2	2	4.47		12	NM_D2_Y02_V447_F12
450	New Mast, Flap	D2	2	4.90		12	NM_D2_Y02_V490_F12

Appendix B

Drag Force Plots

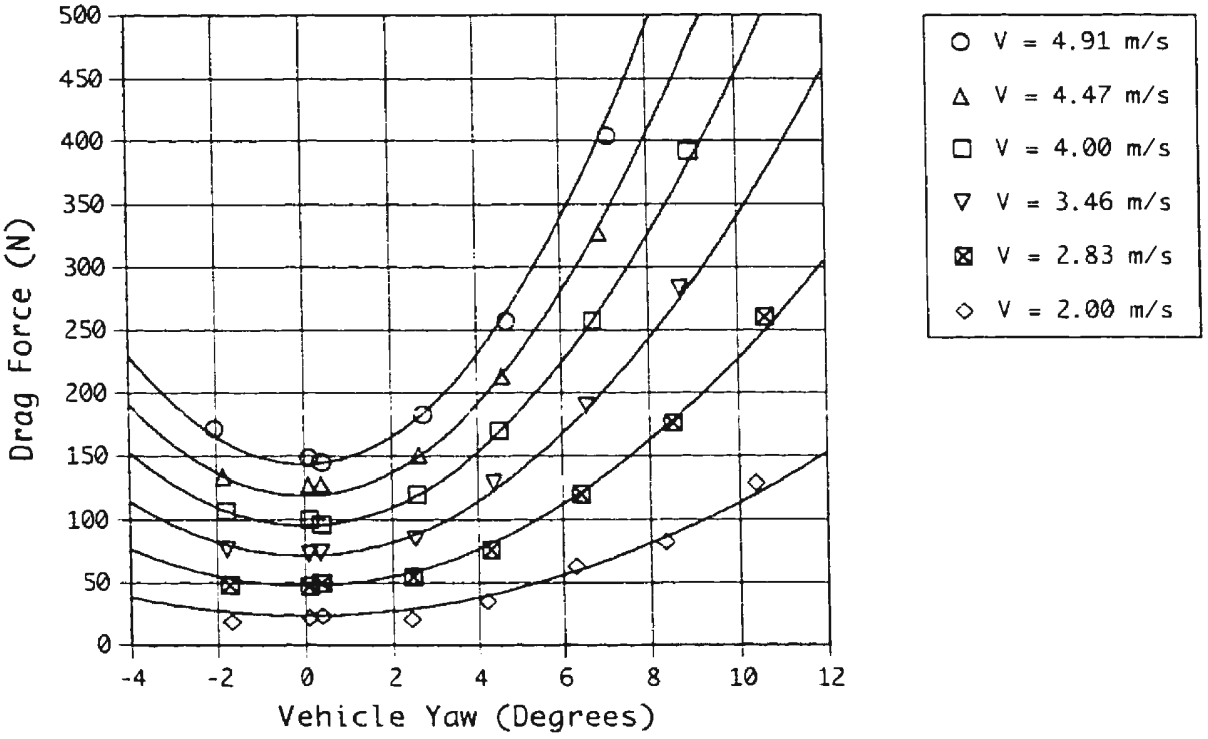

Figure B.01 - *Drag Force vs. Vehicle Yaw Angle; M0 (No Mast)*

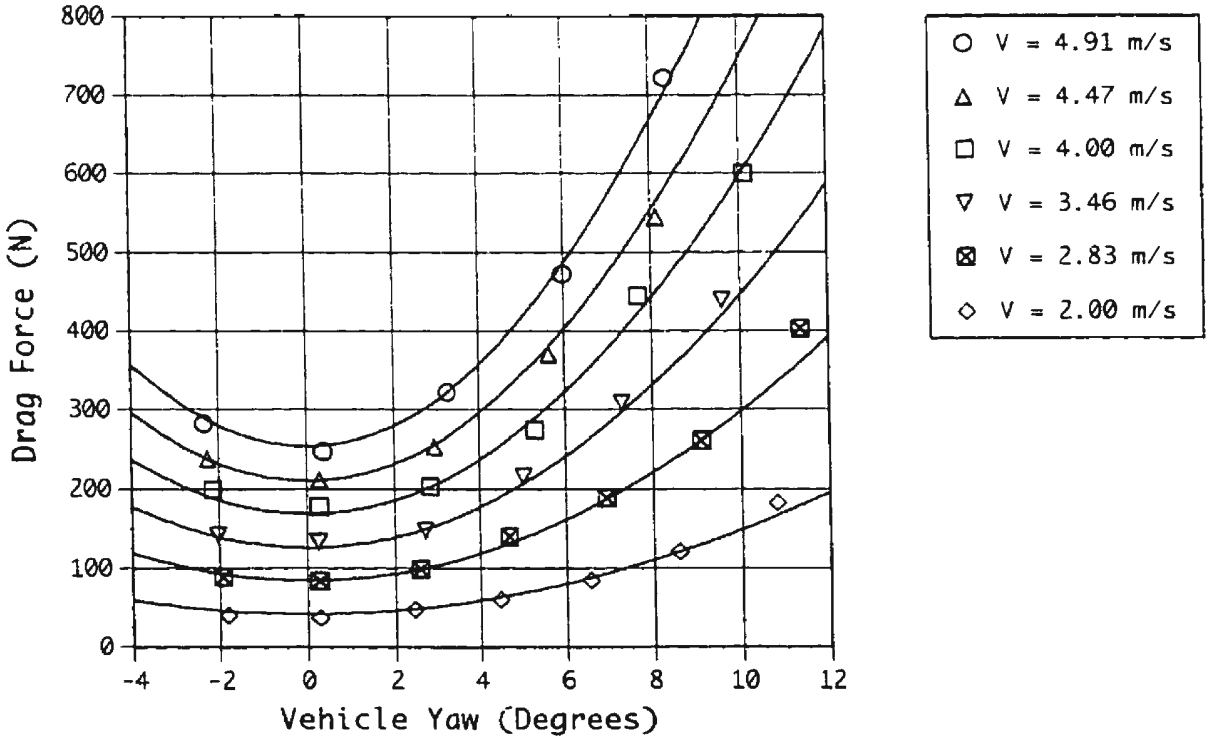

Figure B.02 - *Drag Force vs. Vehicle Yaw Angle; M1 @ D1*

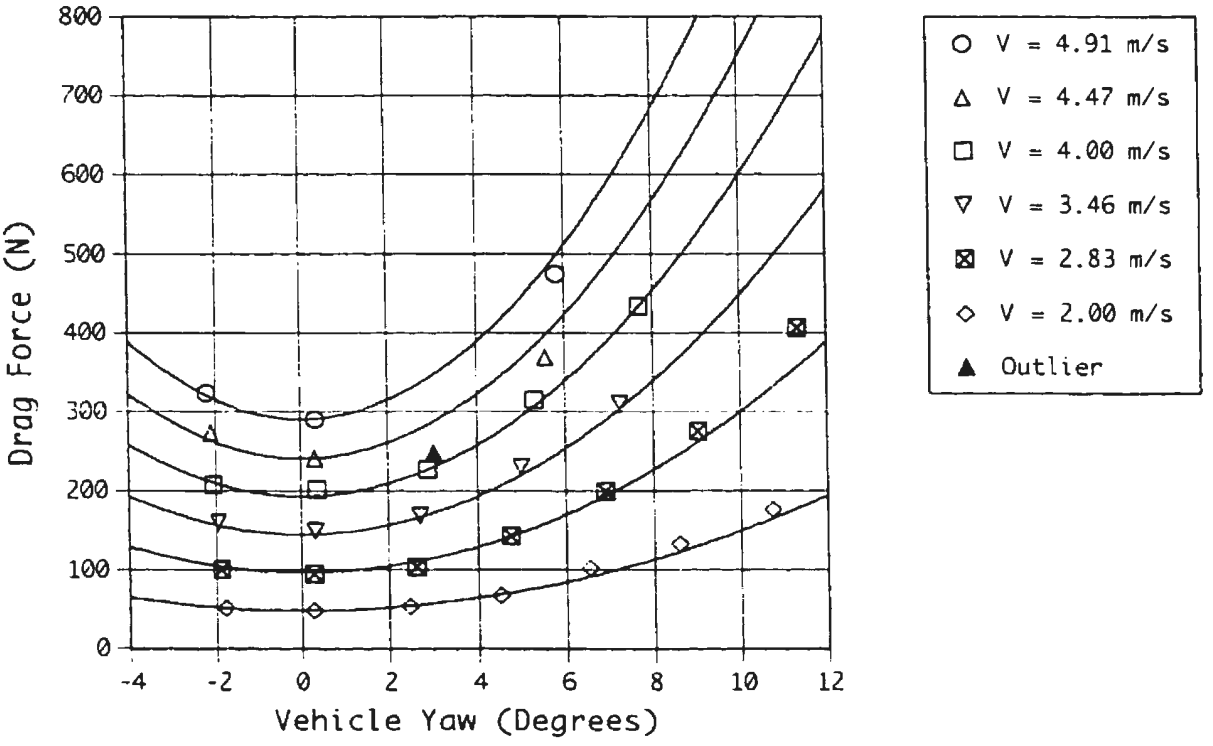

Figure B.03 - *Drag Force vs. Vehicle Yaw Angle; M1 @ D2*

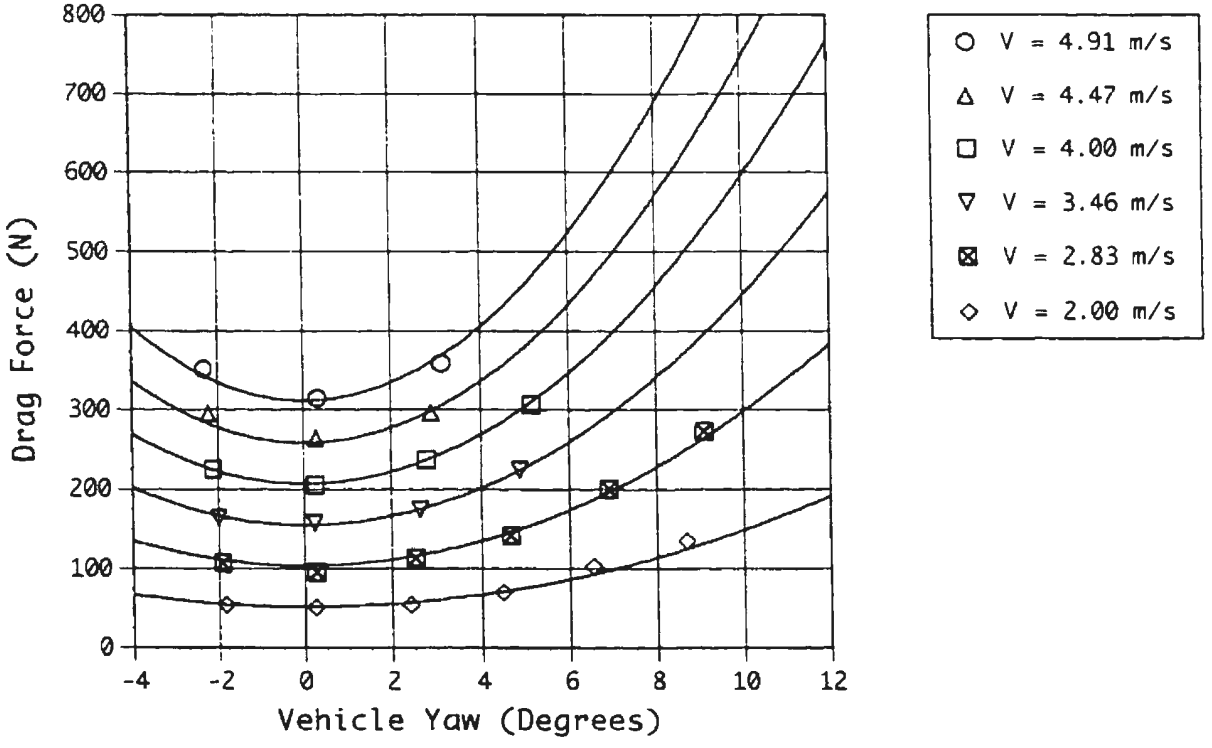

Figure B.04 - *Drag Force vs. Vehicle Yaw Angle; M1 @ D3*

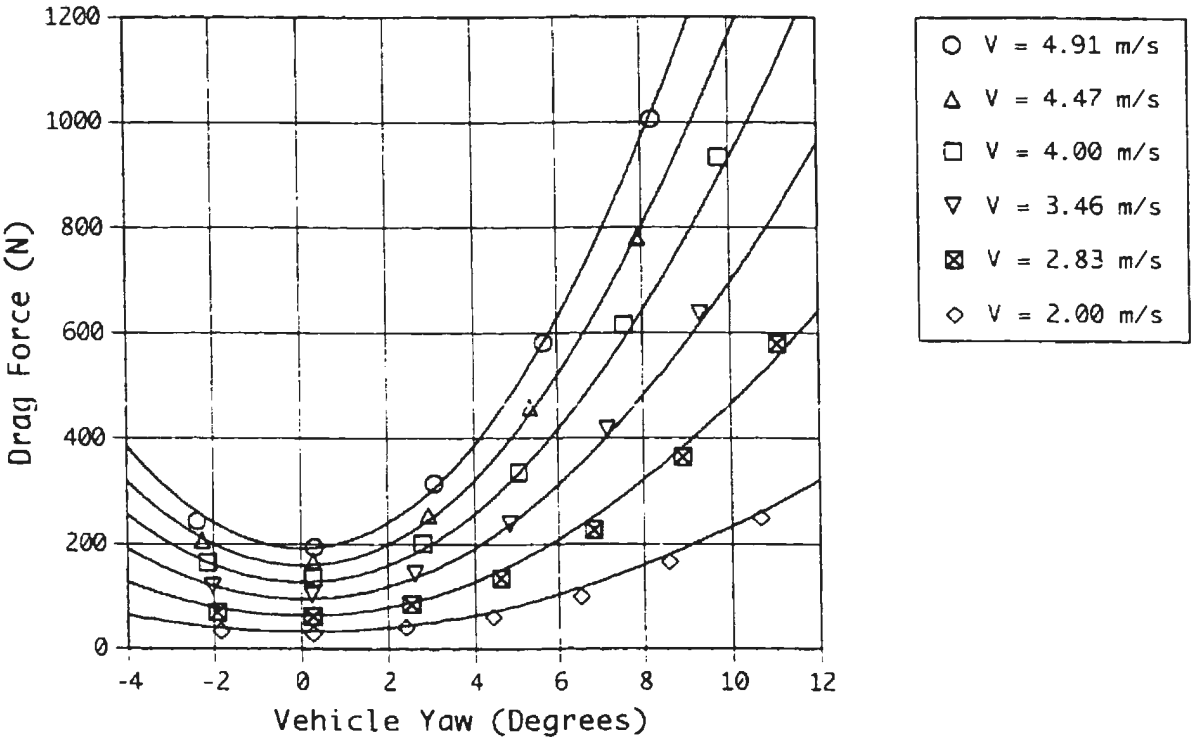

Figure B.05 - *Drag Force vs. Vehicle Yaw Angle; M2 @ D1*

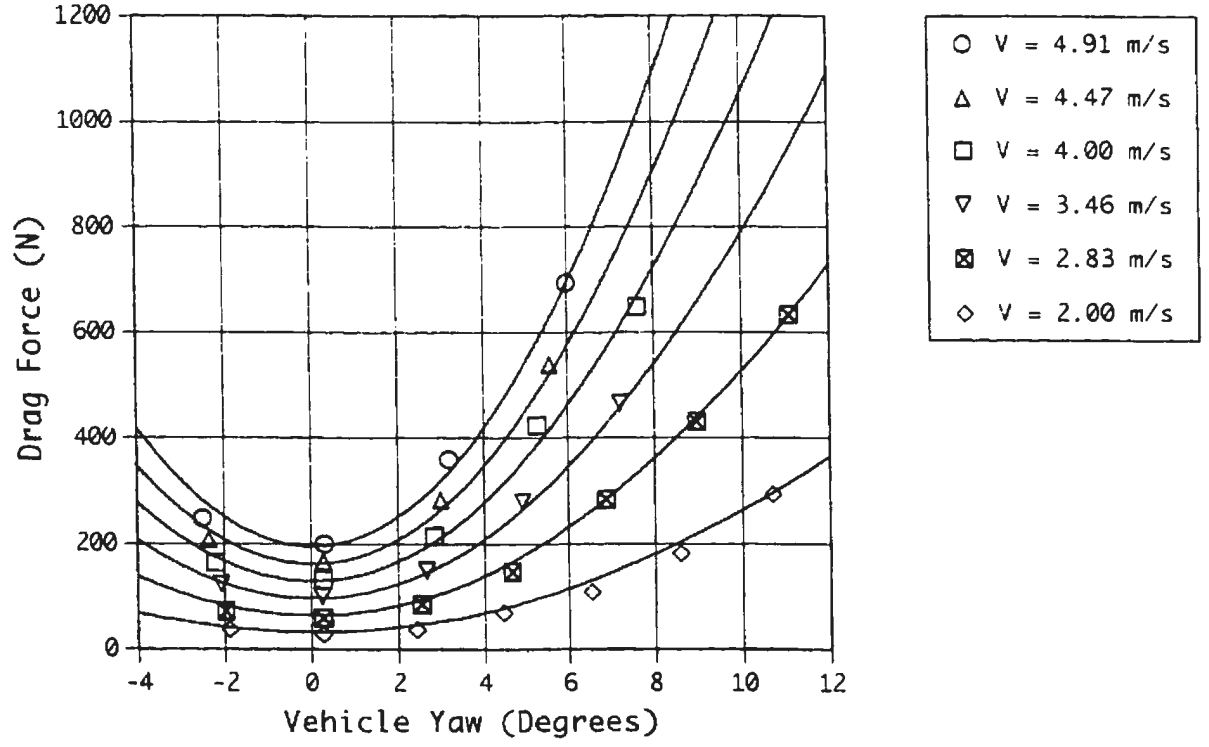

Figure B.06 - *Drag Force vs. Vehicle Yaw Angle; M2 @ D2*

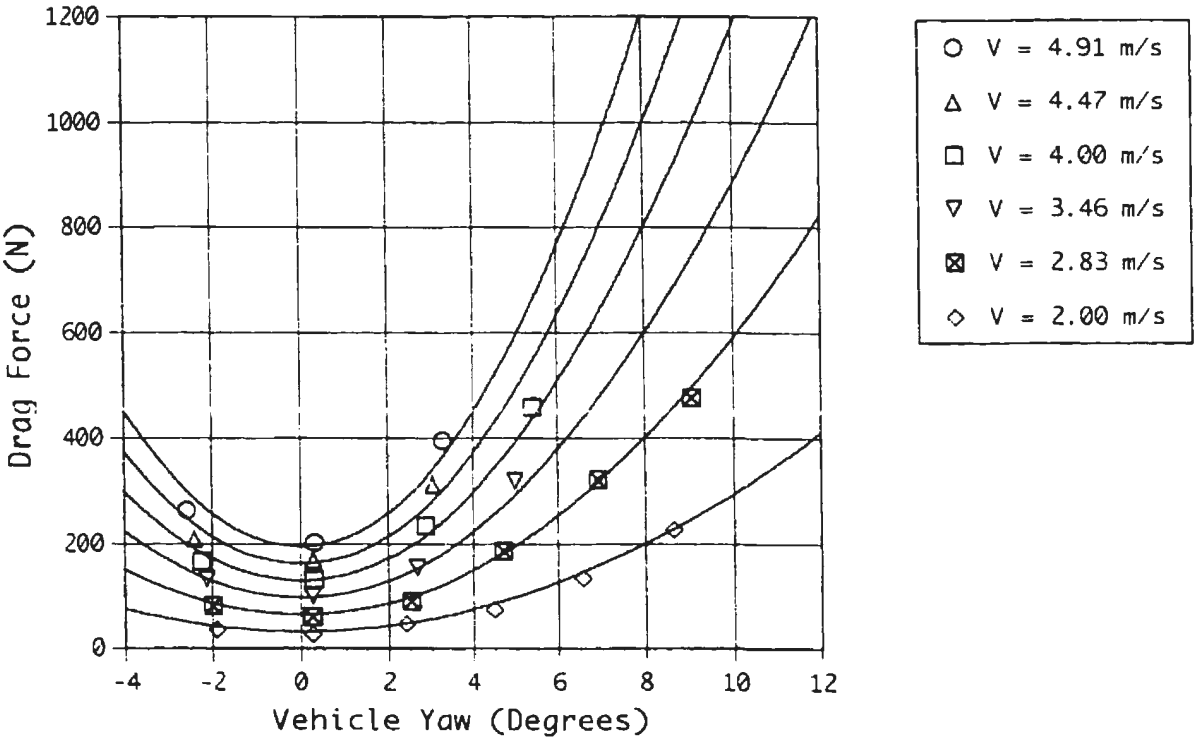

Figure B.07 - *Drag Force vs. Vehicle Yaw Angle; M2 @ D3*

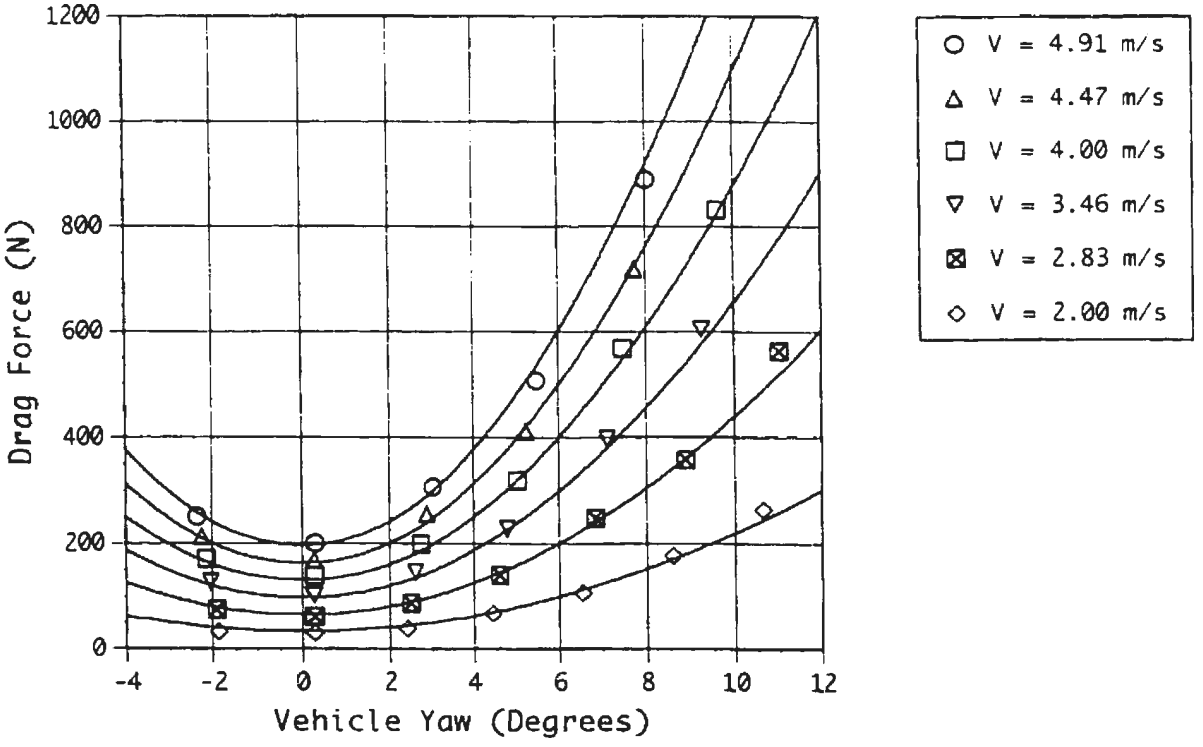

Figure B.08 - *Drag Force vs. Vehicle Yaw Angle; M2B @ D1*

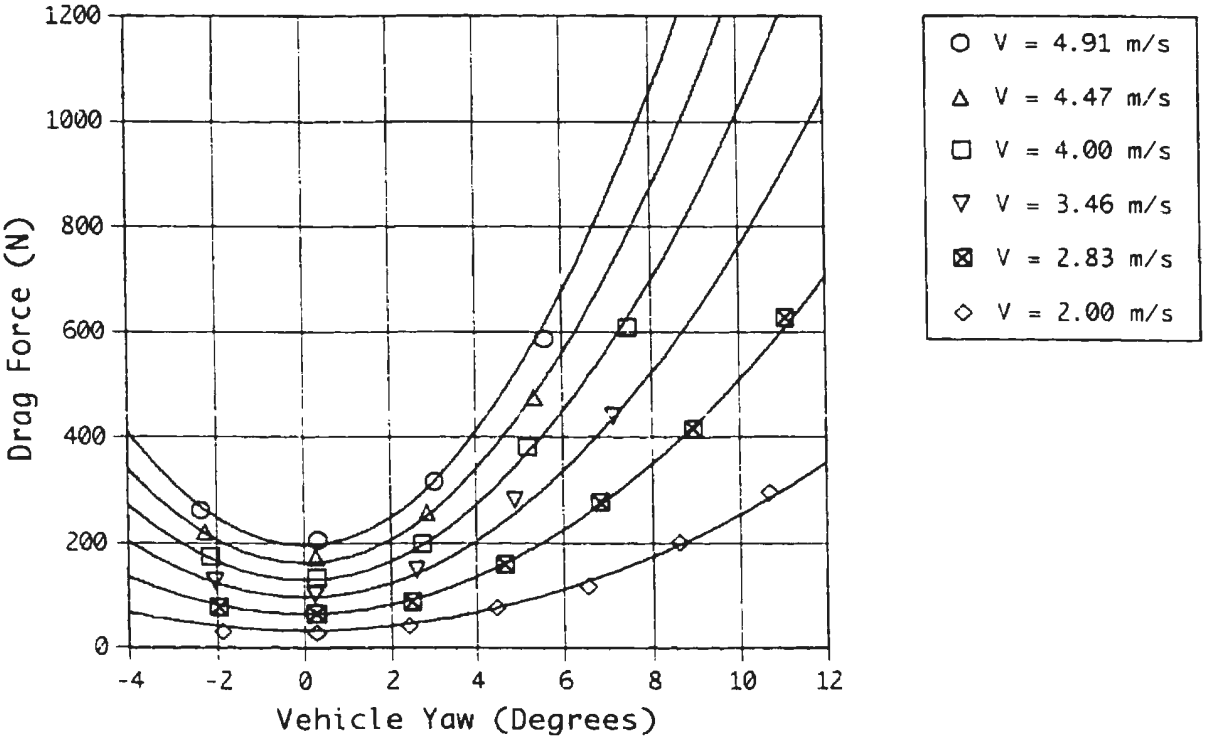

Figure B.09 - *Drag Force vs. Vehicle Yaw Angle; M2B @ D2*

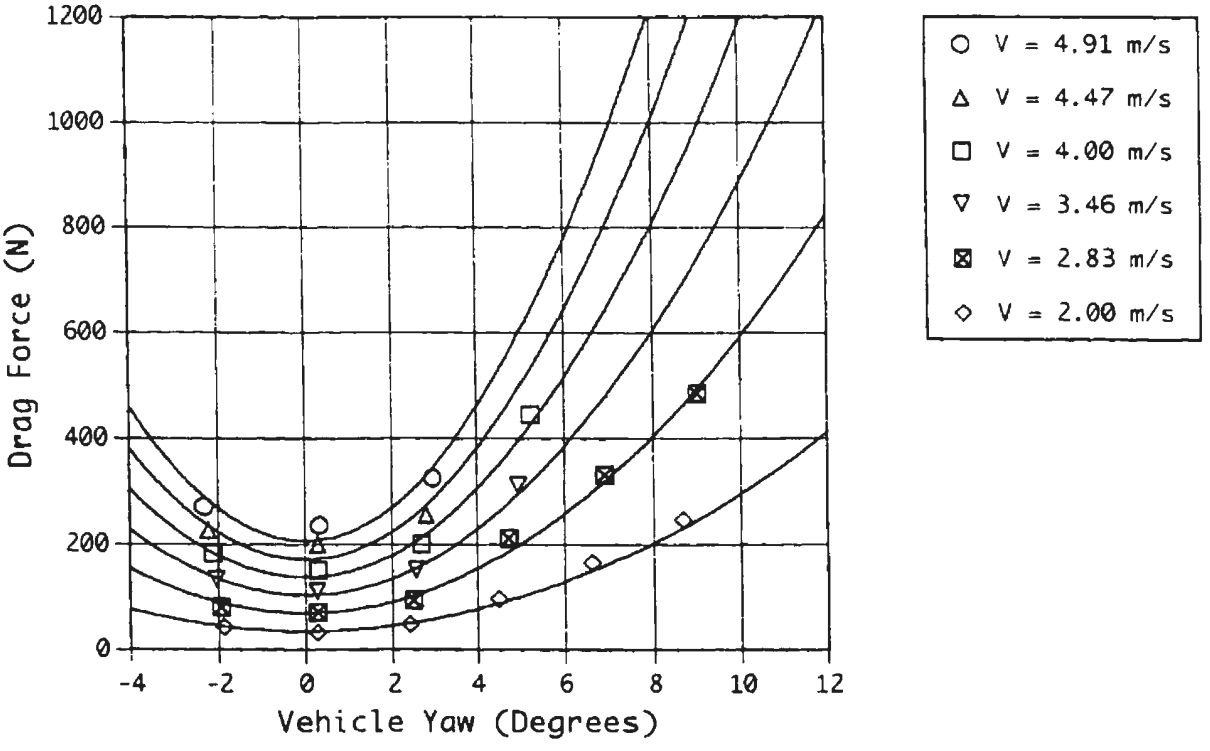

Figure B.10 - *Drag Force vs. Vehicle Yaw Angle; M2B @ D3*

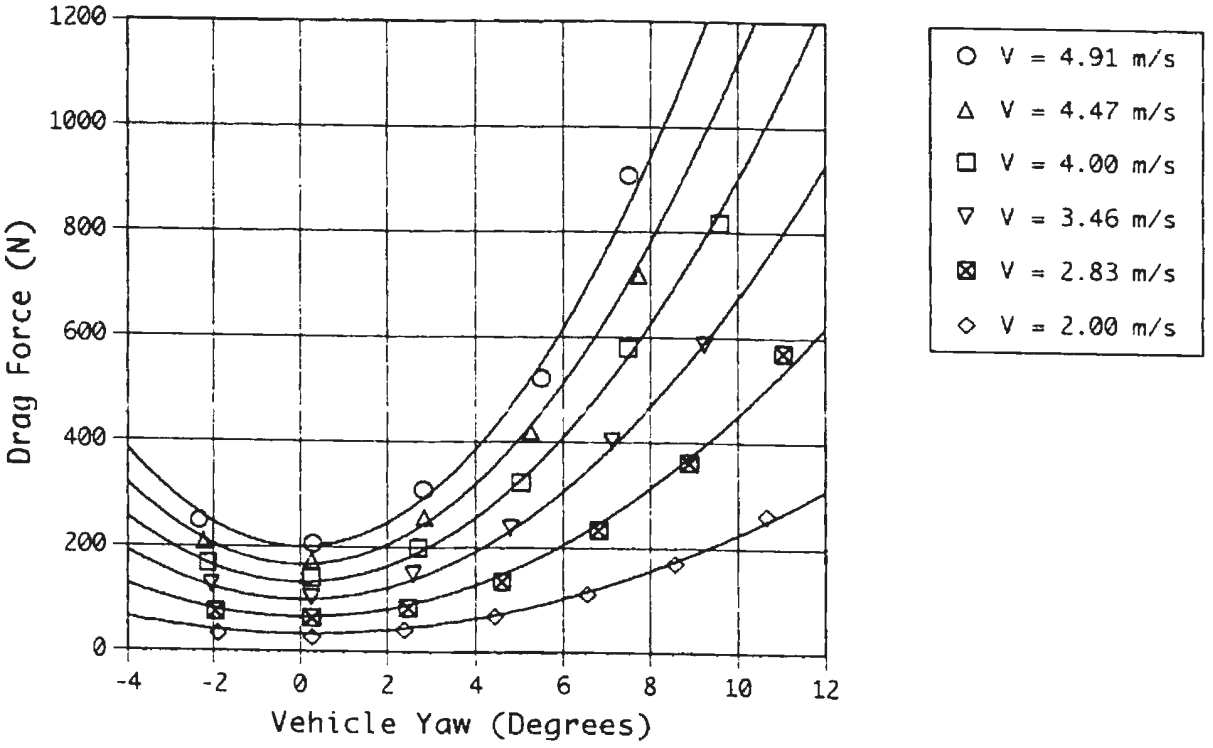

Figure B.11 - *Drag Force vs. Vehicle Yaw Angle; M2A @ D1*

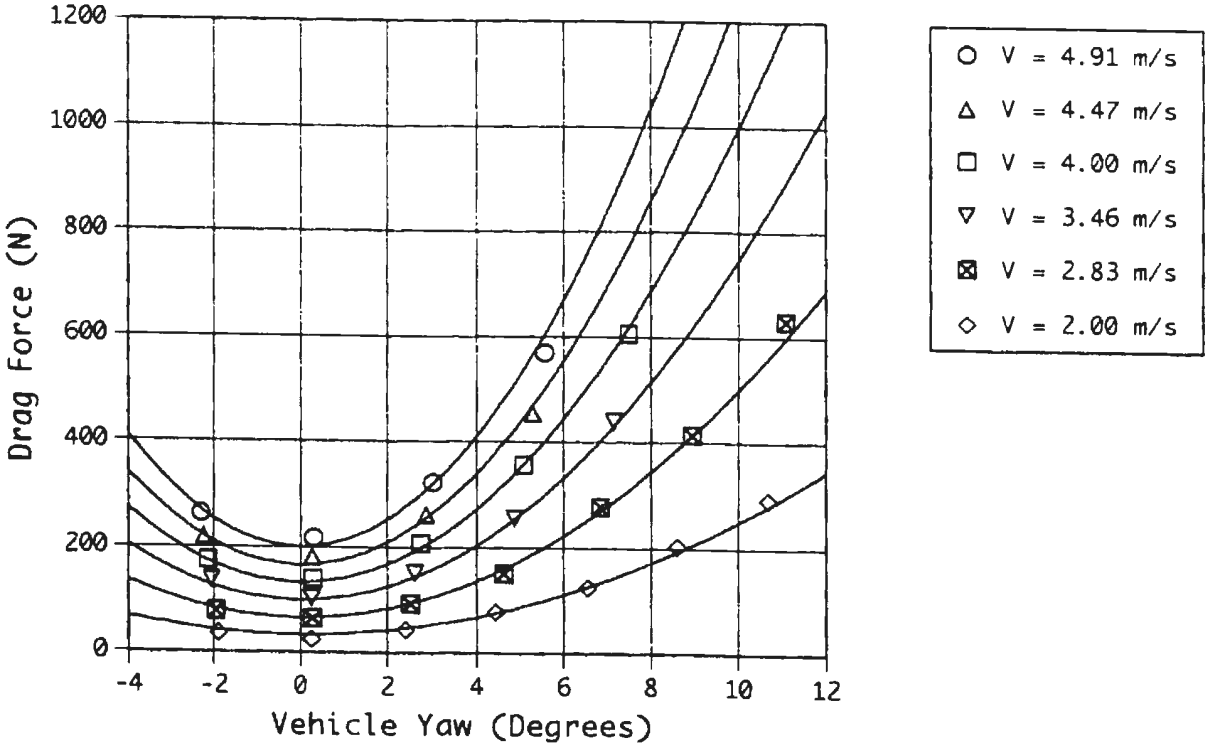

Figure B.12 - *Drag Force vs. Vehicle Yaw Angle; M2A @ D2*

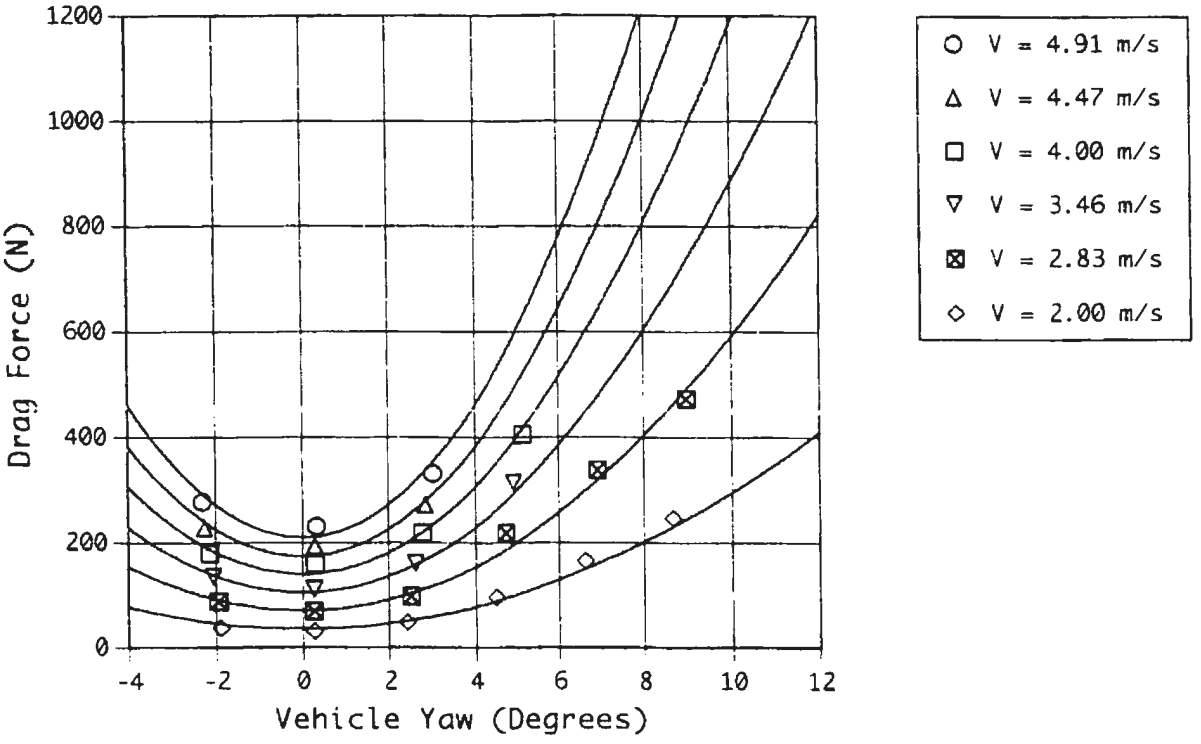

Figure B.13 - *Drag Force vs. Vehicle Yaw Angle; M2A @ D3*

Appendix C

Lift Force Plots

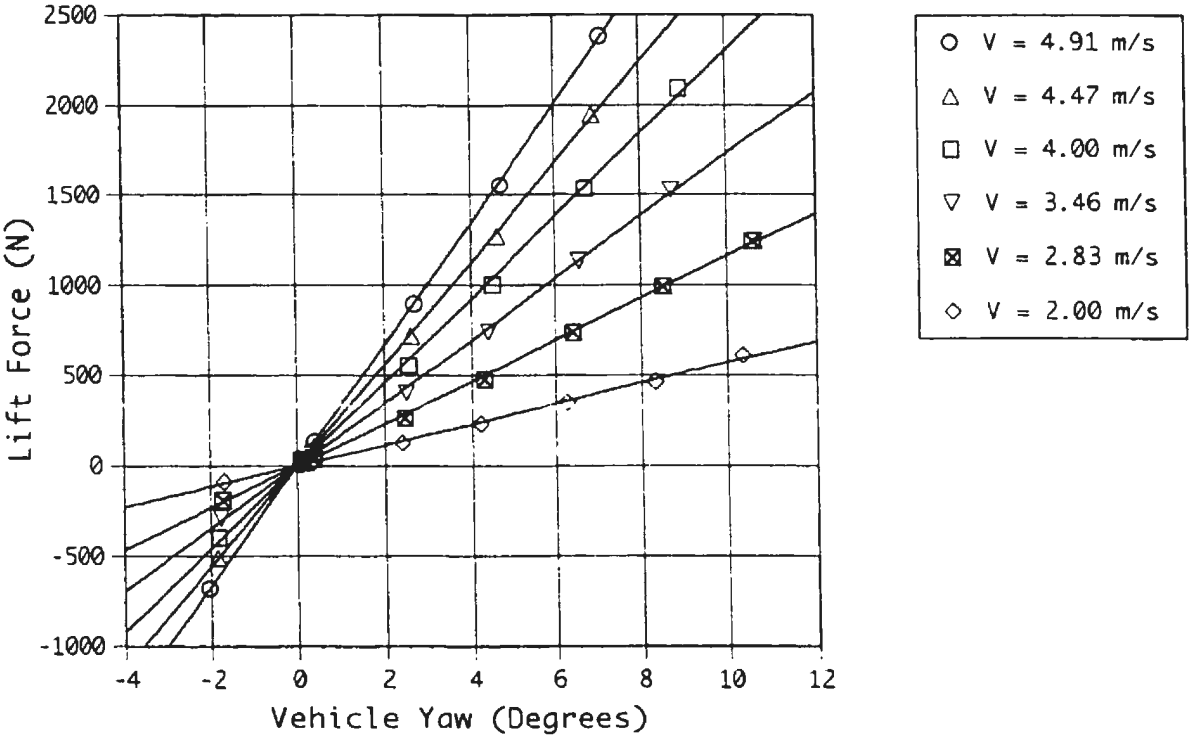

Figure C.01 - *Lift Force vs. Vehicle Yaw Angle; M0 (No Mast)*

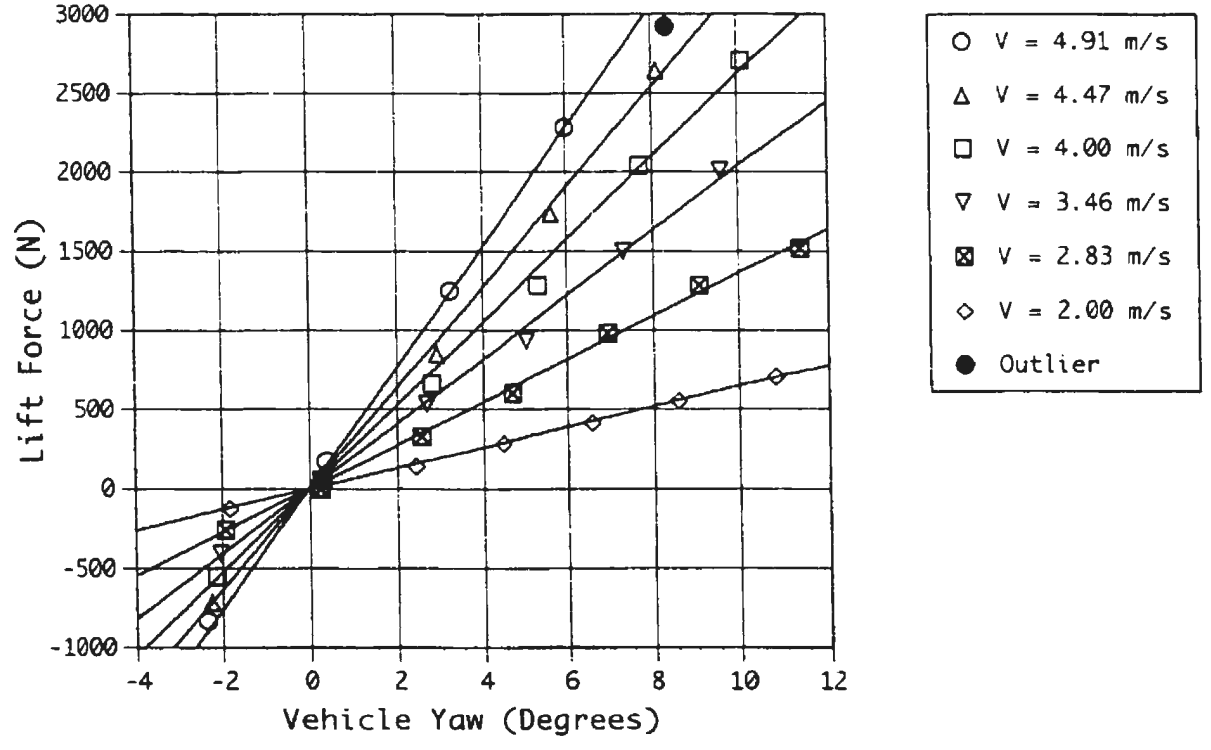

Figure C.02 - *Lift Force vs. Vehicle Yaw Angle; M1 @ D1*

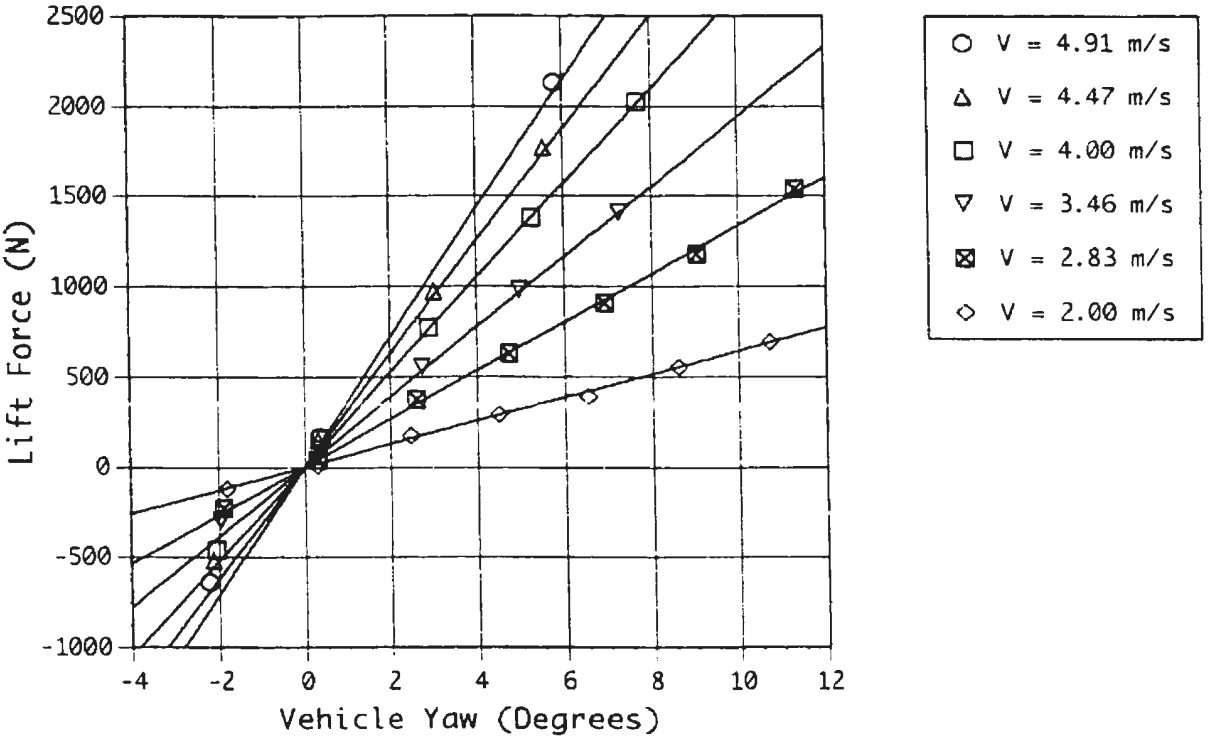

Figure C.03 - *Lift Force vs. Vehicle Yaw Angle; M1 @ D2*

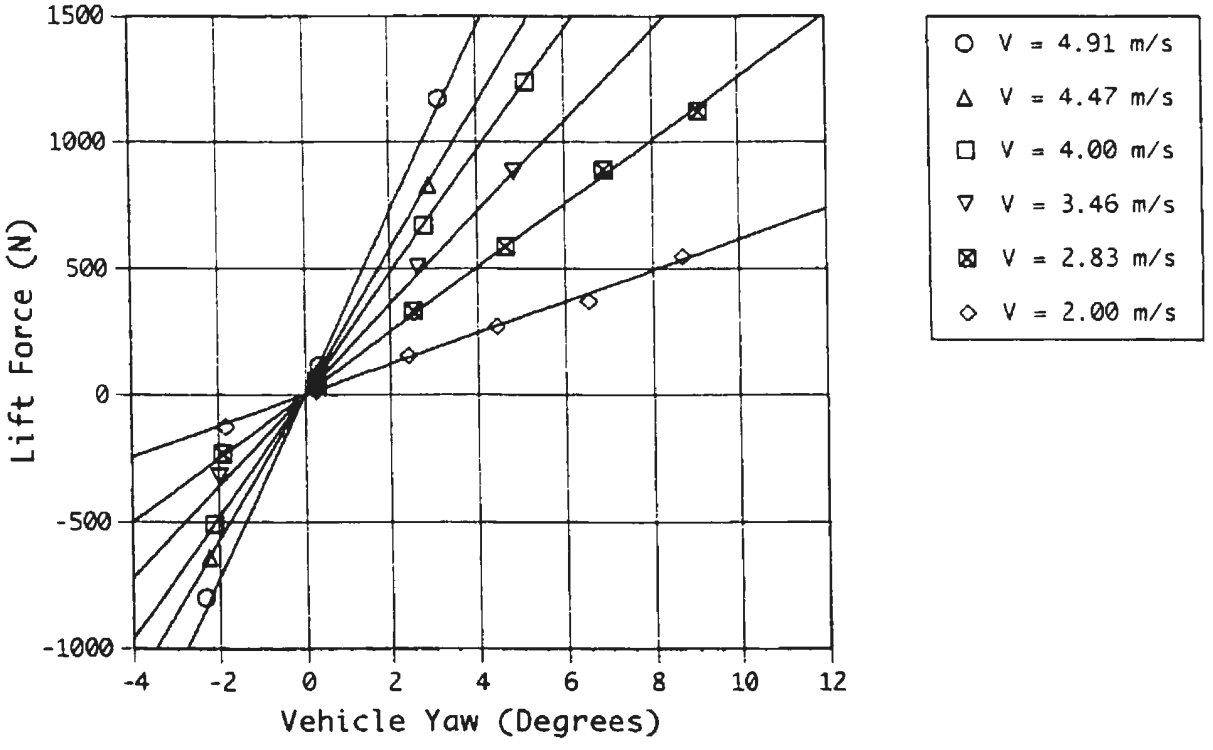

Figure C.04 - *Lift Force vs. Vehicle Yaw Angle; M1 @ D3*

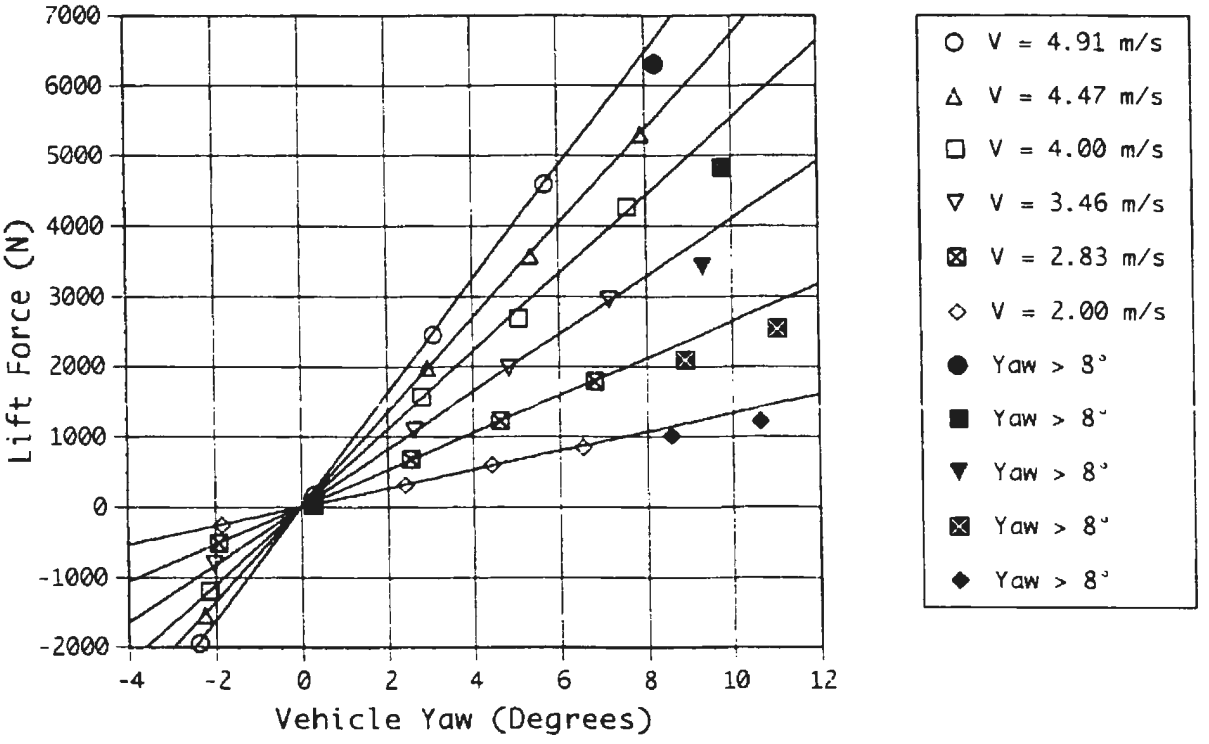

Figure C.05 - *Lift Force vs. Vehicle Yaw Angle; M2 @ D1*

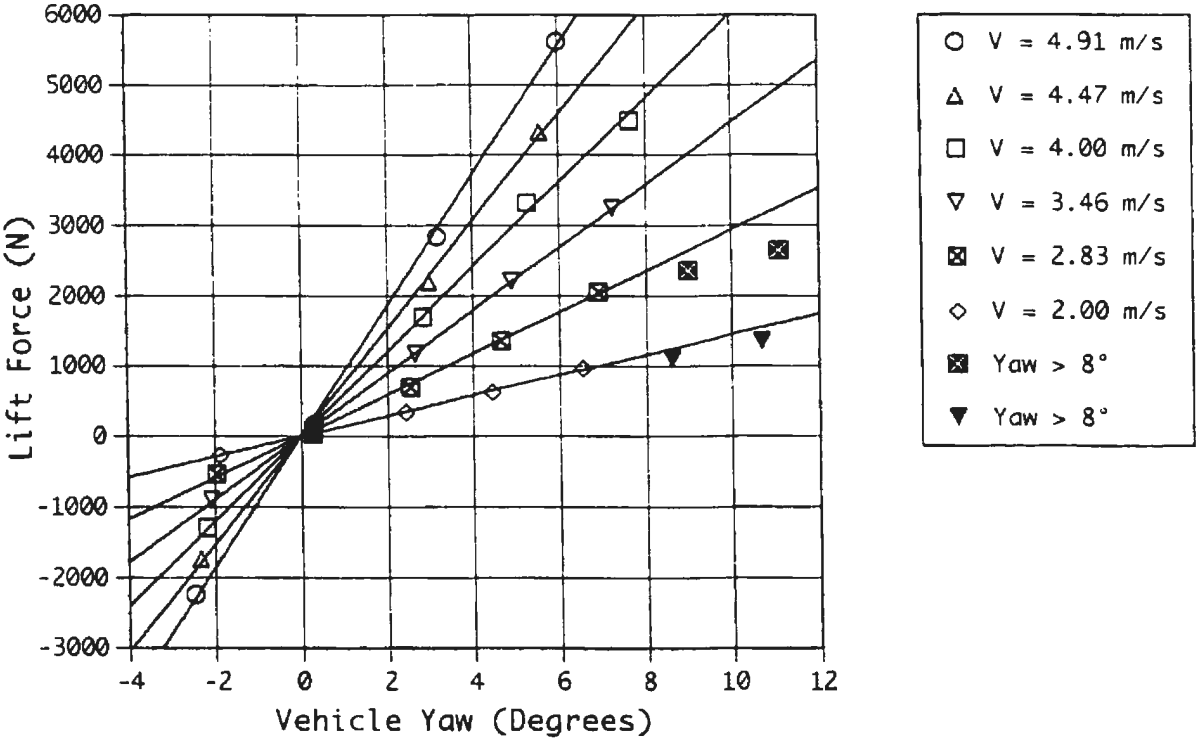

Figure C.06 - *Lift Force vs. Vehicle Yaw Angle; M2 @ D2*

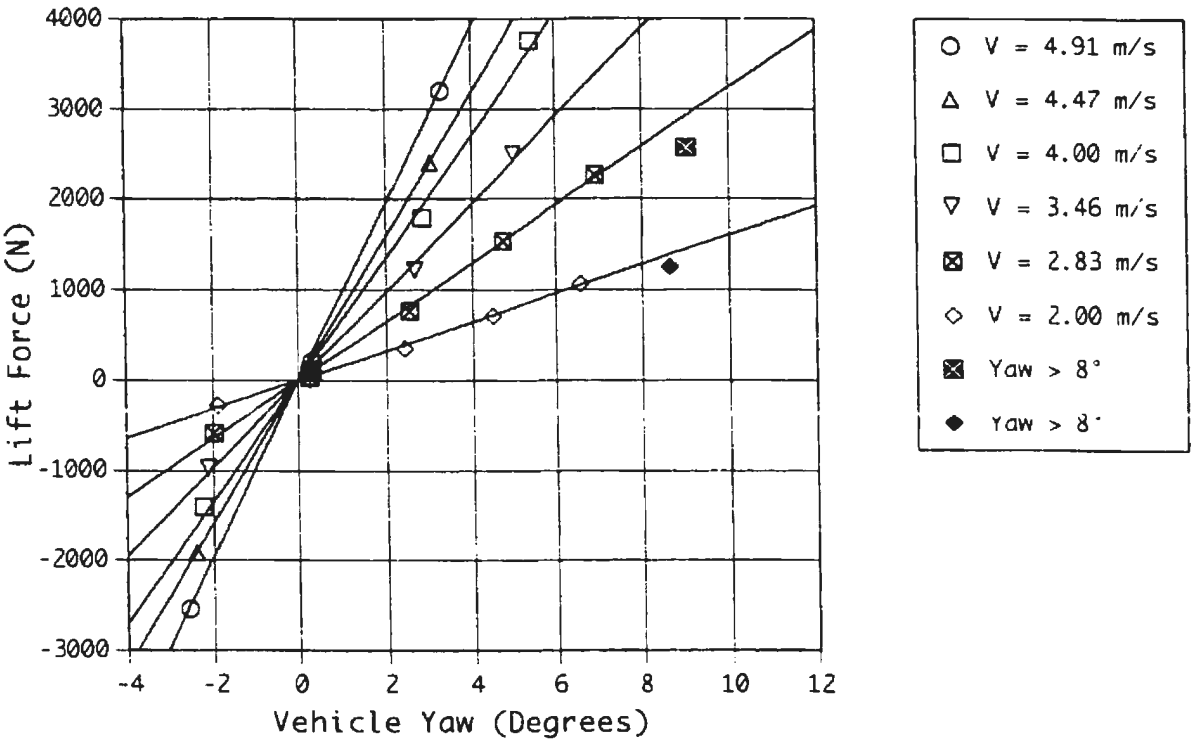

Figure C.07 - *Lift Force vs. Vehicle Yaw Angle; M2 @ D3*

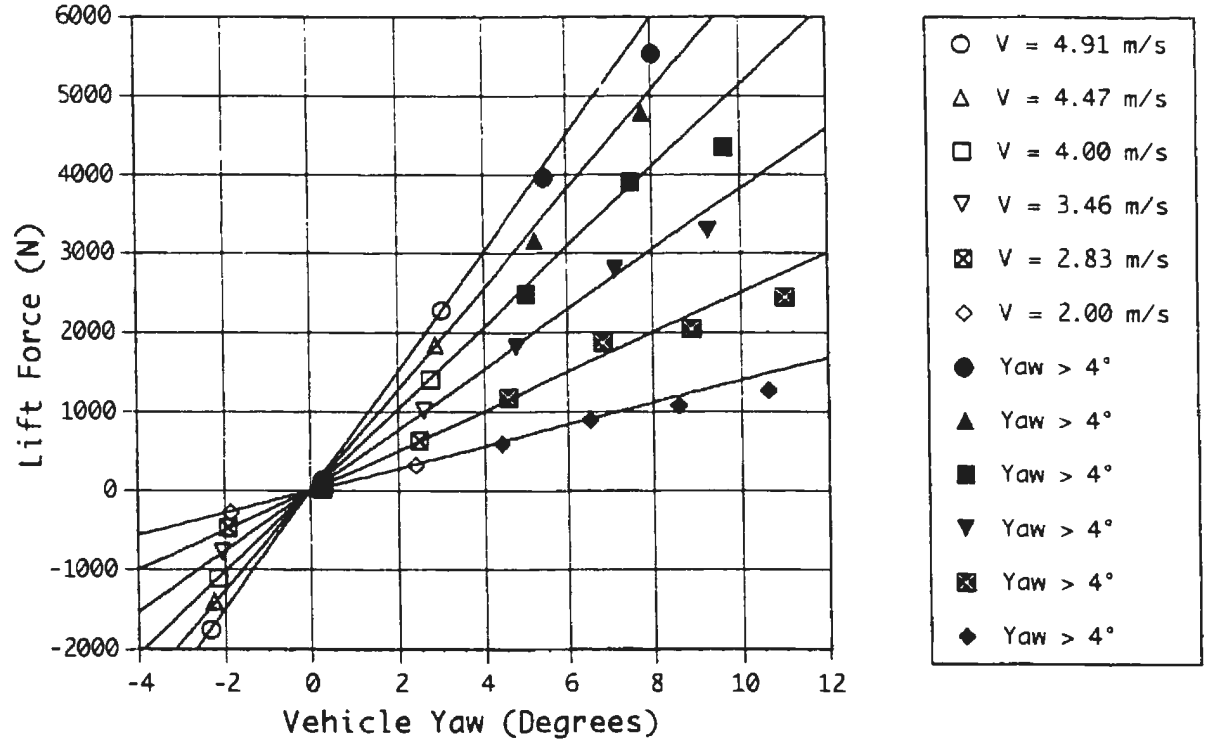

Figure C.08 - *Lift Force vs. Vehicle Yaw Angle; M2B @ D1*

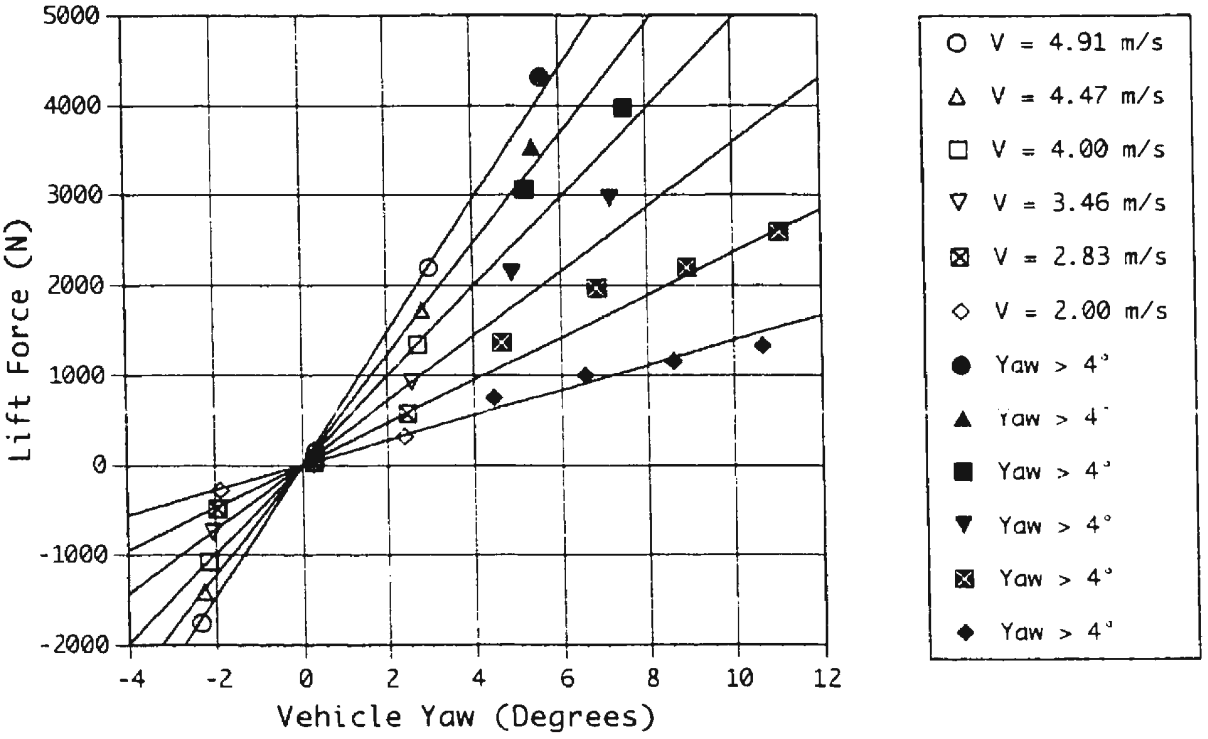

Figure C.09 - *Lift Force vs. Vehicle Yaw Angle; M2B @ D2*

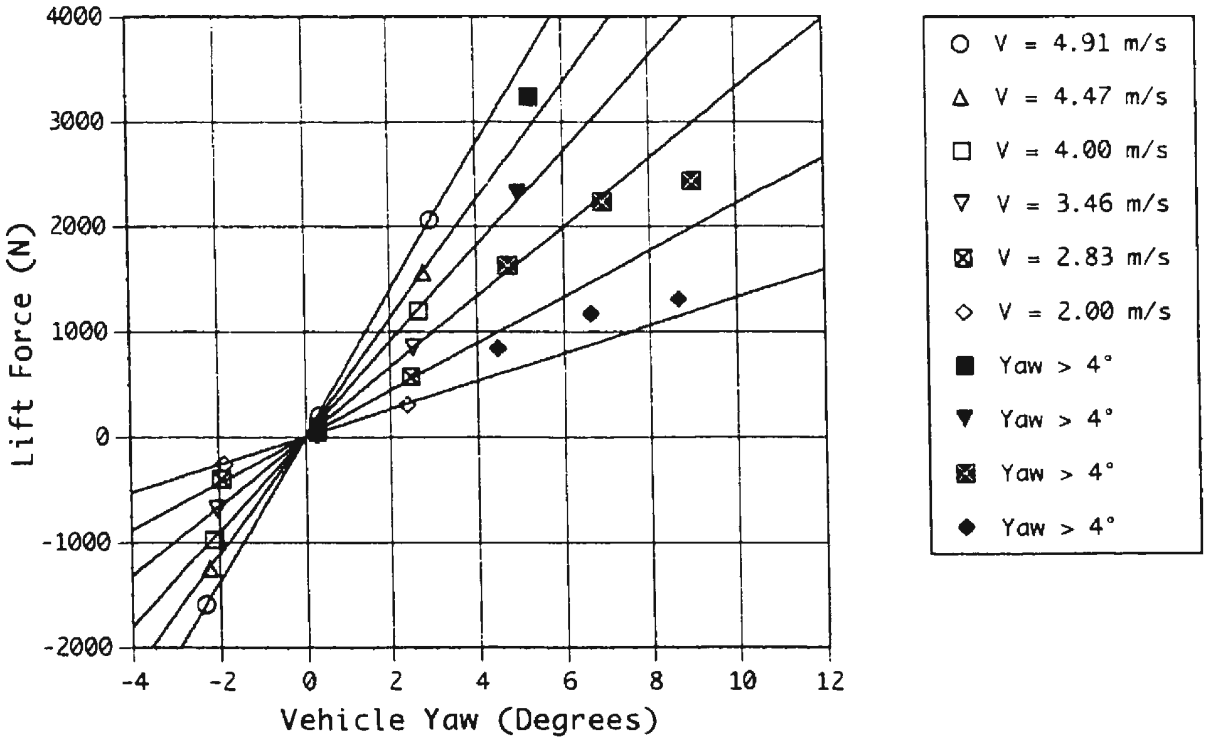

Figure C.10 - *Lift Force vs. Vehicle Yaw Angle; M2B @ D3*

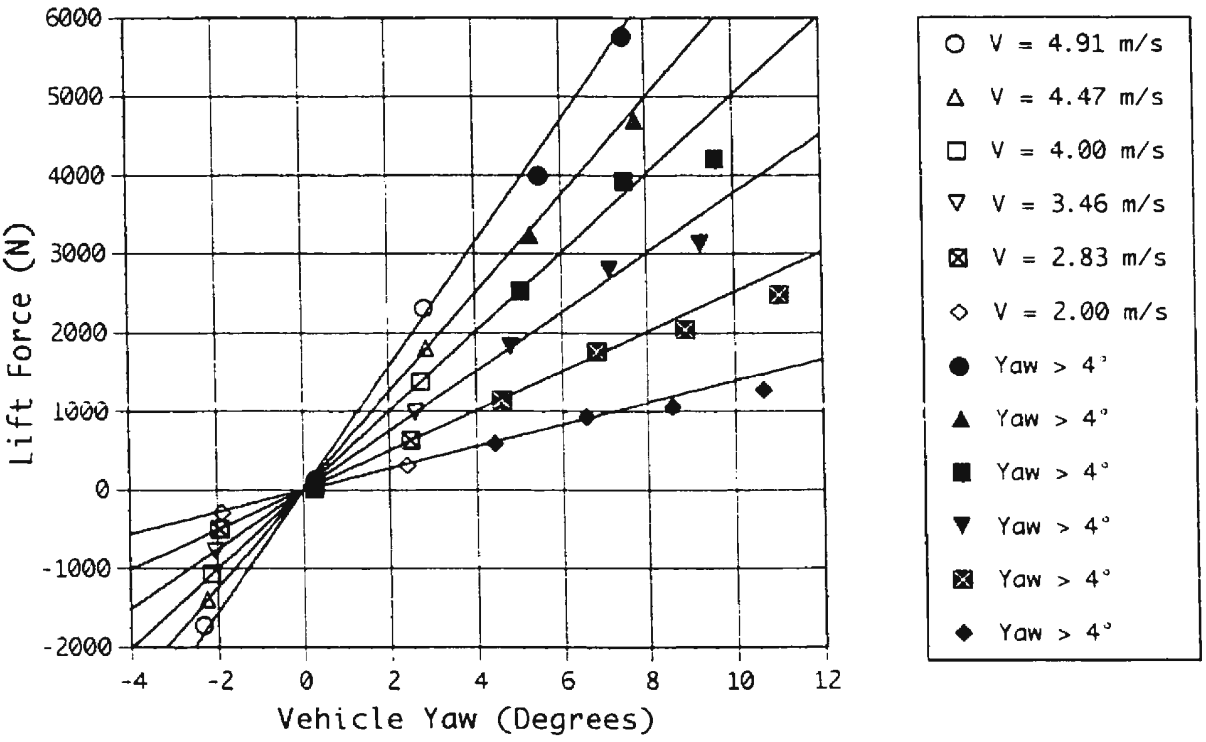

Figure C.11 - *Lift Force vs. Vehicle Yaw Angle; M2A @ D1*

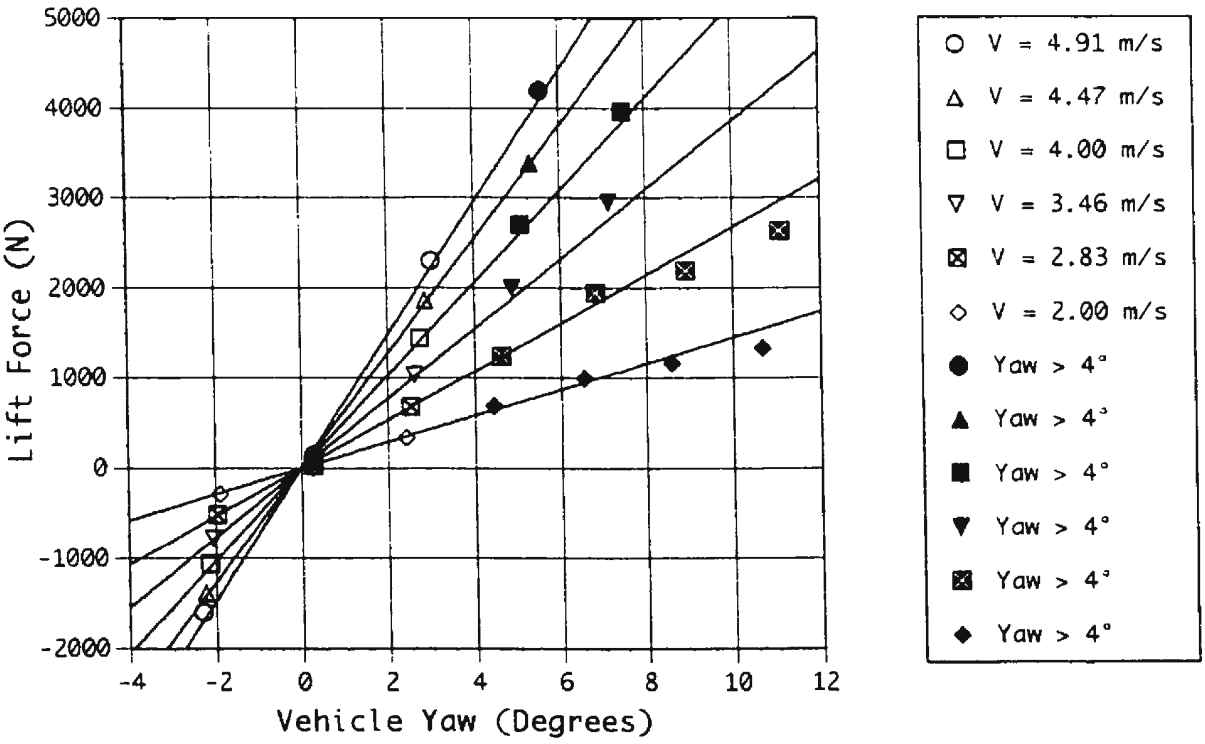

Figure C.12 - *Lift Force vs. Vehicle Yaw Angle; M2A @ D2*

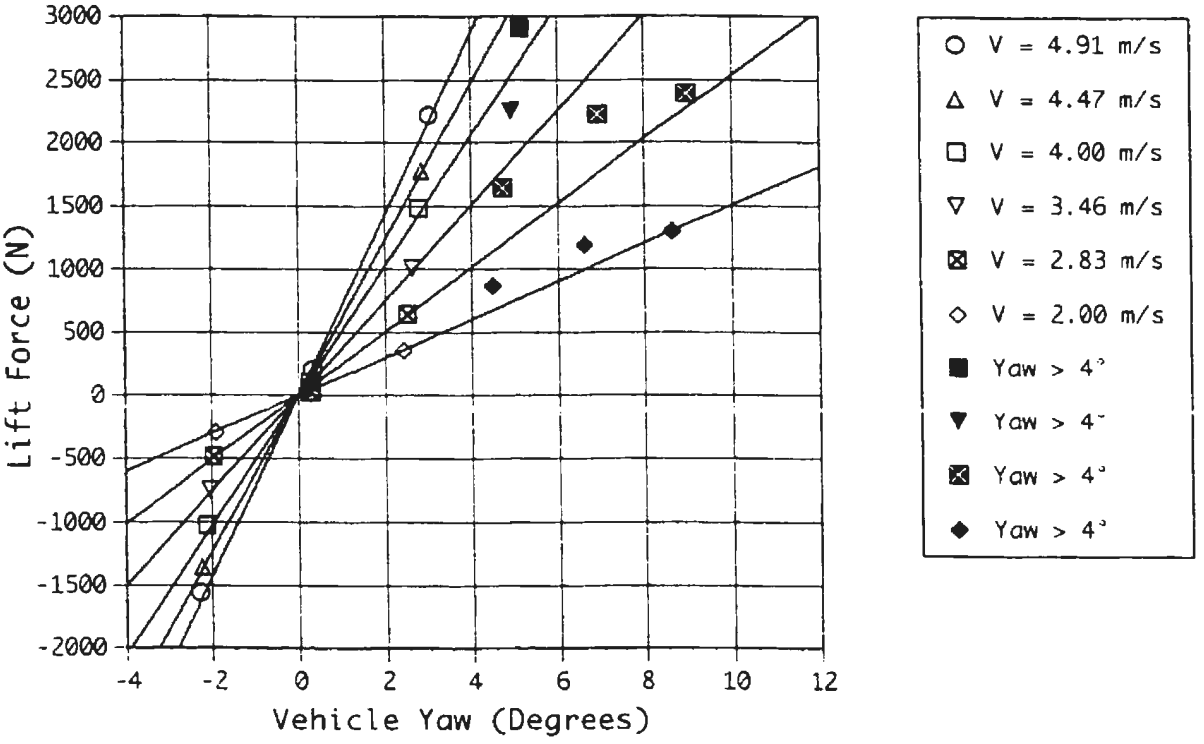

Figure C.13 - *Lift Force vs. Vehicle Yaw Angle: M2A @ D3*

Appendix D

Roll Moment Plots

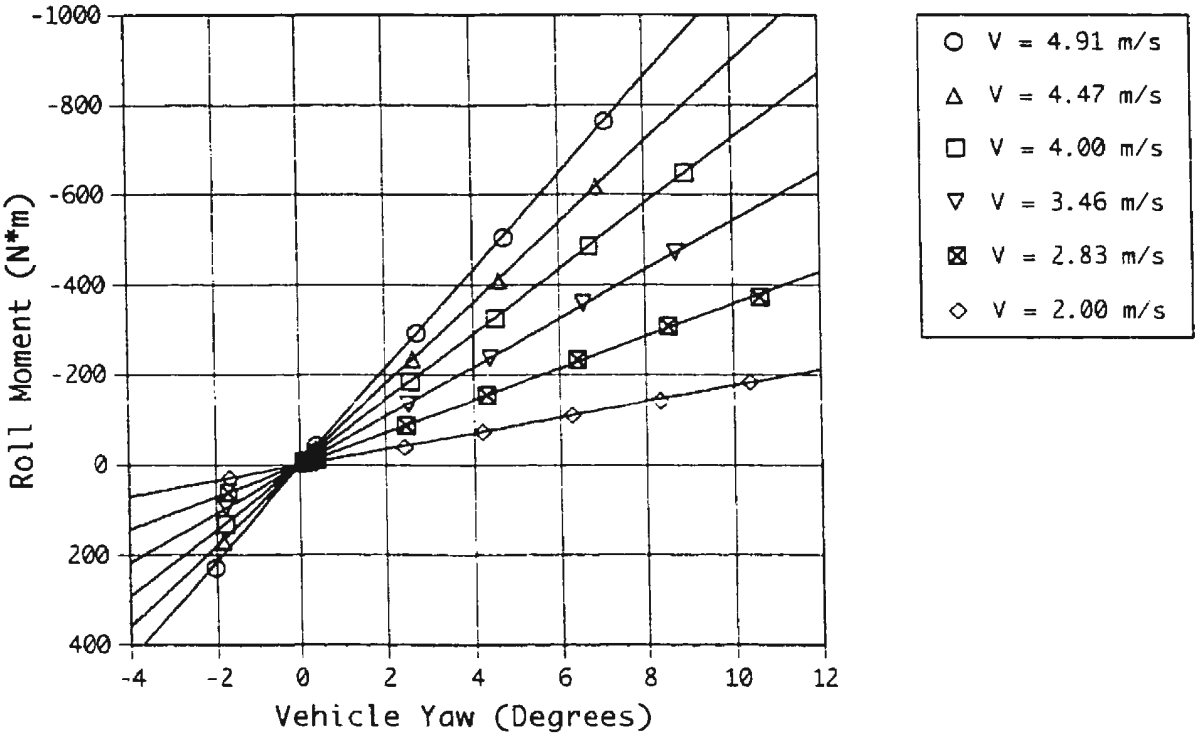

Figure D.01 - *Roll Moment vs. Vehicle Yaw Angle; M0 (No Mast)*

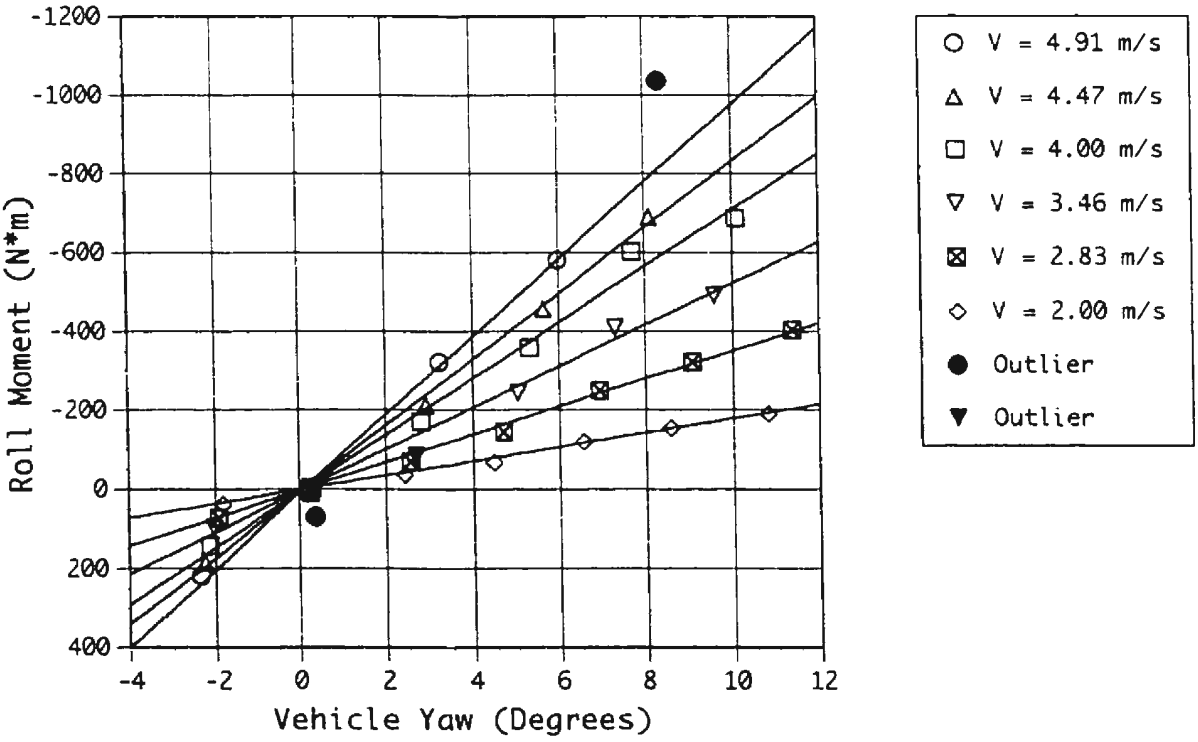

Figure D.02 - *Roll Moment vs. Vehicle Yaw Angle; M1 @ D1*

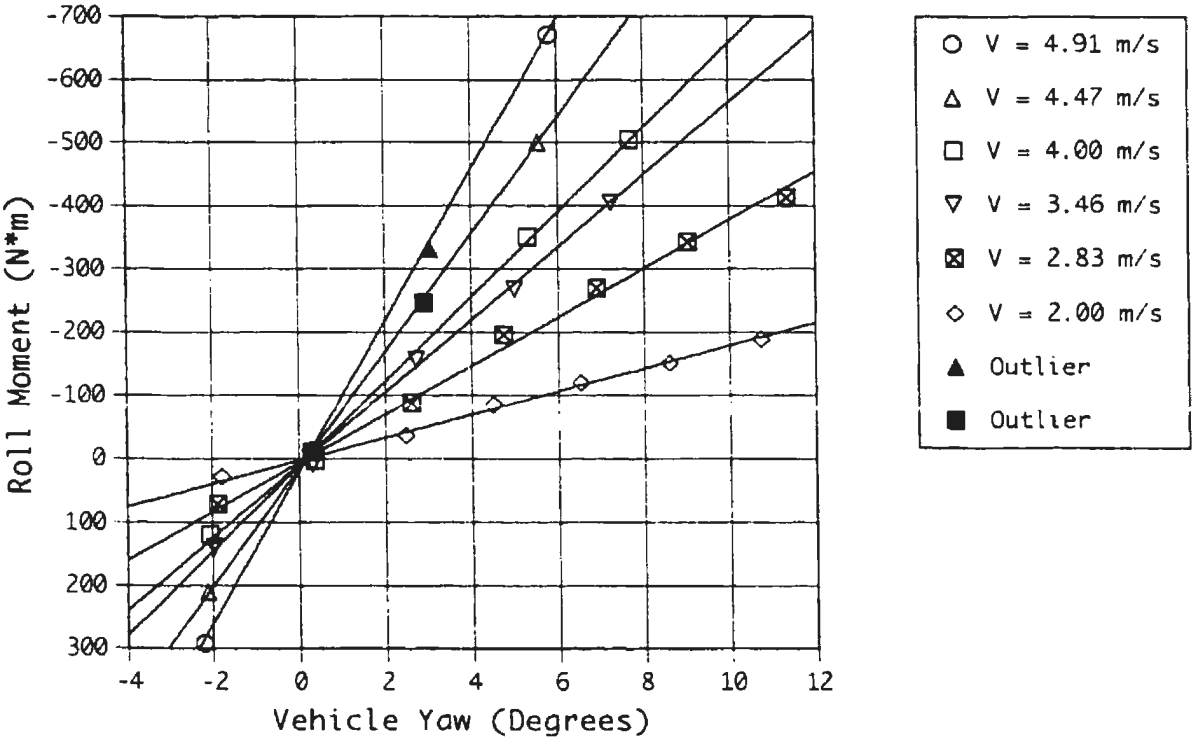

Figure D.03 - *Roll Moment vs. Vehicle Yaw Angle; M1 @ D2*

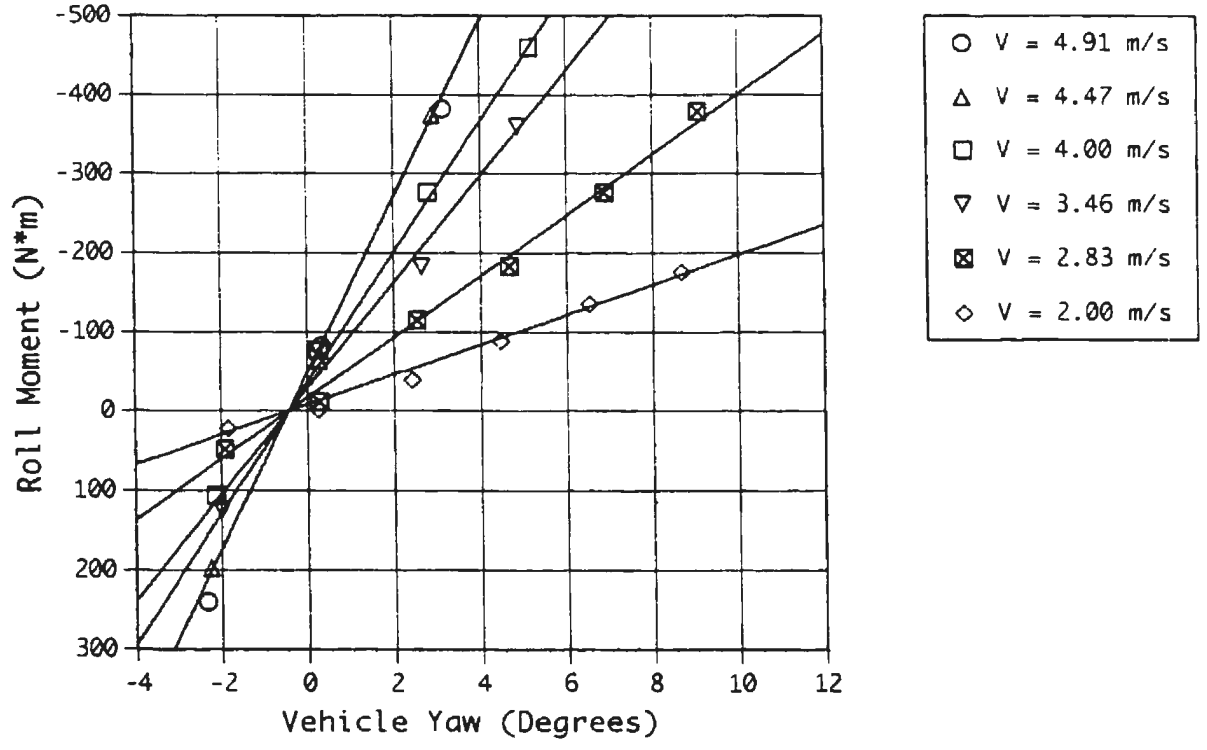

Figure D.04 - *Roll Moment vs. Vehicle Yaw Angle; M1 @ D3*

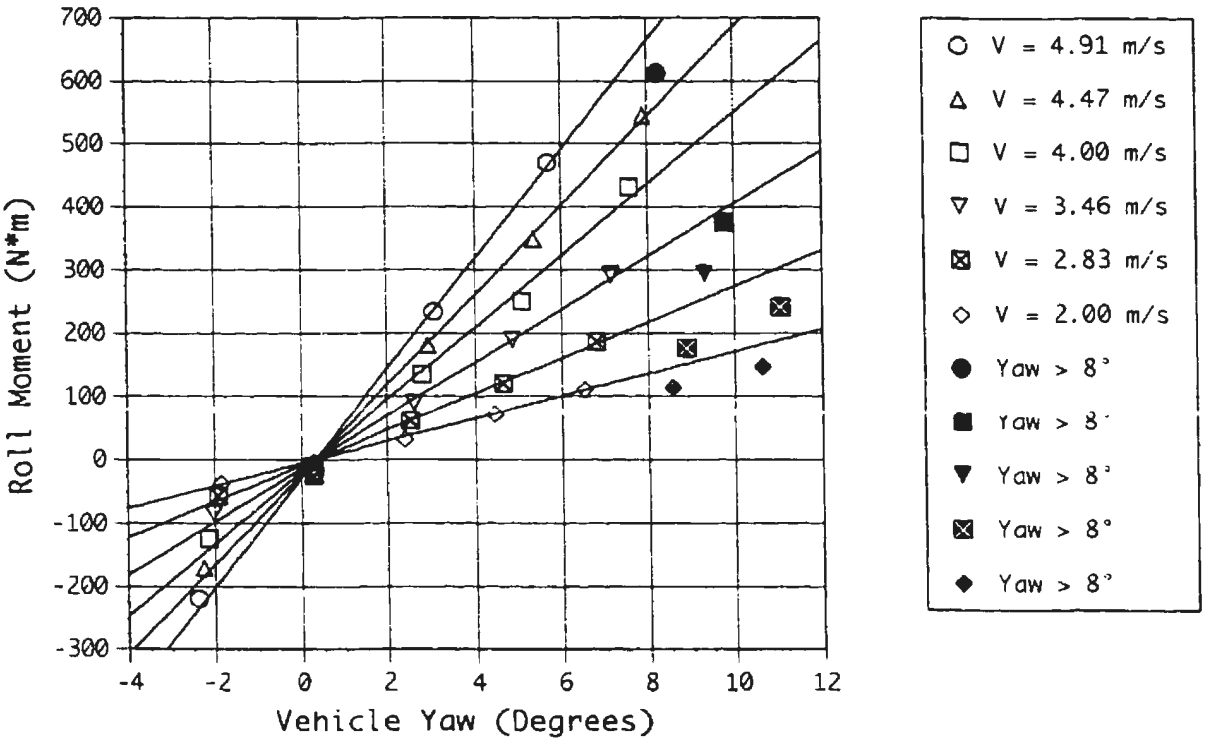

Figure D.05 - *Roll Moment vs. Vehicle Yaw Angle; M2 @ D1*

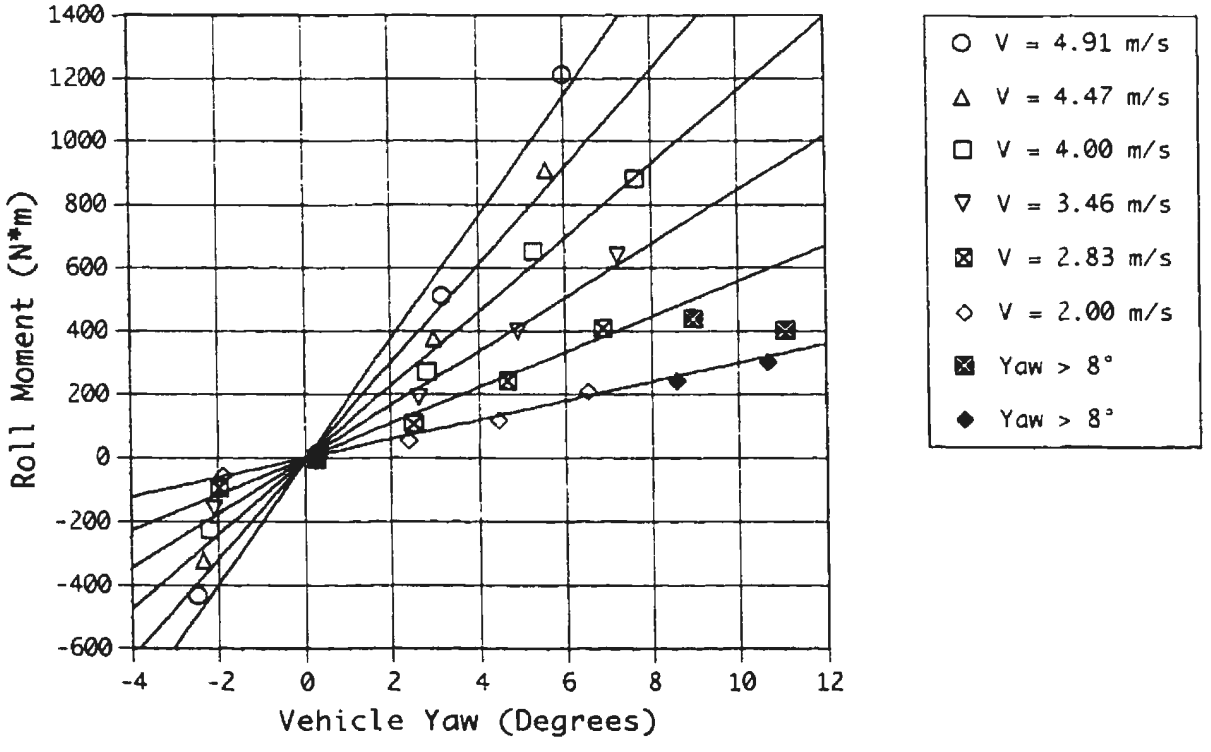

Figure D.06 - *Roll Moment vs. Vehicle Yaw Angle; M2 @ D2*

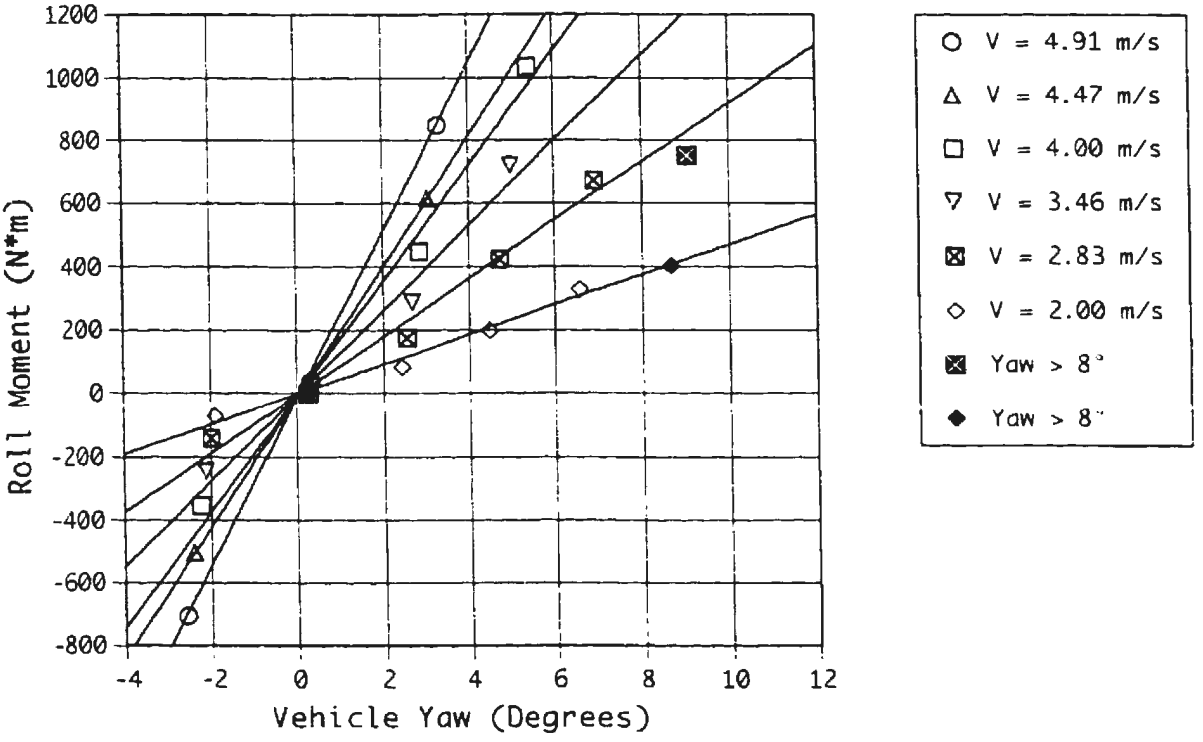

Figure D.07 - *Roll Moment vs. Vehicle Yaw Angle; M2 @ D3*

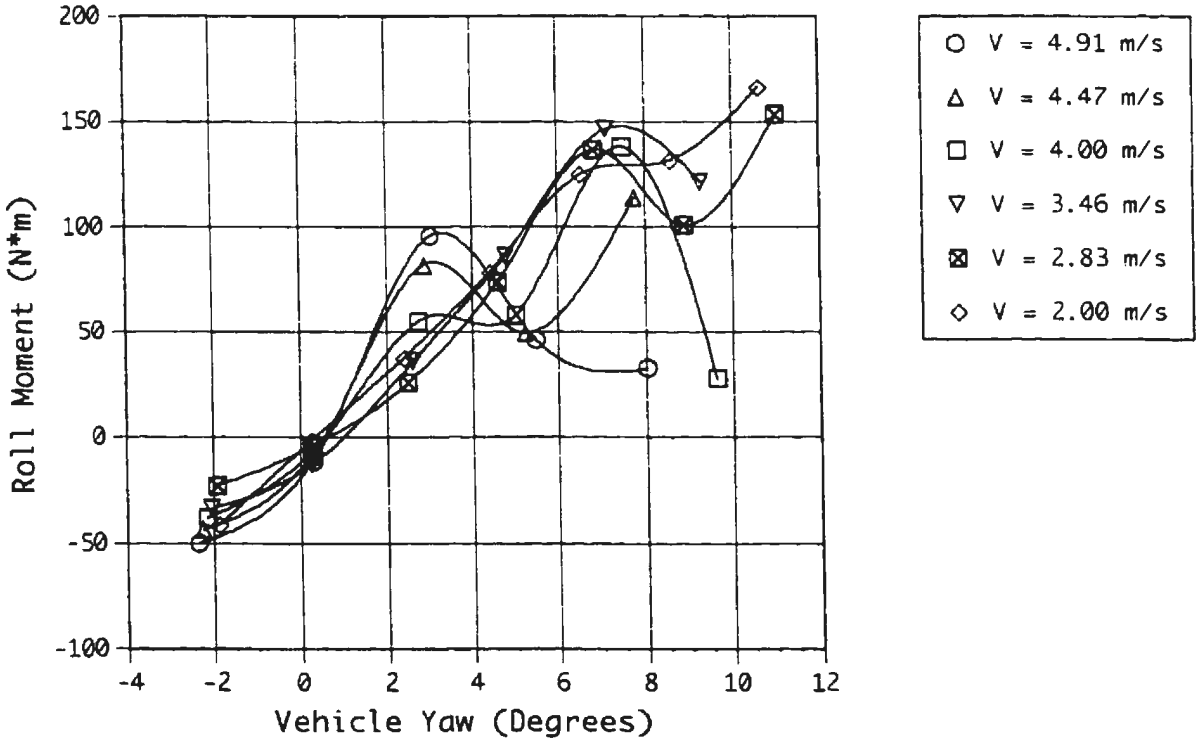

Figure D.08 - *Roll Moment vs. Vehicle Yaw Angle; M2B @ D1*

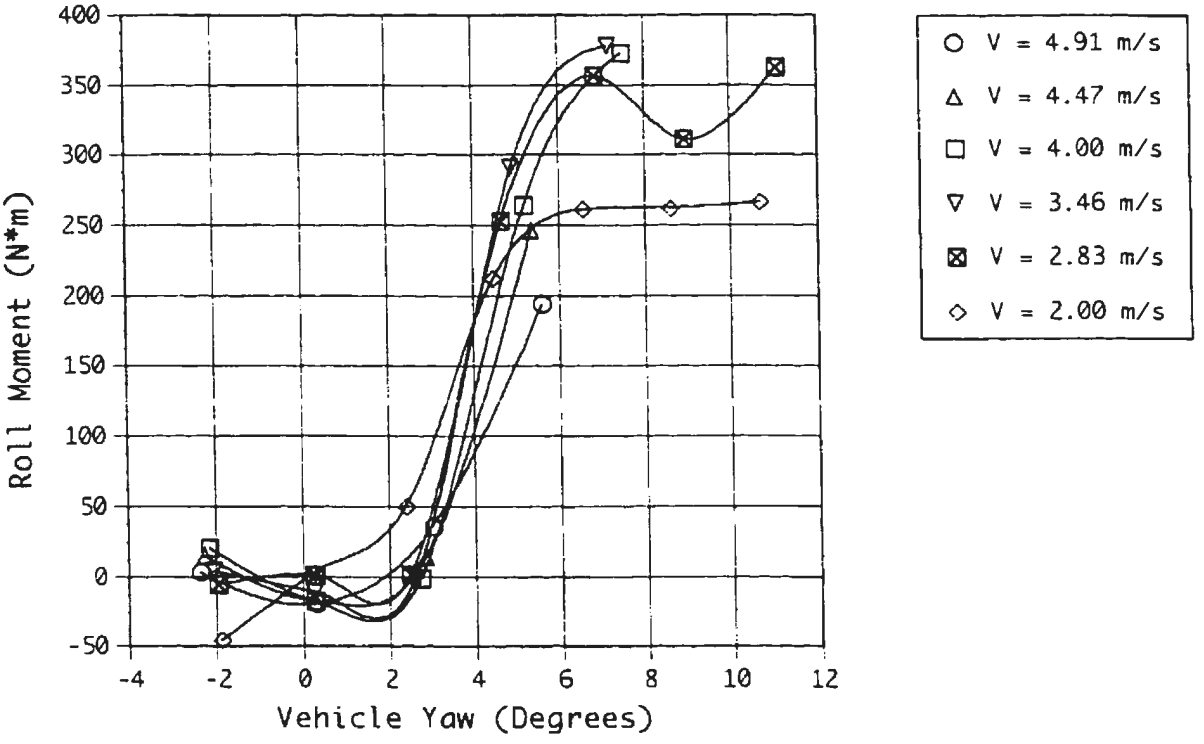

Figure D.09 - *Roll Moment vs. Vehicle Yaw Angle; M2B @ D2*

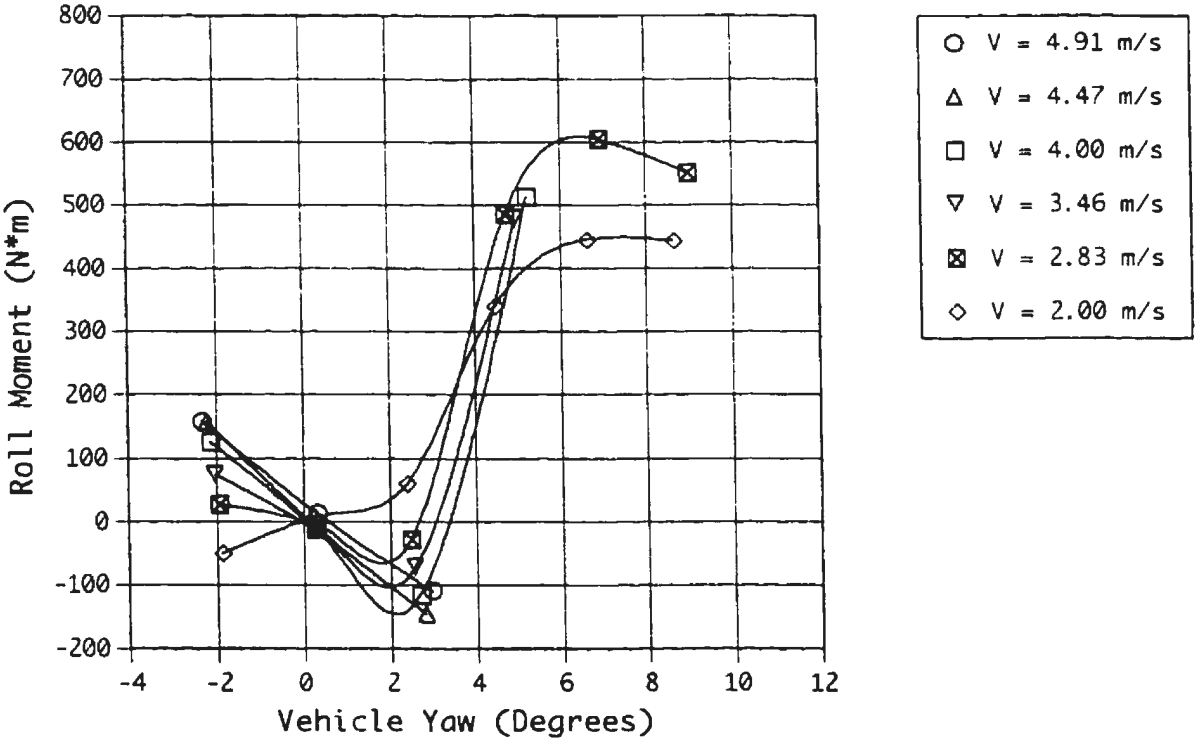

Figure D.10 - *Roll Moment vs. Vehicle Yaw Angle; M2B @ D3*

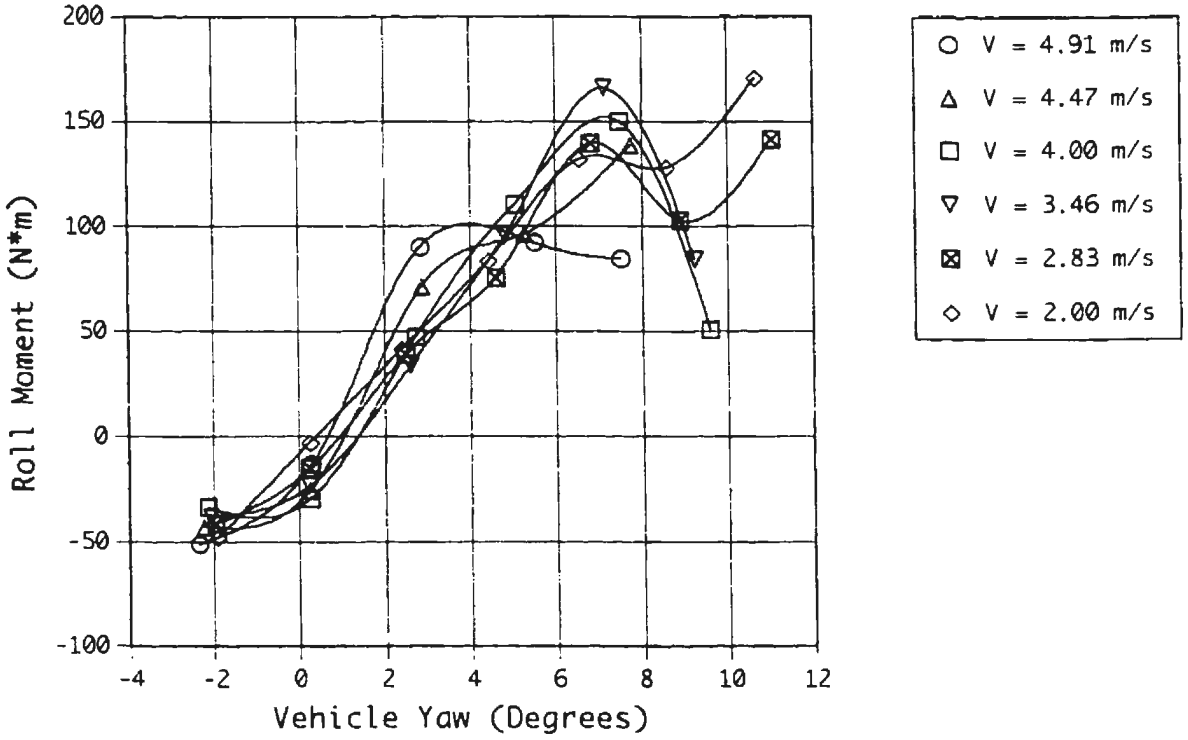

Figure D.11 - *Roll Moment vs. Vehicle Yaw Angle; M2A @ D1*

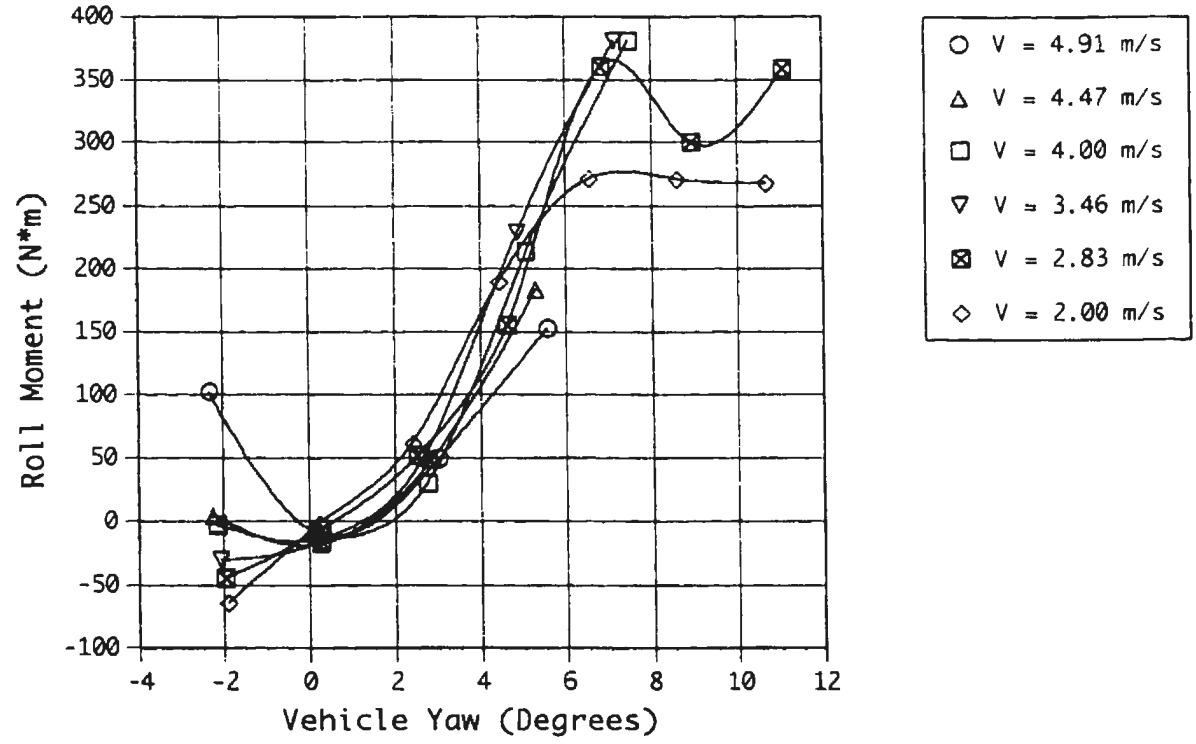

Figure D.12 - *Roll Moment vs. Vehicle Yaw Angle; M2A @ D2*

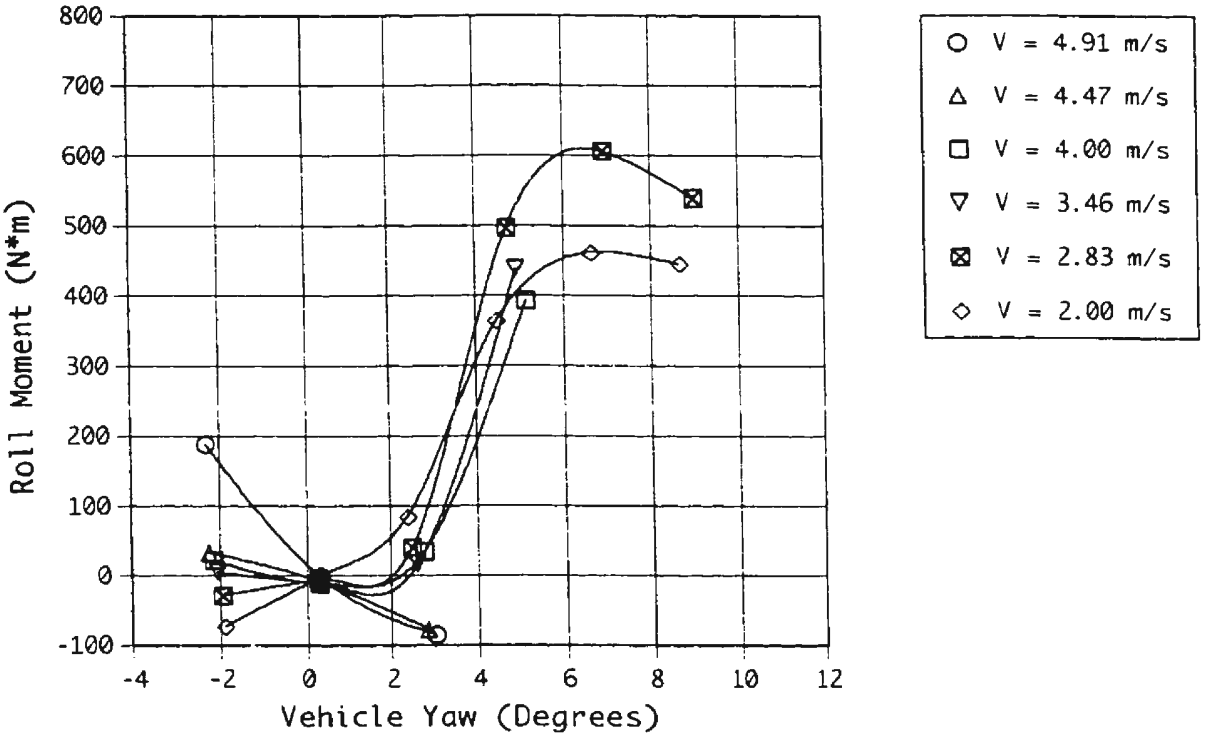

Figure D.13 - *Roll Moment vs. Vehicle Yaw Angle; M2A @ D3*